

## **ABSTRACT**

Title of dissertation: THE EFFECT OF SURFACTANT VAPOR ON  
MARANGONI CONVECTION IN ABSORPTION AND  
CONDENSATION

Zhe Yuan, Doctor of Philosophy, 2005

Dissertation directed by: Dr. Keith E. Herold, Associate Professor,  
Department of Mechanical Engineering

Mass and heat transfer enhancement by the addition of a class of surfactant additives is in common use in absorption machines based on aqueous lithium-bromide (LiBr). It is observed that the addition of on the order of 100 ppm of a surfactant such as 2-ethyl-hexanol (2EH) introduces Marangoni convection on the liquid surface and thereby enhances absorption and condensation rates. The Vapor Surfactant Theory (Kulankara and Herold, 2000) proposed that such Marangoni convection is driven by the surface tension gradient caused by surfactant that circulates through the machine and arrives at the liquid surfaces as a vapor by bulk flow along with water vapor.

The objective of this work was to fully understand the vapor surfactant induced enhancement mechanism and to quantify the relationship between the enhancement and the key variables. This goal was achieved by conducting experimental and numerical

analyses including the measurement of surface tension with surfactant 2EH in the vapor, determination of 2EH surface concentrations in aqueous LiBr and water, experimental study of Marangoni convection in an absorption and condensation pool with surfactant 2EH in the vapor and modeling of Marangoni convection in the presence of surfactant vapor.

The surface tensions were measured with controlled 2EH concentration in the vapor by using the drop volume method. The results show that for both aqueous LiBr and water the surface tensions are reduced with increased 2EH concentration in the vapor. The 2EH concentration in the vapor is a primary variable in determining the surface tension of aqueous LiBr. Calculated surface concentrations show that the presence of LiBr results in a reduction in 2EH solubility, and that the surface concentration of 2EH is more sensitive to surfactant in the vapor than to surfactant in the liquid. Furthermore, the experimental and numerical analyses show that surfactant in the vapor alone can initiate the Marangoni convection; the strength of Marangoni convection is primarily dependent on the 2EH concentration in the vapor. The current studies show that surfactant in the vapor is a necessary condition for significant absorption and condensation enhancement.

THE EFFECT OF SURFACTANT VAPOR ON MARANGONI CONVECTION  
IN ABSORPTION AND CONDENSATION

By

Zhe Yuan

Dissertation submitted to the Faculty of the Graduate School of the  
University of Maryland at College Park in partial fulfillment  
Of the requirements for the degree of  
Doctor of Philosophy  
2005

Advisory Committee:

Professor Keith E. Herold, Chair/Advisor  
Professor James H. Duncan  
Professor Reinhard Radermacher  
Professor Janice E. Reutt-Robey  
Professor Tien Mo Shih

©Copyright by

Zhe Yuan

2005

## **ACKNOWLEDGEMENTS**

I would like to express my sincere appreciation to my advisor, Dr. Keith Herold, for his guidance, support and encouragement throughout the course of this study at the University of Maryland. The motivating discussions I had with him and constant pushing from him over the years were essential in completing this work. The educational experience received from him and serious attitude toward work learned from him have undoubtedly contributed to my academic career development.

I would also like to thank my dissertation committee Dr. James Duncan, Dr. Reinhard Radermacher, Dr. Reutt-Robey and Dr. Tien Mo Shih for their time, suggestions and comments.

I would also like to appreciate Dr. Kenneth Kiger for providing the flow visualization particles for my experiments.

My thanks also go to my wife, Chunhui Pan, for her constant support and patience and my son for being able to take my mind off my work.

Special thanks also go to my parents for their faithful support and encouragement. I hope I have not disappointed them for taking such long time to finish this work.

Financial support of this research by the companies in the Sorption Systems Consortium (SSC) is gratefully acknowledged. In particular, the support from Carrier Corp., FMC Corp., Gas Research Institute, Trane Co., Wolverine Tube Co. and York International.

## TABLE OF CONTENTS

ACKNOWLEDGEMENTS .....	ii
LIST OF TABLES .....	vi
LIST OF FIGURES .....	vii
NOMENCLATURE .....	x
CHAPTER 1 INTRODUCTION .....	1
1.1 Background and Motivation .....	1
1.2 Objectives of This Study .....	3
1.3 Dissertation Outline .....	5
CHAPTER 2 SURVEY OF LITERATURE.....	7
2.1 Surface Tension of Aqueous LiBr with Surfactants .....	7
2.2 Marangoni Convection in the Presence of Surfactants .....	10
2.3 Published Surfactant Enhancement Theories.....	18
2.4 Absorption and Condensation Enhancement by Surfactants .....	23
CHAPTER 3 SURFACE TENSION MEASUREMENT WITH SURFACTANT 2-ETHYL-HEXANOL.....	30
3.1 Introduction.....	30
3.2 Description of the Measurement Method .....	31
3.2.1 Measurement Apparatus .....	32
3.2.2 Preparation of the Liquid Samples .....	35
3.2.3 Experimental Procedure .....	36
3.2.4 The Effect of Air Velocity.....	36
3.2.5 Determination of the Vapor Concentration .....	37
3.2.6 Examination of Measurement Accuracy .....	39
3.3 Surface Tension Measurement Results .....	40
3.3.1 Surface Tension Results for Water.....	40
3.3.1.1 Surface tension of water with 2-ethyl-hexanol in air.....	40
3.3.1.2 Surface tension of water with 2-ethyl-hexanol in the liquid sample .....	41
3.3.2 Surface Tension Results for Aqueous LiBr.....	44
3.3.2.1 Surface tension of aqueous LiBr with 2-ethyl-hexanol in air .....	44
3.3.2.2 Surface tension of aqueous LiBr with 2-ethyl-hexanol in aqueous LiBr..	50
3.4 Solubility Limit of 2EH in 60% Aqueous LiBr and Water .....	50
3.5 Comparison with Literature Data.....	55
3.6 Discussion .....	59
CHAPTER 4 DETERMINATION OF THE SURFACE CONCENTRATION .....	61
4.1 Introduction.....	61
4.2 Data Reduction and Gibbs Adsorption Theory.....	61
4.3 Surface Concentration Results .....	63
4.3.1 Surface Concentration of 2-Ethyl-Hexanol in Water .....	63
4.3.2 Surface Concentration of 2-Ethyl-Hexanol in Aqueous LiBr .....	68
4.4 Discussion .....	74

<b>CHAPTER 5 EXPERIMENTAL STUDY OF MARANGONI CONVECTION IN ABSORPTION/CONDENSATION IN THE PRESENCE OF SURFACTANT VAPOR</b>	81
5.1 Introduction.....	81
5.2 Experimental Apparatus and Procedure.....	82
5.2.1 Description of the Measurement Apparatus.....	82
5.2.2 Experimental Procedure .....	86
5.3 Main Issues in the Experiments .....	89
5.3.1 Preparation of a Vapor Sample.....	89
5.3.2 The Effect of Evacuation on the 2EH Concentration.....	89
5.3.3 The Particles for Visualization .....	91
5.3.4 The Cooling System .....	91
5.3.5 Examination of Measurement Accuracy .....	92
5.4 Absorption of Water + 2EH Vapor in Aqueous LiBr.....	92
5.4.1 Adiabatic Absorption.....	92
5.4.1.1 Adiabatic Absorption with $\geq$ 2500 ppm 2EH .....	93
5.4.1.2 Adiabatic absorption with 400-1500 ppm 2EH .....	97
5.4.2 Absorption with Cooling .....	102
5.4.3 Evaporation with Heating.....	108
5.5 Condensation of Water + 2EH Vapor.....	111
5.5.1 Adiabatic Condensation.....	111
5.5.2 Condensation with Cooling .....	112
5.6 Discussion .....	113
<b>CHAPTER 6 NUMERICAL STUDY OF CONDENSATION IN THE PRESENCE OF SURFACTANT VAPOR.....</b>	119
6.1 Introduction.....	119
6.2 Physical Model.....	120
6.3 Governing Equations, Initial and Boundary Conditions.....	121
6.4 Numerical Formulation.....	125
6.5 Simulation Study.....	128
6.5.1 Simulation Algorithm.....	128
6.5.2 Grid Study.....	128
6.5.3 Relationship Between Surface Tension and Surface Concentration .....	130
6.5.4 Mass Diffusivity of 2EH in Water and Aqueous LiBr .....	132
6.5.5 Time Step Size .....	133
6.5.6 Numerical Approximation of the Advection Term .....	134
6.6 Results and Discussion .....	135
<b>CHAPTER 7 DISCUSSION.....</b>	147
7.1 Effect of Surfactant 2-ethyl-hexanol on Surface Tension.....	147
7.2 Effect of Surfactant Vapor on Marangoni Convection .....	151
7.3 Absorption and Condensation in the Presence of 2-ethyl-hexanol Vapor .....	153
7.4 Comparison of Numerical and Experimental Results.....	155
7.4.1 Comparison of Geometries and Assumptions in Simulations and Experiments .....	155
7.4.2 Discussion of Major Results.....	156

7.5 Interpretation of Results in Terms of the Vapor Surfactant Theory .....	157
<b>CHAPTER 8 CONCLUSIONS AND RECOMMENDATIONS FOR FUTURE WORK</b>	<b>160</b>
8.1 Summary .....	160
8.2 Conclusions.....	162
8.3 Recommendations for Future Work.....	165
<b>APPENDIX A SOURCE CODE FOR 1-D SURFACTANT MASS TRANSFER EQUATION.....</b>	<b>167</b>
<b>APPENDIX B EXPERIMENTAL PROCEDURE FOR POOL ABSORPTION/CONDENSATION MEASUREMENTS .....</b>	<b>178</b>
<b>APPENDIX C REGRESSION OF THE PROPERTIES OF AQUEOUS LITHIUM BROMIDE BY GIBBS FREE ENERGY METHOD.....</b>	<b>182</b>
C.1 Introduction.....	182
C.2 Multi-property Gibbs Free Energy Correlation Method.....	183
C.3 SSC-4 Correlation.....	184
C.3.1 Database Used to Generate the SSC-4 Correlation.....	184
C.3.2 Functional Form of Gibbs Free Energy and Other Thermodynamic Properties .....	186
C.3.3 SSC-4 Regression Results.....	190
C.4 Verification and Discussion.....	191
C.5 Thermodynamic Property Plots .....	198
C.6 Conclusion .....	200
<b>APPENDIX D PROPERTY ROUTINE: FOR AQUEOUS LIBR AND WATER IN VISUAL BASIC .....</b>	<b>201</b>
D.1 Introduction.....	201
D.2 Visual Basic Routine and Its Main Features.....	201
D.3 Verification .....	205
D.4 Summary .....	206
<b>APPENDIX E SPECIFIC HEAT MEASUREMENTS ON AQUEOUS LITHIUM BROMIDE .....</b>	<b>207</b>
E.1 Introduction.....	208
E.2 Measurement Method .....	208
E.3 Specific Heat Results .....	213
E.4 Comparison With Selected Literature Data .....	214
E.5 Verification of Measurement Method Accuracy .....	215
E.6 Uncertainty Analysis.....	216
E.7 Conclusion .....	217
<b>BIBLIOGRAPHY .....</b>	<b>224</b>

## LIST OF TABLES

Table 3.1	Examination of measurement accuracy .....	40
Table 4.1	2EH surface concentration and surface tension for water with 2EH .....	68
Table 4.2	2EH saturated surface concentration and solubility limit .....	73
Table 4.3	2EH system concentration producing a 20 mN/m reduction in surface tension, $x_{20}$ , and the ratio of $x_{sol}/x_{20}$ along with saturated surface concentration and solubility limit .....	78
Table 5.1	The change of the amount of sample in the sample flask before and after evacuation .....	90
Table 5.2	Comparison of the experimental conditions and results for representative adiabatic absorption and condensation .....	117
Table 6.1	Grid study results showing total condensation rate and average velocity at the free surface (time = 5 sec) for two grid choices.....	130
Table C.1	Summary of the property data set used to generate SSC-4.....	185
Table C.2	The sources of experimental vapor pressure and density data used in SSC-4 .....	185
Table C.3	Coefficients for SSC-4 .....	191
Table C.4	Enthalpy difference between the SSC-4 correlation and McNeely's data (Unit for enthalpy difference: kJ/kg) .....	193
Table E.1	Experimental specific heat data for aqueous Lithium Bromide.....	218
Table E.2	Coefficients for the specific heat correlation for aqueous lithium bromide (Eq. E.2) .....	219

## LIST OF FIGURES

Figure 1.1	Schematic of absorption refrigeration cycle .....	2
Figure 2.1	Surface tension of LiBr solution versus concentration of 2EH .....	11
Figure 3.1	Schematic of force balance for a drop on the tip of the surface tension measurement apparatus.....	32
Figure 3.2	Schematic of the surface tension facility .....	34
Figure 3.3	The surface tension facility .....	34
Figure 3.4	The effect of air velocity on surface tension.....	38
Figure 3.5	Surface tension of water versus drop frequency and 2EH concentration in air .....	42
Figure 3.6	Surface tension of water versus concentration of 2EH in air.....	43
Figure 3.7	Surface tension of water versus drop frequency and 2EH concentration in the water.....	45
Figure 3.8	Surface tension of water versus 2EH concentration in sample.....	46
Figure 3.9	Surface tension of 60% aqueous LiBr versus drop frequency with 2EH concentration in air .....	48
Figure 3.10	Surface tension of pure water and 60% aqueous LiBr with 2EH concentration in air .....	49
Figure 3.11	Surface tension of 60% aqueous LiBr versus 2EH concentration in the liquid .....	51
Figure 3.12	Determination of solubility limit of 2EH in 60% aqueous LiBr.....	54
Figure 3.13	Determination of solubility limit of 2EH in water.....	56
Figure 3.14	Surface tension of LiBr solution versus concentration of 2-ethyl-hexanol .....	58
Figure 4.1	Surface tension and 2EH surface concentration versus 2EH system concentration (where system is water in a glass flask) .....	65
Figure 4.2	Surface tension versus 2EH surface concentration for water (Equation 4.7) .....	67
Figure 4.3	Surface tension versus 2EH system concentration for aqueous LiBr .....	70
Figure 4.4	2EH surface concentration versus 2EH system concentration for aqueous LiBr .....	71
Figure 4.5	Surface tension versus 2EH surface concentration for aqueous LiBr .....	72
Figure 4.6	Surface tension versus dilution time of sample .....	75
Figure 4.7	2EH surface concentrations for water computed from different surface tension data sources .....	77
Figure 4.8	2EH surface concentration versus 2EH vapor concentration in air .....	80
Figure 5.1	Schematic of absorption/condensation pool apparatus .....	83
Figure 5.2	A photograph of the absorption/condensation pool apparatus.....	84
Figure 5.3	Schematic of the connection between the thermocouples and the feedthroughs on the wall of the chamber.....	86
Figure 5.4	Evolution of surface during adiabatic absorption (2EH vapor concentration = 2500 ppm, sample solution = 60% aqueous LiBr) .....	94
Figure 5.5	The pressure history during adiabatic absorption for high 2EH vapor concentrations .....	96

Figure 5.6	Evolution of surface during adiabatic absorption (2EH vapor concentration = 400 ppm, sample solution = 60% aqueous LiBr) .....	99
Figure 5.7	The pressure history during adiabatic absorption including low 2EH vapor concentrations .....	100
Figure 5.8	Evolution of surface with cooling from the center underneath the pool (2EH vapor concentration = 2500 ppm, sample solution = 60% aqueous LiBr) 105	105
Figure 5.9	Evolution of the surface with cooling from the center underneath the pool showing two cells at 1 sec (2EH vapor concentration = 2500 ppm, sample solution = 60% aqueous LiBr) .....	106
Figure 5.10	Evolution of the surface with cooling from the center underneath the pool showing an annulus ring at 60 sec (2EH vapor concentration = 2500 ppm, sample solution = 60% aqueous LiBr).....	107
Figure 5.11	Cross sectional schematic of the pool showing recirculating flow to explain surface clearing seen in Figures 5.8 to 5.10.....	108
Figure 5.12	Evolution of the surface when heating was applied from the center underneath the pool (2EH vapor concentration = 2500 ppm, sample solution = 60% aqueous LiBr).....	110
Figure 5.13	Evolution of surface in a water pool for adiabatic condensation (2EH vapor concentration = 10300 ppm) .....	114
Figure 5.14	Evolution of surface in a water pool for condensation with cooling (2EH vapor concentration = 10300 ppm) .....	115
Figure 6.1	Schematic of the condensation pool .....	120
Figure 6.2	Schematic of grid and control volume for the internal and boundary points .....	126
Figure 6.3	Flow chart for the Fluent based simulation of Marangoni convection during condensation in the presence of surfactant in the vapor .....	129
Figure 6.4	Relationship between surface tension and surfactant surface concentration used in simulation .....	131
Figure 6.5	Surfactant surface concentration and steam condensation flux .....	136
Figure 6.6	Shear stress distribution at upper surface as a function of position and time .....	138
Figure 6.7	Surfactant surface concentration distribution as a function of position....	138
Figure 6.8	Condensation flux distribution along surface as a function of position....	139
Figure 6.9	Velocity distribution along surface as a function of position and time ....	139
Figure 6.10	Condensation rate versus time for surfactant enhanced condensation simulation.....	142
Figure 6.11	Surfactant surface concentration versus time at different locations .....	143
Figure 6.12	Streamline contours ( $D = 10^{-7} \text{ m}^2/\text{sec}$ ).....	144
Figure C.1	Vapor pressure error plot .....	194
Figure C.2	Specific heat error plot.....	194
Figure C.3	Volume error plot.....	195
Figure C.4	Comparison of specific heat between SSC-4 correlation and experimental data.....	195
Figure C.5	Comparison of vapor pressure between SSC-4 correlation and McNeely's data .....	196

Figure C.6	Comparison of volume between SSC-4 correlation and experimental data .....	196
Figure C.7	Comparison of enthalpy between SSC-4 correlation and McNeely's data .....	197
Figure C.8	Gibbs free energy property plot .....	198
Figure C.9	Chemical potential of water property plot .....	199
Figure C.10	Entropy property plot .....	199
Figure D.1	About window in Visual Basic routine .....	202
Figure D.2	Main window in Visual Basic routine .....	203
Figure D.3	Two phase window for aqueous lithium bromide.....	205
Figure E.1	Layout of Setaram C80 heat flux calorimeter .....	209
Figure E.2	C80 output for a run with distilled water .....	212
Figure E.3	Specific heat data of aqueous LiBr solution .....	220
Figure E.4	Specific heat data compared with SSC-4 correlation .....	220
Figure E.5	Error plot of differences between our experimental data and the SSC-4 correlation. ....	221
Figure E.6	Comparison of specific heat between our correlation and other data sources .....	221
Figure E.7	Comparison of specific heat between our correlation and the data of Zaytsev and Aseyev (1992) .....	222
Figure E.8	Calorimeter sensitivity function verification using pure water literature data .....	222
Figure E.9	Verification of the specific heat measurement system for a sample (ethanol) with lower specific heat .....	223

## NOMENCLATURE

C	Association factor of solvent in Eq. 6.16 ( $C = 2.6$ for water, $C = 1.5$ for ethyl-alcohol)
D	Diameter (m); Diffusion coefficient of surfactant on surface ( $m^2/s$ )
e	The east face of a selected control volume
E	Neighbor grid point of P at east side
Fr	Froude number, $Fr = V^2/gL$
g	The gravitational acceleration ( $m/s^2$ )
G	The configuration parameters applied to the electrical cooling chip
$h_{fg}$	Latent heat (kJ/kg)
H	Height (m)
I	Current (A)
k	The notation of time step
L	Characteristic length (m)
m	Mass (kg)
M	Molecule weight (g/mole)
$M_2$	molecular weight of solvent (kg/kmol)
N	The configuration parameters applied to the electrical cooling chip
P	pressure (Pa), The center grid point
Pe	Mass transfer Peclet number, $Pe = \rho VL/D$
Q	Heat flux ( $kJ/m^2$ )
r	Radius (m)
R	Universal gas constant ( $8.31 \text{ J/mol}\cdot\text{K}$ )
S	Mass flux of steam condensation on the upper surface from vapor phase ( $\text{kg}/\text{s}\cdot\text{m}^2$ )
t	Time (s)
T	Temperature ( $^\circ\text{C}$ , K)
u	Velocity (m/s)
$u_h$	Velocity on upper surface (m/s)
V	Volume of a drop ( $\text{m}^3$ ); Voltage (V); Characteristic velocity (m/s)
$V_1$	Molar volume of solute 1 at its boiling temperature ( $\text{cm}^3/\text{mol}$ )
w	The west face of a selected control volume
W	Neighbor grid point of P at west side
x	Mass fraction (%; ppm)
$X_s$	Surface concentration of surfactant ( $\text{mg}/\text{m}^2$ )
$q''$	Cooling flux at bottom of film ( $\text{W}/\text{m}^2$ )
$\Delta t$	Time step size (second)
$\Delta T$	Temperature difference ( $^\circ\text{C}$ )
$\beta$	Thermal expansion coefficient ( $1/\text{K}$ )
$\delta$	The grid interval (m)
$\lambda$	Thermal conductivity ( $\text{W}/\text{m}\cdot\text{K}$ )

$\mu$	Dynamic viscosity of water (kg/m·s)
$\rho$	Density (kg/m <sup>3</sup> )
$\sigma$	Surface tension (mN/m)
$\nu$	Kinematic viscosity of water (m <sup>2</sup> /s)
$\mu$	Dynamic viscosity of water (kg/m·s); Dynamic viscosity of solvent, (mPa·s)
$\Gamma$	Surfactant surface excess concentration (mg/m <sup>2</sup> )

### Subscripts

ave	Averaged
c	Cold side
h	Hot side
sat	Saturation
sol	Solution
sur	Surfactant
wall	Wall

### Abbreviations

2EH	2-ethyl-hexanol
2MP	2-methyl-1-pentanol
CMC	critical micelle concentration
LiBr	Lithium-Bromide
SLVSA	the solubility limit of vapor surfactant with adsorption
UDF	user defined function

# CHAPTER 1

## INTRODUCTION

### 1.1 Background and Motivation

Enhancements of both absorption and condensation show significant potential for application in absorption refrigeration systems. The enhancement of absorption and condensation by the addition of a class of surfactant additives is common in absorption machines based on aqueous Lithium-Bromide (LiBr).

An absorption chiller based on aqueous LiBr as the working fluid consists of the major components shown in Figure 1.1. The cycle uses water vapor as the refrigerant and a thermal compressor which utilizes aqueous LiBr as a liquid absorbent for the refrigerant. The cycle can be understood by starting at the evaporator where liquid refrigerant (water) evaporates at a low temperature due to heat transfer from the chilled water (i.e. the cooling load). The pressure in the evaporator is held at a low value by the thermal compressor which consists of the absorber and the desorber. The vapor coming from the evaporator is absorbed into aqueous LiBr in the absorber while rejecting heat at temperatures close to ambient (typically via a cooling tower). The combined refrigerant and absorbent is pumped to the desorber where the refrigerant is boiled off by heat transfer from a high temperature heat source (e.g. a natural gas flame or a waste heat source). The desorber operates at a higher pressure than the absorber. The refrigerant vapor leaving the desorber flows to the condenser where it changes to liquid phase accompanied by heat rejection at temperatures close to ambient (cooling tower). The

liquid refrigerant then flows back to the evaporator by the pressure difference caused by the thermal compressor.

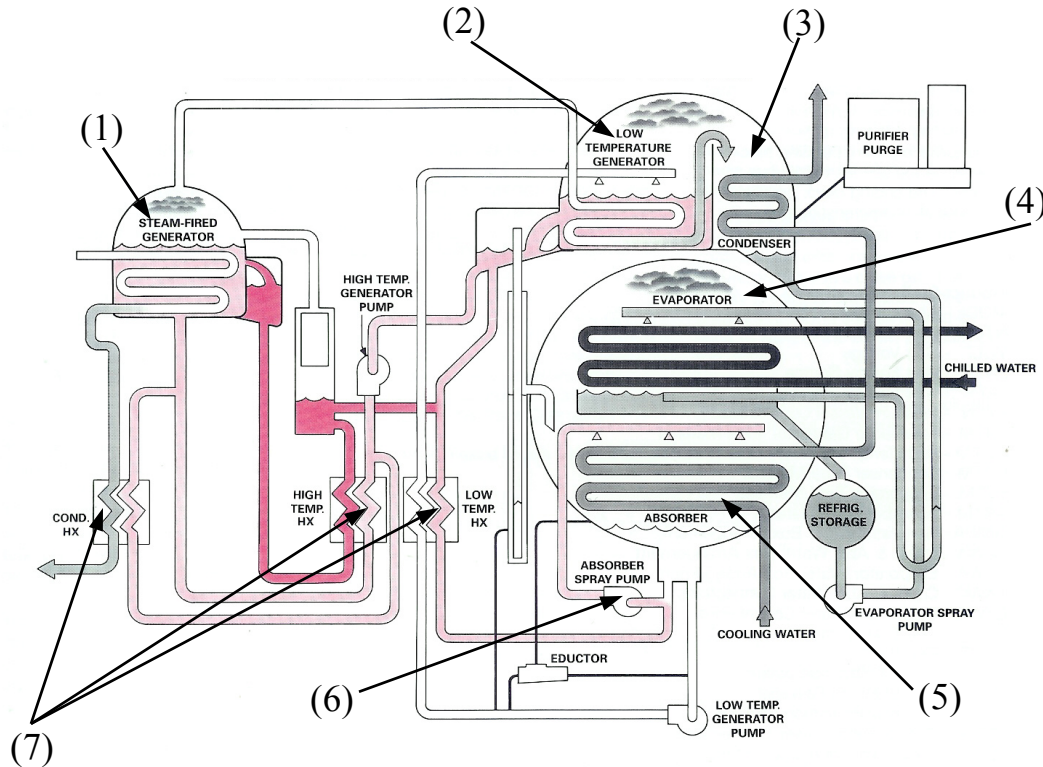


Figure 1.1 Schematic of absorption refrigeration cycle

- (1: High temperature desorber; 2: Low temperature desorber; 3: Condenser;
- 4: Evaporator; 5: Absorber; 6: Absorber spray pump; 7: Heat exchanger)

The performance of such an absorption machine and thus the economics are largely dependent on the absorption process where large surface areas are needed. The transfer processes occurring in the absorber are strongly coupled heat and mass transfer where the mass transfer normally is very slow owing to the small driving force (the difference between vapor pressure and equilibrium pressure of aqueous LiBr), and the slow mass transport in the liquid.

The role of the surfactant is to enhance the heat/mass transfer rate in the absorber. It also enhances the rate in the condenser, although this is less significant for the economics since the condenser is controlled, in most designs, by the water side characteristics. The surfactant flows around the chiller in a surfactant cycle along with the refrigerant. The surfactant is soluble in the liquids, although the solubility in aqueous lithium bromide is quite low (on the order of 25 ppm). It is observed that the addition of surfactant additive, even on the order of 100 ppm, introduces a surface flow, which dramatically disrupts the absorption boundary layer and, thereby, enhances the absorption rate. A similar phenomenon is observed in condensation. Thus, the use of a surfactant reduces the size of absorber significantly and reduces the cost of the entire machine.

The enhancement role of the surfactant is well-known but the details of the mechanism have been obscured by many studies. Several published theories attribute the enhancement to interfacial convection (Marangoni convection) due to surface tension gradients. However, the cause of the surfactant surface concentration gradients was not well explained. Many studies focused on the presence of the surfactant in the liquid and largely ignored the presence of the surfactant in the vapor until a recent theory, called the vapor surfactant theory (Kulankara and Herold, 1999), proposed that the heat and mass transfer enhancement is due to Marangoni convection caused by surfactant which arrives at the surface primarily from the vapor along with the water being absorbed.

## 1.2 Objectives of This Study

The primary objective of the present study was designed to clarify enhancement mechanism of surfactant-induced augmentation of absorption and condensation and to

quantify the relationship between the enhancement and the key variables by experiment, with emphasis on flow visualization, and via simulation. A clear understanding of the way the surfactant reaches the surface, and how it induces Marangoni convection, was sought.

In order to achieve the objectives, four tasks were planned. These tasks are the measurement of surface tension with surfactant 2-ethyl-hexanol (2EH), determination of 2EH surface concentration, experimental study of Marangoni convection in a pool with absorption/condensation in the presence of surfactant 2EH, and modeling of Marangoni convection in the presence of surfactant vapor.

Surface tension plays a key role in the enhancement mechanism. A literature survey revealed considerable scatter in the data on the surface tension of aqueous LiBr with surfactants. According to the vapor surfactant theory, the surfactants in an absorption chiller are delivered to the surface from the vapor where they change the surfactant surface concentration and the surface tension. Therefore, in this study, the surface tension was measured with well-controlled surfactant concentration in the vapor. The drop volume method was applied with 2EH as the surfactant. Two series of surface tension measurements were conducted. The first was to quantify the effect of drop frequency on the measured surface tension. The second was to quantify the relation between surface tension and surfactant vapor concentration. Measurements of surface tension for both aqueous LiBr and water were conducted.

It is known that the presence of surfactant on the surface changes the surface tension and the surface tension is a function of the equilibrium surface excess concentration of surfactant (Rosen, 1989). A more complete understanding of Marangoni

convection and the enhancement mechanism in absorption/condensation requires knowledge of the surface concentration. Thus, the surface concentration for both aqueous LiBr and water were derived from equilibrium surface tension data based on a Gibbs adsorption analysis, and the relationship of surface concentration to the vapor concentration and surface tension was determined.

The Marangoni convection in a typical absorption system is a complicated surface flow on a falling film outside tubes cooled internally by cooling water. In order to study the effect of surfactant in the vapor on the Marangoni convection while avoiding the complexity of surfactant-driven unstructured flow seen in a falling film configuration, experiments were conducted in a simpler absorption/condensation pool with controlled surfactant vapor concentration and water vapor concentration. This simpler configuration provided a very effective geometry for understanding the enhancement mechanism. The transfer rates were quantified by recording pressure data for both absorption and condensation, and the flow patterns with different 2EH concentrations in the vapor for both absorption and condensation were observed and recorded on video. A numerical simulation of the surface motion in a similar configuration as the experiments was carried out. The simulation is based on a two-dimensional pool and the surfactant surface concentration was modeled using a one-dimensional surfactant mass balance at the interface. The simulation results are compared with the experimental results.

### 1.3 Dissertation Outline

The previous research, both experimental and theoretical, on the effect of surfactant on mass transfer enhancement is first reviewed in Chapter 2. The main

experimental and theoretical aspects of the current work are described in Chapters 3 to 6, which include the surface tension measurements, determination of the surface concentrations, experimental study of Marangoni convection in absorption/condensation and numerical study of condensation. In Chapter 7, a discussion of the results and observations from the experiments and numerical simulations is presented; the results are interpreted in the context of the vapor surfactant theory. Finally, conclusions and some proposals for future work are given in Chapter 8. In addition, a simulation code used in the current study and some related early stage work (i.e. a property routine for aqueous LiBr and water was developed) are included in appendices.

## CHAPTER 2

### SURVEY OF LITERATURE

In this chapter the most relevant previous work on the effect of surfactants on absorption and condensation enhancement are reviewed. The review of previous work is divided into four sections: 1) surface tension of aqueous lithium bromide (LiBr) with surfactants, 2) Marangoni convection in the presence of surfactants, 3) theories of surfactant enhancement, and 4) experimental and computational work in absorption and condensation enhancement in the presence of surfactants.

#### **2.1 Surface Tension of Aqueous LiBr with Surfactants**

Studies on enhancement of absorption of water vapor into aqueous LiBr in the presence of surfactants require information about the surface tension, since surface tension gradients at the liquid surface induce Marangoni convection which is the mechanism of enhancement.

Yao et al. (1991) measured surface tension of aqueous LiBr with surfactant 2-ethyl-hexanol (2EH) using a drop-volume apparatus. In their experiments, the 2EH was added to the solution by a micropipet, and the samples were homogenized in an ultrasonic bath. The authors found considerable difference as compared to previous data by Grosman and Naumov (1984), Kashiwagi et al. (1985), Hozawa et al. (1989) without clear explanations. None of these papers emphasized the effect of a key factor, the vapor side conditions, on the measurement results.

Hihara and Saito (1991) measured surface tension of LiBr solution with surfactant 2EH using a ring method. In the preparation of the samples, the surfactant 2EH was mixed with a certain amount of LiBr solution to obtain the required concentration of the surfactant. They found that on increasing the concentration of the surfactant, the surface tension decreased and reached a plateau value at a certain concentration which was interpreted as the solubility limit. The solubility limit of 2EH in 55% aqueous LiBr (by mass) was determined to be about 100 ppm. Based on these experiments, they concluded that the 2EH concentration in the LiBr solution is a main factor in determining the surface tension. However, in their experiments, the effect of vapor side conditions was not mentioned.

Kim et al. (1994) employed the Du Nouy ring method (a ring method using Du Nouy apparatus) to determine the surface tension of aqueous LiBr with surfactant 2EH. The 2EH was added into the solutions, which were then mixed by a magnetic stirrer and then left at room temperature for at least 48 hours. All preparations and measurements were at normal atmospheric pressure with surface exposed to air. The measurement results show that the surface tension in the presence of 2EH decreases as surfactant concentration increases, and increases as solution temperature increases. This is in contrast to the case without 2EH where the surface tension decreases with increasing solution temperature. The measured surface tension was found to be higher than the data from the drop volume method (Yao et al., 1991). The authors speculated that the measurement error could be traced to the Du Nouy ring method due to an additional volume detachment from the ring. The authors noticed that the values of surface tension varied with time, and proposed that a long time is required (48 hours in these

experiments) to allow the solution to reach equilibrium with the 2EH. But in the context of the Vapor Surfactant theory, this procedure would be expected to cause the 2EH concentration in the vapor to vary with time due to evaporation of 2EH, which would also explain the high values of surface tension found since after 48 hours, most of the surfactant had evaporated from the system.

Kim and Janule (1994) measured surface tension of aqueous LiBr with 2EH using the maximum bubble pressure method. 2EH was added to aqueous LiBr solutions and then solutions were mixed by a magnetic stirrer. The surface tension of aqueous LiBr at the different time was measured in order to obtain the dynamic surface tension (i.e., surface tension before the solution reaches its equilibrium condition). Their results showed that the surface tension decreased versus time and was proportional to  $1/t^{0.5}$  (where t is time), and the time required for the solution to reach its equilibrium values are dependent on the mass diffusivity of surfactant in the aqueous LiBr.

Gustafsson et al. (1996) measured the surface tension of aqueous LiBr with fluorinated alcohols as surfactants. The drop-volume method was employed and the effect of solution temperature and measuring time were tested. They found that for a given concentration of surfactant the solubility of the surfactant increases as the temperature increases, resulting in a lower surface excess and hence a higher surface tension. The authors also pointed out that because the equilibrium surface is not established as fast in highly concentrated electrolytes as compared to pure water, due to the lower diffusivity at the high salt concentration, measured surface tension values may depend on time.

Ishida and Mori (1996) measured the surface tension of aqueous LiBr with surfactant 1-octanol using a surface tensiometer utilizing laser-beam reflection, and they speculated that the disagreement with previous measured data might be due to inappropriate use of non-static measuring techniques.

Kulankara and Herold (2002) measured the surface tension of both aqueous LiBr and water with surfactant 2EH using a drop volume method. In order to achieve better accuracy in the surface tension measurement by this method, a correction factor recommended by Harkins (1952), which is a function of the drop tip and the volume of drop, was included in the calculation of surface tension. They realized that during the measurements the surface tension of aqueous LiBr was strongly affected by the presence of surfactant vapor around the liquid drop interface. They attributed the scatter in surface tension data in the literature to the sensitivity to the 2EH vapor environment but were not equipped to measure the 2EH vapor concentration in their surface tension measurements.

In summary, Figure 2.1 shows the surface tension data of aqueous LiBr with 2EH from the authors mentioned above and selected data from Grosman and Naumov (1981) and Ziukanov et al. (1984). The data in Figure 2.1 show considerable disagreement. One of the main motivations of the current work was to better explain this disagreement and to describe the steps needed to obtain meaningful surface tension data on such systems.

## 2.2 Marangoni Convection in the Presence of Surfactants

It has been known since 1960-70's (Bourne and Eisberg, 1966; Albertson et al., 1971, Chi et al., 1971 and Zawacki et al., 1973) that the addition of a trace amount of alcohol additives, such as 2EH, in an absorption refrigeration machine based on aqueous

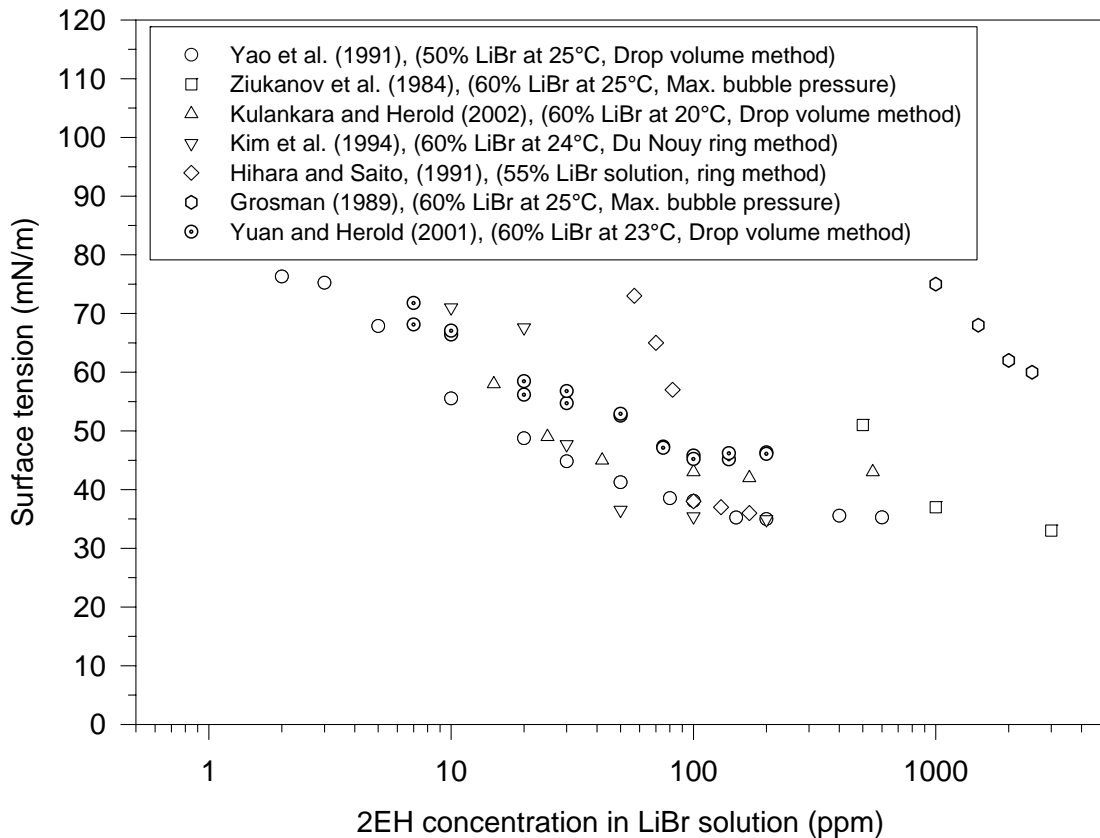


Figure 2.1 Surface tension of LiBr solution versus concentration of 2EH

LiBr produces a substantial increase in the heat and mass transfer rates. It is widely accepted that the improved absorption rates are due to the surfactant properties of the alcohol that causes Marangoni convection, a hydrodynamic instability at the liquid-vapor interface, arising from surface tension gradients. This instability enhances the mixing of the solution on the surface of heat transfer tubes and thereby improves the heat and mass transfer rates. This section summarizes prior experimental and theoretical studies on Marangoni convection in the presence of surfactants.

During the 1950-60's Marangoni convection was studied as a problem of hydrodynamic stability with diffusion and interfacial movement. The methods of linear stability theory were applied to determine the conditions for the onset of instability. Sternling and Scriven (1959) were apparently the first to analyze the stability of a disturbance caused by a concentration gradient of solution in addition to thermal instability. A conclusion for vapor-liquid systems was that an increase in surface tension due to mass transfer (i.e. causing a concentration gradient) might lead to instability.

Extensive studies on the basic mechanism of Marangoni convection in aqueous LiBr systems started in the mid-1980's. Kashiwagi (1988) did pioneering work on Marangoni convection including a number of experiments that implied the importance of vapor side effects. However, this work did not get much attention.

Ji et al. (1993, 1993b) performed a linear stability analysis for Marangoni convection during absorption of water vapor into LiBr solution with surfactant 1-octanol. In their model, it was assumed that the bulk concentration of a surfactant in the gas phase is initially zero and that surfactant is desorbed from the solution to the gas. Their numerical analysis predicted that Marangoni convection is triggered mainly by the absorption of water vapor when the surfactant causes a surface tension increase with increasing solution temperature. Their analysis also demonstrated that the absorption system is destabilized by desorption of the surfactant and stabilized by the adsorption of surfactant.

To identify the dominant factors in inducing Marangoni convection, Suzuki et al. (1996) carried out an experiment by using an ethanol-water binary mixture in an enclosed cell with an applied temperature difference across the cell. They concluded that the

combined concentration and temperature gradients at the surface gave rise to surface tension gradients, but concentration induced Marangoni convection dominates the surface motion, resulting in a surface flow in the opposite direction to the buoyancy-induced flow. This viewpoint, although very valid for ethanol-water, is not very useful for 2EH induced Marangoni convection due to the unique properties of this system.

Fujita and Hihara (1999) conducted an experiment in a thin liquid film of aqueous LiBr in the presence of surfactant n-octanol. In the experiment, temperature fluctuations on the vapor-liquid interface were measured using an infrared thermometer, and flow direction on the vapor-liquid interface was recorded. Contrary to Suzuki's prediction, their tests showed that the surface flow induced by the surface tension gradient took place from the area of low temperature toward that of high temperature. Therefore, they concluded that the Marangoni convection is mainly dominated by the temperature effect rather than the LiBr concentration effect because the surface tension increases with increasing solution temperature in the presence of surfactant (Kim et al, 1994). It should be pointed that the surfactant concentration gradients on the interface and vapor surfactant concentration were not considered in these studies. Since these factors are understood now (proposed by Kulankara and Herold (2000) and highlighted by Koenig and Grossman's study (2003)) to be the most important factors, a reinterpretation of the experiments in terms of these variables is needed.

Kim et al. (1996) conducted an experiment on water absorption into aqueous LiBr with surfactants and reported that Marangoni convection is initiated by the surface tension gradient caused by surfactant concentration and solution temperature as well as

LiBr concentration. Again, several of the main variables (surfactant vapor concentration) are not reported or described.

Koenig and Grossman (1999) numerically studied the Marangoni instability and found that in addition to the effect of solution temperature and solution concentration, for surfactants with high diffusion coefficient in the absorbent solution, surfactant concentration is highly variable along the interface, and its gradients affect surface tension in a way that reinforces the surface mixing, resulting in relatively significant absorption rate enhancement.

Kang et al. (1999) investigated Marangoni convection experimentally in aqueous LiBr with various surfactants including 2EH. The effects of LiBr concentration, the surfactant concentration and the solution temperature on the surface tension gradients were studied. They concluded that the temperature gradient of the surface tension ( $\partial\sigma/\partial T$ ) could not be the initial cause for inducement of Marangoni convection. They further concluded that the magnitude of the surface tension played an important role for inducement of Marangoni convection. The negative solution concentration gradient of the surface tension ( $\partial\sigma/\partial x_{\text{LiBr}}$  (with surfactant)  $< 0$ ) was found to be a trigger for inducement of Marangoni convection at surfactant concentration below the surfactant solubility limit, while the imbalance of the surface tension of aqueous LiBr solution and the interfacial tension between aqueous LiBr solution and surfactant is a trigger above the solubility limit. Vapor concentration of the surfactants was not considered an important variable in this work.

Kim and Lee (1999) carried out absorption experiments of water vapor into LiBr solution with eight-carbon alcohol surfactants using a simple static pool absorber. Sample

solutions containing surfactant was prepared prior to each experiment and was placed in an absorption chamber. Four surfactants (n-octanol, 2-octanol, 3-octanol and 2EH) and four different solution concentrations were investigated. They found that the surfactant concentration required for onset of mass transfer enhancement is dependent on the surfactants, and most are in the range of 5 to 8 ppm. There was no mention of vapor concentration of surfactant in this work.

Gustafsson (2000) presented a stability analysis for a vertical falling film system with aqueous LiBr solution and surfactant. The analysis showed that the rate of the surface tension decrease is more important than the surface tension value itself. The surfactant diffusivity appeared to be an important value for surface tension relaxation time and subsequently for the absorption rate. However, this analysis assumes that the surfactant arrives at the surface from the liquid side. The physics implied by the Vapor Surfactant theory implies that the stability considerations are much different from those included in this analysis.

Koening et al. (2003) numerically analyzed the role of surfactant adsorption rate in inducing Marangoni convection in LiBr-H<sub>2</sub>O solution with surfactant 2EH. They reported that in order to achieve Marangoni convection and absorption enhancement, an effective surfactant should reduce the surface tension of the solution quickly enough to cause Marangoni instability within a short absorption process period. Beutler et al., (1996) carried out experimental studies on a column of horizontal tubes, the strong solution of LiBr was sprayed onto the top tube and trickled down. The surfactants were added to the solution. Their heat transfer coefficient results have also shown that the lowering of static surface tension of absorbent solution itself is not a sufficient condition

for the occurrence of the Marangoni convection. The surface tension must be lowered, but the time required for lowering surface tension is critical in determining the ultimate success of a surfactant in enhancing absorption rates. However, these studies did not clearly address the vapor surfactant issues.

Kim et al. (1993) and Kulankara and Herold (2000) both conducted falling film absorption experiments on a single vertical tube. The surfactant 2EH with water vapor entered from the top of the absorber resulting in parallel flow with aqueous LiBr. Their observations confirmed that the intensity of the Marangoni convection decreased from the top to the bottom of the tube, possibly because the concentration of 2EH in the falling film increased along the tube and approached saturation near the bottom of the tube. These studies demonstrated vapor effects very clearly since the Marangoni convection was observed to start immediately upon introduction of the surfactant at a location remote to the absorbing surface where the only communication was via the vapor.

Kim et al. (2004a, 2004b) theoretically studied the effects of surfactant on the onset of Marangoni convection using the propagation theory. In their model, surfactant 2EH was assumed to pre-exist in the solution, and surfactant on the surface was assumed to be neither soluble in absorbent liquid nor volatile to gas phase when the absorbate transfers from the gas phase to the liquid phase, and surface tension is positively related to the concentration of solute (i.e.,  $\partial\sigma/\partial x_{LiBr} > 0$ ) and negatively related to the surface excess concentration of surfactant (i.e.,  $\partial\sigma/\partial \Gamma < 0$ ). They found that it is not always advantageous to increase the mass transfer coefficient in the gas phase to enhance the absorption rate and that there is an optimum mass transfer condition in the gas phase to affect Marangoni instability at the surface and produce the maximum absorption rate. The

surface properties of the surfactant (surfactant surface excess concentration and adsorption) were thought to be more significant than that of the solute (i.e., diffusivity) to analyze Marangoni instability. A higher surface excess concentration of surfactant acts as a stabilizer while a higher diffusivity of surfactant from the surface acts as a destabilizer for the onset of Marangoni convection. This work did not address the vapor concentration of surfactant.

Studies of Marangoni convection have also been reported by several investigators in the case of condensation and in systems other than water and aqueous LiBr. Hijikata et al. (1994) theoretically and experimentally studied the droplet growth mechanism in condensation in a water-ethanol binary mixture. In their theoretical work, instability analysis was used to determine a transition from the film wise condensation to pseudo-dropwise condensation. Both surface tension itself and the surface tension change due to the change in temperature and concentration were considered. Their results show that the Marangoni effect plays a more important role than the absolute value of the surface tension. The change of condensation type from film wise to pseudo-drop wise is only realized when the temperature dependency of the surface tension becomes positive.

Morrison and Deans (1997) reported enhancements in the condensation of steam in the presence of a low ammonia concentration due to significant disturbance in the condensate film that authors attributed to Marangoni convection. Further studies by Morrison et al. (1998) on the condensation of steam in the presence of methylamine also showed enhanced non-film wise condensation.

Kang et al. (1999b) observed Marangoni convection inducement in NH<sub>3</sub>-H<sub>2</sub>O system and concluded that the concentration and temperature gradients of the surface

tension should not be a criterion for Marangoni convection inducement in NH<sub>3</sub>-H<sub>2</sub>O system. The magnitude of the surface tension did not affect the occurrence of Marangoni convection. They proposed that because of stronger hydration force between water molecules and electrolyte ions NH<sub>4</sub><sup>+</sup> and OH<sup>-</sup>, surfactant is segregated from the bulk solution (authors called it “salting-out”) leading to a significant reduction of the surface tension. This was viewed as a key criterion for Marangoni convection inducement at the concentration below solubility limit in NH<sub>3</sub>-H<sub>2</sub>O system.

Kang and Kashiwagi (2002) conducted an experiment in an ammonia-water absorption pool to visualize Marangoni convection in the presence of surfactant, n-octanol, in the pool. They reported that Marangoni convection was observed near the interface only in the cases with surfactant, and that the Marangoni convection was very strong just after absorption started and weakened as time elapsed.

### 2.3 Published Surfactant Enhancement Theories

As mentioned in the Introduction, a small amount of certain surfactants causes interfacial convection (Marangoni convection) leading to higher heat and mass transfer performance in both condensation and absorption in absorption chillers. The basic mechanism of Marangoni convection in aqueous LiBr has been extensively investigated for decades. This section summarizes the published surfactant enhancement theories.

Regarding enhancement theories by surfactants, most papers attribute the enhancement to Marangoni convection due to surface tension gradients, which result from surfactant concentration gradients on the surface. However, the explanations for what causes the surfactant concentration gradients are divergent.

Kashiwagi et al. (1985, 1988) suggested that Marangoni convection is induced by the unbalance of surface tension around droplets of the surfactant floating on the solution surface. They proposed that the existence of surfactant droplets at the surface of the absorbent solution is necessary to obtain a drastic absorption enhancement. According to this theory, the onset of interfacial turbulence requires excess surfactant beyond the solubility limit. However, Elkassabgi and Perez-Blanco (1991), Perez-Blanco and Sheehan's (1995) as well as work in our group show that the enhancement does not require surfactant droplets. Thus, other theories were sought to explain a wider range of the observed phenomena.

Hozawa et al. (1991) and Kim et al. (1993, 1996) reported that the presence of an island of surfactant is not a necessary condition to initiate Marangoni convection, but it can provide and maintain more violent convection for a longer time by acting as a reservoir of surfactant on the surface. Hozawa et al. (1991), Pearson (1958) and Daiguji et al. (1997) proposed the so-called “salting-out” theory. This theory holds that an increase in the concentration of aqueous LiBr causes a rejection of surfactant molecules from the liquid bulk, because the hydration force between water molecules and electrolyte ions,  $\text{Li}^+$  and  $\text{Br}^-$ , is larger than the bonding force between water molecules and surfactants molecules. As a result, the surfactant molecules are segregated from the bulk solution and move to the surface and cause a decrease of surface tension. This theory proposed that the salting-out effect is the initial cause of Marangoni convection. The data from Saito (1991), Hoffmann et al. (1996) and Beutler et al. (1996) were interpreted to support this theory. However, Daiguji et al. (1997) also pointed out that it was difficult to explain the Marangoni instability only by the salting-out effect in the

cases where the departure from equilibrium is large or the concentration of surfactant exceeds the solubility limit.

Kang et al. (1999) compared the Kashiwagi model (1985, 1988) with the salting-out model (Hozawa et al., 1991) and concluded that the salting-out effect is a trigger for the induction of Marangoni convection at the concentration below the surfactant solubility while the imbalance of the surface tension of the solution and interfacial tension between the solution and surfactant is a trigger inducing Marangoni convection above the solubility limit.

The mechanism of enhancement by surfactants was also the subject of intense study in our group where a new theory was introduced to explain surfactant enhancement. This new theory, called the Vapor Surfactant theory, was proposed by Kulankara and Herold (2000, 2002). This theory maintains that the surfactant circulates through the machine and arrives at the liquid surfaces by bulk flow along with water vapor. Previous theories emphasized the presence of the surfactant in the liquid phase. The major departure provided by the Vapor Surfactant theory is the emphasis on the presence of the surfactant in the vapor phase. The surfactant arrives at the liquid surface along with the absorbing vapor by bulk flow, not by diffusion. The action of the surfactant occurs on the surface of the liquid in the form of Marangoni convection that continuously renews the surface layer, sweeping away the dilute layer and exposing the high-affinity concentrated liquid. For aqueous LiBr at high concentration, once the surfactant reaches the surface, it tends to stay on the surface due to its strong affinity for the surface. The presence of the surfactant on the surface disrupts the bonding between water molecules and thus reduces the surface tension. Based on this theory, an effective surfactant should have several

properties that enable a surfactant cycle. These include solubility in water that enables transport from condenser to evaporator and sufficient vapor pressure in addition to the surfactant properties. The authors have verified this theory in their absorption, condensation, static pool and surface tension measurements. Further experimental and numerical studies from our group on surface tension measurements (Yuan and Herold, 2001), enhancement of absorption by 2EH in an absorption machine (Ghosh and Herold, 2002), surface tension driven flow due to condensation with a vapor surfactant (Qiao et al., 2000) and study of phase distribution of surfactant (Zhou and Herold, 2002) strongly support this theory.

Regarding other theories, one called the steric hindrance or catalytic effect theory holds that the surfactant provides a lower energy path for the absorption of water by lithium ions. Since branched surfactants have a weaker bond than straight chain surfactants in combining with lithium ions, the branched surfactants should be more effective and faster in forming Li-H<sub>2</sub>O bonds. Therefore, it is also not necessary for the surfactant to exist in a separate liquid phase for the enhancement to occur. Indeed, Chandler's experiment (1993) found an enhancement at small surfactant concentrations that are below the solubility limit. However, Perez-Blanco and Sheehan's data (1995) conflict with this theory. A constant enhancement in their experiments was not expected from steric hindrance theory, since as the hydration limit is approached, the surfactant effectiveness should decrease. Based on their experiment, both branched and straight chain surfactants provide effective enhancement, and relatively constant enhancement was observed with brine concentration.

Hihara and Saito (1993) proposed an instability theory that relates the surface tension change to the properties of solution with surfactants. They concluded that surface tension changes with temperature and LiBr mass fraction are the key variables to predict enhancement. The data from Jao et al. (1991) and Kim et al. (1994) showed that the enhancement was related to the property of  $\partial\sigma/\partial T > 0$  for LiBr solution with surfactants and this seemed to support their theory.

Sheehan and Perez-Blanco (1996) proposed an explanation of enhancement, called the diffusion theory where the time taken for the diffusion of the surfactant to the liquid-vapor interface is considered as a key factor. According to this theory, the ability of a surfactant to enhance mass transfer may be related not so much to its activity at the interface, but to its ability to diffuse and adsorb at the interface. This theory seemed to be supported by the fact that surfactants are more effective when presented in the vapor phase, rather than in the liquid (Bennett, 1995; Kulankara and Herold, 1999). Although vapor effects are mentioned in this paper, the main focus of the paper is on liquid side effects. Koenig and Grossman (2003) also proposed a similar mechanism of enhancement by surfactant and stated that an effective surfactant must not only reduce the surface tension of the solution; it must do so quickly enough to cause the Marangoni instability within the short absorption process time. The effect of the absorption process on the surface tension relaxation rate is mainly influenced by initial solution concentration and temperature, cooling side heat flux and vapor phase pressure. A key difference between these theories and the Vapor Surfactant theory is that the Vapor Surfactant theory holds that the surfactant arrives at the surface primarily by bulk flow and not by diffusion.

## **2.4 Absorption and Condensation Enhancement by Surfactants**

The Vapor Surfactant theory leads to the realization of the importance of two variables that are seldom reported in studies on enhancement. These are the concentration of the surfactant in the vapor and the absorption flux, which can be reported as either mass or heat flux. In the current literature review, there was mention of vapor concentration in only a few studies but many studies reported flux values and these are emphasized in the review.

A substantial body of work exists on absorption enhancement with surfactants in LiBr/water systems (both in falling film and static pool absorption). In contrast, the work on condensation enhancement using surfactants is limited to a few papers. In this section, previous work on absorption and condensation enhancement with surfactants is surveyed.

Vliet and Cosenza (1990, 1991) investigated the effects of surfactants on water vapor absorption into aqueous LiBr flowing over a smooth horizontal tubular surface using surfactant 2EH at 500 ppm. In their tests, they struggled with air leakage (a common problem in such systems) and carefully documented the presence of less than 0.1% air in their system. The results showed that heat flux was augmented to about 45  $\text{kW/m}^2$  which has a nominal three-fold improvement in absorption rate compared to the case without the surfactant. The authors related this enhancement to the presence of totally de-structured film flows described as “ropey” with “rivulets” moving back and forth laterally along the tubes.

Hihara and Saito (1991) conducted falling film absorption experiments on an inclined plate with surfactant 2EH (60 ppm) added into the LiBr solution. The results

show that the absorption heat flux is about  $120 \text{ kW/m}^2$ , an increase about 5 times as compared the case without surfactant. They observed that this enhancement was accompanied by active surface-disturbances and an improvement in wetting of the heat transfer area. In comparison, when the surfactant was not added, the surface of the liquid solution was smooth, and free of waves.

Kim et al. (1996) conducted a vertical falling film experiment on absorption into aqueous LiBr with 2EH. A turbulent coolant flow rate was selected to greatly reduce the heat-transfer resistance on the cooling water side. Their results showed that the absorption heat flux in the presence of 2EH (50 ppm in the liquid) is about  $7.8 \text{ kW/m}^2$ , an increase of 72% in the absorption heat flux as compared to the case without 2EH. A “vigorous mixing” was observed in their experiments. They also reported that the heat transfer coefficient appeared to reach a plateau after the surfactant concentration reached 50 ppm.

Hoffmann et al. (1996) studied the combined effect of surfactants (1-octanol and 2EH) and an enhanced tube surface on the absorption of water vapor into aqueous LiBr in a horizontal-tube falling film absorber. They found that the rivulet flows were most distinct in the region with strongest absorption, and surfactants provided more enhancement than the enhanced tube surface and an increase of 60-140% in heat transfer coefficient was achieved in the case with surfactant as compared to the case without surfactant. For this study, the mass and heat flux cannot be estimated due to a lack of data about the heat transfer area.

Park et al. (2004) conducted experiments on an absorber consisting of 24 horizontal tubes in a column to investigate the effect of surfactant on the absorption

performance. The working fluid is H<sub>2</sub>O/LiBr solution with various inlet concentrations of LiBr. Surfactant 1-octanol is used with the concentration of 400 ppm in the liquid. It was found that the absorption heat flux with surfactant is about 12.7 kW/ m<sup>2</sup> representing an enhancement of 3.8 times that without surfactant.

Jung et al. (1994) conducted their experiments in a falling film mini-absorber to study the effect of four different surfactants (1-heptanol, 1-octanol, 3-octanol and 2EH) on the absorption of water in aqueous LiBr (58.5% by mass). Based on their experiments, 1-heptanol gave the highest absorption enhancement of 24%. The absorption heat flux was about 1.6 kW/ m<sup>2</sup>. 2EH was second with an enhancement of 20%. The low enhancement values reported here are consistent with the low heat flux values.

Kashiwagi et al. (1993) conducted experiments on absorption with 1-octanol. In their experiments, surfactant 1-octanol was boiled into the vapor space. Surfactant vapor concentration was set at 100 ppm by boiling a certain amount of water and surfactant in a flask-type boiler. The enhancement effects caused by vapor 1-octanol surfactant were studied. Based on their results, the mass flux for the case with 100 ppm 1-octanol in the liquid is almost the same as the one for the case with 100 ppm 1-octanol in the vapor. The maximum mass flux occurred when 1-octanol was added to both liquid and vapor. For this case, the absorbed mass flux was about 1.8 g/m<sup>2</sup>·s, corresponding to heat flux of 4.4 kW/m<sup>2</sup>, 26% higher than without 1-octanol. The authors attributed this enhancement to the formation of 1-octanol droplets on the surface of the solution. The flow with both 1-octanol in liquid and vapor phases showed complicated interference fringes compared with the case without 1-octanol.

Kulankara and Herold (1999) conducted absorption experiments of water vapor into aqueous LiBr on a vertical falling film facility using 2EH. The results showed an increase of 29% in the heat transfer coefficient when the concentration of surfactant increased from 15 to 85 ppm in the liquid. The heat transfer coefficient also increased about 30% with increases in heat flux from 10.5 to 20.5 kW/m<sup>2</sup>. Vigorous and unstructured motions were observed in their experiments. These experiments clearly show the importance of heat flux and were the basis of the Vapor Surfactant theory of absorption enhancement.

Ghosh and Herold (2002) investigated the enhancement by surfactant 2EH in an absorption machine. Based on their experiments, they deduced that enhancement by 2EH occurred in both the absorber and condenser. Furthermore, it was concluded that the surfactant flowed around the machine in a cycle.

Glebov and Setterwall (2002) investigated the influence of surfactant 2-methyl-1-pentanol (2MP) on the performance of an absorption chiller experimentally in their two experimental series. In one experimental series, the surfactant was injected into LiBr liquid; in the second experiments, the surfactant was injected into the refrigerant sump located in the evaporator. They found that the enhancement ratio was up to 20% for the first experiment and 32% for the second experiment. They concluded that the presence of the surfactant in the vapor phase, even in very small amounts, favors the enhancement more than the surfactant in the liquid solution.

An absorption enhancement experiment was also performed by Setterwall et al. (1991) in a static pool. The absorption rates were increased from 6% to 30% depending on the surfactants, the concentration of surfactants and the solution temperature.

Kim et al. (1999) conducted experiments on absorption of water into LiBr solution with surfactant 2EH using a simple stagnant pool apparatus. Sample solution containing a desired amount of surfactant was prepared prior to each experiment. A vigorous interfacial turbulence was observed during absorption with surfactants. The water vapor absorption rate increased with increasing surfactant concentration up to about 200 ppm in the liquid in their experiments. The maximum absorption heat flux was about  $2.4 \text{ kW/m}^2$  (absorption mass flux was about  $1 \text{ g/m}^2\cdot\text{s}$ ), in which mass transfer rate with 2EH was found to be about four times higher than that without the surfactant. The surfactant concentration for onset of mass transfer enhancement was in the range 5 to 8 ppm.

Tests of heat transfer coefficients in an actual LiBr absorption chiller were performed by Grosman and Naumov (1991). In their tests, 2EH was used and the increase of the overall heat transfer coefficients for absorber, condenser, generator and evaporator were found to be 90.2%, 32.2%, 0% and 0%, respectively.

Very little work was found that relates directly to condensation enhancement with surfactants. The physics of binary condensation bears some resemblance although the use of surfactants typically involves only trace amounts of the second species. The literature related to condensation enhancement is discussed next.

An early work conducted by Mirkovich and Missen (1961) observed streak and dropwise condensation of binary vapors. The nature of the condensation was found to be related to the type of binary vapors, the concentration of components and the sub-cooling temperature. Goto and Fujii (1982) presented a comparison of heat transfer coefficients between experiment and theory using an R114-R11 mixture. Their theoretical analysis

was based on the two-phase boundary layer equation. Their experimental data with a smooth film was consistent with the theoretical analysis. However, the experimental data with ringwise or turbulent ringwise films showed the heat flux of  $10 \text{ kW/m}^2$  and condensation rates 50% higher than the value from the analysis. The authors attributed the increase to the turbulent motion due to interfacial convection.

Morrison and Deans (1996) conducted water condensation experiments with small amounts of ammonia. They found that heat flux increased from  $132 \text{ kW/m}^2$  to  $179 \text{ kW/m}^2$  and heat transfer coefficient was enhanced about 13% with an ammonia concentration in the vapor from 0.23 to 0.88% by mass. They also found that no further enhancement happened with continued increase in ammonia concentration. Morrison et al. (1997) also carried out steam condensation experiments with methylamine as surfactant. Based on their experimental results, when the vapor mass fraction of methylamine is 0.03%, the heat flux was about  $192 \text{ kW/m}^2$  and the heat transfer coefficients were enhanced 20-50% over the heat transfer coefficient of pure steam at the same conditions. The highest heat transfer coefficient was found at a mass fraction of methylamine of 0.2%, and at larger mass fraction values the heat transfer coefficient decreased, apparently due to vapor diffusion resistance. “Pseudo-dropwise” and “rippled band” condensation patterns were observed.

Utaka and Terachi (1995) conducted experiments on the condensation of steam with small amounts of ethanol on horizontal tubes. They investigated the relation between heat transfer coefficient and the surface sub-cooling temperature difference  $\Delta T$  ( $=T_{\text{sat}} - T_{\text{wall}}$ ) with 0.17-0.74% ethanol by mass. They found that the heat transfer coefficient at  $\Delta T = 20-25 \text{ K}$  is five times as much as the heat transfer coefficient for pure

steam. In a more recent work, Utaka (1998) used a high-speed digital camera to observe the relation between the heat transfer coefficient and the flow characteristics. He found that with an increase of ethanol concentration and sub-cooling  $\Delta T$ , the size of condensing drops and the distance between drops reduced and the film between drops became thinner, with a corresponding increase in heat transfer coefficient.

# CHAPTER 3

## SURFACE TENSION MEASUREMENT WITH SURFACTANT 2-ETHYL-HEXANOL

### 3.1 Introduction

Heat and mass transfer enhancement in a lithium bromide (LiBr) based absorption chiller can be achieved by adding trace amounts of a surfactant like 2-ethyl-hexanol (2EH). In order to fully understand this enhancement mechanism, accurate surface tension data are needed.

Surface tension data are available for pure water (Haar et al. 1984) and pure LiBr solution (Foote Mineral Co. 1995). Surface tension data for aqueous LiBr with 2EH have also been reported but the inconsistency and scatter of the data is significant (Yao et al, 1991; Hihara and Saito, 1991; Kim and Berman, 1994; Kulankara and Herold, 1999). The poor agreement is believed to be due to the fact that some key variables were not controlled during the measurements.

A new explanation of the surfactant physics called the Vapor Surfactant theory (Kulankara and Herold, 1999) was recently published, which explains how the surfactant reaches the interface in an absorption machine. According to this theory, surfactant molecules are delivered to the liquid surface mainly from the vapor by bulk flow along with the absorbing water vapor. A non-uniform surface concentration of surfactant results from non-uniform absorption flux. Based on this theory, the surfactant concentration in

the vapor has a strong influence on surface tension and any measurement method that does not control this variable is not expected to yield reproducible data.

The work presented in this chapter is focused on surface tension measurements with well-controlled surfactant concentration in the vapor. The drop volume method is applied with 2EH as the surfactant. The main experiment is arranged such that air mixes with 2EH vapor and flows over the sample drops in the test chamber and delivers 2EH to the surface of the drops in a controlled manner. The 2EH adsorbs on the surface of the drops causing significant reduction of the surface tension. Two primary series of surface tension measurements were conducted. One was to observe the effect of drop frequency on the measured surface tension with the objective of establishing an appropriate drop frequency to obtain accurate surface tension data. The other was to measure the effect of surfactant vapor concentration on surface tension. Measurements of surface tension for both aqueous LiBr solution (60% by mass) and pure water were conducted. In addition, a series was run to find the difference between cases with 2EH in the vapor versus 2EH in the liquid.

### 3.2 Description of the Measurement Method

The drop volume method (also called the drop weight method) was used to measure surface tension (Becher, 1965). This method is based on a force balance on drops as they separate from a small diameter tube as shown in Figure 3.1. The weight of the drop is assumed to be balanced by the surface tension as

$$mg = 2\pi r\sigma \quad 3.1$$

where  $m$  is the mass of one drop,  $g$  is the gravitational acceleration,  $r$  is the

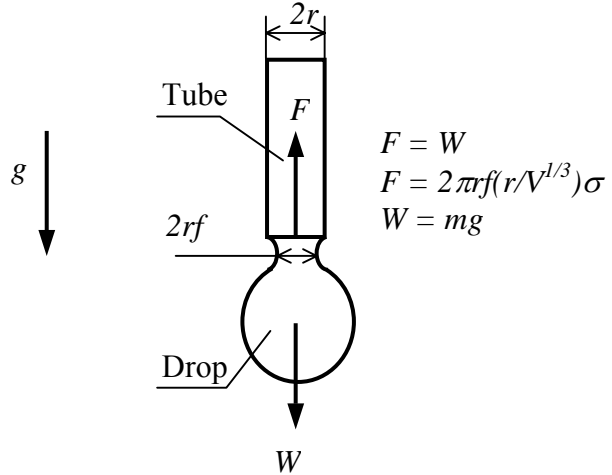


Figure 3.1 Schematic of force balance for a drop on the tip of the surface tension measurement apparatus

outside radius of the tip and  $\sigma$  is the surface tension of the liquid. However, it has been found that a small portion of the drop remains on the tip and causes an error in the calculated surface tension. Therefore, a modification factor  $f(r/V^{1/3})$ , introduced by Harkins (1952), is used to correct for this effect to achieve better accuracy. This modification factor is a function of the outside radius of the tip,  $r$ , and the volume of a drop,  $V$ . With the modification factor, the surface tension can be expressed as

$$\sigma = \frac{mg}{2\pi r f\left(\frac{r}{V^{1/3}}\right)} \quad 3.2$$

### 3.2.1 Measurement Apparatus

A facility was built to measure surface tension with well-controlled surfactant concentration in the vapor. A schematic and photograph of this facility are shown in Figures 3.2 and 3.3, respectively. The facility consists of a test chamber, drop creator, collection flask, balance, surfactant flask, heating mantle and rotameter.

The test chamber is made of transparent plastic pipe with an inside diameter of 0.1 m. The drop creator is made from a stainless tube whose outside diameter is 1.59 mm, a valve, a connecting tube and a large cross-section reservoir. The valve was modified to include a large handle to allow fine control of the flow. The major factors that affect drop frequency were found to be surfactant vapor concentration and liquid level. Due to the large surface area of the reservoir, the level in the reservoir does not change significantly during a test run so that the drop frequency is constant if the surfactant concentration in air remains constant. During the measurements, the solution is poured into the reservoir and then it flows by gravity to form the drops at the tip. The drops fall into a collection vessel that is positioned below the tip. To determine the average weight of a drop, 10 drops are collected in the collection vessel for each operating condition and the collection vessel is weighed using a high accuracy balance before and after collecting the drops.

Surfactant (2EH) vapor in the chamber is supplied by boiling the surfactant in a flask equipped with a heating mantle. The flow rate of surfactant vapor is controlled by varying the heat input to the surfactant boiler. The facility is connected to an air supply such that the surfactant vapor is mixed with a known flow rate of air flowing into the test chamber. The system was operated under steady state conditions with constant heat input to the surfactant boiler implying a constant surfactant vapor concentration flowing through the test chamber.

Turbulent flow upstream of the test section effectively mixes the air and 2EH vapor. The turbulent time scale for mixing in the channel was calculated (Tennekes and Lumley, 1982) to be 0.2 s while the time required for the air to flow from the 2EH injection port to the test section is 2.5 s. Therefore, it is concluded that the 2EH is

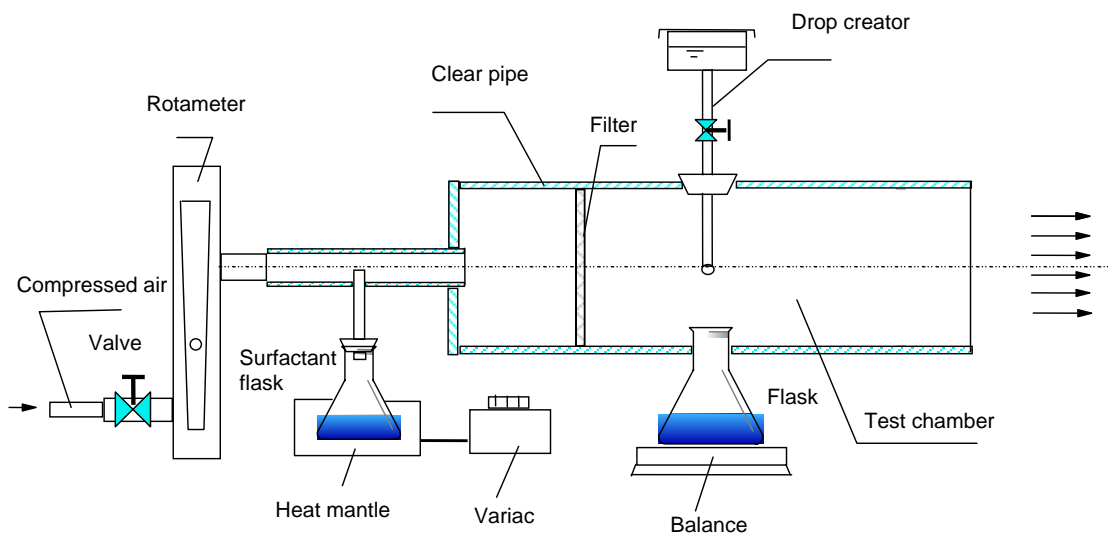


Figure 3.2 Schematic of the surface tension facility

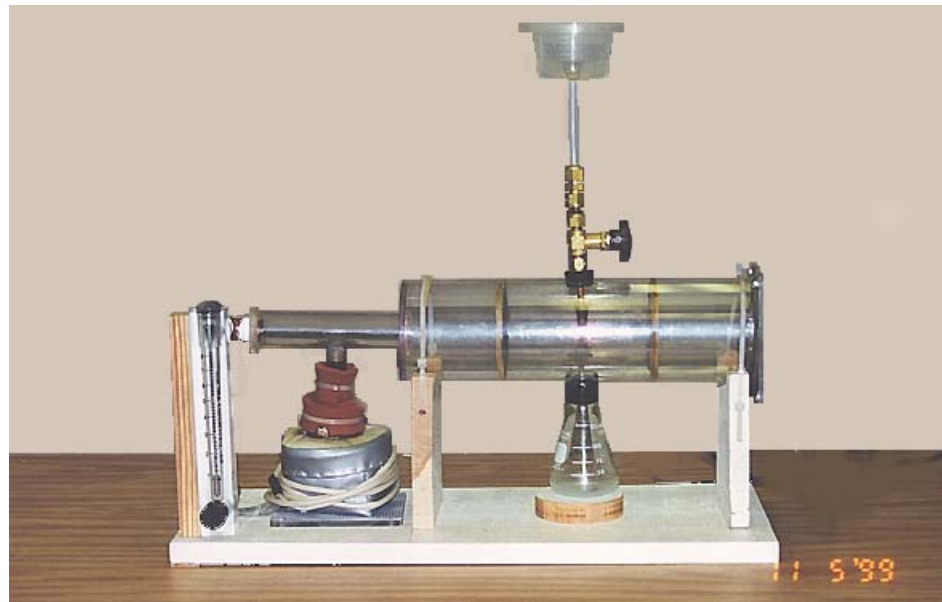


Figure 3.3 The surface tension facility

uniformly mixed with air before reaching the test section. It was also observed that under certain conditions the 2EH produced fog and the jet entering the test section was observed to expand and fill the test section, apparently due to residual turbulent eddies. Based on these observations, it is concluded that the vapor velocity in the test section is well characterized by the average velocity. The average velocity of the air in the test section was 0.06 m/s. This low value was chosen so that it would have negligible effect on the drop creation process while dependably establishing the vapor environment around the forming drops. Tests were done with and without air flow and it was found that the air flow did not have any detectable influence on drop frequency.

### **3.2.2 Preparation of the Liquid Samples**

Surface tension measurements were made on both water and 60% aqueous LiBr. In the measurements on pure water, distilled water was used. In the measurements on aqueous LiBr solution, 53% stock solution was first concentrated to above the target by boiling and then 60% LiBr solution was made by dilution with distilled water.

In order to find the mass fraction of aqueous LiBr, the temperature and density of the sample solution were measured and then a LiBr property routine (Yuan and Herold, 1998) was used to infer the mass fraction. Besides giving the mass fraction of aqueous LiBr, this routine is also used to calculate other thermodynamic and transport properties of aqueous LiBr and water used during the data processing. This routine was written by the author and is described in Appendices D and E.

To measure the surface tension with 2EH in the liquid, the sample liquid was made by mixing the liquid and 2EH in a clean mixing vessel. Then this vessel was shaken

vigorously until the liquid appeared uniformly milky before transferring the sample liquid to the reservoir which feeds the drop creator.

### **3.2.3 Experimental Procedure**

After transferring the sample liquid to the reservoir, the air flow rate was adjusted to the proper value and the power to the surfactant flask was turned on and variac was adjusted. The drop frequency was adjusted and the drops of liquid sample were collected in a collection vessel. The weight of a certain number of drops is the primary measurement.

Before conducting each test series, the surface tension of the surfactant free liquid (either distilled water or LiBr solution) was measured with only air flowing through the facility. The results were compared with literature data to establish a baseline. Such tests yield a probable error of  $\pm 1.43 \text{ mN/m}$  as discussed later in Section 3.2.6. For the cases with surfactant in the liquid sample, the drop creator was disassembled and cleaned thoroughly using warm water and detergent between runs. Vapor concentration of 2EH for a series of runs was varied from low to high values.

### **3.2.4 The Effect of Air Velocity**

The facility was designed to provide a slow flow (the Reynolds number based on the drop diameter is on the range of 10 to 100) sweeping past the drops with known surfactant concentration in the air. One possible source of error in this design is evaporation of water from the droplet that would be expected to cause a decrease in

temperature. The rate of evaporation would depend on the humidity in the air and in this study the humidity was not measured. A comparison between the present surface tension data and the literature data for the pure liquids seems to show that this effect was minor. The effect of air velocity was checked for pure water, with and without 2EH in the air and the results are shown in Figure 3.4. The drop frequency was held constant at 0.033 Hz and the mean temperature of the system was 22°C. For the case without 2EH in the air, the surface tension increased by less than 1% when the air velocity increased from 0 to 0.18 m/s. For the case with 2EH in the air (37 ppm), the surface tension decreased by 8.3% as the air velocity increased from 0.06 to 0.18 m/s. The small reduction in surface tension is apparently due to the presence of 2EH and is thought to be due to enhanced convective transport of 2EH to the droplet surface at higher velocity. For subsequent measurements, the velocity was fixed at 0.06 m/s as the minimum controllable velocity in our facility.

### **3.2.5 Determination of the Vapor Concentration**

The concentration of 2EH in the air is determined by the ratio of the mass flow rates of the 2EH and the air injected into the chamber. The air flow rate is measured by a rotameter with a full scale reading of  $2.36 \times 10^{-3}$  m<sup>3</sup>/s and an estimated accuracy of  $\pm 4.72 \times 10^{-5}$  m<sup>3</sup>/s. The density of air is calculated from temperature and pressure using the ideal gas law. The flow rate of 2EH is determined by weighing the surfactant flask before and after a measurement run and assuming steady state conditions during the interval. Air

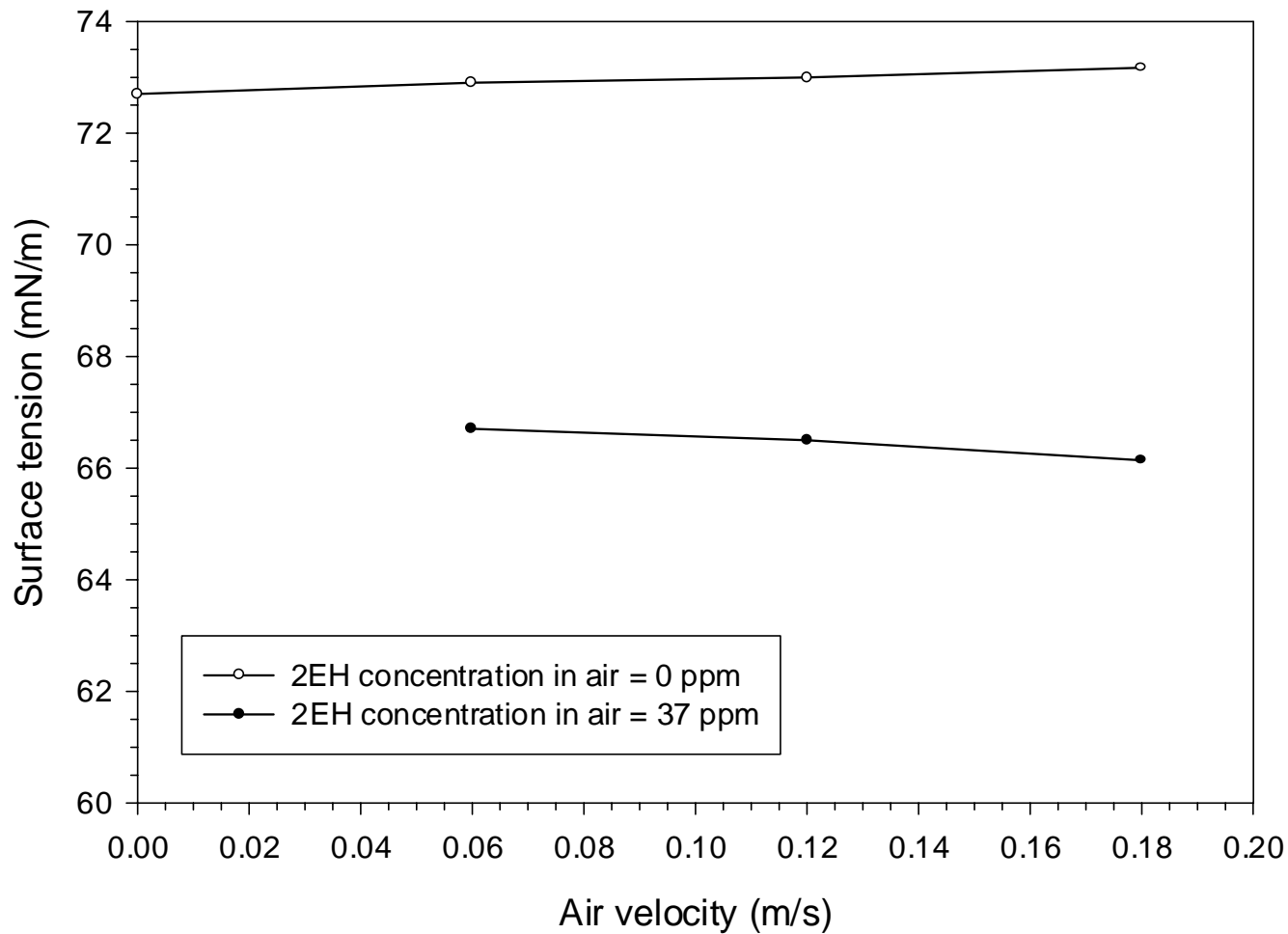


Figure 3.4 The effect of air velocity on surface tension

enters the surfactant flask as it cools down from boiling temperature of 2EH (184°C) to room temperature during the weighing process. To minimize errors from this, the time taken in weighing the surfactant flask was kept as short as possible. In addition, the lowest reading from the balance was taken (the reading increases as the temperature of the flask decreases). Several measurements at a single operating condition were checked and the probable error of the vapor concentration measurement was estimated to be  $\pm 5.4\%$ .

### **3.2.6 Examination of Measurement Accuracy**

Typical results for both distilled water and 60% LiBr solution are listed in Table 3.1 along with literature data. The drop frequency used for the tests from the current study listed in this table was 0.033 Hz. Based on comparison with literature data, the probable error for surface tension is  $\pm 0.18$  mN/m for water and  $\pm 0.28$  mN/m for 60% aqueous LiBr. In addition, the effect of the change of temperature was also examined. During the series of measurements, room temperature varied between 21.6 and 28.5 °C. Based on the water data by Haar et al. (1984) and the aqueous LiBr data from Foote Mineral Co. (1995), this temperature variation would cause a maximum change in surface tension of approximately 1.1 mN/m for pure water and 1.4 mN/m for 60% aqueous LiBr. Based on all of these effects, it is estimated that the probable error for the surface tension measurement is  $\pm 1.4$  mN/m.

Table 3.1 Examination of measurement accuracy

Sample	Tempera-ture (°C)	Number of measure-ments	Surface tension (Range of values, mN/m) (Current study)	Surface Tension (Average) (mN/m) (Current study)	Surface Tension (mN/m) (Literature)
Water	23.5±1.9	5	72.3 ~ 72.9	72.5	72.2 <sup>(1)</sup>
60% LiBr solution	25.4±0.2	6	93.8 ~ 94.8	94.5	96.0 <sup>(2)</sup> 91.2 <sup>(3)</sup>

(1) Haar et al. (1984)

(2) Kulankara (1999)

(3) Foote Mineral Company technical data, Bulletin 145 (1995)

### 3.3 Surface Tension Measurement Results

#### 3.3.1 Surface Tension Results for Water

##### 3.3.1.1 Surface tension of water with 2-ethyl-hexanol in air

In this series of measurements, the liquid water charged into the drop creator was free of 2EH. Figure 3.5 shows the surface tension of water versus drop frequency and 2EH concentration in air. It can be seen that the surface tension decreases significantly as drop frequency decreases. Because of the limitations on our ability to control the drop frequency, the lowest drop frequency used in our measurement is around 0.03 Hz.

Surface tension measurements at low frequency yield accurate results using the Harkin correction factor (Harkin, 1952) to account for the portion of drop remaining on the tip. At higher frequency, a dynamic error has been identified which is apparently due to the additional liquid flowing out of the drop creator during the process of drop off (necking) (Scheele and Meister, 1968). Based on their model, this necking effect at a drop frequency of 1 Hz causes an increase of 5.8 mN/m over the surface tension at very low frequency which is consistent with our experimental results (5.3 mN/m increase from 0.03 to 1 Hz as shown in Figure 3.5), and at drop frequency of 0.1 Hz, the increase of

surface tension is about 1 mN/m. Therefore, at low drop frequency the necking effect diminishes. Further surface tension measurements were conducted with drop frequencies between 0.05 and 0.033 Hz to minimize such dynamic errors.

Figure 3.6 is a plot of surface tension versus 2EH concentration in air at a drop frequency of 0.04 Hz. The solid curve was computed by the least squares method and the resulting function is shown on the plot. The surface tension decreases with an increase in 2EH concentration in air until it reaches a plateau.

The plateau surface tension is 39 mN/m which is approached within 1% by 1000 ppm. This minimum value of surface tension is in good agreement with the data given by Kulankara and Herold (1999) who measured equilibrium surface tension as low as 38 mN/m using a different experimental configuration.

### **3.3.1.2 Surface tension of water with 2-ethyl-hexanol in the liquid sample**

Surface tension measurements with 2EH in the liquid sample were also conducted. The surfactant was well mixed with water in a mixing vessel prior to transfer to the reservoir for the drop creator. For this series of tests there was no 2EH in the air flowing past the droplets.

Figure 3.7 is a plot of surface tension versus drop frequency with 2EH concentration in the liquid as a parameter. The data are plotted versus the system concentration. It should be pointed out that because of the tendency of 2EH to adsorb on surfaces, the 2EH concentration in the liquid passing through the drop creator is expected to be lower than the 2EH concentration charged in the reservoir. Because the

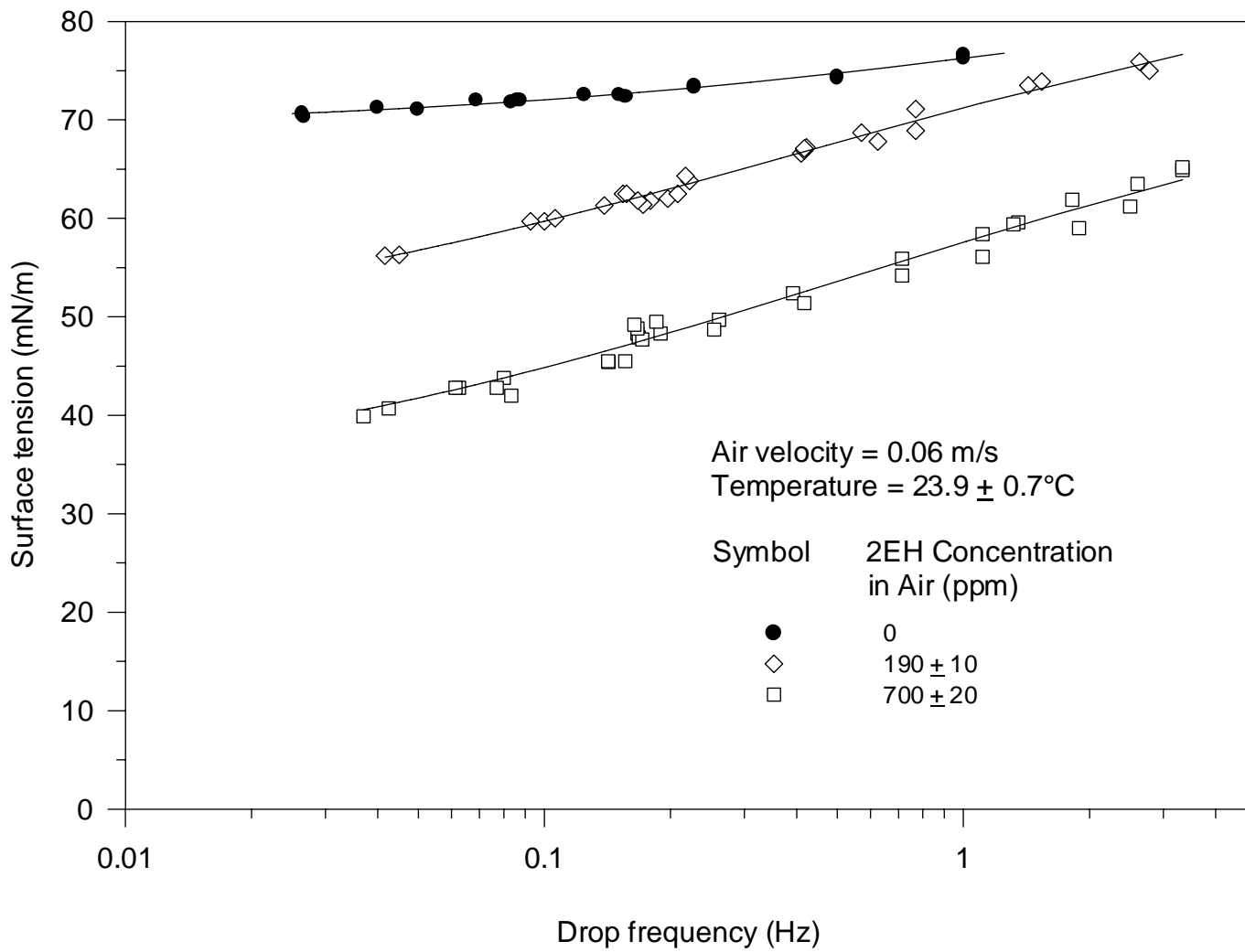


Figure 3.5 Surface tension of water versus drop frequency and 2EH concentration in air

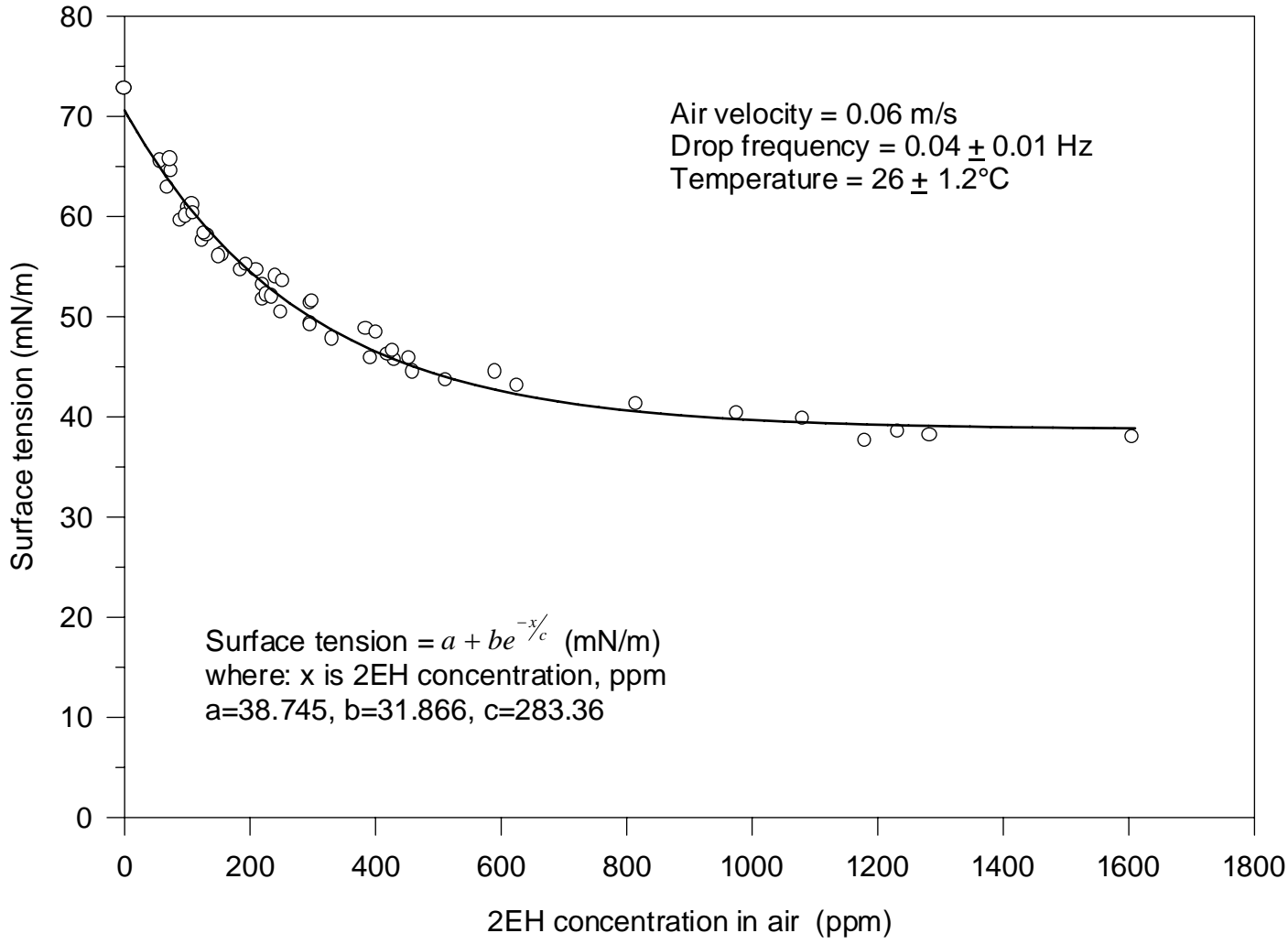


Figure 3.6 Surface tension of water versus concentration of 2EH in air

actual 2EH concentration in the droplets is not known, the 2EH concentration charged in the reservoir is used in this plot and is referred to as the system concentration. Figure 3.7 shows that the surface tension significantly decreases with an increase of 2EH concentration in the sample. The shape of the surface tension versus 2EH concentration is somewhat different from the case with 2EH in air as in Figure 3.5. In Figure 3.7 the surface tension is seen to be essentially independent of the drop frequency below 0.1 Hz. This phenomenon was also observed by Kulankara (1999). Apparently, the surfactant molecules diffuse to the free surface from the liquid bulk on a time scale shorter than the period between drops, with the result that the equilibrium state on the surface is achieved relatively quickly for the water case.

Figure 3.8 is a plot of surface tension versus 2EH concentration in the sample. The data in Figure 3.8 were taken at a drop frequency of 0.04 Hz. As can be seen, the surface tension decreases with an increase in 2EH concentration (in the liquid) until it reaches a plateau. The plateau value of surface tension is found to be 41 mN/m which is approached within 1% at  $850 \pm 50$  ppm.

### 3.3.2 Surface Tension Results for Aqueous LiBr

#### 3.3.2.1 Surface tension of aqueous LiBr with 2-ethyl-hexanol in air

A series of surface tension measurements were conducted for 60% aqueous LiBr with 2EH vapor in air and the results are shown in Figure 3.9. The surface tension is seen to significantly decrease with an increase of 2EH concentration in air. It is interesting to note the difference in shape observed here as compared to the water data in Figure

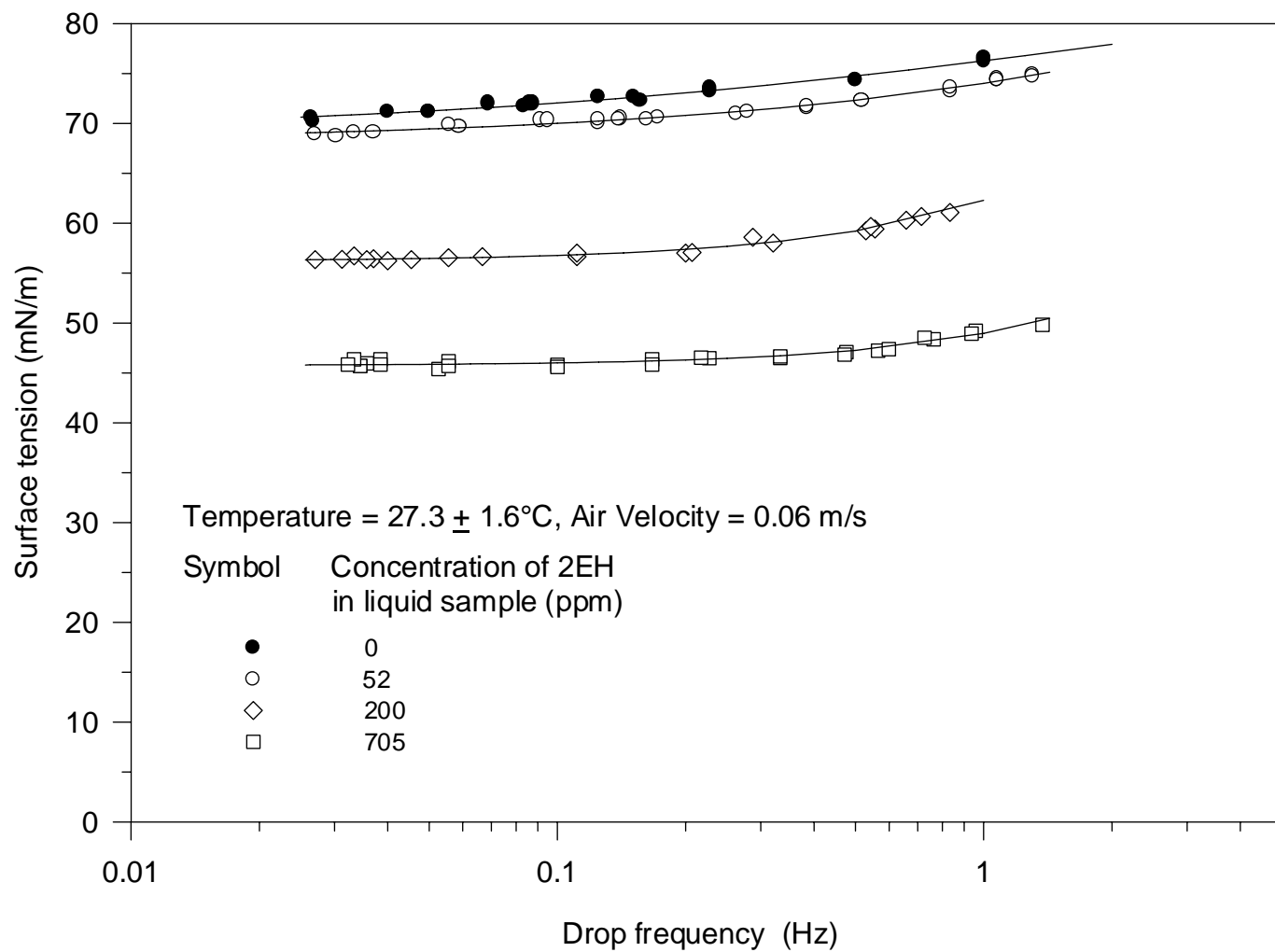


Figure 3.7 Surface tension of water versus drop frequency and 2EH concentration in the water

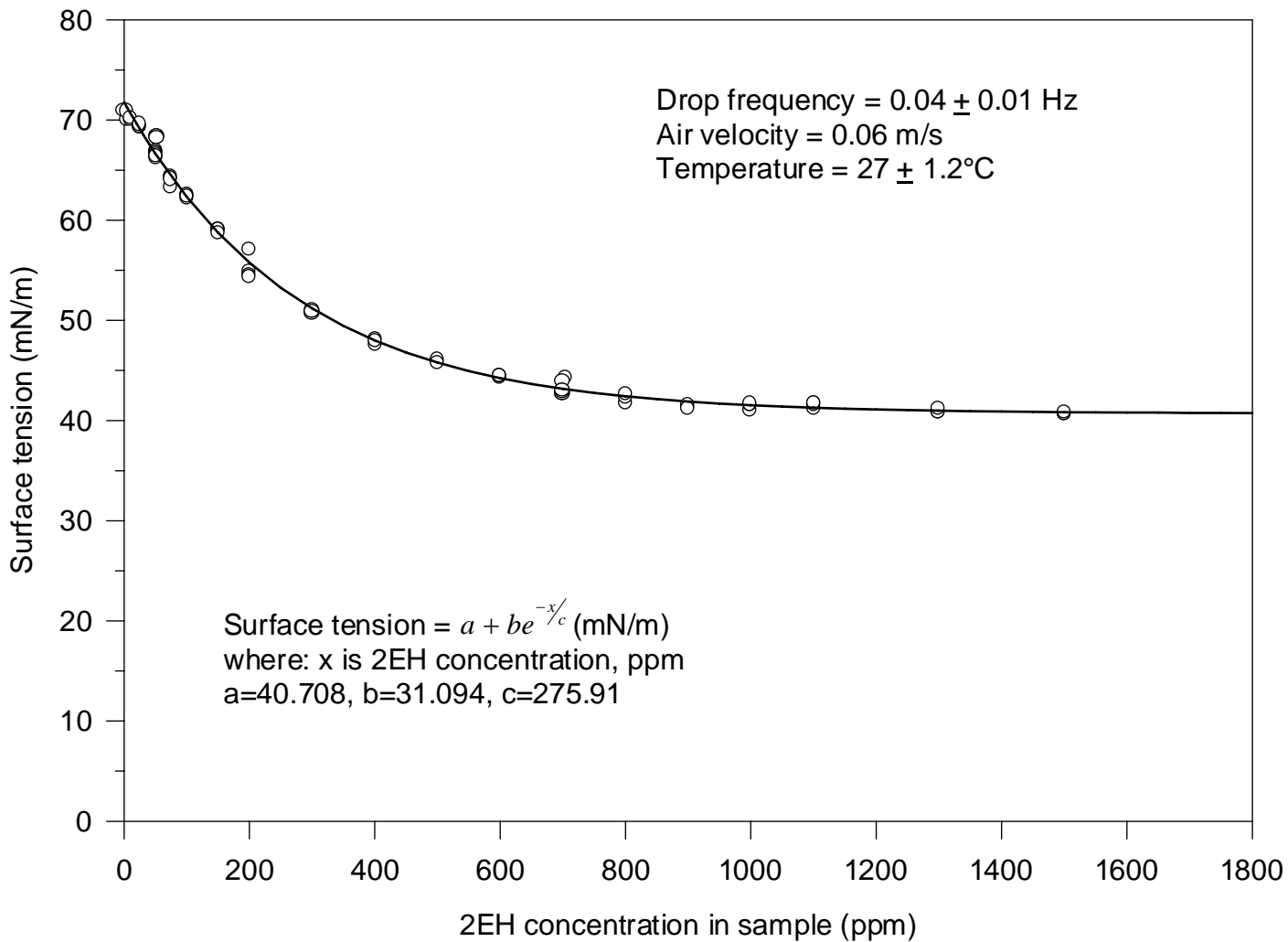


Figure 3.8 Surface tension of water versus 2EH concentration in sample

3.5. When the drop frequency is smaller than approximately 0.2 Hz, the surface tension is essentially independent of drop frequency. It is also noticed that at high drop frequency the surface tension curves with and without 2EH in air show a different shape.

Figure 3.10 presents surface tension data for 60% aqueous LiBr solution as a function of 2EH concentration in air. For comparison, water data obtained under the same measurement conditions are also shown along with the curve fit results. As can be seen, the surface tension for 60% LiBr solution decreases with increasing 2EH concentration and reaches a plateau surface tension value of 37 mN/m. By comparison, the minimum surface tension for 60% aqueous LiBr from Kulankara and Herold (1999) was found to be 42 mN/m under somewhat different conditions.

Figure 3.10 also shows that the surface tension of aqueous LiBr is higher than that of water for the case with no 2EH. But when 2EH is present, the curves cross such that the plateau value is higher for water. One possible explanation of this crossover phenomenon may be attributed to the difference in 2EH solubility between aqueous LiBr and water. The addition of LiBr to water creates an electrolyte structure where water molecules group with the salt ions. This reduction in the number of free water molecules is thought to be a key factor in the decrease in both diffusivity and solubility of 2EH in this system. Although the presence of the electrolyte repels the hydrophobic part of 2EH, the data seems to indicate that the presence of the LiBr actually increases the surface concentration possibly due to the fact that the hydrophilic part of the 2EH has a stronger affinity for the electrolyte surface than it does for the pure water surface. The result of this is that for the same 2EH concentration in air, more 2EH is adsorbed on the surface for the aqueous LiBr and hence the surface tension is lower.

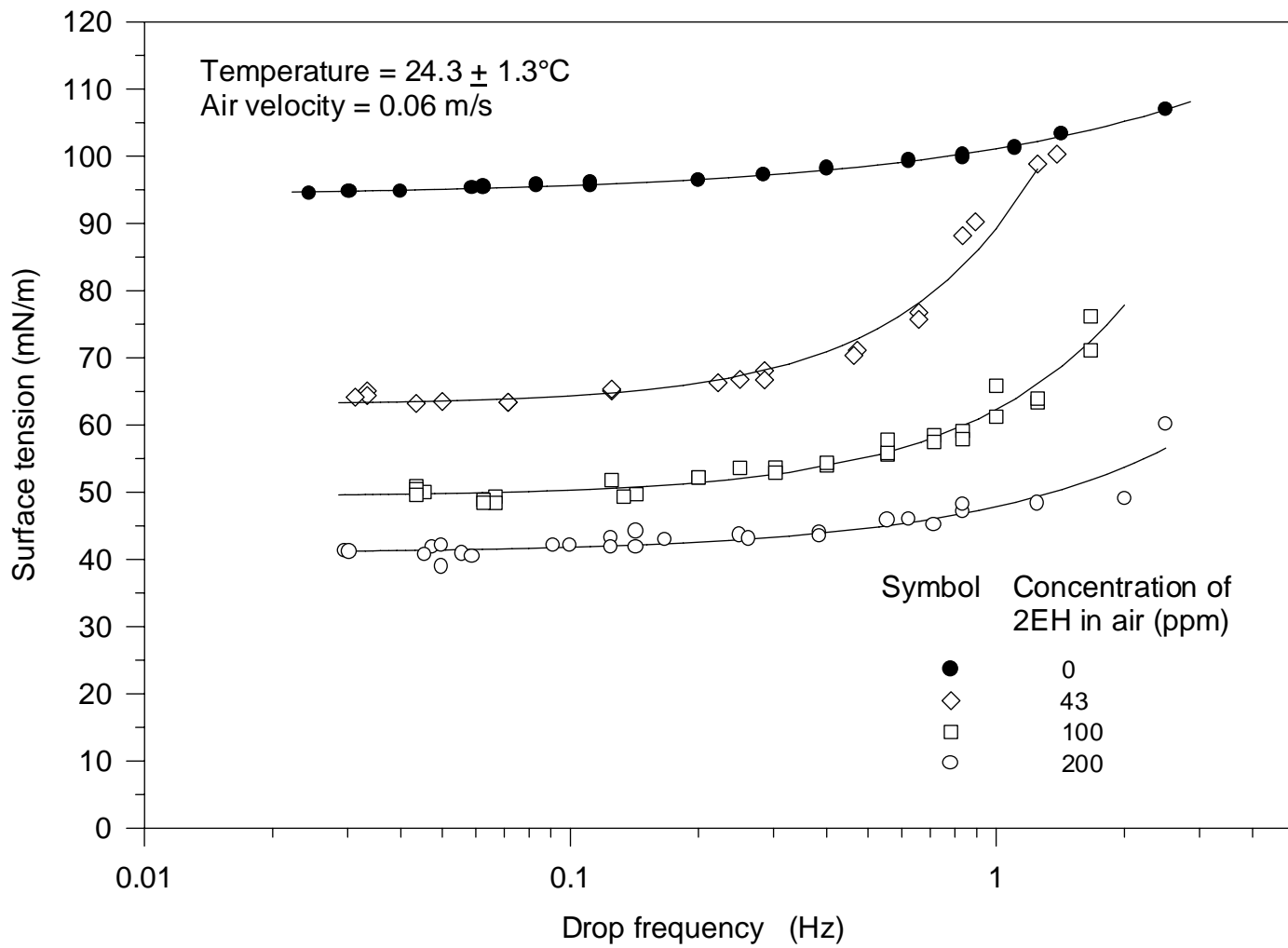


Figure 3.9 Surface tension of 60% aqueous LiBr versus drop frequency with 2EH concentration in air

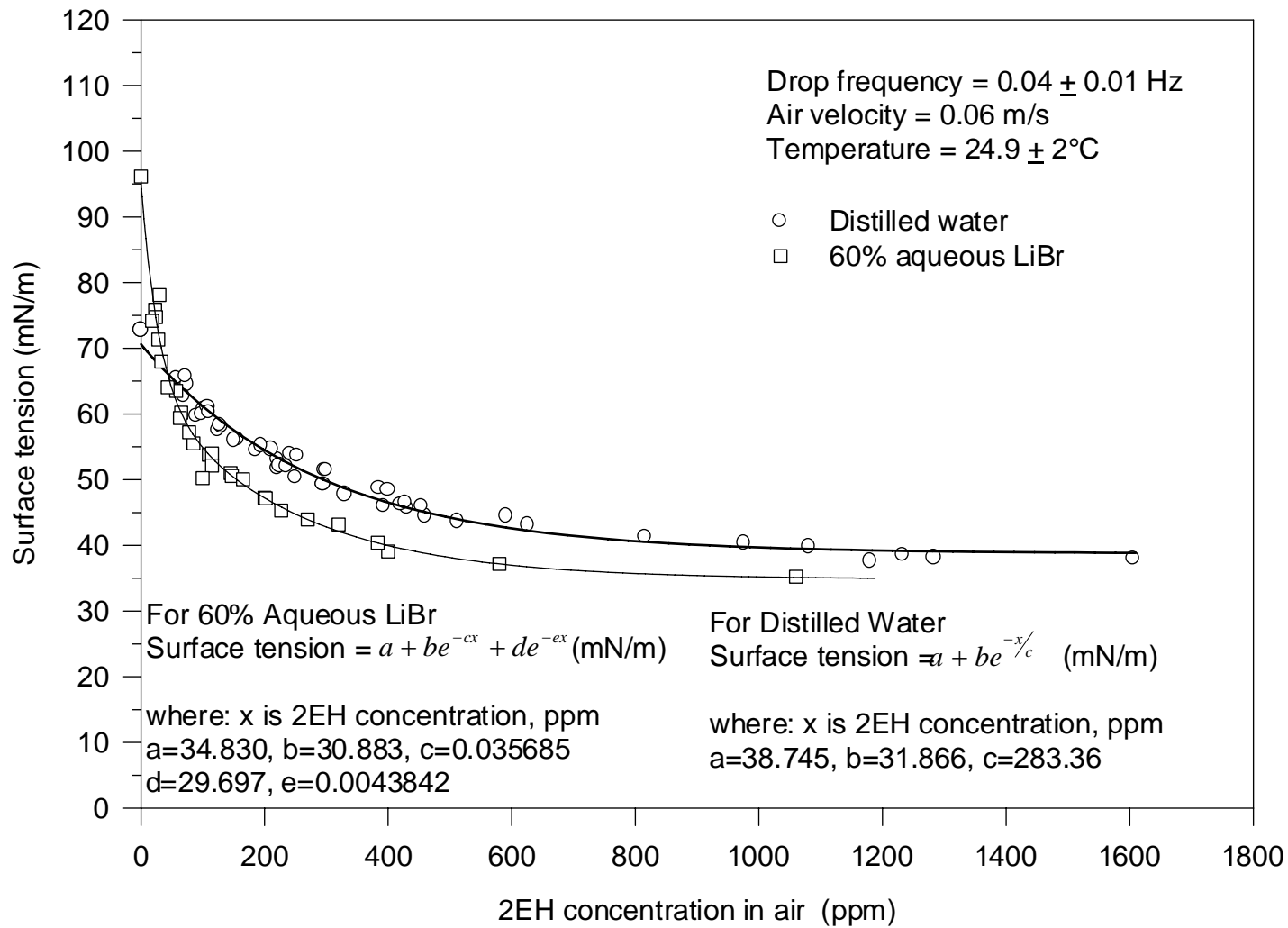


Figure 3.10 Surface tension of pure water and 60% aqueous LiBr with 2EH concentration in air

### **3.3.2.2 Surface tension of aqueous LiBr with 2-ethyl-hexanol in aqueous LiBr**

The surface tension of 60% aqueous LiBr with 2EH only in the liquid was measured over a range of drop frequency as shown in Figure 3.11. The upper curve was generated in a procedure closely similar to that used to generate Figure 3.8. It shows a small but measurable reduction in surface tension. For comparison, an additional series of experiments were performed with a different procedure that was first developed by Kulankara (1999).

In this case, the drop measurements were done with the tip of the drop creator placed inside the collection flask such that the vapor conditions around the drop are defined by the collected liquid. The collected liquid was the liquid left in the collection vessel from the previous test. The lower curve measurement was finished right after the upper curve measurement for each point. For the lower curve, there was no air flow. As shown in the lower curve in Figure 3.11, the surface tension in this configuration is significantly lower than the value measured with no vapor side effects (top curve). This indicates that the effect of the 2EH vapor is more efficient in reducing the surface tension for 60% aqueous LiBr as compared to water.

## **3.4 Solubility Limit of 2EH in 60% Aqueous LiBr and Water**

The solubility limit is an important property affecting surface tension characteristics. In order to understand these effects, the determination of the solubility of 2EH is discussed here.

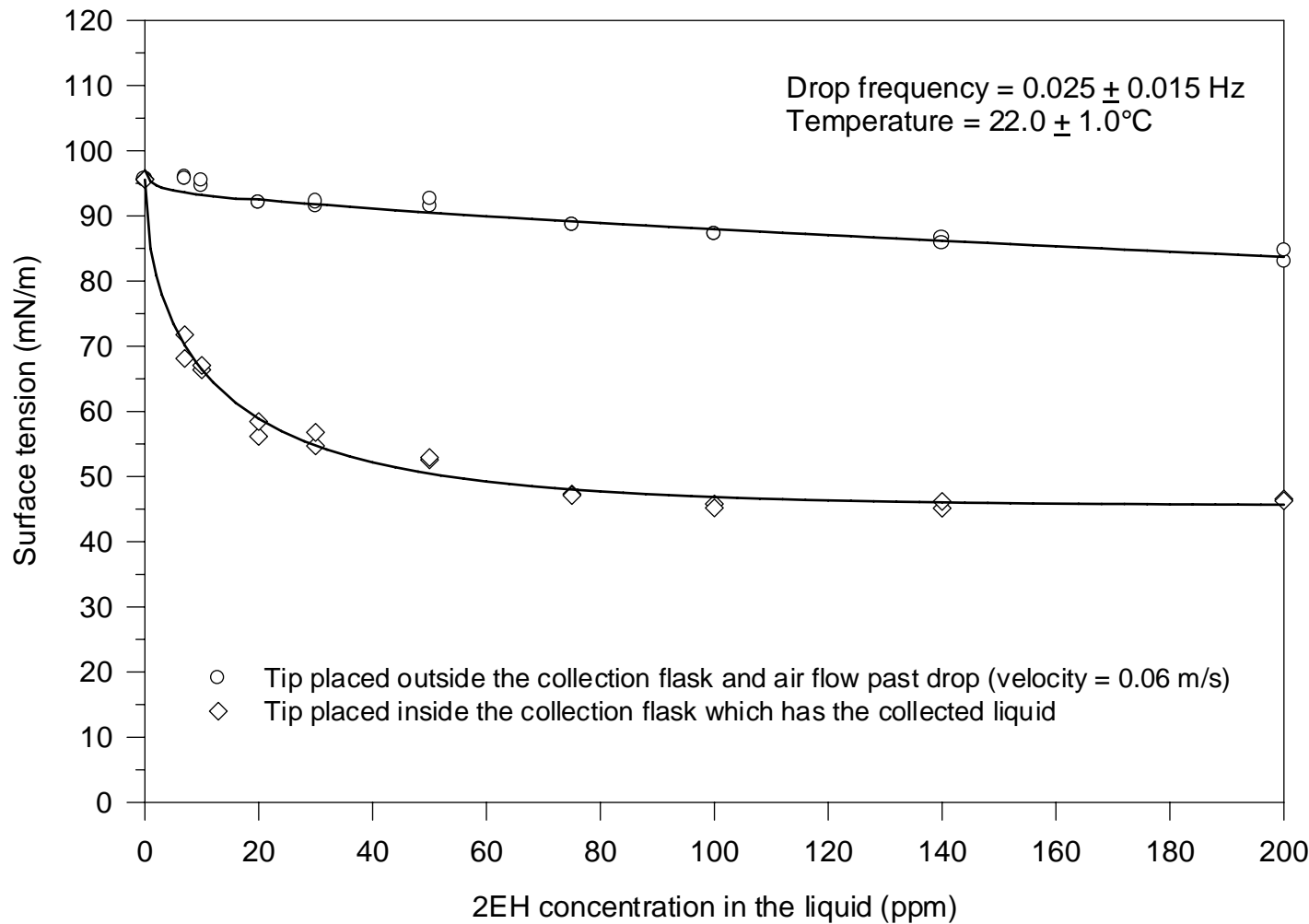


Figure 3.11 Surface tension of 60% aqueous LiBr versus 2EH concentration in the liquid

Due to the difficulty in direct determination of solubility, the usual method is to infer the solubility limit from the shape of the surface tension versus surfactant system concentration characteristics. The solubility limits of 2EH in 60% aqueous LiBr and water were determined here by a new method which we call the SLVSA method (solubility limit of vapor surfactant with adsorption). This method consists of two steps: conducting a calibration test series and then running the actual sample.

The solubility of 2EH in aqueous LiBr is low, often quoted as 100 ppm based on surface tension measurements. However, there is considerable doubt about this figure based on the present surface tension measurements that imply that the system concentration of 2EH is largely irrelevant in determining the surface tension unless the entire system is in equilibrium. Thus, conclusions based on surface tension versus system concentration are dubious for studies that do not even mention equilibrium. Furthermore, it is found that 2EH adsorbs strongly and adheres to solid surfaces to the extent that very careful procedures are necessary to eliminate 2EH from vessels between experiments. In a series of initial experiments on 60% aqueous LiBr, it was found that the amount of 2EH adsorbed on the walls of a beaker is sufficient to cause the surface tension of a 2EH-free sample to reach the lowest measured value when the drop creator is positioned inside the collection vessel such that the vapor around the drops is saturated by 2EH evaporating from the walls. Based on the above described experiments, it was concluded that extra effort is required to assure an equilibrium condition.

The SLVSA method was designed to account for these effects. In particular, the amount of 2EH that adheres to the vessel wall is taken into account. The SLVSA calibration involves measuring the surface tension of 2EH-free aqueous LiBr with the

drop creator positioned within the collection vessel. The collection vessel is prepared by charging with a known quantity of aqueous LiBr (50 g) and 2EH such that the system concentration of 2EH is known. The vessel is shaken vigorously to distribute the 2EH throughout the system. The measured surface tension is found to vary with the amount of 2EH charged in the collection vessel as shown in Figure 3.12.

To run an actual sample with saturated 2EH in aqueous LiBr, excess 2EH (17.7 mg) was mixed with 79 g of 60% aqueous LiBr (the 2EH system concentration is 225 ppm). This solution was mixed in a vessel with a free surface. Numerous surfactant droplets were observed on the free surface, supporting the idea that the 2EH liquid concentration was at the solubility limit. 50 g of this solution was extracted from the bottom of the mixing vessel in such a way as to avoid entraining 2EH from the surface. The resulting sample was free of excess 2EH, containing only the dissolved fraction. A surface tension measurement was then done on the sample to determine the 2EH liquid concentration. The flask used in the calibration tests was employed and the tip of the drop creator was positioned identically as in the calibration tests. The surface tension was found to be 41.4 mN/m. By interpolation from the calibration curve, the amount of surfactant in this 50 g sample was determined to be 1.349 mg. The solubility limit was then calculated as  $1.349 \text{ mg} / 50 \text{ g} = 27.0 \text{ ppm}$ .

To verify the repeatability of this method, two additional tests were conducted with higher amounts of 2EH charged in the mixing vessel (25.2 mg 2EH in 86.7 g LiBr solution (the 2EH system concentration is 290 ppm) and 33.0 mg 2EH in 83.2 g LiBr solution (the 2EH system concentration is 400 ppm)). Although the 2EH amount in these cases is larger than the amount in the first case, the solution sample taken from

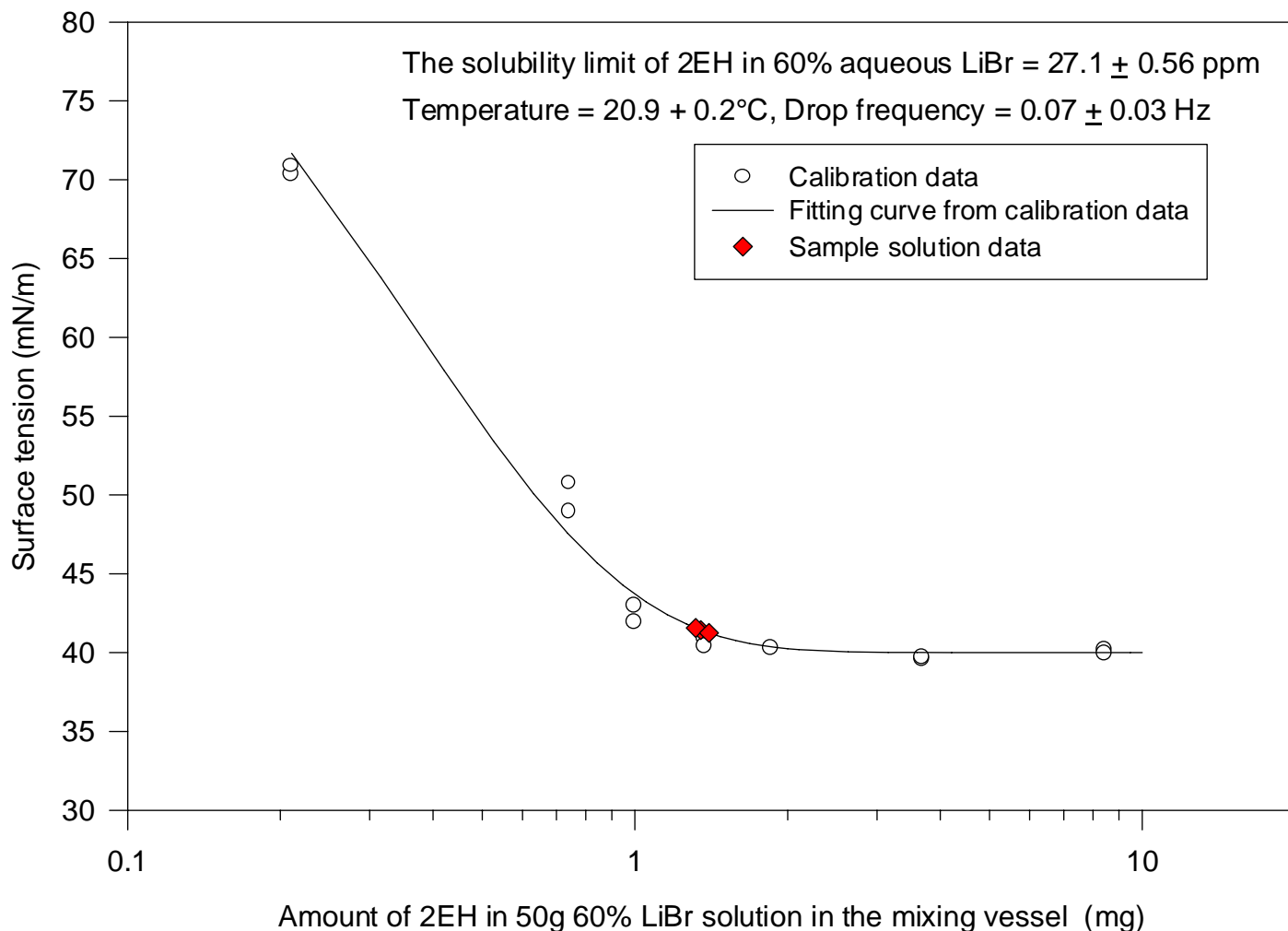


Figure 3.12 Determination of solubility limit of 2EH in 60% aqueous LiBr

the bottom of the mixing vessel is still expected to be at the solubility limit. The measured surface tension values for these two cases were 41.57 and 41.26 mN/m which are quite close to the first value. All three data points are plotted on Figure 3.12. The scatter of the surface tension is approximately  $\pm 0.1$  mN/m based on these three data and thus the corresponding probable error of solubility in this surface tension range is estimated as  $\pm 0.6$  ppm. Thus, based on the above measurements, the solubility limit of 2EH in 60% aqueous LiBr at temperature of 29 °C is determined to be  $27.1 \pm 0.6$  ppm.

The SLVSA method was also used to determine the solubility limit of 2EH in water. The results are shown in Figure 3.13. Two samples were 202.4 mg 2EH in 100 g water (the 2EH system concentration is 2000 ppm) and 326 mg 2EH in 100 g water (the 2EH system concentration is 3260 ppm). 75 mg of these samples were acquired and tested and the surface tension was found to be  $45.75 \pm 0.38$  mN/m. By interpolation from the calibration curve, the amount of 2EH was determined to be  $62.5 \pm 3.5$  mg and the solubility limit at temperature of 27.3 °C was calculated to be  $835 \pm 45$  ppm.

### 3.5 Comparison with Literature Data

Limited literature data on the surface tension of aqueous LiBr with 2EH were found as shown in Figure 3.14. For comparison, our data from the lower curve in Figure 3.11 are included in Figure 3.14. As can be seen, the data show considerable disagreement and scatter. However, if we discard Ziukanov's data, the tendencies of the surface tension with 2EH concentration are consistent. Based on the measurement methods described in the original papers, all the data were obtained without controlling

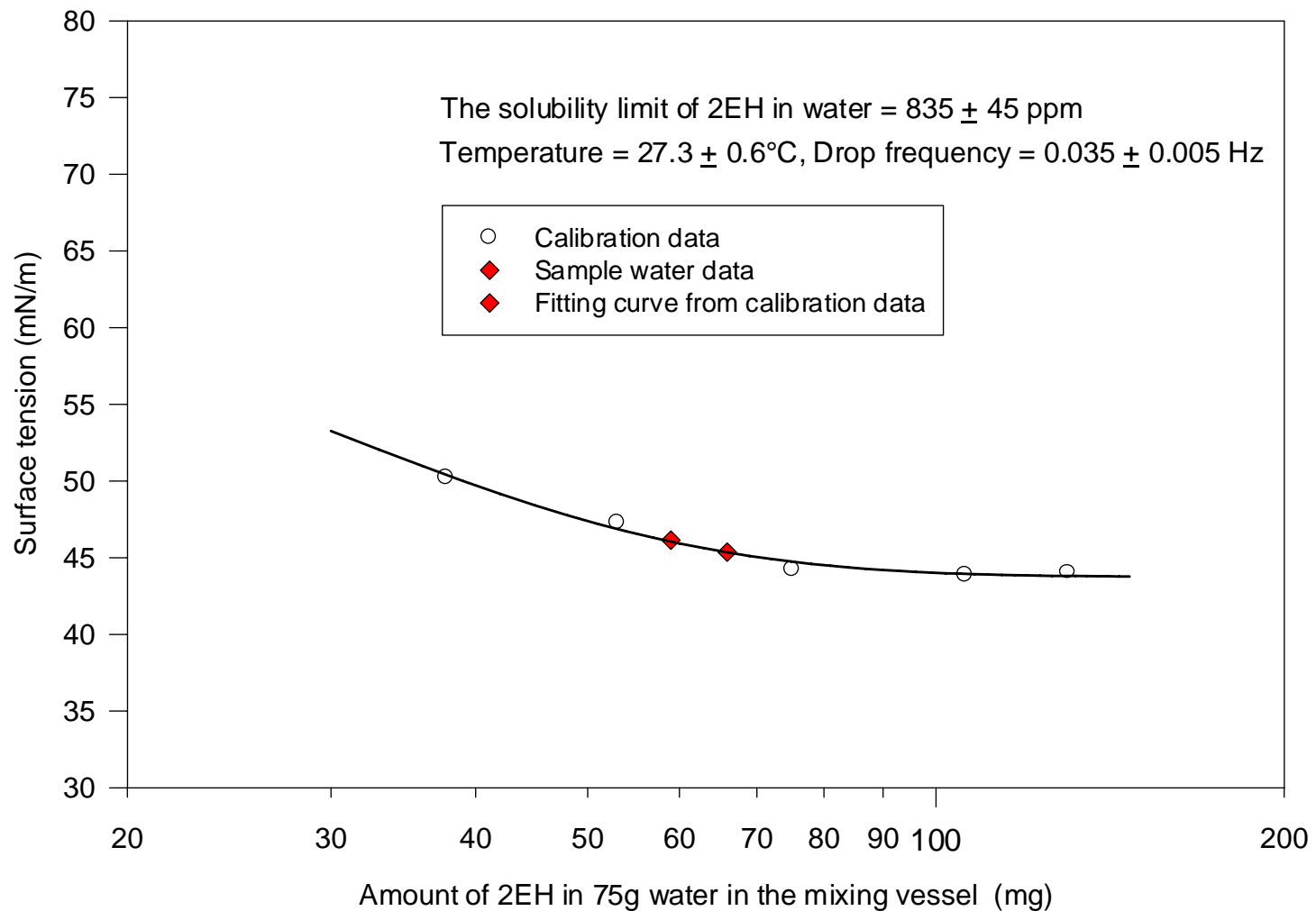


Figure 3.13 Determination of solubility limit of 2EH in water

the vapor side conditions, which is shown in this study to be critical. Another factor is inaccuracy in the liquid concentration of 2EH. Because of the adsorption characteristics, some of the 2EH is found on the free surface and the walls, especially when the surfactant concentration is greater than the solubility limit. Therefore, the actual surfactant concentration in solution may be significantly different from the system concentration of a prepared sample. The 2EH concentrations for all data in Figure 3.14 (including our data) are not true liquid concentrations. The difference is estimated in Section 4.3. In the literature, some authors (Kim and Janule, 1994; Sheehan et al., 1996; Gustafsson et al., 1996; Ishida and Mori, 1996) attribute the surface tension measurement error to dynamic effects in the liquid, i.e. the effect of time on surface tension. Our results show conclusively that the surfactant vapor concentration at the vapor/liquid interface around the drops must be controlled to obtain repeatable surface tension data. Complete equilibrium of the system is a time consuming process due to the very low mass diffusivity of 2EH in aqueous LiBr. However, the kinetics of equilibrium between the vapor and the liquid surface are quite fast in comparison. Since the 2EH is supplied to the liquid surface from the vapor in the absorption chiller application, the kinetics of diffusion in the liquid is not particularly important in understanding surfactant enhancement of absorption.

It should be noted that our data in Figure 3.14 were obtained under different conditions as compared with other sources. As described in the discussion of Figure 3.11, the solution in the collection flask is from the drop tip and therefore, the 2EH vapor concentration in the collection vessel is limited by the solubility limit. For this

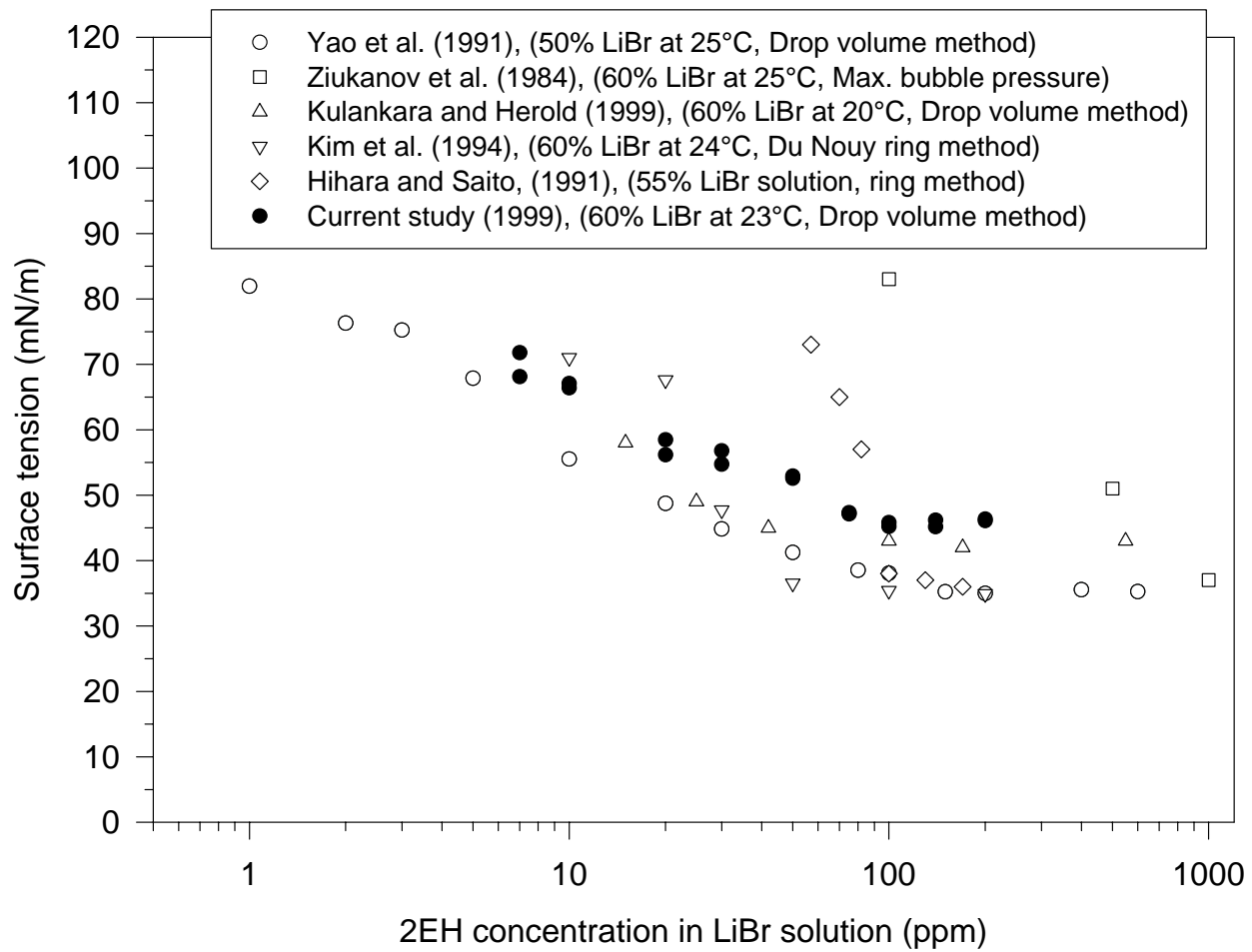


Figure 3.14 Surface tension of LiBr solution versus concentration of 2-ethyl-hexanol

measurement condition, the surface tension plateau is somewhat higher than the literature data.

### 3.6 Discussion

The shape of the curves of surface tension versus drop frequency shown in Figure 3.5 for water and Figure 3.9 for 60% aqueous LiBr are different. It is believed that the surface tension is mainly determined by 2EH surface concentration. A discussion of this is deferred to the end of Chapter 4 which focuses on a quantitative discussion of surface concentration.

The surface tension values for both water and 60% LiBr solution with 2EH in air, shown in Figure 3.10, display similar tendencies but the sensitivity of surface tension to 2EH concentration for 60% LiBr solution is larger than that for water, especially in the lower 2EH concentration range.

The surface tension results with 2EH only in the liquid are shown in the upper curve in Figure 3.11 for 60% aqueous LiBr. In these experiments, no 2EH was delivered from the vapor and the air continuously swept over the drops. In other words, the measurements were taken under a non-equilibrium 2EH vapor concentration condition. These measurement results show only a slight reduction of surface tension (as 2EH liquid concentration increases) from 96 mN/m with no 2EH to 86 mN/m with 200 ppm 2EH. Slow diffusion of 2EH from the liquid to the surface, and evaporation of 2EH molecules that reach the surface, result in a low 2EH surface concentration. The diffusion rate of 2EH molecules from the bulk to the surface is believed to be enhanced by free water molecules (Kim and Berman, 1996). Because there is no free water in 60% LiBr solution,

the diffusion of 2EH molecules from the bulk to the surface is restricted. Thus the 2EH in the liquid bulk slowly diffuses to the surface such that the surface concentration stays low and the surface tension stays high. In contrast, the diffusivity of 2EH molecules in water is apparently much higher than for LiBr solution, thus resulting in a higher 2EH surface concentration and a significant change in surface tension as shown in Figure 3.8.

Based on Figure 3.11, it is observed that for aqueous LiBr, diffusion of 2EH from the liquid does not result in reduction in surface tension on the time scales of interest in absorption. But if the 2EH is present in vapor form, it results in a significant reduction in surface tension even on very short time scales.

At first glance, it seems that the surface tension data from the lower curve in Figures 3.11 and 3.12 are not in agreement, because the surface tension plateau is 46 mN/m in Figure 3.11 and 41.5 mN/m in Figure 3.12. However, this difference is due to different 2EH vapor concentrations. The 2EH vapor concentration in Figure 3.11 is limited by the 2EH solubility in the flask but the 2EH vapor concentration in Figure 3.12 can go to a much higher value because the 2EH system concentration in the flask is very high.

## CHAPTER 4

### DETERMINATION OF THE SURFACE CONCENTRATION

#### **4.1 Introduction**

Marangoni convection is flow caused by surface tension gradients. Surface tension gradients can be caused by non-uniform surface concentration of surfactant. The Vapor Surfactant theory (Kulankara and Herold, 1999) holds that the non-uniformities in surfactant surface concentration result from delivery of surfactant to the surface with the absorbing vapor in a spatially non-uniform manner. Based on surface tension data presented in Chapter 3, surface tension decreases with an increase of 2EH concentration, in either the vapor or liquid, for both water and aqueous LiBr. According to surfactant theory (Rosen, 1989) the reduction of the surface tension mainly depends on the number of adsorbed 2EH molecules on the surface, i.e. on the 2EH surface concentration. Thus, a more complete understanding of the mechanism of Marangoni convection in the system of interest requires knowledge of the surface concentration.

#### **4.2 Data Reduction and Gibbs Adsorption Theory**

Aqueous surfactants characteristically have a molecular structure consisting of both hydrophilic and hydrophobic groups. The hydrophilic group promotes solubility in water and the hydrophobic group is basically insoluble. As a result, surfactants concentrate on free surfaces with the hydrophilic group in the water and the hydrophobic

group oriented away from the water. The presence of surfactant on the surface changes the surface tension by disrupting the tightly bonded symmetry with a weaker link. Based on Gibbs adsorption theory, the equilibrium surface excess concentration of surfactant is functionally related to the surface tension and the chemical potential of each species in the liquid (Rosen, 1989). For a binary system where the solvent has a surface excess concentration of zero, the surface excess concentration of the surfactant,  $\Gamma$ , can be written as

$$\Gamma = \frac{\partial \sigma}{\partial \mu} \quad 4.1$$

where  $\mu$  is the chemical potential of the surfactant in the liquid. For ideal solutions, the variation in chemical potential can be expressed in terms of the variation in mole fraction,  $x$ , as

$$d\mu = -RTd \ln x \quad 4.2$$

resulting in

$$\Gamma = -\frac{1}{RT} \left( \frac{\partial \sigma}{\partial \ln x} \right)_T \quad 4.3$$

In the present study, the solute is 2EH and the solvent is either water or aqueous lithium bromide. In order to deduce the 2EH surface concentration from the surface tension data in Chapter 3, Equation 4.3 can be rewritten in terms of the mass fraction,  $x_{2EH}$ , as

$$\begin{aligned} \Gamma_{2EH} &= -\frac{1}{RT} \left[ x_{2EH} + \left( \frac{M_{H2O}}{M_{2EH}} - 1 \right) x_{2EH}^2 \right] \left( \frac{\partial \sigma}{\partial x_{2EH}} \right)_T \\ &\approx -\frac{x_{2EH}}{RT} \left( \frac{\partial \sigma}{\partial x_{2EH}} \right)_T \end{aligned} \quad 4.4$$

where the second form is accurate when  $x_{2EH}$  is close to zero as in the current considerations ( $0 < x_{2EH} < 0.001$ ).

The Gibbs adsorption analysis is based on an equilibrium state, which implies that the vapor, surface and liquid are all in equilibrium. That explains why only the 2EH liquid concentration appears in the formulation. However, it should be noted that equilibration in this system is slow due to the low mass diffusivity of 2EH in the liquid. In addition, the Gibbs adsorption analysis cannot be applied to concentrations above the CMC (critical micelle concentration, a concentration in which micelles first form). Micelles form a separate phase in which the hydrophobic ends of surfactant molecules are oriented toward the micelle and the hydrophilic ends are in aqueous contact. As a result, when the overall concentration rises above CMC, only the size and number of the micelles increase, but the dissolved surfactant stays constant (Tsujii, 1997; Bikerman, 1970).

### 4.3 Surface Concentration Results

#### 4.3.1 Surface Concentration of 2-Ethyl-Hexanol in Water

The surface tension data displayed in Figure 3.8 for water with 2EH are used to calculate the surface concentration. The surfactant liquid mass fraction in Equation 4.4 is replaced by the system mass fraction to accomplish the calculation. It is believed that this replacement is a good approximation due to the high solubility of 2EH in water (835 ppm). In Figure 3.13, when the system reaches the saturation point where the surface tension reaches a plateau value, the amount of 2EH is approximately 78 mg in 75 g water.

From this figure, it can also be observed that the solubility limit of 2EH in the liquid is 62 mg in 75 g water. Therefore, the difference between the 2EH system concentration and 2EH liquid concentration is estimated to be about 20% ((78-62)/78) for water in this particular system. These surface tension data were taken with 2EH free air flowing past the drops. Although the vapor is far from equilibrium, the data still show a significant reduction in surface tension that indicates that the diffusion of 2EH from the liquid to the surface is relatively fast for pure water. Thus, the data are interpreted as equilibrium data.

Figure 4.1 is a plot of surface concentration for 2EH in water, calculated from the surface tension data in Figure 3.8 using Equation 4.4. The surface tension data from Figure 3.8 is reproduced in Figure 4.1 along with a curve fit. The surface concentration results are computed from the curve fit. The curve fit was based on the Szyszkowski equation (Reid et al., 1988)

$$\sigma = a - b \ln(1 + cx_{2EH}) \quad 4.5$$

All the data at system concentration below the saturation point (where the surface tension reaches a plateau) were included in the curve fit. This type of saturation point has been interpreted as the CMC (critical micelle concentration) by Bikerman (1970) and the solubility limit (Kim and Berman, 1996). In the present work, it is interpreted as the solubility limit. The point is determined from the data by the following steps. First, the plateau surface tension was calculated by averaging the surface tension data at the largest system concentrations. For this case, data at concentrations of 1000, 1100, 1300 and 1500 ppm were identified as part of the plateau region by inspection of the plot. The data with system concentration less than 1000 ppm was then fit with a curve as in Equation 4.5.

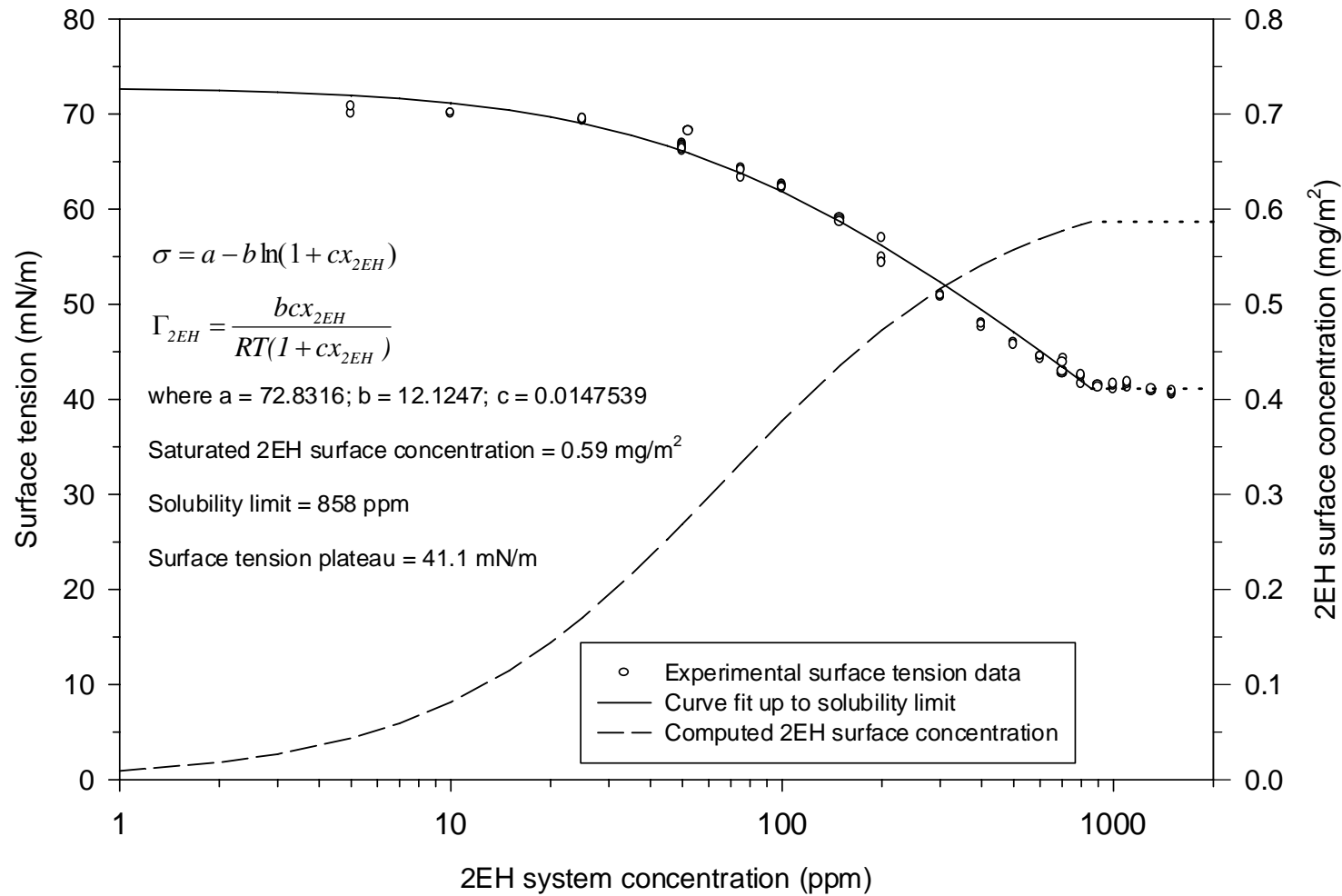


Figure 4.1 Surface tension and 2EH surface concentration versus 2EH system concentration (where system is water in a glass flask)

The solubility limit was determined from the intersection of the curve fit and the horizontal line representing the plateau.

The 2EH surface concentration was calculated from Equation 4.4 using Equation 4.5 resulting in

$$\Gamma_{2EH} = \frac{bcx_{2EH}}{RT(1+cx_{2EH})} \quad 4.6$$

or

$$\sigma = a - b \ln \left[ 1 + \frac{RT \Gamma_{2EH}}{b - RT \Gamma_{2EH}} \right] \quad 4.7$$

The value of the surface concentration at the solubility limit (835 ppm) is 0.59 mg/m<sup>2</sup> and is interpreted as the saturated surface concentration in this system.

Figure 4.1 can be divided into several 2EH system concentration ranges. In the low 2EH system concentration range (for example, below 100 ppm in Figure 4.1), a slight reduction in surface tension is accompanied by a significant increase in the 2EH surface concentration. In contrast, in the high 2EH system concentration range, relatively small changes in 2EH surface concentration result. The increase of the surface concentration in the low system concentration range is attributed to population of the surface with 2EH molecules; while changes in the surface concentration in the high system concentration range are attributed to the direct influence of 2EH liquid concentration on surface tension (Rosen, 1989).

Figure 4.2 presents an alternative view of the relationship between surface tension and 2EH surface concentration (Equation 4.7). As can be seen in Figure 4.2, the surface tension decreases gradually as surface concentration increases starting from a clean surface. However, as the surface concentration approaches the saturated value, the

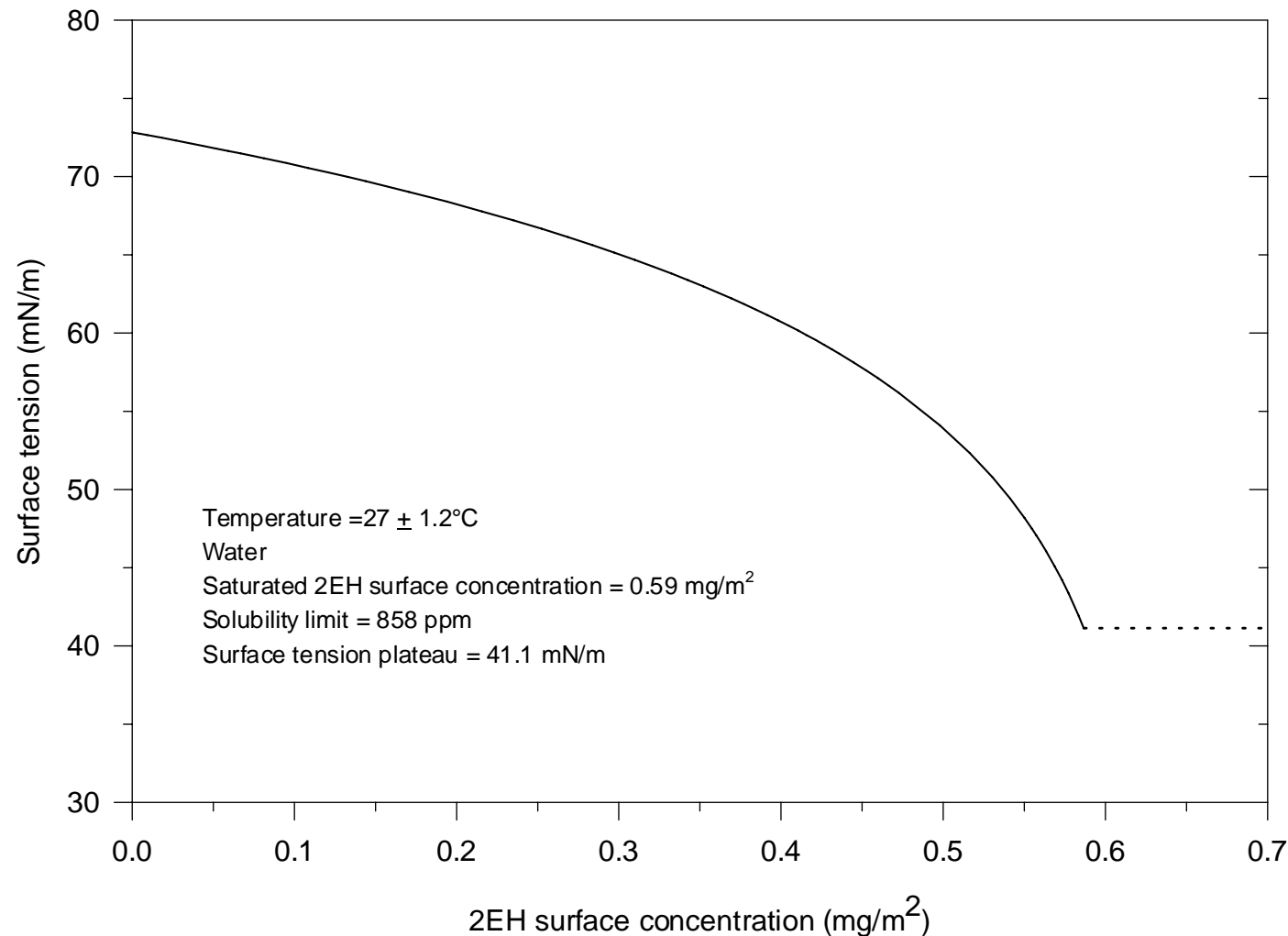


Figure 4.2 Surface tension versus 2EH surface concentration for water (Equation 4.7)

surface tension drops quickly. Selected surface concentration values from Equations 4.5 and 4.6 are also provided in Table 4.1 for reference.

Table 4.1 2EH surface concentration and surface tension for water with 2EH

2EH system concentration (ppm)	0	5	10	20	30	40	50	100	150	200	250
Surface tension (mN/m)	72.8	72.0	71.1	69.7	68.4	67.2	66.1	61.8	58.7	56.2	54.1
2EH surface concentration (mg/m <sup>2</sup> )	0.0	0.043	0.081	0.144	0.194	0.235	0.269	0.377	0.436	0.473	0.498
2EH system concentration (ppm)	300	350	400	450	500	550	600	650	700	800	858
Surface tension (mN/m)	52.3	50.8	49.4	48.2	47.1	46.0	45.1	44.2	43.4	41.9	41.1
2EH surface concentration (mg/m <sup>2</sup> )	0.516	0.530	0.541	0.550	0.558	0.564	0.569	0.573	0.577	0.584	0.587

#### 4.3.2 Surface Concentration of 2-Ethyl-Hexanol in Aqueous LiBr

In order to find the surface concentration of 2EH in aqueous LiBr, the surface tension was measured for a range of LiBr mass fraction. These data were collected by another student with continuous consultation by the author (Zhou et al., 2001). Figure 4.3 is a plot of 2EH surface tension versus 2EH system concentration based on those data along with their curve fits.

These data were measured by the drop weight method. A series of experiments were done which showed that very representative results could be obtained by feeding

2EH free aqueous LiBr through the drop creation system while allowing the drops to form in a vapor environment where the 2EH vapor concentration is defined by the prepared sample. This method works because the surface tension of this system is much more sensitive to the 2EH vapor concentration than it is to the liquid concentration. The advantage of this approach is that it avoided the need to clean the drop creator between each data point. The data are presented as a function of the 2EH system concentration of the sample prepared in the drop collection vessel which was allowed to equilibrate in a sealed vessel for 24 hours after mixing.

The system concentration of 2EH is used in place of the liquid concentration in the Gibbs adsorption analysis for the calculation of surface concentrations. The curve fits were constructed in a manner similar to that described in Section 4.3.1. In particular, the solubility limit was determined first by inspection of the data and then only data below the solubility limit concentration were used in the fit.

Based on the curve fits for surface tension shown in Figure 4.3, the 2EH surface concentration was calculated (Equation 4.6) and the results are plotted in Figures 4.4 and 4.5. Figure 4.4 is a plot of surface concentration versus 2EH system concentration and Figure 4.5 is a cross plot of surface tension versus 2EH surface concentration. The saturated 2EH surface concentration was determined for each LiBr mass fraction as represented by the maximum values in Figure 4.4. These saturated values are listed in Table 4.2 along with the solubility limits and surface tension plateau values. As can be seen from Table 4.2, the 2EH saturated surface concentration increases from 0.474 to 0.904 mg/m<sup>2</sup> as mass fraction of LiBr increases from 0 to 57%. The results listed for 60% aqueous LiBr are extrapolated as discussed later in Section 4.4.

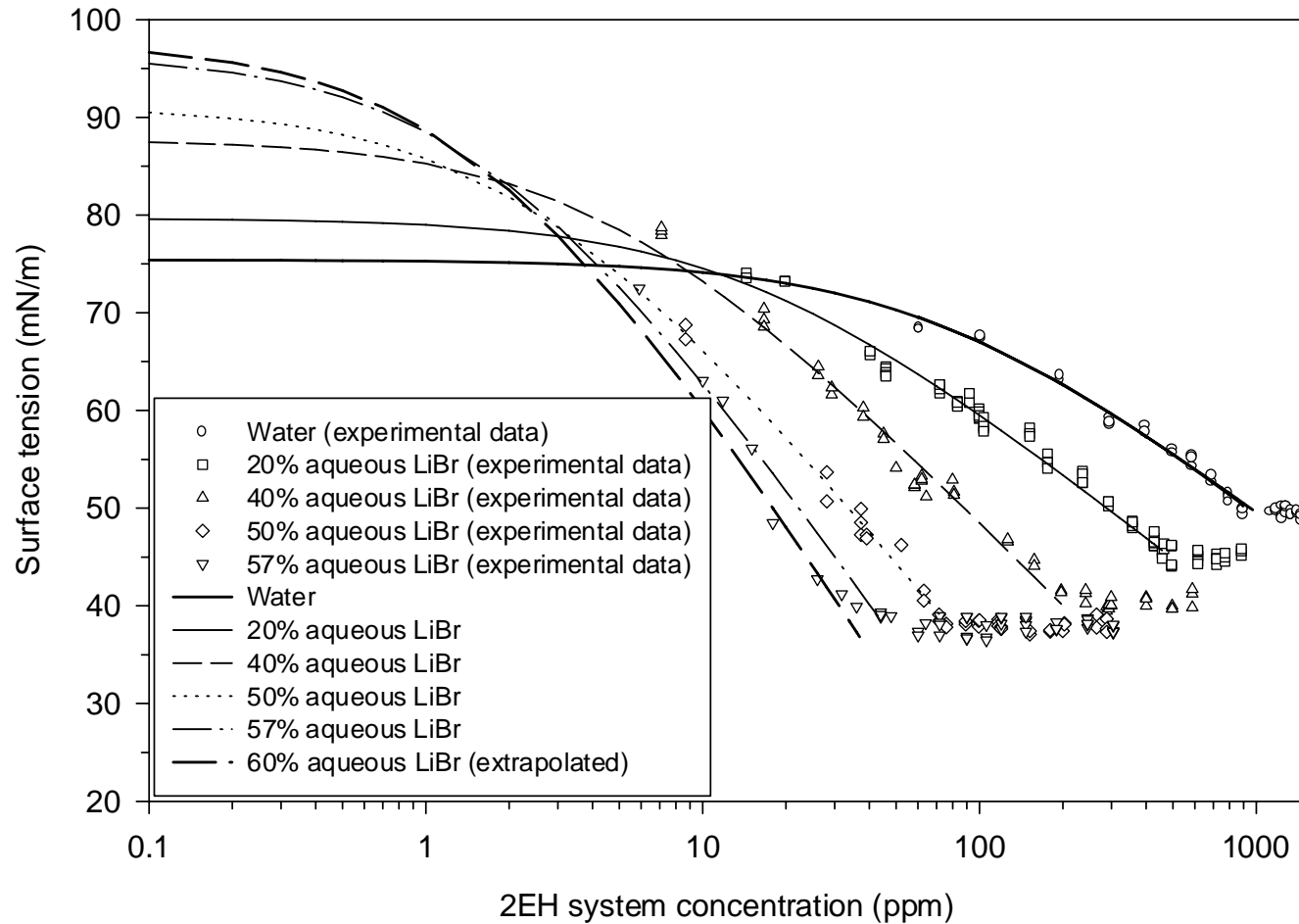


Figure 4.3 Surface tension versus 2EH system concentration for aqueous LiBr

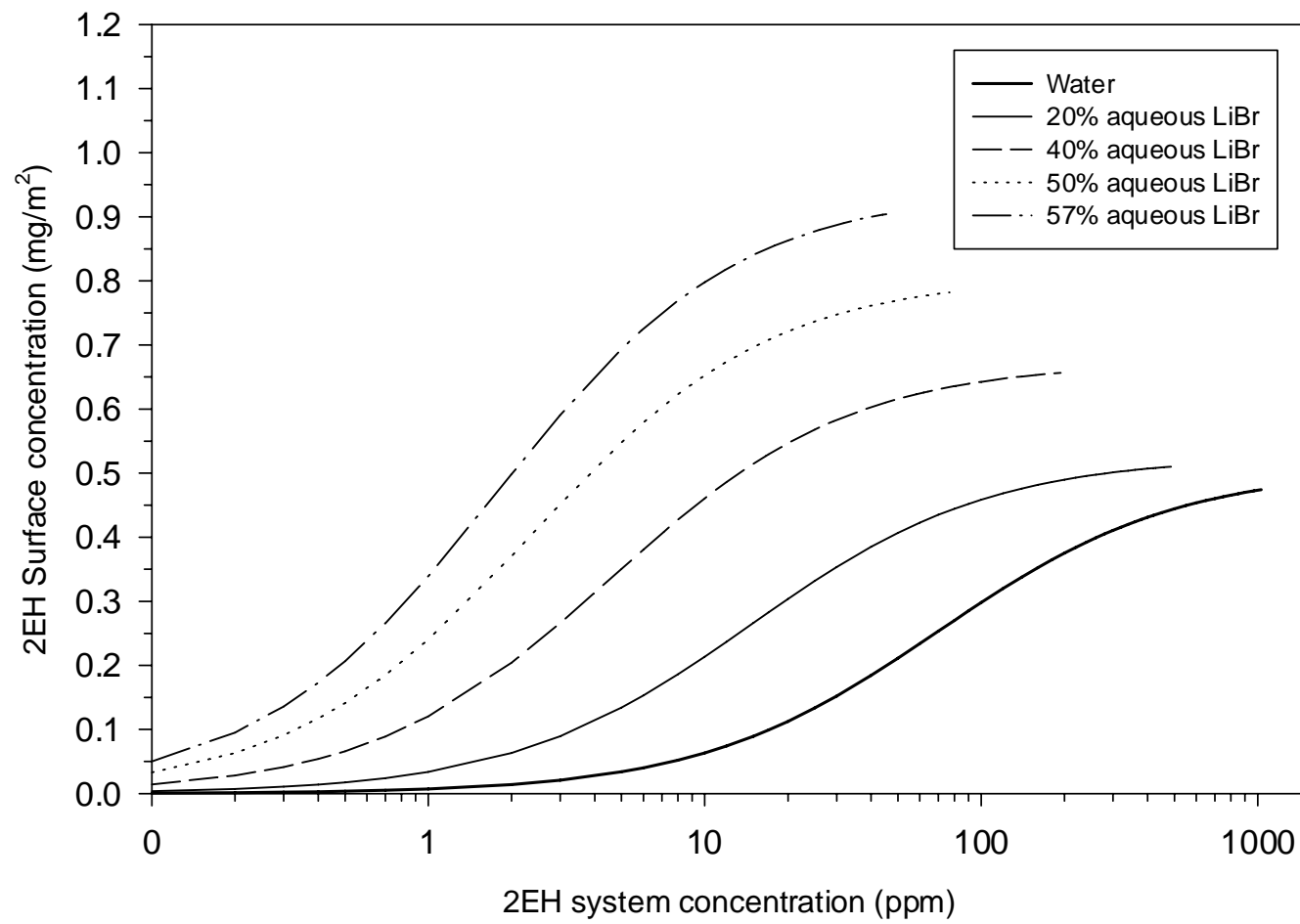


Figure 4.4 2EH surface concentration versus 2EH system concentration for aqueous LiBr

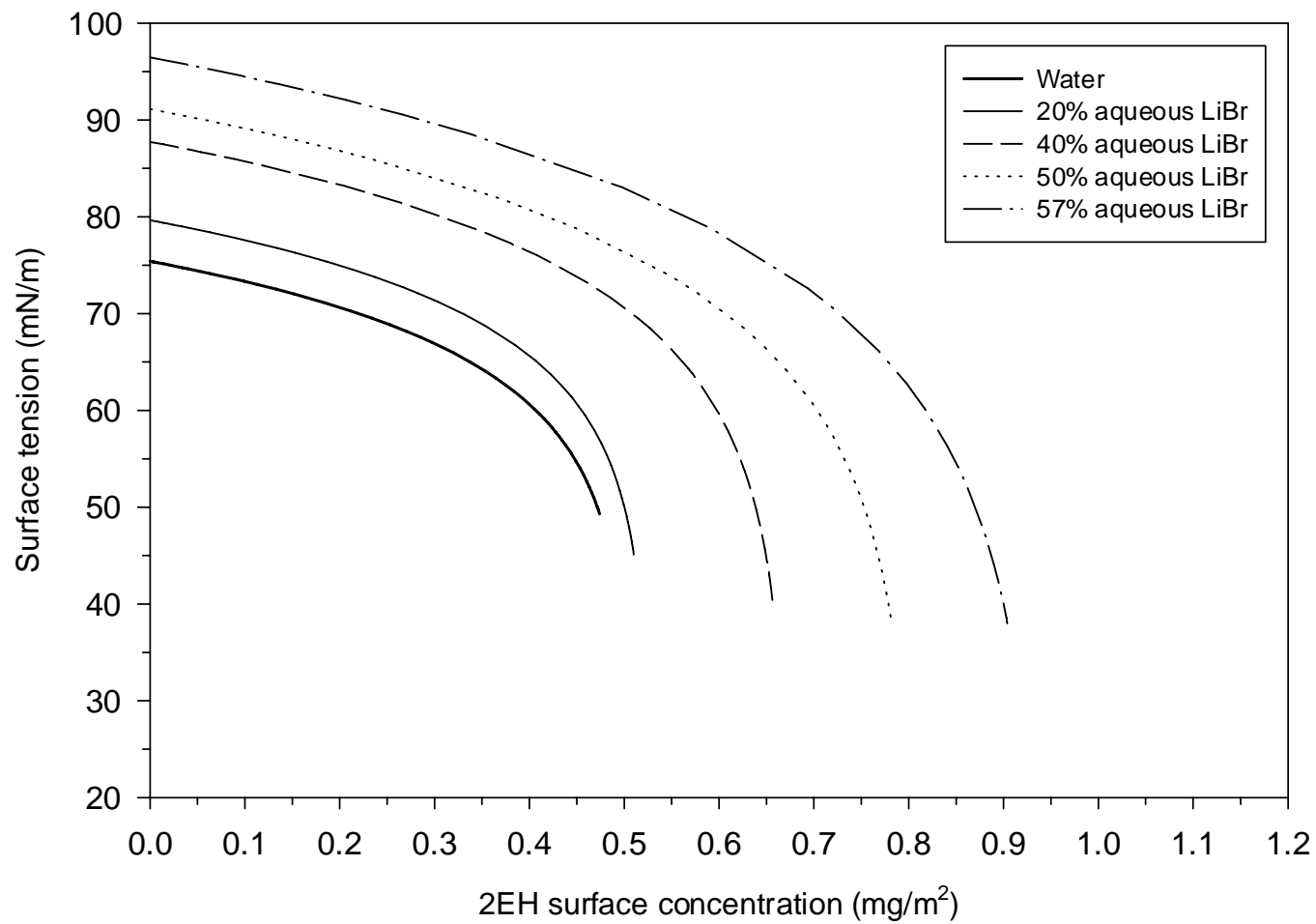


Figure 4.5 Surface tension versus 2EH surface concentration for aqueous LiBr

Table 4.2 2EH saturated surface concentration and solubility limit

	<b>Water</b>	<b>20% LiBr</b>	<b>40% LiBr</b>	<b>50% LiBr</b>	<b>57% LiBr</b>	<b>60% LiBr<sup>(1)</sup></b>
<b>Surface tension plateau (mN/m)</b>	49.3	45.1	40.4	38.1	38.0	36.8
<b>Solubility limit (ppm)</b>	1030	486	194	77	45	37
<b><math>\Gamma_{\text{sat}}</math> (mg/m<sup>2</sup>)</b>	0.474	0.510	0.657	0.782	0.904	0.993
<b>Coefficients in Equation 4.5</b>	a	75.407	79.649	87.733	91.115	96.474
	b	9.4729	9.7742	12.560	15.077	17.825
	c	0.01431	0.06849	0.21792	0.42461	0.56345

(1) Extrapolated results

The increase in saturated 2EH surface concentration with increase in mass fraction of LiBr solution has been observed elsewhere for electrolyte solutions (Rosen, 1989; Schick, 1962). From the point of view of molecular arrangements, this increase in saturated 2EH surface concentration represents a more compressed and tightly packed structure of 2EH molecules on the surface. For non-ionic surfactants like 2EH, the solubility limit can be explained by the extent of hydration of the hydrophilic heads of the surfactant molecules through the formation of hydrogen bonds between the water and the surfactant (Schick, 1962). With the reduction of free water molecules on addition of electrolyte, more surfactant molecules are rejected from the liquid to the surface. The solubility limit of 2EH in aqueous LiBr decreases with the increase of mass fraction of aqueous LiBr. The present results show that the presence of LiBr increases the 2EH surface concentration and this seems to indicate that the hydrophilic part of 2EH has a stronger affinity for the electrolyte surface than it does for the pure water surface. The result of this is that for the same 2EH system concentration, more 2EH is adsorbed on the surface for the aqueous LiBr and hence the surface tension is lower.

## 4.4 Discussion

In the surface tension measurements shown in Figure 4.3, the concentration of 2EH is the system concentration of the sample. The fact that 2EH adsorbs on the walls of the flask makes it difficult to accurately determine the 2EH liquid concentration in this low concentration range. A simple rinsing experiment was done to illustrate this point. The results are plotted in Figure 4.6. After mixing and equilibration of a sample, the surface tension of the sample was measured and then the sample was discarded and a fresh charge of aqueous LiBr was added to the sample flask without cleaning. The sample was then mixed and allowed to equilibrate, and surface tension measurements were run as before. This rinsing sequence was repeated and the surface tension results were examined as a function of the rinsing stage. The results show that after the first rinse, the measured surface tension is close to that found for the original sample. However, after the second rinse, the surface tension rises steadily toward the 2EH free value. This implies that the amount of 2EH clinging to the vessel walls was comparable to the amount of 2EH required to reduce the surface tension to the lowest level ever observed in the system. Thus, when a sample is made at a particular system concentration, the amount of 2EH dissolved in the aqueous LiBr may be as low as half of the system concentration. However, because the actual liquid concentrations are not known, the data in this effort is analyzed as if the system concentration is equal to the liquid concentration (in the range below the solubility limit).

The 2EH surface concentrations in water were calculated based on surface tension data obtained using two different procedures as shown in Figures 4.1 and 4.3. A comparison between the results is shown in Figure 4.7. The results show that the

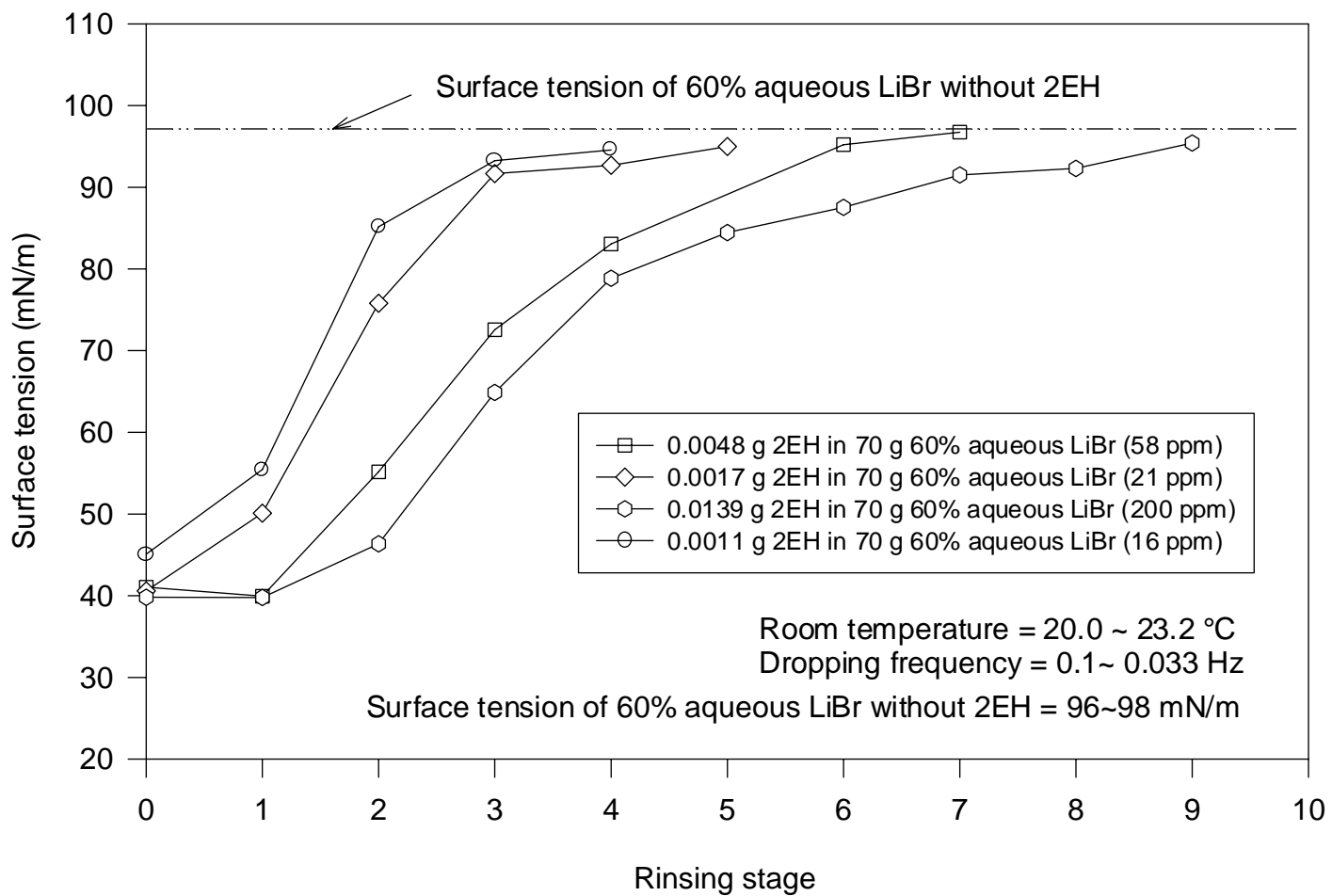


Figure 4.6 Surface tension versus dilution time of sample

saturated surface concentrations are 0.47 mg/m<sup>2</sup> from Zhou et al. (2001) and 0.59 mg/m<sup>2</sup> from my experimental data. The differences are believed to be associated with the approach to equilibrium in the surface tension measurements. The present surface tension data were taken with 2EH in the liquid sample used to form the droplets and 2EH free air flowing past the drops. In this mode, 2EH diffuses from the liquid to the drop surface where it adsorbs on the surface and lowers the surface tension. Although the vapor is clearly not in equilibrium, the values of surface tension obtained seem to indicate that the delivery of 2EH to the surface by diffusion from the liquid is rapid enough so that the surface is relatively close to equilibrium with the liquid. In contrast, the data of Zhou et al. (2001) were taken in a mode that was found useful for aqueous LiBr but extended to water for consistency. This method emphasizes equilibrium between the vapor and the liquid surface and it works well for aqueous LiBr where diffusion in the liquid is very slow but it may not be appropriate for water. The calculated surface concentrations from these two data sets, shown in Figure 4.7, show similar trends. The fact that the surface tension plateau value is lower for the data set with air flowing seems to indicate that this data set is closer to equilibrium.

In order to measure the effect of surfactant system concentration on the surfactant surface concentration, a parameter, symbolized by  $x_{20}$ , is introduced (Rosen, 1989).  $x_{20}$  is a concentration required to produce a 20 mN/m reduction in surface tension. Based on theoretical analysis by Rosen (1989), for most surfactants 20 mN/m reduction in surface tension due to the adsorption of surfactant results in a surfactant surface concentration close to its saturated value (0.84-0.99  $\Gamma_{\text{sat}}$ ). Using this parameter, the strength of adsorption and micellization processes can be further indicated by the ratio of  $x_{\text{sol}}$

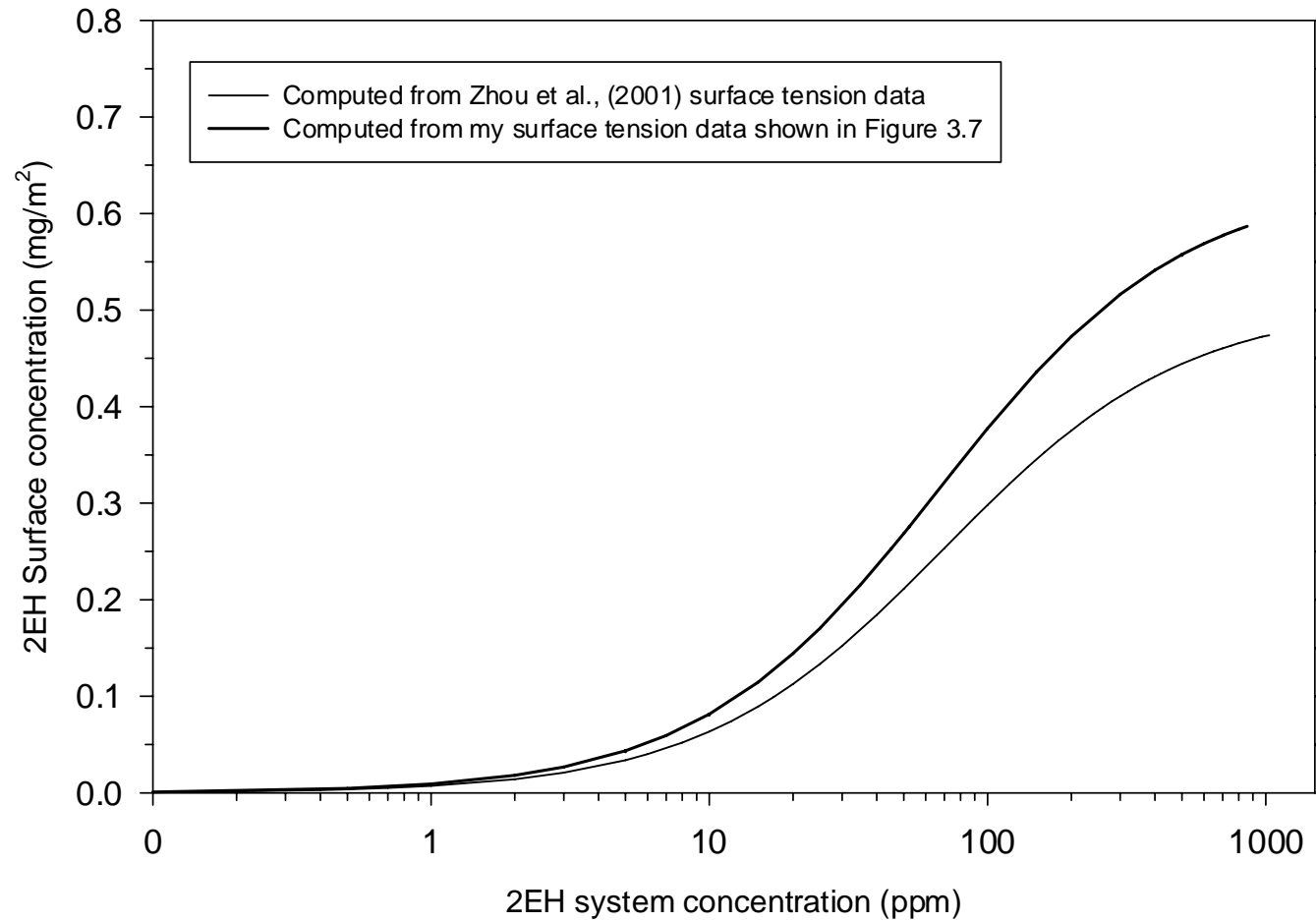


Figure 4.7 2EH surface concentrations for water computed from different surface tension data sources

Table 4.3 2EH system concentration producing a 20 mN/m reduction in surface tension,  $x_{20}$ , and the ratio of  $x_{\text{sol}}/x_{20}$  along with saturated surface concentration and solubility limit

	<b>Water (1)</b>	<b>Water (2)</b>	<b>20% LiBr</b>	<b>40% LiBr</b>	<b>50% LiBr</b>	<b>57% LiBr</b>
<b><math>\Gamma_{\text{sat}}</math> (mg/m<sup>2</sup>)</b>	0.587	0.474	0.510	0.657	0.782	0.904
<b><math>x_{\text{sat}}</math> (ppm)</b>	858	1030	486	194	77	45
<b><math>x_{20}</math> (ppm)</b>	286	507	99	18	6.5	3.7
<b><math>x_{\text{sol}}/x_{20}</math></b>	3.0	2.0	4.9	10.8	11.8	12.2

(1) From Figure 4.1

(2) From Figure 4.3 (Zhou et al. 2001)

(solubility limit)/ $x_{20}$ . A large ratio of  $x_{\text{sol}}/x_{20}$  indicates that after the system concentration reaches  $x_{20}$ , surfactant can still be dissolved in the solvent. Therefore, the micellization is inhibited and adsorption is facilitated. A relatively small ratio of  $x_{\text{sol}}/x_{20}$  indicates that the formation of micelles is facilitated more than adsorption. In the current study, the  $x_{20}$  and the ratio of  $x_{\text{sol}}/x_{20}$  are calculated for all cases. The results are listed in Table 4.3.

The  $x_{\text{sol}}/x_{20}$  ratio increases with the mass fraction of aqueous LiBr, which indicates that the adsorption of 2EH is more favorable than the formation of micelles. Therefore, 2EH molecules are adsorbed on the surface more readily at higher values of mass fraction of LiBr. In addition,  $x_{20}$  is about one-third of the solubility limit or less. This indicates that a small increase in 2EH system concentration results in a large reduction in surface tension and a rapid increase in surface concentration. In other words, the reduction in surface tension is mainly caused by the 2EH surface concentration at low values of system concentration.

Values for 2EH surface concentration versus surface tension for water and aqueous LiBr are shown in Figures 4.2 and 4.5. The results of the surface tension versus 2EH vapor concentration are shown in Figure 3.10. By combining both results, the value

of the 2EH surface concentration corresponding to a certain 2EH vapor concentration in air can be estimated.

Figure 4.8 shows the 2EH surface concentration versus 2EH vapor concentration in air for both water and 60% aqueous LiBr. The curves terminate at the saturated surface concentration. It can be seen from Figure 4.8 that when the 2EH surface concentration reaches the saturation value (the end points of the curves), the 2EH vapor concentrations are 1180 and 615 ppm for water and 60% aqueous LiBr, respectively. Because the mixed air and 2EH vapor density is quite low ( $\approx 1.2 \text{ kg/m}^3$ ), only a small amount of 2EH is required to achieve a certain vapor concentration and the results in Section 3.3.2 show that adding such a small amount of 2EH to the vapor has a dramatic effect on surface tension. This demonstrates the sensitivity of this system to vapor borne surfactant.

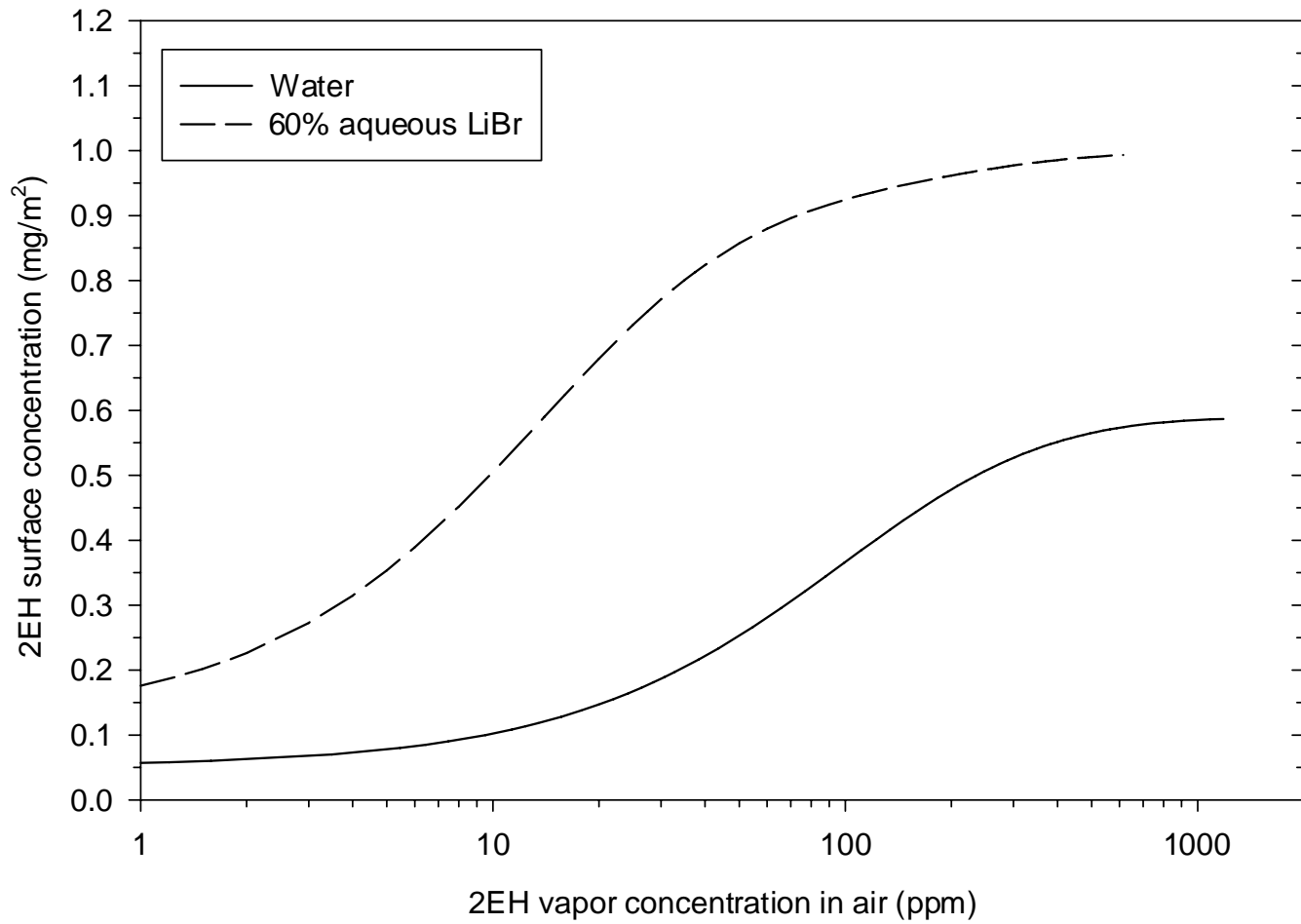


Figure 4.8 2EH surface concentration versus 2EH vapor concentration in air

# **CHAPTER 5**

## **EXPERIMENTAL STUDY OF MARANGONI CONVECTION IN ABSORPTION/CONDENSATION IN THE PRESENCE OF SURFACTANT VAPOR**

### **5.1 Introduction**

The effect of 2-ethyl-hexanol (2EH) vapor on the surface tension was discussed in Chapter 3. It was concluded that the surface tension decreased significantly with an increase in 2EH vapor concentration. Based on surfactant theory, the reduction of surface tension is mainly due to the adsorption of 2EH on the surface. Non-uniform surface concentration implies surface tension gradients that drive Marangoni convection. One of the key aspects of this chapter is the demonstration that non-uniform absorption or condensation results in significant Marangoni flows when 2EH is present in the vapor.

The importance of surfactant vapor can be easily demonstrated in a bench top test. In this test, a 2EH drop was held above the surface of a quiescent pool of aqueous lithium bromide (LiBr) at atmospheric pressure. When the surfactant drop was positioned near the surface, the surface was observed to move away from the point right below 2EH drop. This movement is apparently caused by lower surface tension at the point below the 2EH drop due to adsorption of 2EH vapor from the drop. Similar results were obtained for water although the induced surface motion was found to be weaker than that for aqueous LiBr.

In this chapter, a series of absorption/condensation tests are discussed. These tests were designed to observe Marangoni convection with controlled 2EH vapor concentration in a configuration amenable to modeling. The absorption rates are quantified by recording the pressure history.

## 5.2 Experimental Apparatus and Procedure

### 5.2.1 Description of the Measurement Apparatus

The absorption/condensation pool apparatus consists of a test chamber, cooling system, sample flask, mixing flask, pipe and vacuum system, pressure and temperature transducers and a lighting and video recording system. A schematic of this apparatus and a photograph are shown in Figures 5.1 and 5.2, respectively.

The test chamber, a vacuum vessel that houses the absorption/condensation pool, is made of transparent plastic with diameter (I.D.) by height of  $10 \times 11$  cm. The cover of the vessel is sealed by a rubber O-ring between the cover and the chamber. A glass petri dish (diameter (O.D.) by height =  $9 \times 5.0$  cm) is placed inside this vessel to hold the sample solution. The purpose of using the petri dish was to simplify the cleaning procedure and avoid contact between the LiBr sample and the plastic to prevent chemical attack.

The cooling system consists of a thermoelectric cooler (the cooling capacity varied with liquid pool temperature from 0.6 to 1.1 W), heat sink and a fan. The thermoelectric cooler is installed on the underside of the bottom of the chamber. Thermal grease was applied on both sides of the cooler and thermal grease with a thermal pad were applied between the chamber and the petri dish, to ensure good thermal contact.

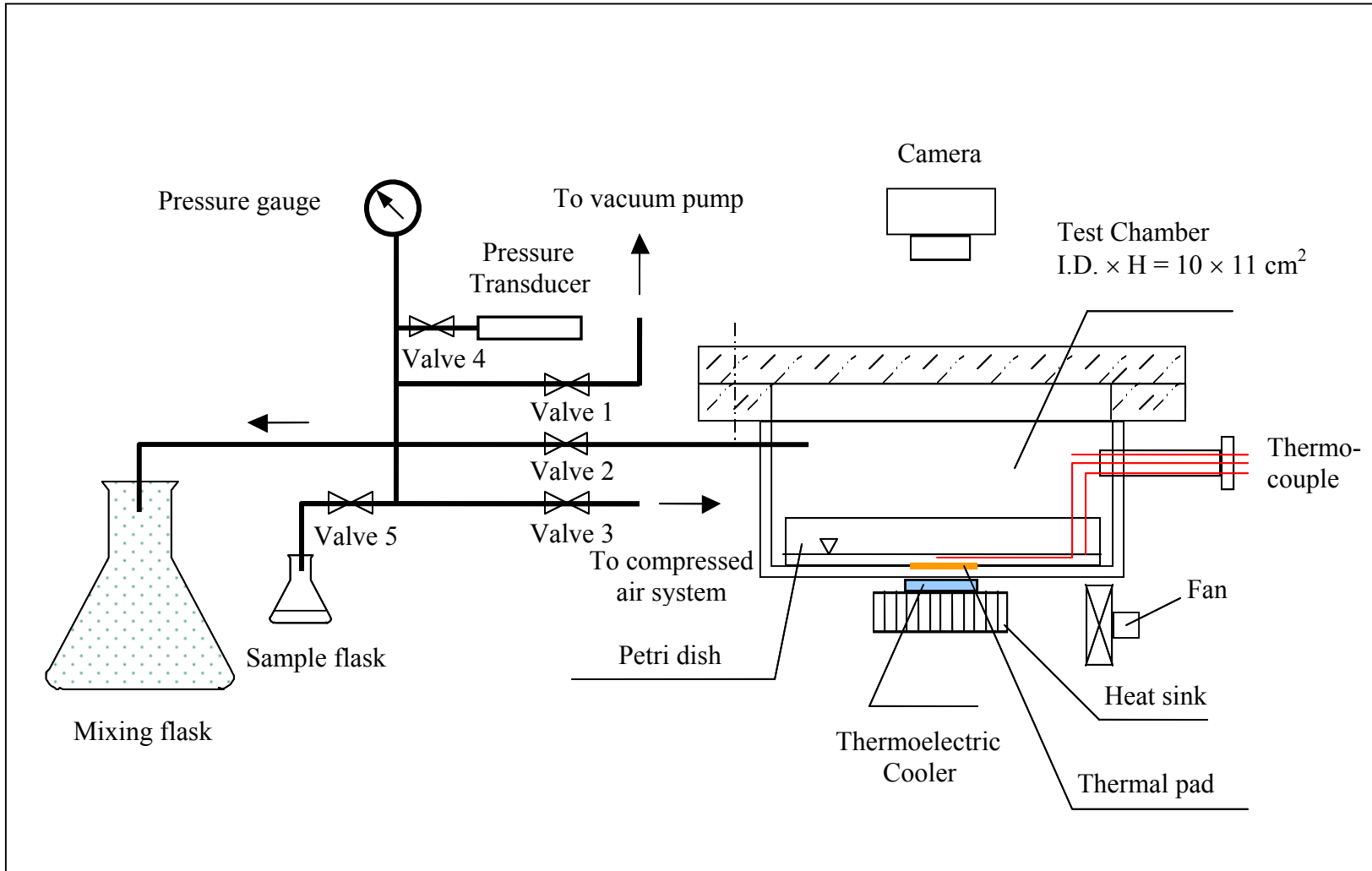


Figure 5.1 Schematic of absorption/condensation pool apparatus

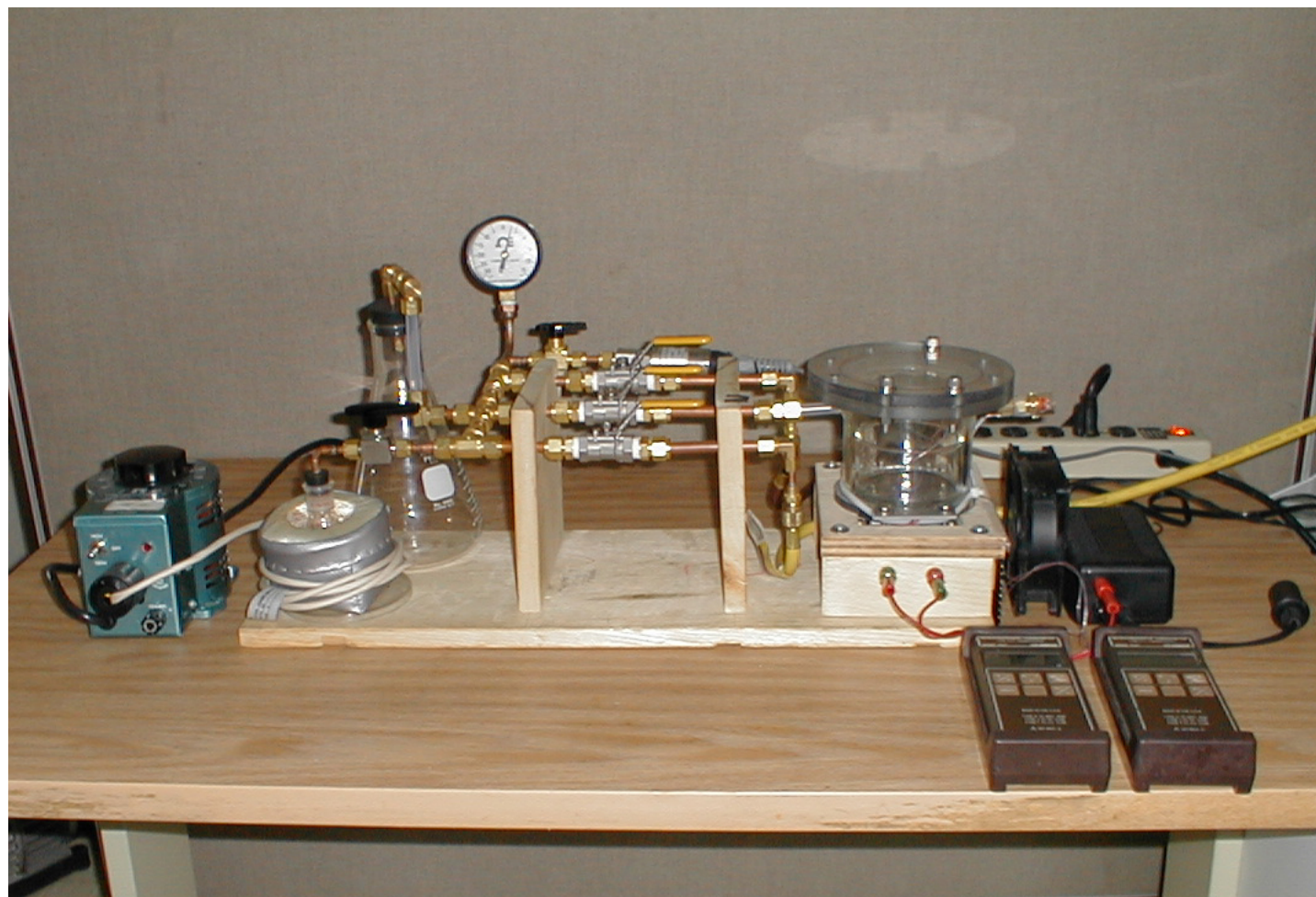


Figure 5.2 A photograph of the absorption/condensation pool apparatus

A sample flask was connected to the chamber to provide controlled amounts of both 2EH and water vapor. The weights of both 2EH and water in the sample flask were measured by a balance with a resolution of 0.1 mg. A heater was used to warm the sample flask to ensure that the sample vaporized totally. The mixing flask provides sufficient volume such that the pressure remains below the saturation pressure at room temperature (this avoids condensation of the sample). The mixing flask is used to store the vapor sample before introduction to the test chamber.

Five valves are used to support different functions during the experiments. The system pressure and temperature are monitored using a pressure transducer with a resolution of 0.1 mmHg and three thermocouples with a resolution of 0.1°C. The thermocouples were positioned at the center, the edge in the solution and the vapor, respectively.

In order to prevent leakage around the thermocouples, the feedthroughs for the thermocouples were cast in a plastic plate (see Figure 5.3) that then was glued on the wall of the chamber, and the thermocouple wires were soldered on the feedthroughs on each end. Because the feedthroughs were copper cylinders, they are expected to be close to isothermal at both ends and thus do not cause errors in the thermocouple circuit.

Flow visualization was achieved by illumination of particles on the liquid surface. The particles are chemically inert silver coated micro-spheres (PQ Corporation, 2001). The particles were initially mixed with the sample solution. After a series of tests, it was found that the best observation effect was achieved with 0.015 g of particles in 30 g of 60% aqueous LiBr or 17.5 g of water. A non-reflecting black paper was placed beneath the petri dish to improve contrast. The camera was positioned over the chamber looking

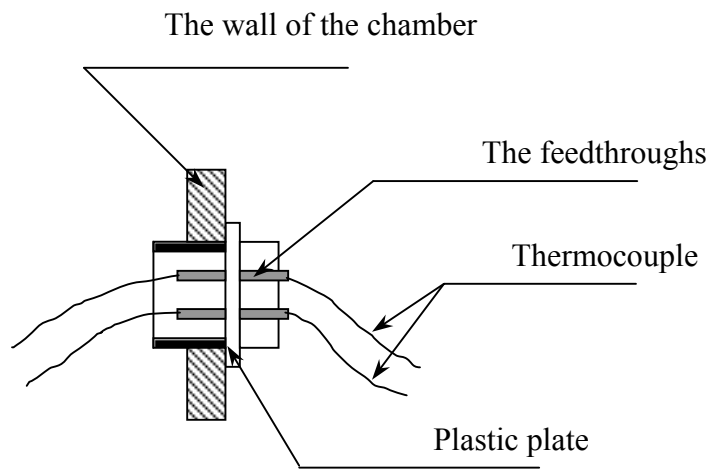


Figure 5.3 Schematic of the connection between the thermocouples and the feedthroughs on the wall of the chamber

down normal to the liquid surface. The images were recorded in VHS video format and transferred to a computer for further processing.

### 5.2.2 Experimental Procedure

The main steps of the experimental procedure are as follows:

1. The system was cleaned by compressed air and detergent water. The piping system was flushed with compressed air for one hour and the sample flask, the mixing flask and the test chamber were rinsed by detergent water to eliminate any 2EH remaining in the system from previous runs.
2. The thermal pad and thermal grease on the upper surface of the plastic plate were checked or replaced if necessary to ensure good thermal contact.
3. The absorption/condensation pool was set up. The petri dish with sample solution was first positioned in the chamber. In order to create a pool with a 3 mm depth in the

petri dish, the sample solution for each run was either 29.2 g of 60% aqueous LiBr (density of 60% aqueous LiBr =  $1.717 \text{ kg/m}^3$ ) or 17.0 g of water. Then the thermocouples were positioned in the solution; one was in the center, one was in the edge of the pool, and another one was in the vapor space, respectively. These thermocouples were fixed by adhesive on the side wall of the petri dish. The liquid sensors were positioned at the mid-height of the liquid layer and the readings are interpreted as the average liquid temperature.

4. 0.015 g of silver coated micro-sphere particles (diameter = 50  $\mu\text{m}$ ) were introduced to the pool and the apparatus was shaken to distribute the particles on the surface and in the liquid uniformly. The cover of the chamber was sealed.

5. A metered amount of 2EH and water were introduced to the sample flask, which was then connected to the system with all valves in the system closed.

6. The camera was mounted above the chamber and connected to the VCR, and two fluorescent lights were placed around the chamber. Clear visualization was achieved by adjusting the lighting angle.

7. The chamber, and the mixing flask and the sample flask were evacuated with a vacuum pump. The chamber and the mixing flask were first evacuated with Valves 5 and 3 closed and then the sample flask was evacuated with Valves 2 and 3 closed. The test section was pumped on until air bubbles stopped rising from the liquid. The evacuation of the sample flask was stopped when the pressure reached 50 mmHg. This pressure was a compromise between limiting the effect of air and avoiding removal of 2EH and water (the saturation pressure of water ranges from 23.8 to 31.8 mmHg when the temperature changes from 25 to 30°C). Because of the small size of the sample flask (5 ml), the air

mass fraction in the sample flask at the end of the evacuation process calculated on the basis of 1 g of water was 0.04%. Based on the analysis by Dai and Zheng (1980), 0.1% air mass fraction causes 1% degradation of the performance in actual machines. Therefore, the effect of this 0.04% of air on the absorption/condensation in the current study is considered negligible (further discussion of this is given in Section 5.3.3).

Because of the significant effect of air in this type of system (Dai and Zhang, 1980; Suzuki, 1996), the system leakage rate was checked before each run. The maximum leakage rate tolerated was 1.2 mmHg/hr (the time needed for one run was about a half hour).

8. The sample flask was warmed by the sample flask heater, with Valve 5 opened and Valve 2 closed, and the sample vapor was delivered to the mixing flask. Thus, unlike the studies by Elkassabgi and Perez-Blanco (1991) and Fujita and Hihara, (1999), the present study introduced 2EH into the absorption/condensation pool from the vapor not from liquid.

9. After Valve 2 was opened, the pressure and temperature readings were recorded and the surface motion was captured on video. During each run, three phases were observed. The first phase was adiabatic absorption/condensation, where no cooling or heating power was applied. This phase started with an initial surface motion when the 2EH vapor was delivered and ended with no surface motion. In the second phase, the thermoelectric cooler was turned on. This phase led to a steady state surface motion with the particles circulating back and forth between the center and the edge of the circulation region. In the final phase, the power to the cooler was reversed to supply heat to the test

section. This phase ended with a motionless surface. A sample data sheet showing details of the procedure is included as Appendix B.

### **5.3 Main Issues in the Experiments**

#### **5.3.1 Preparation of a Vapor Sample**

Preparation of a vapor sample required weighing small quantities of both water and 2EH. In order to obtain the desired pressure, the amount of water was 1 g. The smallest 2EH drop from a syringe needle was about 2.5 mg, which resulted in a 2EH concentration (in 1 g water) of 2500 ppm, which was too high as a starting point. It was found that a smaller drop of about 0.2 mg could be captured on a fine wire (0.02 mm diameter). This allowed preparation of a sample with 200 ppm 2EH.

By vaporizing all of the sample in the sample flask, the 2EH vapor concentration was determined by the liquid sample charged in the flask. To ensure all liquid in the sample flask was vaporized, the liquid was warmed by the sample flask heater. It was determined by weighing the sample flask before and after a run, that the amount of sample left in the sample flask was too small to be measured.

#### **5.3.2 The Effect of Evacuation on the 2EH Concentration**

Two approaches were tried in introducing 2EH to the sample flask. One approach was to evacuate the system first and then introduce 2EH to the sample flask using a syringe. The other approach was to deliver a known amount of water and 2EH to the sample flask first at atmospheric pressure and then connect this flask to the vacuum

system. It was found that the first approach did not work because all of the 2EH in the syringe was sucked into the sample flask under the low pressure condition and thus the amount of 2EH introduced to the flask could not be controlled and determined. Therefore, this approach was not pursued.

In order to use the second approach, the effect of evacuation of the sample flask on the 2EH concentration needed to be quantified. Table 5.1 shows the change of the amount of sample in the sample flask before and after evacuation. During this test of the evacuation procedure, the sample flask was weighed initially, and then the sample flask was pumped down to 50 mmHg (the actual pressure used in the experiments) and weighed again after air was reintroduced into the sample flask such that the pressure in the flask was back to ambient pressure. The difference in weight was a loss of sample during the evacuation process. It was found that the amount of sample evaporated during the evacuation was on the order of 0.005 g. Due to intermolecular forces in the liquid, the 2EH concentration in the vapor would be expected to be lower than that in the liquid. Even if it is assumed that the 2EH vapor concentration is the same as that in the liquid, the evacuation process only resulted in a 0.044% (0.005 g/ 1.14 g) change in the 2EH concentration, which is considered negligible.

Table 5.1 The change of the amount of sample in the sample flask before and after evacuation

	Weight of sample in the sample flask		Weight change (g)
	Before evacuation (g)	After evacuation (g)	
<b>Run 1</b>	1.150	1.146	0.004
<b>Run 2</b>	1.144	1.142	0.002
<b>Run 3</b>	1.124	1.117	0.007

### **5.3.3 The Particles for Visualization**

The particles used in current study were silver coated micro-sphere particles (PQ Corporation, 2001). The diameter and density of these particles are 50  $\mu\text{m}$  and 0.7 g/cm<sup>3</sup>, respectively. Because the size of particles is small and the density is close to that of water, the particles tend to suspend in the liquid bulk or float on the surface. Therefore, the surface movement can be easily visualized when these particles are added to the system.

### **5.3.4 The Cooling System**

The cooling was supplied by a thermoelectric cooler (i.e. cooling chip) (Melcor, 2000). During operation, DC current flows through the cooler causing heat to be transferred from one side to the other and creating a cold side and a hot side. The cooling capacity depends on the configuration of the chip, the electrical input and the temperature on both sides of the chip as follows (Melcor, 2000):

$$Q_C = 2N \left( aIT_C - \frac{I^2 p}{2G} - kG(T_H - T_C) \right) \quad 5.1$$

$$I = \frac{G}{p} \left( \frac{V}{2N} - a(T_H - T_C) \right) \quad 5.2$$

where the coefficients  $a$ ,  $p$ ,  $k$  are known for a particular chip and the voltage,  $V$ , is 12 V. For a particular cooling chip, the configuration parameters  $N$  and  $G$  can be found from the manufacturer. Thus, by substituting Equation 5.2 for the current into Equation 5.1, the cooling is directly related to the temperatures on both sides of the chip. For the present study, the solution temperature and the temperature on the heat sink were measured.

Equations 5.1 and 5.2 were solved for the cooling rate by combining with a heat conduction model of the wall of the vessel and the heat sink plate. It was found that the cooling rate varied from 0.6 to 1.1 W for the tests reported here.

### 5.3.5 Examination of Measurement Accuracy

The system pressure and temperature were measured by a pressure transducer system with a resolution of 0.1 mmHg and a thermocouples system with a resolution of 0.1 °C. The mass of the sample solution was measured using a balance with resolution of 0.1 mg. The estimated uncertainty for the internal energy of the sample solution for a typical run with 30 g of 60% aqueous LiBr is:

$$\Delta u \approx \frac{\partial u}{\partial T} dT = m \cdot Cv \cdot dT = 3.0 \times 10^{-2} \text{ kg} \times 1.8 \frac{\text{kJ}}{\text{kg} \cdot \text{K}} \times 0.1 \text{ K} = \pm 5.4 \text{ J}$$

## 5.4 Absorption of Water + 2EH Vapor in Aqueous LiBr

### 5.4.1 Adiabatic Absorption

At the beginning of each run, the liquid in the solution pool was stationary and the particles were uniformly distributed on the surface. During test preparation Valve 2 (in the line between the absorption/condensation pool chamber and the mixing flask) was closed. Then the valve was abruptly opened and the mixed sample vapor was allowed to flow into the chamber. No cooling was applied during this initial phase of the experiment. The purpose of this phase was to observe the surface movement resulting from adiabatic

absorption in an aqueous LiBr pool. It was found that the observed Marangoni flow depended on the vapor concentration of 2EH and so the observations are keyed to that variable.

#### **5.4.1.1 Adiabatic Absorption with $\geq 2500$ ppm 2EH**

Figure 5.4 shows a typical example of the surface movement for high 2EH vapor concentration. The experiment was conducted with 2EH vapor concentration of 2500 ppm. The series of images show the evolution of the surface with time. At time = -2 sec the pool was static. At time = 0 sec (the moment when Valve 2 was opened), the entire surface began to move. Cellular motion could be observed immediately although it took some time before the surface particles made the cells unmistakable. At time = 40 sec, the cells became very clear. Although not visible in Figure 5.4, in each cell there was a circulation with particles in the liquid bulk moving from the center to the edge of the cell on the surface and back from the edge to the center of the cell under the surface. With time, these cells grew and merged and the surface movement died out. The adiabatic absorption process took about 3 minutes from sample vapor introduction until the surface movement stopped.

As a part of the observations of the surface movement, the pressure histories for several high 2EH vapor concentrations were recorded to quantify the effects of 2EH vapor concentration on the surface movement. Figure 5.5 shows a pressure history at 2EH vapor concentration of 5600 ppm. It should be mentioned that during the measurements, one concern was water condensation in the pipes and the wall of the

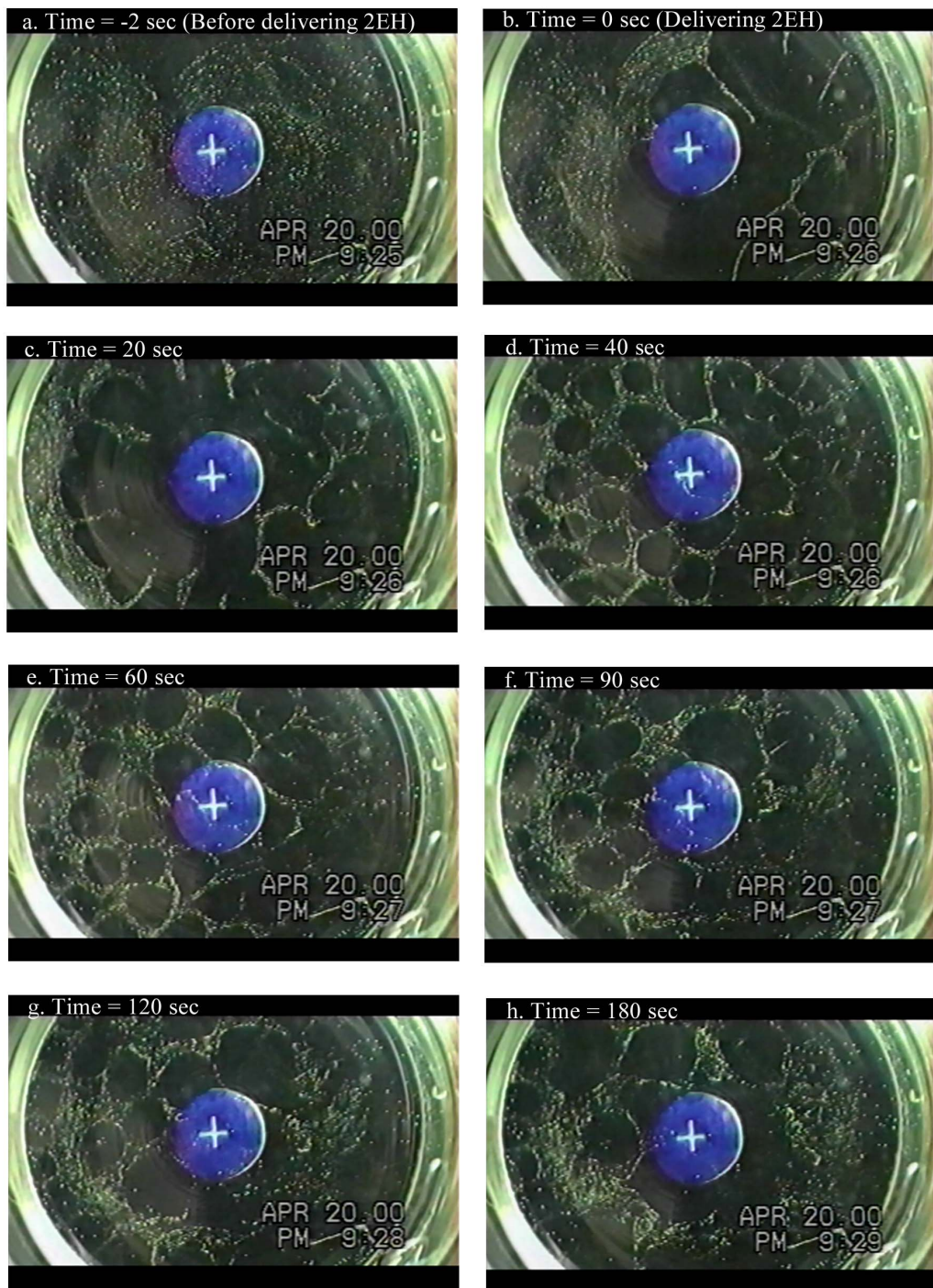


Figure 5.4 Evolution of surface during adiabatic absorption (2EH vapor concentration = 2500 ppm, sample solution = 60% aqueous LiBr)

mixing flask. Therefore, a test was run with no 2EH in the system and no aqueous LiBr in the petri dish, the results of this run are included as the top curve in Figure 5.5. In addition, as a baseline, the pressure with no 2EH in the vapor was measured and the results are plotted. The initial pressure was taken while Valve 2 was closed. In order to reach the same initial pressure in the mixing flask for these runs, the amount of water introduced to the sample flask was close to the same for each (about 1 g).

As can be seen, without absorption the pressure decreased from 26.5 to 25.9 mmHg in 500 sec which is small compared to the pressure changes of interest ( $\sim$  15 mmHg). The test with no 2EH shows a relatively steady decrease with time with a total pressure change of about 11 mmHg in 500 sec. No surface movement was observed in this case, but it is assumed that there was weak natural convection in the pool. In contrast, in the case with 2EH vapor concentration of 5600 ppm, the pressure decreased more quickly. The multi-cell flow pattern was observed in this case.

The multi-cell pattern is believed to be caused by weak Marangoni convection coupled with natural convection. The Marangoni convection was caused by adsorption of surfactant (2EH) on the liquid surface as 2EH molecules arrived with the water vapor (it is noted that the liquid was 2EH free initially). When the sample vapor entered the vessel, absorption of water vapor began accompanied by adsorption of 2EH on the liquid surface. Marangoni convection driven by adsorbed 2EH amplifies spatial non-uniformities by bringing fresh solution to the surface at locations of high absorption. Under low-flux absorption conditions such as adiabatic absorption, this leads to a cellular convection. The boundary of each cell was constrained by adjacent cells. As seen in Figure 5.4, the particles collected between the cells where the surface flows

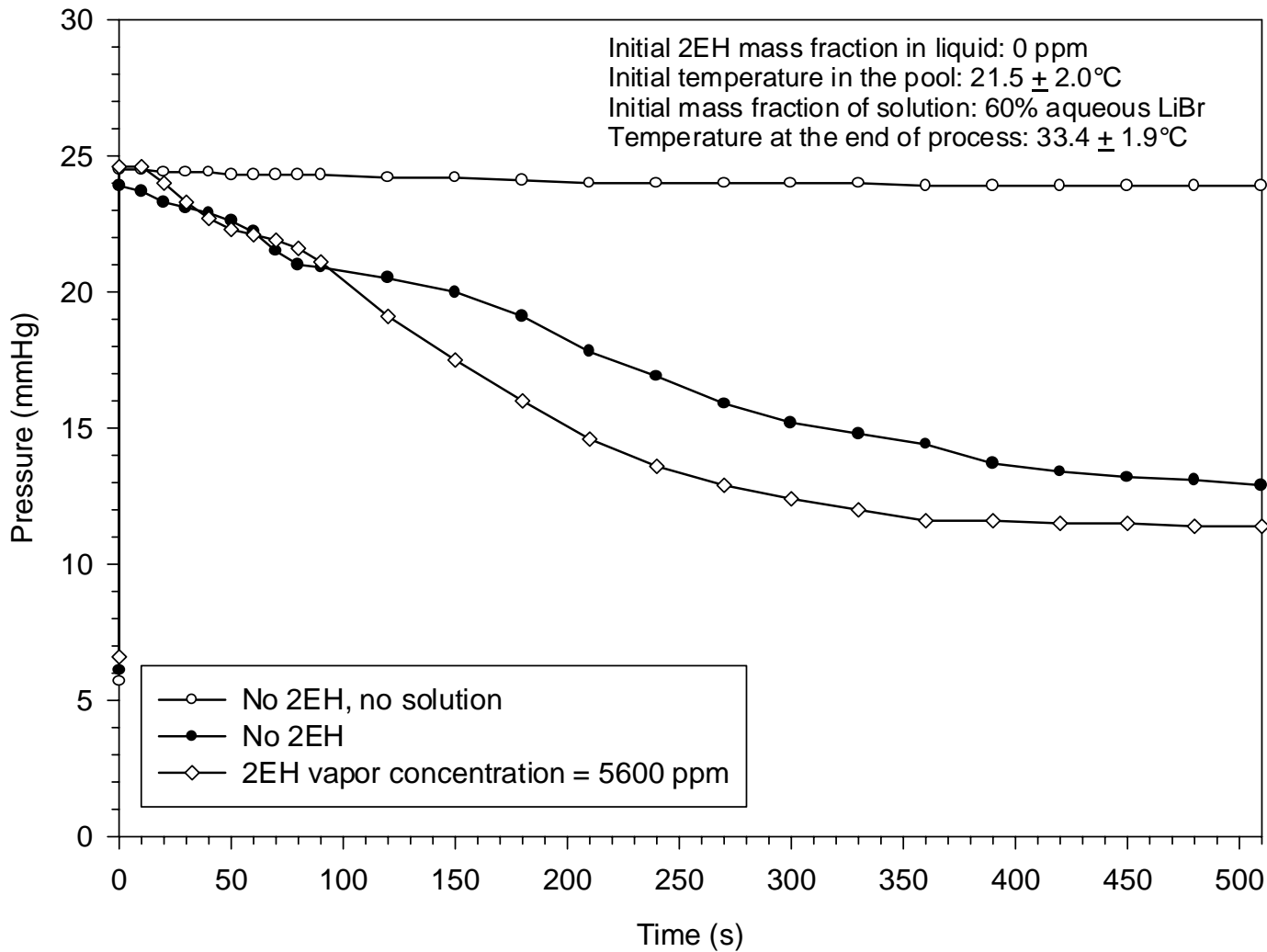


Figure 5.5 The pressure history during adiabatic absorption for high 2EH vapor concentrations

collided. When the 2EH concentration is higher than 1500 ppm, relatively low absorption rates were observed and this is attributed to increased vapor side mass transfer resistance. When the 2EH vapor concentration is very high (>15000 ppm), only weak Marangoni flow was observed.

#### **5.4.1.2 Adiabatic absorption with 400-1500 ppm 2EH**

The surface flow in adiabatic absorption with a vapor concentration of 400 ppm 2EH is illustrated in Figure 5.6. The pressure histories for 2EH vapor concentrations of 400 and 1500 ppm are shown in Figure 5.7. For comparison, the pressure histories for the cases shown in Figure 5.5 are also included in this figure. In Figure 5.6 it can be seen that the flow features before 20 sec are similar to the high 2EH vapor concentration case shown in Figure 5.4. When the vapor sample was introduced to the vessel (the moment defined as time = 0 sec), the multi-cell surface movement started. For 2EH concentration in the range 400 – 1500 ppm, the multi-cell pattern organized faster because the surface velocities were higher. For these cases, the velocity continued to increase and ultimately the multi-cell pattern broke down into a much less organized flow involving the entire surface of the pool (from time = 40 sec). Particles suspended in the liquid were observed to move rapidly (~ 2 cm/sec) and apparently randomly.

In addition, a rapid decrease in the pressure was also observed beginning around 40 to 50 sec as seen in Figure 5.7. This corresponded to the time when the multi-cell flow broke up and vigorous surface motion was observed. The pressure drops observed in the cases with 2EH concentration of 400 to 1500 ppm were much faster than for the case with high 2EH concentration (5600 ppm).

The breakdown of the multi-cell flow is apparently due to strong Marangoni flow. Initially the absorption flux is relatively low and the multi-cell pattern appears. As time goes on, the absorption rate increases due to stronger Marangoni flow. This process finally stops because the pressure drop implies a lower absorption driving potential. When the 2EH vapor concentration is lower than 200 ppm, no Marangoni flow was seen. For those cases, absorption was slow and steady and assumed to be accompanied by weak natural convection in the liquid.

An estimate was done to determine the amount of 2EH delivered to the surface, and the resulting surface concentration was compared with the saturated surface concentration. In this calculation, it was known that for 60% LiBr solution the solubility of 2EH in the liquid is 27 ppm (Section 3.4) and the 2EH saturated surface concentration is  $1 \text{ mg/m}^2$  (Section 4.3.2). Therefore, the amount of 2EH needed to reach the solubility limit and the saturated surface concentration is known (the mass of LiBr solution = 30 g, the surface area of the pool =  $54 \text{ cm}^2$ ) are  $0.81 \text{ mg}$  ( $30 \text{ g } 60\% \text{ LiBr solution} \times 27 \text{ ppm} = 0.81 \text{ mg}$ ) and  $5.4 \times 10^{-3} \text{ mg}$ , respectively.

$$m_{sol} = m_s x_{sol} = 30 \text{ g} \cdot 27 \text{ ppm} = 0.81 \text{ mg}$$

$$m_{sur} = A_{sur} \Gamma_{2EHin60\%LiBr} = 5.4 \times 10^{-3} \text{ m}^2 \cdot 1 \frac{\text{mg}}{\text{m}^2} = 5.4 \times 10^{-3} \text{ mg}$$

For the high 2EH vapor concentration case (2EH vapor concentration = 2500 ppm), the solution temperatures before delivering the sample vapor and when the multi-cell flow died out were 21.5 and  $33.5^\circ\text{C}$ , respectively. Thus it was calculated that the increase of internal energy of the solution during this phase was 670 J. Based on an energy balance, this energy implies that the amount of water vapor absorbed in the pool

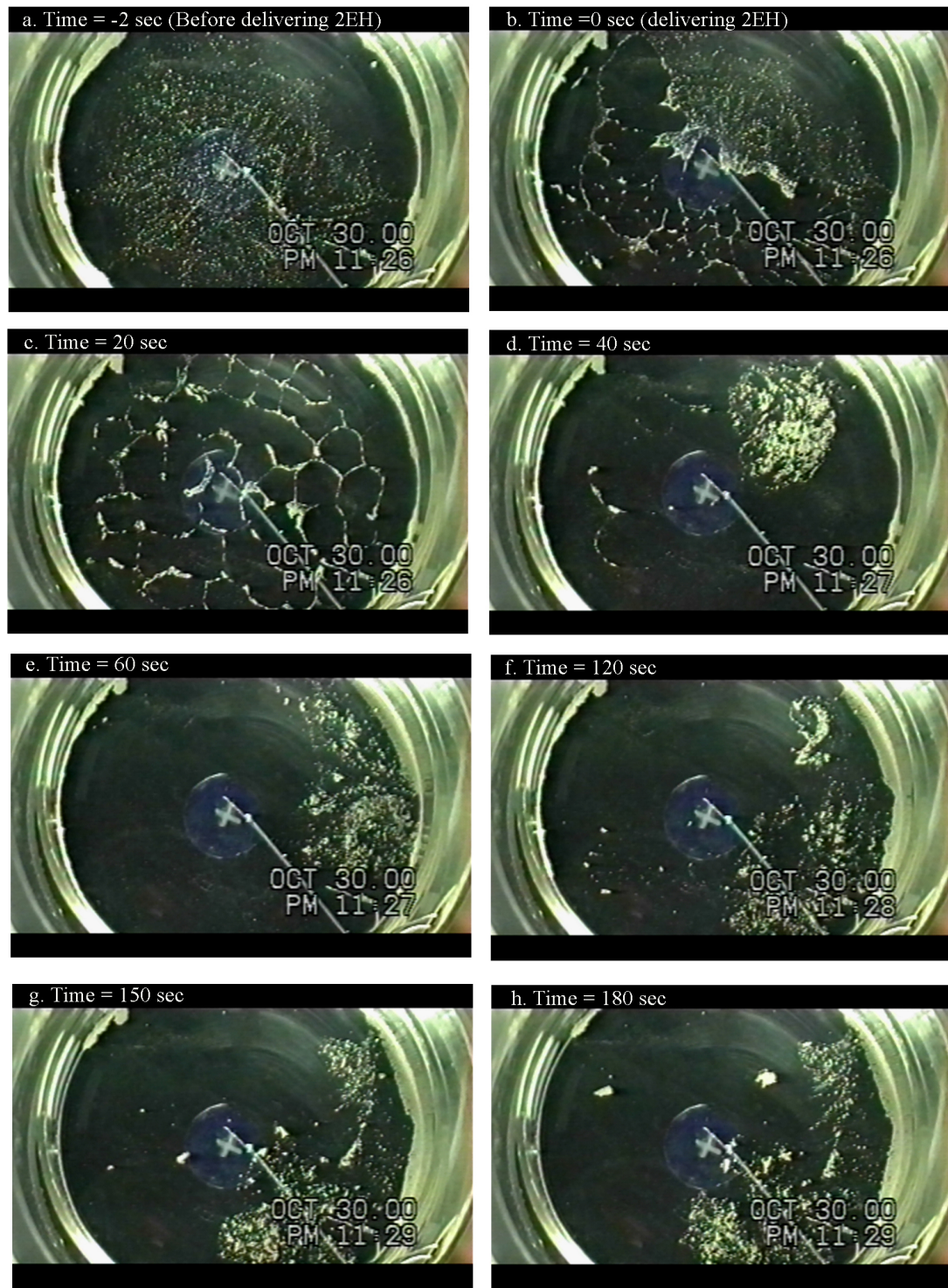


Figure 5.6 Evolution of surface during adiabatic absorption (2EH vapor concentration = 400 ppm, sample solution = 60% aqueous LiBr)

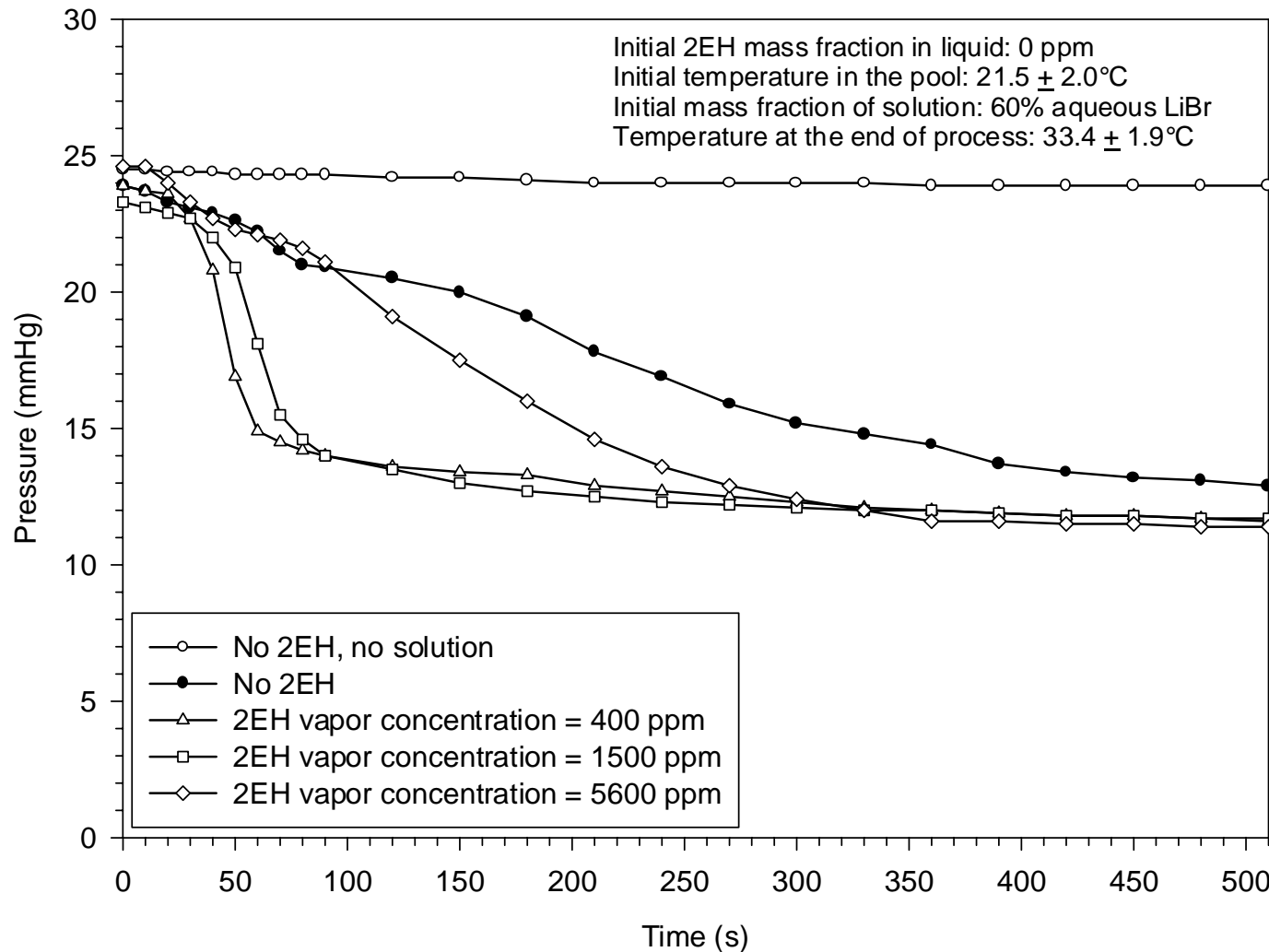


Figure 5.7 The pressure history during adiabatic absorption including low 2EH vapor concentrations

was about 0.28 g. If the 2EH vapor was mixed with water vapor uniformly and if it changed phase like azeotrope without leaving an excess of one constituent behind in the vapor, then the amount of 2EH vapor absorbed in the pool along with water vapor was 0.7 mg. This amount is very close to the amount of 2EH needed to reach the solubility limit and the saturated surface concentration (0.81 mg). For comparison, a similar calculation was done for the low 2EH vapor concentration case (2EH vapor concentration = 400 ppm) and it was found that the amount of 2EH transferred to the pool during the time period from the start of the test to the time when the multi-cell flow broke up was 0.3 mg, which was much smaller than the amount of 2EH needed to reach the saturation point (0.81 mg).

Therefore, it is concluded that the break-up of the multi-cell flow can be explained as follows. If the 2EH vapor concentration is in the range of 400 to 1500 ppm, the 2EH concentration in the liquid does not reach the solubility limit and 2EH surface concentration does not reach the saturated surface concentration after the multi-cells flow breaks up. Thus, as the absorption flux increases the Marangoni forces increase until they pass the critical value that allows the multi-cell structure to exist. The absorption rate was significantly enhanced by the vigorous Marangoni flow, as shown by the pressure decrease and this point is discussed further in Section 5.6.

In addition, the time period during which multi-cell motion was observed was much different between high and low 2EH vapor concentration cases. It was found that the multi-cell motion in the high 2EH vapor concentration case (180 sec at 2500 ppm in Section 5.4.1.1) lasted much longer as compared to the low 2EH vapor concentration case (40 sec at 400 ppm in Section 5.4.1.2). This is attributed to the effect of 2EH saturation

surface concentration. At high 2EH vapor concentration, the 2EH surface concentration reached the saturation surface concentration quickly and therefore, the absorption of water was slow after the surface was saturated and the duration of the multi-cell pattern was longer. By comparison, in the low 2EH vapor concentration case, the surface concentration remained below the saturated condition until the surface motion destabilized under the influence of larger surface concentration gradients.

Suzuki et al. (1996), Morrison and Deans (1997) and Morrison et al. (1998) also found a decrease of absorption and condensation rates with too high vapor concentration. They attributed this reduction to the vapor side mass transfer. Based on the measurements of the pressure history and the observations of the surface movement in the present study, it is believed that the absorption rate during the multi-cell flow is smaller than that accompanying the vigorous surface motion. Because no surface movement was observed both with no 2EH and very high 2EH vapor concentration (7800 ppm), it is expected that there is an optimal 2EH vapor concentration that maximizes Marangoni convection and absorption rate. Near the optimal 2EH concentration, large surface tension gradients form during absorption and the 2EH vapor mass transfer resistance is small. If the 2EH vapor concentration is above this optimal concentration, the 2EH mass transfer resistance limits the absorption rate.

#### **5.4.2 Absorption with Cooling**

After the surface movement associated with adiabatic absorption stopped ( $\sim 500$  sec) for the case with 2500 ppm 2EH, the apparatus was shaken to redistribute the particles uniformly on the surface of the pool, and then cooling was applied (the cooling

power varied with the solution temperature from 0.6 to 1.1 W). The purpose of this experiment was to observe surface movement due to spatially non-uniform cooling.

Figure 5.8 is a typical series of images from one of the cooling experiments. This experiment was conducted with a 2EH vapor concentration of 2500 ppm. It was found that at time = -2 sec, the particles are uniformly distributed and motionless. At time = 0 sec (defined as the beginning of the surface movement, which happened 65 sec after the cooling was turned on), a surface movement was observed near the edge of the cooling chip. At time = 1 sec, a particle free circular region formed near the center of the pool. The average surface speed from 0 to 1 sec was estimated to be 1 cm/s (note: the diameter of the thermal pad is 1.5 cm). From 2 to 60 sec, the surface changed continuously with the diameter of the particle free circle increasing until reaching a steady state diameter of 4 cm. This surface movement appeared as a single cell, in contrast to the multi-cell case described in Section 5.4.1. After the particles floating on the surface stopped moving at 60 sec, the flow below the surface was still in motion as particles could be seen moving. They moved from the center toward the edge near the surface with a speed of approximately 0.5 cm/s and then moved back from the edge to the center underneath the surface with a speed of approximately 0.25 cm/s.

For these cases with cooling, the surface movements observed over the range of 2EH vapor concentrations from 600 to 4600 ppm showed similar features. Figure 5.9 shows another example, also at 2500 ppm, which shows a small variation in the flow pattern. The surface movement began 36 sec after the cooling was turned on in this case. It is seen that two cells formed around the edge of the cooling chip, visible at 1 sec, and then the cells appeared to merge starting at 2 sec. The other features were similar to that

in the example shown in Figure 5.8. Figure 5.10 shows another variation. The surface movement began about 30 sec after the cooling was turned on. At time = 0 sec (defined as the beginning of the surface movement), a surface movement was observed near the edge of the thermal pad, which began to move away from the center. At the same time, the particles located near the circumference of the petri dish detached and moved toward the center. After some time, the particles accumulated in an annulus visible from approximately 5 sec on. This movement from the circumference toward the center was apparently caused by condensed water and 2EH on the petri dish wall, which reduced the surface tension near the wall causing a surface tension force toward the center.

A cooling test was conducted without 2EH in the vapor. Before cooling was applied, the solution temperature was 30.2°C due to adiabatic absorption done first. At 30 min after the cooling was applied, the temperature was 20.3°C at the center and 25.0°C at the edge of the pool. During this 30 min period, the pressure decreased from 25.5 to 22.9 mmHg and no surface movement was observed. Natural convection would be expected to cause surface movement from the edge to the center of the pool since it was cooled in the center at the bottom, but such flow was not observed. Therefore, it is concluded that natural convection is not very strong in this system.

For the case with 2EH in the vapor, the explanation for the single cell surface movement observed with cooling is proposed as follows. When the solution was cooled in the center of the pool, the localized cooling caused more water vapor absorption and this brought 2EH to the surface locally. The 2EH surface concentration increased causing the surface tension to be lower in this center range compared with near the edge of the pool. The surface tension gradient exerts a surface force which drives the particles toward

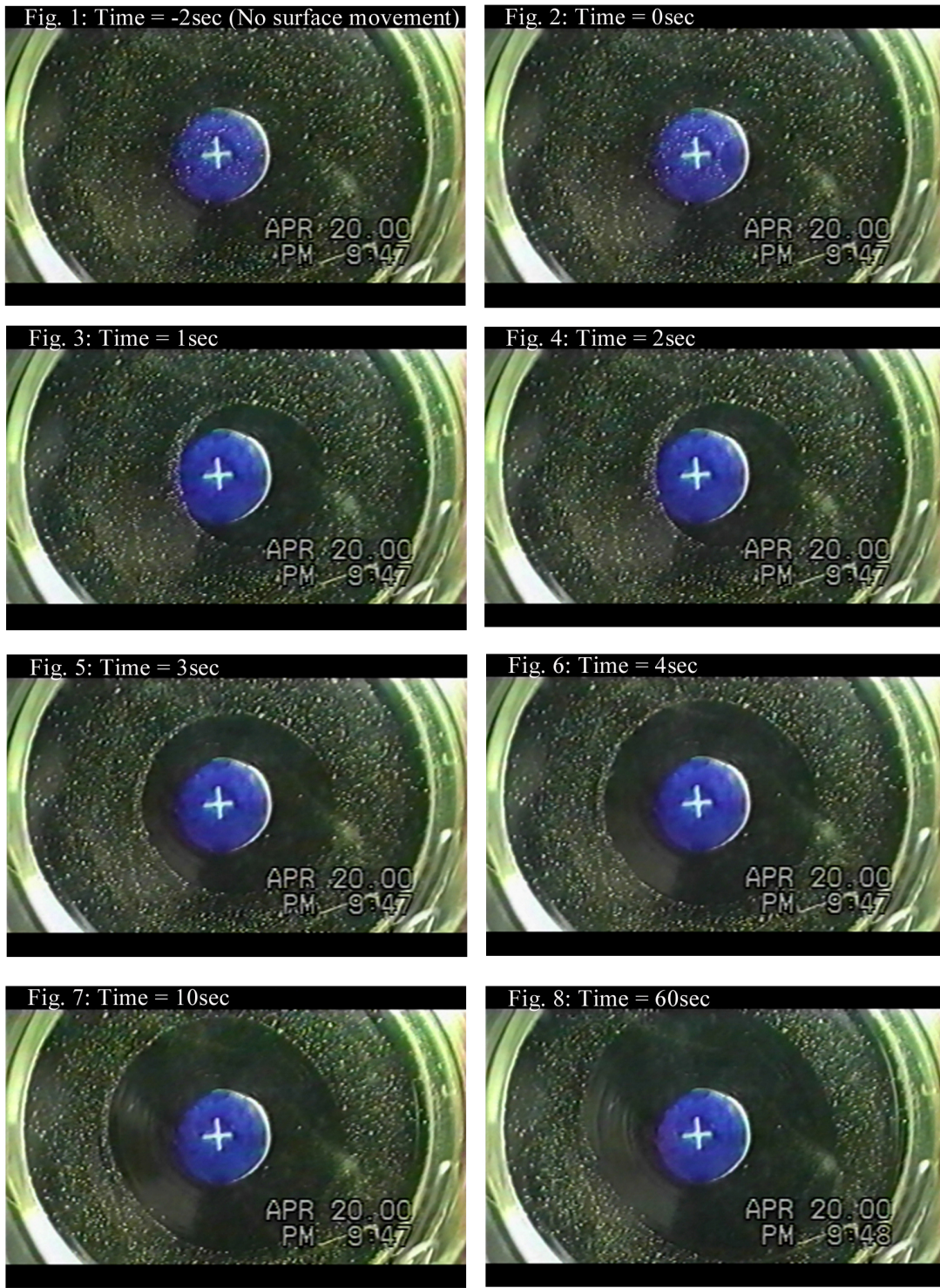


Figure 5.8 Evolution of surface with cooling from the center underneath the pool (2EH vapor concentration = 2500 ppm, sample solution = 60% aqueous LiBr)

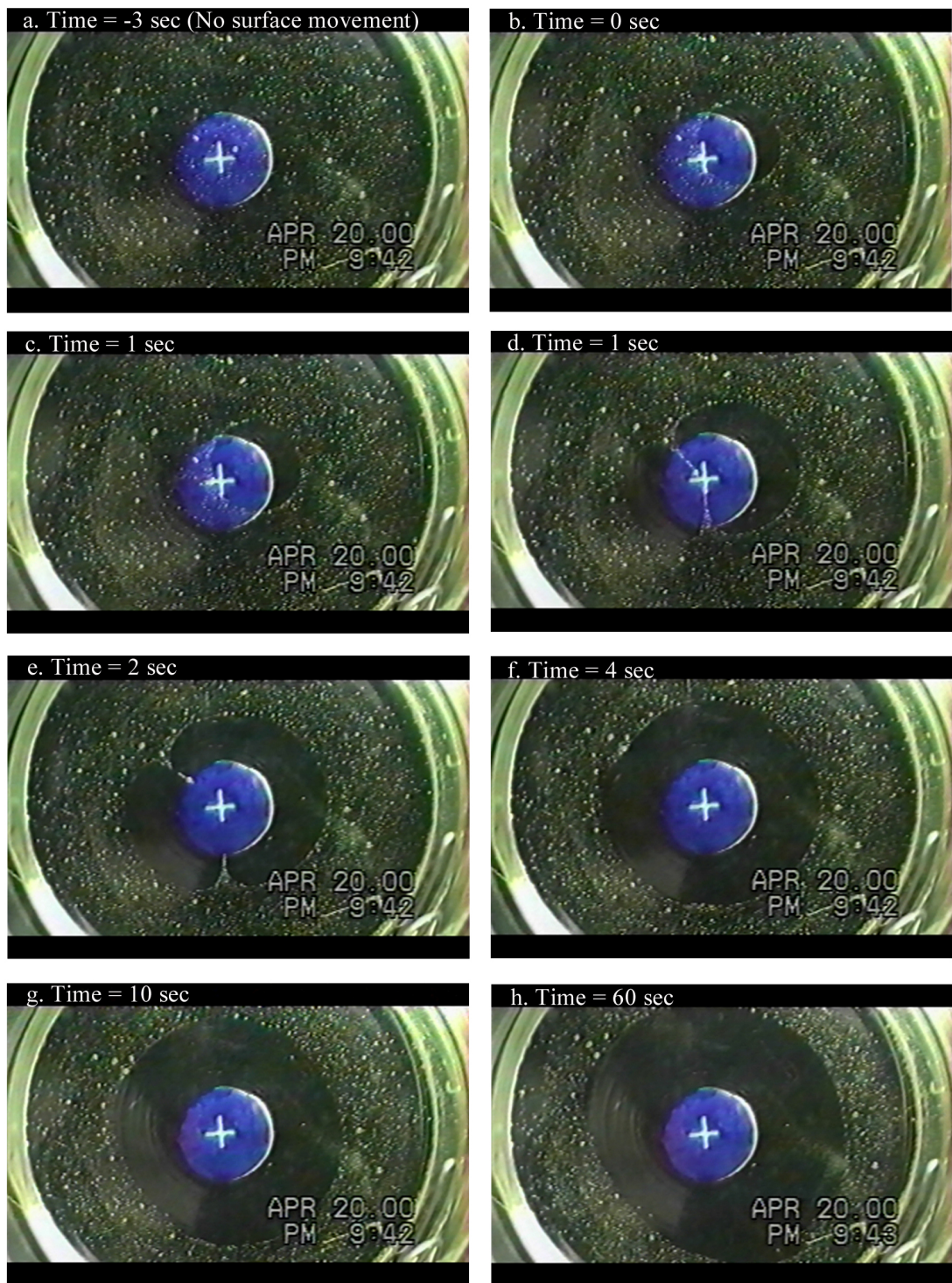


Figure 5.9 Evolution of the surface with cooling from the center underneath the pool showing two cells at 1 sec (2EH vapor concentration = 2500 ppm, sample solution = 60% aqueous LiBr)

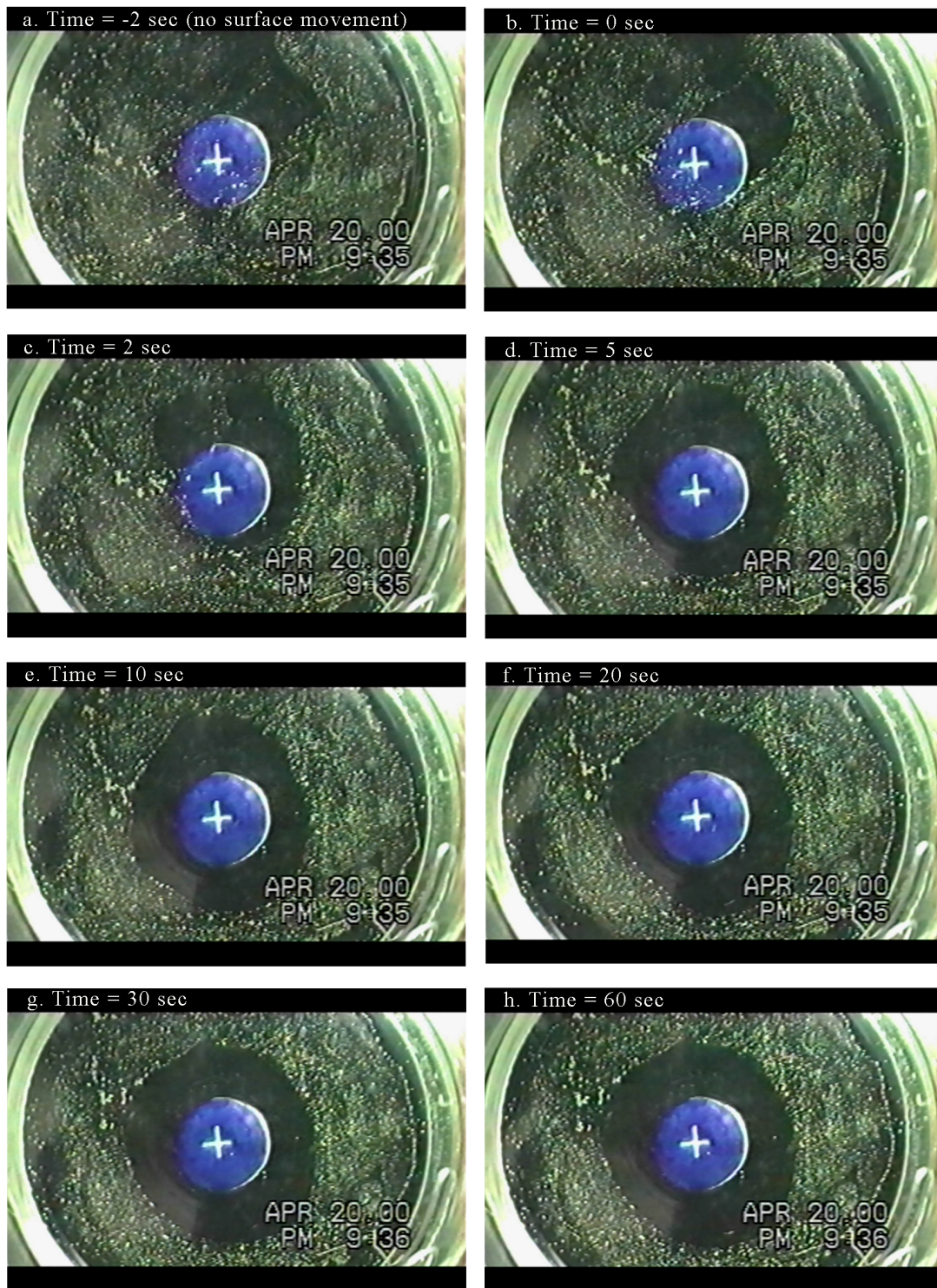


Figure 5.10 Evolution of the surface with cooling from the center underneath the pool showing an annulus ring at 60 sec (2EH vapor concentration = 2500 ppm, sample solution = 60% aqueous LiBr)

the pool edges. As sketched in Figure 5.11, it was observed that after the surface particles stopped expanding, submerged particles continued to circulate in an annular ring whose I.D. is the cooling chip and whose O.D. is the surface particle perimeter. In the center area above the cooling chip, the flow was very weak like a dead zone.

The detachment of particles located near the circumference of the petri dish is believed to be due to condensation of vapor on the wall of the petri dish. When the condensate flows into the pool, it lowers the surface tension at the edge of the Petri dish resulting in the flow from the edge toward the center for cases with cooling.

### 5.4.3 Evaporation with Heating

Surface movement was also observed when the solution was heated (instead of cooled) in the center after the multi-cell motion died out. In this kind of experiment, the

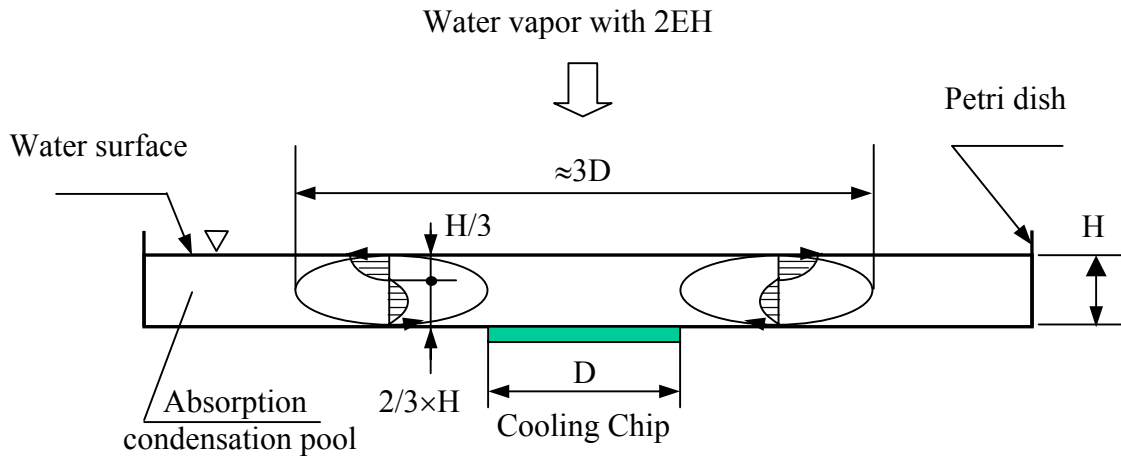


Figure 5.11 Cross sectional schematic of the pool showing recirculating flow to explain surface clearing seen in Figures 5.8 to 5.10

heating was achieved by the same thermoelectric chip by reversing the polarity of the power connection to the chip. The purpose in conducting this experiment was to observe the differences in the surface movements over a range of conditions.

Figure 5.12 shows an example of this surface movement. The 2EH vapor concentration was 2500 ppm. The heat applied by the thermoelectric chip can be calculated based on the solution temperature. The minimum and maximum heat applied in the duration of observation (5 min) were 1.5 and 5.2 W and corresponding average heat in this duration was 2.9 W.

Before the heat was applied, the particles were distributed on the surface uniformly. At time = 0 the heat was applied. The surface remained stationary until time = 2 min 30 sec, when a very slow movement from the edge of the pool toward the center was observed. From 2 min 30 sec to 3 min, the particle distribution caused by surface motion was different from that seen with cooling. The speed of the particles was about 0.1 mm/s, which was very slow compared with the cooling cases described in Section 5.4.2 (10 mm/s). At time = 3 min, the temperatures in the center and the edge of the pool were 31.6 and 26.5°C, respectively. Around time = 3 min 30 sec, a distinct second surface movement was observed. Although this movement was also from the edge toward the center of the pool, a clear difference was that the particles detached from the wall of the petri dish in this second movement. The speed of the particles in this second movement was 0.5 mm/s. The particles in the second movement did not mix with the particles in the first movement and instead surrounded the particles from the first movement and formed an annular ring. After 5 min the surface movement stopped.

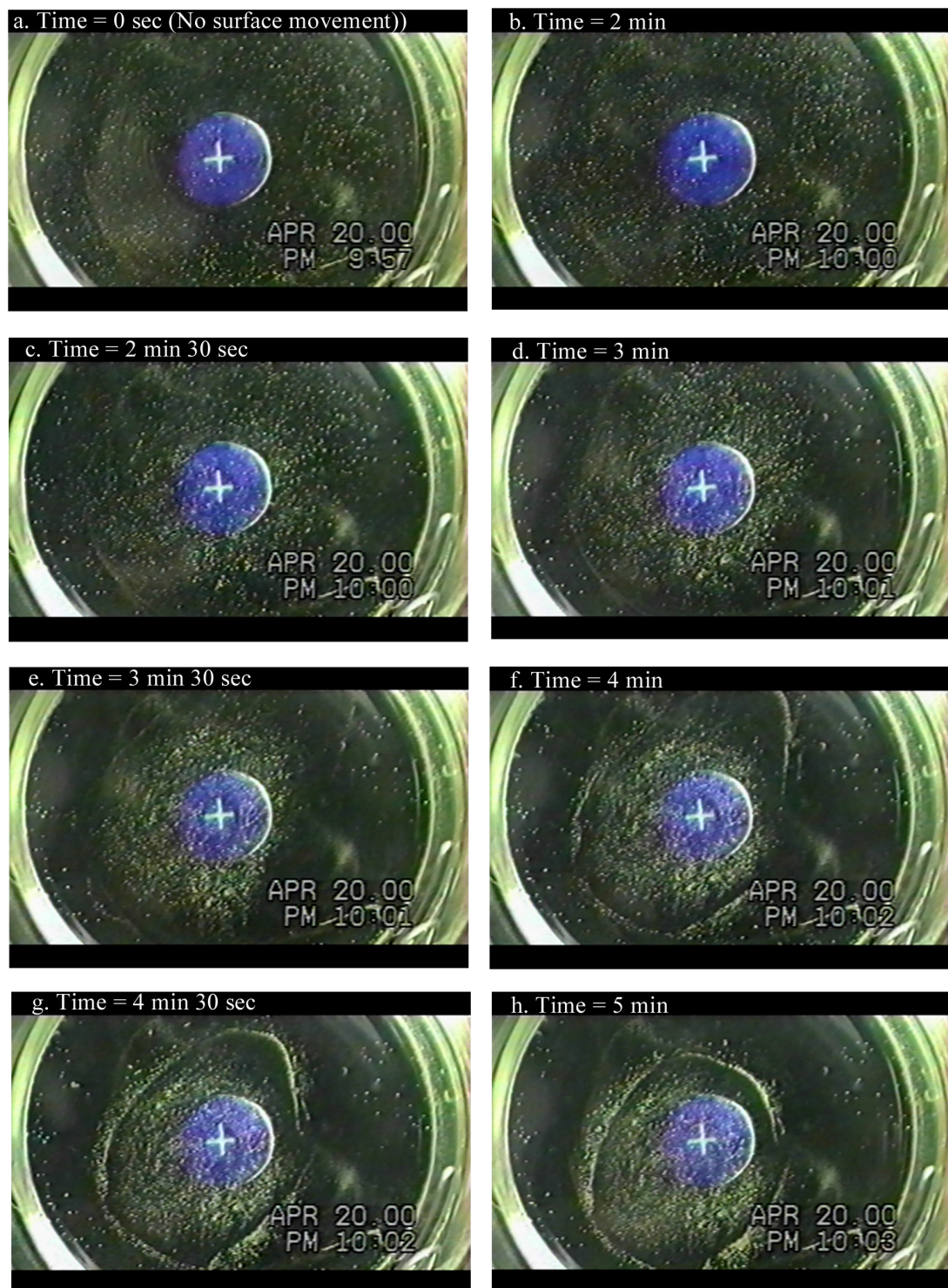


Figure 5.12 Evolution of the surface when heating was applied from the center underneath the pool (2EH vapor concentration = 2500 ppm, sample solution = 60% aqueous LiBr)

The first surface movement is believed to have been caused by evaporation of 2EH on the surface. When the solution was heated in the center of the pool, 2EH evaporated in the area where the solution temperature was relatively high. When the surface tension was high enough in the center due to the low 2EH surface concentration caused by evaporation of 2EH, surface tension caused a flow from the edge toward the center of the pool. The second surface movement is believed to have been caused by condensation of vapor on the walls of the petri dish similar to that explained in the Section 5.4.2. When sample vapor condensed on the wall of the petri dish, it caused a lower surface tension of the solution near the wall. Thus, particles along the wall flowed toward the center.

## 5.5 Condensation of Water + 2EH Vapor

A similar series of tests were run with pure water in the pool and the results of these tests are reported on this section.

### 5.5.1 Adiabatic Condensation

Before introducing the vapor sample to the test vessel, the system was evacuated and the particles were uniformly distributed on the water surface. The water pool appeared stationary. Then Valve 2 (in the line between the test vessel and the mixing flask) was abruptly opened to allow the vapor sample to flow to the test vessel. The purpose of this experiment was to observe the surface movement in a water pool accompanying condensation of water + 2EH vapor.

Figure 5.13 shows a typical example of the results. The experiment was conducted with a 2EH concentration of 10300 ppm in the vapor (note that only in such high 2EH vapor concentration a clear flow pattern was seen). The temperature in the pool before delivering the vapor sample was 20.1°C (corresponding to a saturation pressure of 17.7 mmHg). The pressure in the test vessel immediately after Valve 2 was opened was 25.8 mmHg.

At time = -2 sec, no surface movement was observed. At time = 0 sec, (the moment when Valve 2 was opened), the surface began to move. However, all the particles moved as a united group. Compared with the surface movement in a LiBr solution pool, the speed was very slow (the average speed from 0 to 90 sec was 0.17 mm/s). The multi-cell flow pattern movement seen in absorption was not observed with condensation. At time = 120 sec, the motion slowed further and the pool became almost stationary with an average speed of particles from 120 to 180 sec of only about 0.01 mm/s. At the end of the run, the pressure and average liquid temperature were 24.5 mmHg and 21.4°C.

### 5.5.2 Condensation with Cooling

Following the adiabatic condensation described in Section 5.5.1, in which the pool became static approximately 2 to 3 minutes after the vapor sample was introduced, the petri dish was shaken to redistribute the particles uniformly on the surface, and then cooling was applied.

The surface motion observed during these condensation tests was very weak compared with that in the absorption tests. No surface movement was found with 2EH

vapor concentration of 1500 ppm, a very weak surface movement was observed with 2EH concentration of 3500 to 5000 ppm, and a distinct pattern was clear to see when the 2EH vapor concentration was above 10000 ppm.

Figure 5.14 shows a typical sample of the results. This experiment was conducted with a 2EH vapor concentration of 10300 ppm. The time elapsed from applying the cooling to the appearance of the surface movement was 30 sec. At time = 0 sec (defined as the moment when the surface movement began), the surface movement began near the edge of the cooling chip, and moved toward the edge of the pool with an average speed of the expanding circle of 0.5 mm/s from 0 to 60 sec. At time = 20 sec, a particle free circle was clearly visible centered roughly on the cooling chip. This surface movement stopped at time = 60 sec. The diameter of the particle free circle after motion stopped was about 4 cm. During the whole test period (420 sec), the pressure dropped from 24.2 to 22.8 mmHg, and the liquid temperature reduced from 21.6 to 20.4°C.

## 5.6 Discussion

The series of absorption and condensation experiments described in this Chapter (Sections 5.4 and 5.5) demonstrate Marangoni flow due to 2EH delivered from vapor to the liquid surface. Previous studies have emphasized the temperature gradient on the surface as the primary factor driving Marangoni flow in this system. The effects of temperature gradient on the surface tension are estimated here to put the problem in the literature context.

The effect of surface temperature gradient on Marangoni convection is analyzed here for multi-cell adiabatic absorption. Because higher absorption occurred at the center

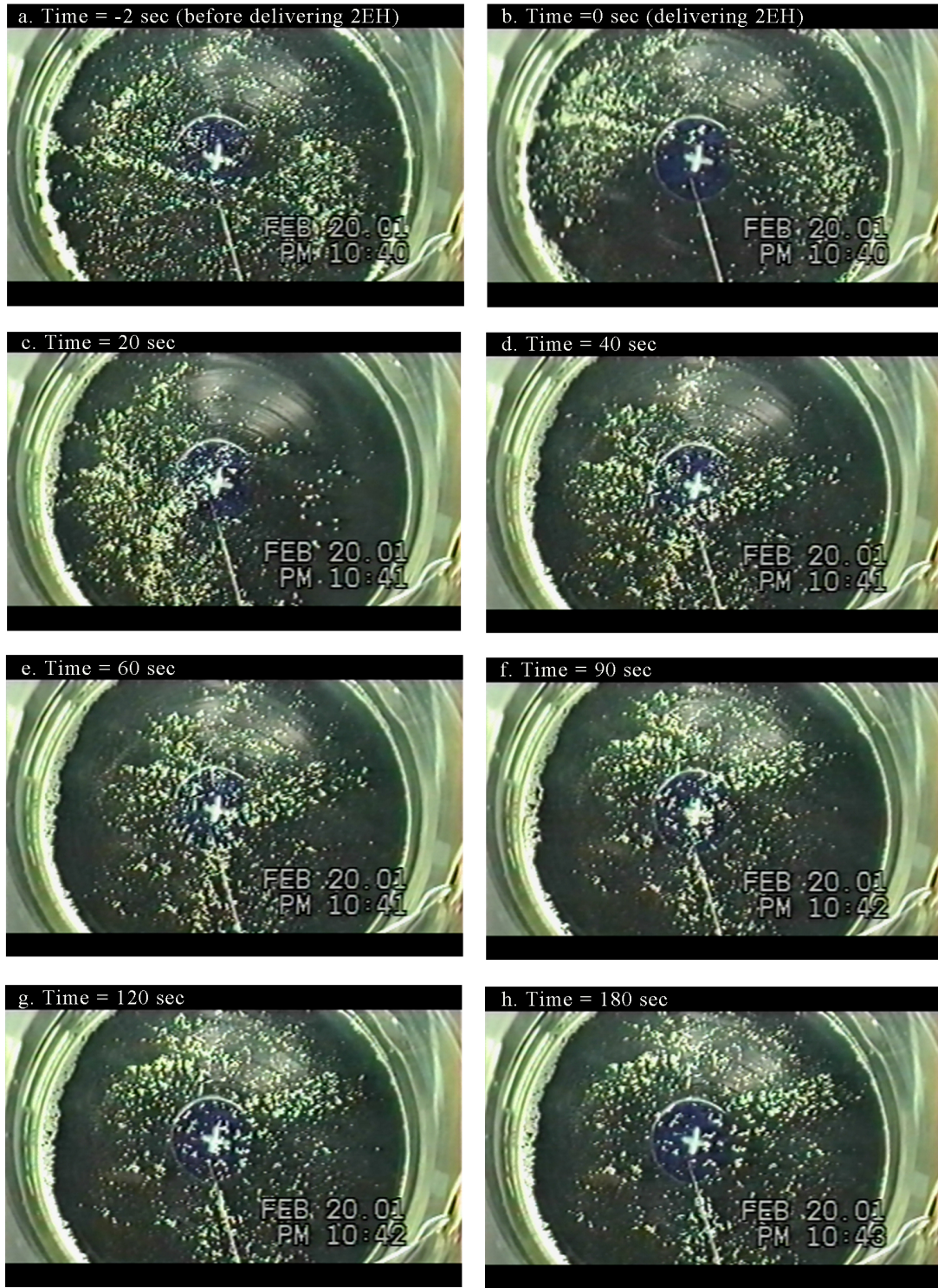


Figure 5.13 Evolution of surface in a water pool for adiabatic condensation (2EH vapor concentration = 10300 ppm)

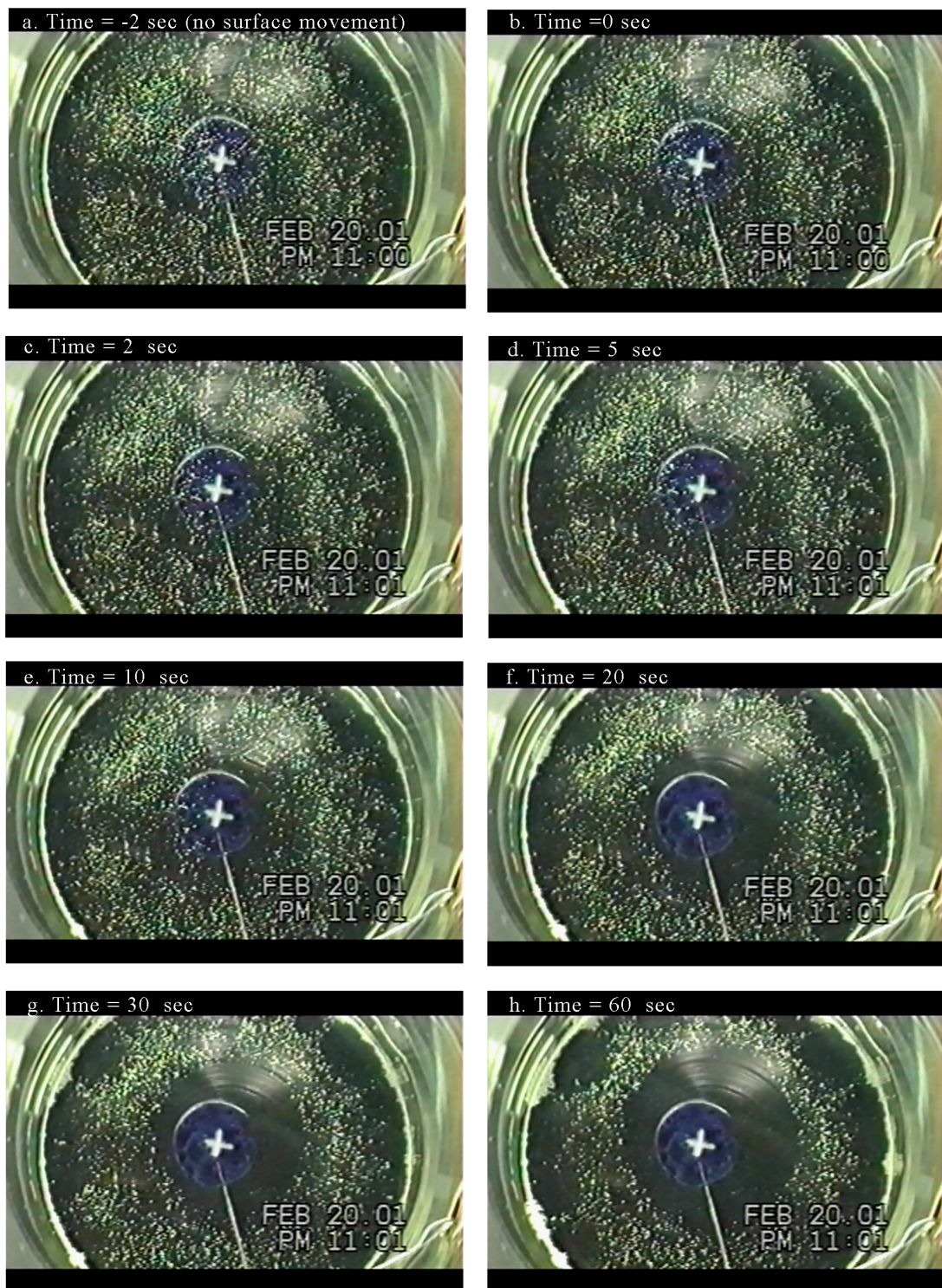


Figure 5.14 Evolution of surface in a water pool for condensation with cooling (2EH vapor concentration = 10300 ppm)

of each cell, the temperature was higher there than at the edge of the cell. This higher temperature at the center is expected to result in a higher surface tension when 2EH is present in the LiBr solution (Kim and Berman, 1994), and therefore, the temperature gradient can only cause a movement from the edge toward the center in each cell, which was opposite to the surface motion observed.

Fujita and Hihara (1999) also observed similar multi-cell pattern surface movement. However, they attributed the multi-cell flow to the existence of air because they only observed it when air was present in the system. For each run in the current study, the multi-cell flow was observed at the beginning and then a single cell pattern was observed when the cooling was applied. Thus it seems likely that Fujita and Hihara's result can be explained better in terms of the absorption rate. One possible explanation is that when air was present in their experiment, the absorption rate was sufficiently low to cause the multi-cell pattern.

The surface movements observed during absorption and condensation were much different. In the case of absorption, when the vapor sample was introduced to the vessel, if the 2EH vapor concentration was high (2EH vapor concentration  $\geq$  2500 ppm), the multi-cell flow was observed. If the 2EH vapor concentration was in the range of 400 to 1500 ppm, the multi-cell flow was followed by a vigorous surface movement. When the cooling was applied, a single cell flow with fast surface movement (10 mm/s) was observed. By comparison, for the condensation case, when the vapor sample was introduced to the vessel, the surface movement was very weak. A clear pattern was seen when the 2EH vapor concentration was above 10000 ppm. Instead of the multi-cell movement seen in absorption, the particles on the surface flowed as an island and the

Table 5.2 Comparison of the experimental conditions and results for representative adiabatic absorption and condensation

	Adiabatic absorption		Adiabatic condensation	
<b>Sample solution</b>	60% LiBr solution		Water	
<b>2EH vapor concentration (ppm)</b>	400		10300	
<b>Time (sec)</b>	0	420	0	420
<b>Solution temperature (°C)</b>	21.5	39.8	20.1	21.4
<b>Pressure (mmHg)</b>	23.9	11.5	25.8	24.5
<b>Saturation pressure (mmHg)</b>	1.6	5.1	17.7	19.1
<b>Condensed water (g)</b>	0.52		0.05	
<b>Condensation heat from water vapor (J)</b>	1256		122	
<b>Change of internal energy of sample solution (J)</b>	1037		92	
<b>The error of energy balance (%)</b>	17.4		24.6	

distribution of the particles changed with time. When the cooling was applied, the single cell flow was observed only in very high vapor sample concentration condition (>10000 ppm), this single cell expended at a very low speed (about 0.5 mm/s).

A comparison of the experimental conditions and results for representative adiabatic absorption and condensation cases are shown in Table 5.2. The reasons for the weak surface motion for adiabatic condensation can be explained as follows.

For condensation, the mass transfer driving potential is low (pressure – saturation pressure = 7.1 ~ 5.4 mmHg) compared with the absorption case (pressure – saturation pressure = 19.9 ~ 6.4 mmHg) and the 2EH vapor side mass transfer resistance is high. Therefore, based on the pressure data, the amount of water condensed on the surface was calculated to be only 0.05 g which was only 10% of that for the absorption case. If the amount of 2EH adsorbed on the surface is assumed to be proportional to the condensed

water, the amount of 2EH adsorbed on the surface for the condensation case is only twice that of the absorption case. However, because of the high solubility and diffusivity of 2EH in water, only a small portion of the 2EH is expected to stay on the surface compared with the absorption case. The largest portion of the 2EH is expected to dissolve in the liquid. Thus, the effective 2EH surface concentration gradient and the surface tension gradient cannot be formed to cause a strong surface movement.

# CHAPTER 6

## NUMERICAL STUDY OF CONDENSATION IN THE PRESENCE OF SURFACTANT VAPOR

### 6.1 Introduction

Significant absorption and condensation enhancement in absorption chillers can be achieved by adding trace amounts of surfactant to the system. Much effort has been expended to understand the mechanism of surfactant enhancement as described in Sections 2.2 to 2.4. Of several theories, Marangoni convection is widely accepted as a key aspect of the enhancement physics (Ziegler and Grossman, 1996).

The recently proposed Vapor Surfactant theory states that the surfactant reaches the surface mainly from the vapor (Kulankara and Herold, 2000). In this theory, the bulk flow of water vapor from the vapor phase to the surface is identified as the primary source of surfactant on the surface, and the non-uniform flux of surfactant arriving at the surface causes a non-uniform surfactant surface concentration. Since the surface tension is largely determined by the surface concentration, the non-uniform surface concentration causes Marangoni convection.

An experimental study guided by this theory is described in Chapter 5. Marangoni convection was observed when 2EH vapor along with water vapor was condensed on the surface of a pool. The results support the conclusion that the surface motion is directly related to non-uniform 2EH surface concentration delivered from the vapor side. However, due to limitations of the experiment set up, some parameters of interest were not measured (e.g. the 2EH surface concentration). For the purpose of the data

interpretation, a numerical study was carried out with the purpose to better understand the mechanism of Marangoni convection in the presence of 2EH in the vapor.

A two-dimensional numerical simulation based on the geometry in Figure 6.1 was conducted (Qiao and Yuan et al., 2000). The geometry is a thin film of liquid water with a small patch of cooling centered on the bottom side. The upper surface is exposed to steam and surfactant vapor so that condensation will occur. The model computes the surface concentration of surfactant and relates that to the surface tension. Calculations show that the condensation rate is much higher when Marangoni convection is occurring, even if the surfactant concentration in the vapor is very small (120 ppm).

## 6.2 Physical Model

The configuration analyzed here is designed to avoid the surfactant-driven unstructured flow (to keep the calculation tractable) seen in falling films while maintaining the most important aspects of the physical phenomena. Thus, the two-dimensional calculation is done on a rectangular geometry that is filled with liquid water (3 mm thick and 10 cm wide).

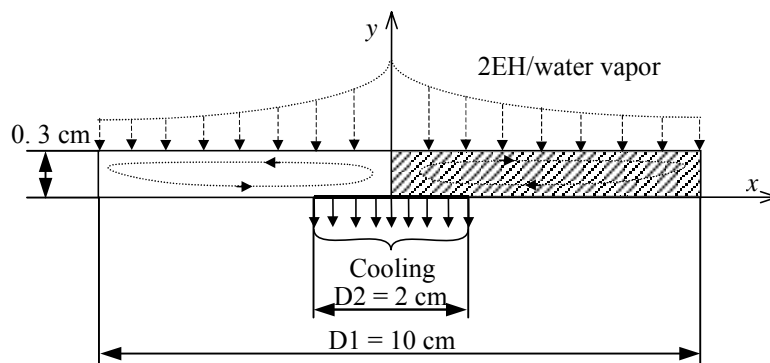


Figure 6.1 Schematic of the condensation pool

Non-uniform cooling is provided to create a non-uniform condensation flux. The upper surface is exposed to water vapor containing surfactant. Initially the liquid is at the saturation temperature corresponding to the partial pressure of the water vapor and the liquid is surfactant free. At time = 0 sec, a cooling flux is imposed on a section at the center of the pool bottom (-1 cm < x < 1 cm), and this eventually causes a non-uniform condensation flux on the upper surface.

The cooling induced condensation acts as a surfactant source at the surface. Because the cooling is localized, the flux of surfactant arriving at the surface is spatially non-uniform. This leads to non-uniform surface tension, which is the driving force for the flow.

### 6.3 Governing Equations, Initial and Boundary Conditions

In the calculation the flow is assumed to be two-dimensional, laminar and incompressible. Since the velocity in the pool is relatively low, the dissipation term in the energy balance is neglected.

In this condensation process, flow and heat transfer are strongly coupled. Also, the surfactant distribution along the upper surface determines the boundary condition for the flow equation. The mass balance of surfactant on the surface, momentum and energy balances all need to be solved simultaneously to model the condensation process.

The simulation was completed using Fluent, a commercial fluid flow software, combined with a UDF (user defined function). The equations solved are listed as follows:

Continuity equation:  $\nabla \cdot \vec{u} = 0$  6.1

Momentum equation:  $\frac{\partial \vec{u}}{\partial t} + (\vec{u} \cdot \nabla) \vec{u} = \beta(T - T_\infty) \vec{g} + \nu \nabla^2 \vec{u}$  6.2

Energy equation:  $\frac{\partial T}{\partial t} + (\vec{u} \cdot \nabla) T = \alpha \nabla^2 T$  6.3

1-D surfactant mass balance on the free surface:

$$\frac{\partial X_s}{\partial t} + \frac{\partial(u_h X_s)}{\partial x} = D \frac{\partial^2 X_s}{\partial x^2} + S(x, t) X_{vapor} \quad 6.4$$

Energy balance on the free surface:  $\lambda \frac{\partial T}{\partial y} = h_{fg} S(x, t)$  6.5

Boundary conditions:

Marangoni force balance:  $\mu \frac{\partial u}{\partial y} \Big|_{y=h} = \frac{\partial \sigma}{\partial x} \Big|_{y=h}$  6.6

No slip:  $\vec{u} = 0 \quad x = 0 \text{ and } L$  6.7  
 $y = 0$

Saturation temperature:  $T \Big|_{y=h} = 300 \text{ K}$  6.8

Cooling flux:  $q'' = -5000 \text{ W/m}^2 \quad -1 < x < 1 \text{ cm}, y = 0$  6.9

Concentration gradient at impermeable walls:

$$\frac{\partial X_s}{\partial x} \Big|_{x=-5cm} = \frac{\partial X_s}{\partial x} \Big|_{x=5cm} = 0 \quad 6.10$$

Initial conditions:

Static pool:  $\vec{u} \Big|_{t=0} = 0$  6.11

Uniform temperature:  $T \Big|_{t=0} = 300 \text{ K}$  6.12

Surfactant free surface:  $X_s \Big|_{t=0} = 0 \text{ mg/m}^2$  6.13

The relationship between surface tension and surface concentration (discussed further in Section 6.5.3) is:

$$\sigma = \begin{cases} 72.16 - 24.30X_s, & mN/m, X_s < 1.2mg/m^2 \\ 43.0 & mN/m, X_s \geq 1.2mg/m^2 \end{cases} \quad 6.14$$

Since the condensation rate is small, it is assumed that the height of the surface does not change during the process. Based on the case with the largest condensation rate during the simulation period (70 sec) the change in height would be only 0.003 mm so this assumption is reasonable. The free surface of the pool was assumed to be flat. The appropriateness of this assumption can be judged (Chanson, 1999) by examining the Froude number defined as

$$Fr = \frac{V^2}{gL} \quad 6.15$$

where  $g$  is gravitational acceleration and  $V$  and  $L$  are characteristic velocity and length, respectively. Taking  $L = 0.003$  m as the pool depth and  $V = 0.5$  mm/s as the maximum computed vertical velocity results in  $Fr = 8 \times 10^{-6}$ . This indicates that the gravitational force is much larger than the inertia force in this system. This calculation supports the assumption of a flat interface.

Initial calculations showed that although the flow driven by natural convection alone is small, when natural convection is coupled with the surface tension driven flow caused by the 2EH surface concentration gradient, the effect of natural convection cannot be neglected. Therefore, the majority of the study focuses on flow induced by surface tension coupled with the effect of natural convection.

On the upper surface (i.e. the free surface), the balance of shear and surface tension forces is given as Equation 6.6, where  $\sigma$  is the surface tension calculated by a

piecewise linear function given as Equation 6.14. The upper surface is assumed to be in equilibrium with the saturated steam in the vapor phase, and the temperature at the upper surface is fixed at the saturation temperature (Equation 6.8). No-slip conditions are applied at the bottom and side walls (Equation 6.7). All walls are perfectly insulated except a small section of the bottom where the cooling is applied (Equation 6.9).

The surfactant mass balance on the upper surface can be expressed as Equation 6.4. It is assumed in this study that the surfactant stays on the surface after it condenses. Therefore, the mass balance is a one-dimensional equation. This assumption follows from the low solubility (25 ppm, Section 3.4) and low diffusivity ( $<10^{-9}$  m<sup>2</sup>/sec, Kim and Janule, 1994) of the surfactant in the liquid and high affinity of the surface to adsorb the surfactant. In terms of observations made in chapters 3 to 5, this assumption would be more accurate for LiBr solution but it was used here as a starting point for such simulations. Of course, this model is only an approximation but it provides a better model than the liquid based models often discussed previously.

It is assumed that the flux of surfactant arriving at the surface is proportional to the steam condensation flux. This assumption is equivalent to assuming that there are no concentration gradients in the vapor. In Equation 6.4,  $u_h$  and  $S(x,t)$  are the liquid velocity and steam condensation flux at the upper surface of the pool respectively and  $X_{vapor}$  is the surfactant concentration in the vapor, which is assumed to be constant in both space and time. The energy release from steam condensation on the surface of the pool is balanced by heat conduction in the liquid (Equation 6.5). The boundary conditions for the 1-D surfactant mass balance (Equation 6.4) are zero flux at both ends of the upper surface as expressed in Equation 6.10.

Initially, the pool is isothermal (Equation 6.12), there is no surfactant on the pool surface (Equation 6.13) and the pool is static (Equation 6.11). The shear stress boundary condition on the pool surface, represented by Equation 6.6, is coupled to the surfactant surface concentration by the properties of the system (Equation 6.14). As a result, these equations must be solved simultaneously. As the surfactant arrives at the surface, it lowers the surface tension locally and the resulting surface flow tends to smooth out the surface tension gradients. The source of surfactant on the surface is the condensation process that is driven by temperature differences in the system. Thus, the mass flow is coupled to the energy flow in the system.

## 6.4 Numerical Formulation

A commercial code (FLUENT Inc, 2000) was used to solve the above equations. Since the code does not directly offer the solution of a 1-D surfactant mass balance in a 2-D problem, the surfactant mass balance equation (Equation 6.4) was solved by a separate program written as a linked function. The source code for the linked function is included as Appendix A. A first-order power law scheme is used for discretization of the convection term in Equation 6.4, and an implicit scheme is used for the computation of the surfactant distribution along the upper surface at each time step. The diffusion coefficient,  $D$ , is an important parameter that affects the flow and heat transfer in the pool through its control of the surfactant distribution on the surface. For the current study two values of diffusivity ( $D=10^{-3}$  and  $10^{-7}$  m<sup>2</sup>/sec) were used for the parametric study.

A discrete approximation to Equation 6.4 was derived using the finite volume method (Patankar, 1980). Only the final equation and its coefficients are given here. A

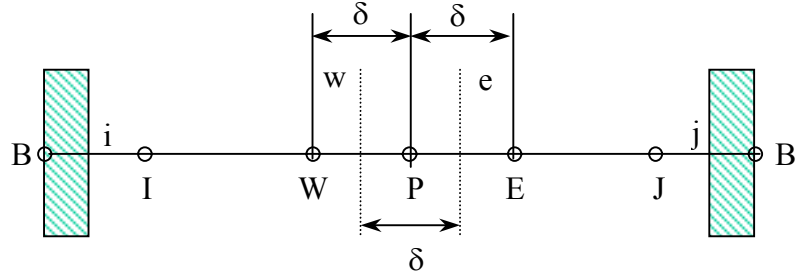


Figure 6.2 Schematic of grid and control volume for the internal and boundary points  
For the internal grid points

schematic of the control volumes for the internal and boundary points are shown in Figure 6.2. A uniform grid is used for the simulations.

$$a_p X_{sp}^k = a_E X_{sE}^k + a_W X_{sW}^k + b \quad 6.16$$

$$a_E = \frac{D}{\delta} A(|Pe_e|) + [-u_e, 0]$$

$$a_w = \frac{D}{\delta} A(|Pe_w|) + [u_w, 0]$$

where:

$$a_p = \frac{\delta}{\Delta t} + a_E + a_W + (u_e - u_w)$$

$$b = S_p^k \delta + \frac{\delta}{\Delta t} X s_p^{k-1}$$

For the left boundary point

$$a_B X_{sB}^k = a_I X_{sl}^k + b \quad 6.17$$

$$a_I = \frac{D}{\delta} A(|Pe_i|) + [-u_i, 0]$$

where:

$$a_B = \frac{\delta}{2\Delta t} + a_I + u_i$$

$$b = S_B^k \frac{\delta}{2} + \frac{\delta}{2\Delta t} X s_B^{k-1}$$

For the right boundary point

$$a_B X_{sB}^k = a_J X_{sJ}^k + b \quad 6.18$$

$$a_J = \frac{D}{\delta} A(|Pe_i|) + [u_j, 0]$$

where:

$$a_B = \frac{\delta}{2\Delta t} + a_J - u_j$$

$$b = S_B^k \frac{\delta}{2} + \frac{\delta}{2\Delta t} X s_B^{k-1}$$

where subscripts  $P$ ,  $W$  and  $E$  denote internal grid points and  $I$ ,  $J$  and  $B$  denote the grid points on the boundary (B) and its neighbors (I,J). The dashed lines show the faces of the control volume and the letters  $e$  and  $w$  stand for the east and west faces.

The mass transfer Peclet number,  $Pe$ , is defined as

$$Pe \equiv \frac{\rho UL}{D} \quad 6.19$$

representing a ratio of the relative strengths of convective and diffusive mass transfer. The function  $A(|P|)$  depends on the particular numerical scheme for the advection term, which is discussed further in Section 6.5.6. The term  $[-u_e, 0]$  denotes the greater of  $-u_e$  and 0. The source term  $S$  is independent of the 2EH surface concentration  $X_s$  (only a function of time and position) and was treated as a constant in the discretization equation.

The resulting set of equations is tri-diagonal and can be efficiently solved by the Thomas (TDMA) algorithm (Patankar, 1980). The TDMA algorithm is fast and memory efficient.

## 6.5 Simulation Study

### 6.5.1 Simulation Algorithm

A flow chart for the simulation algorithm is shown in Figure 6.3. The approach is to solve the momentum and energy equations in Fluent with the 1-D surfactant mass balance equation solved as a user defined function. At the first time step, because the surface is 2EH free, the momentum and energy equations are solved with zero shear stress on the surface. The computed velocity and temperature profiles are then used as inputs to the UDF. The surfactant source strength is calculated based on the condensation flux on the free surface and then the surfactant mass balance equation (Equation 6.4) is solved. The surface tension is calculated by Equation 6.14 and then the shear stress is calculated. This shear stress is used as the boundary condition for the next iteration of the momentum and energy equations. This process continues until the convergence criteria are satisfied (the relative velocities and temperature errors from the  $i$  to the  $i+1$  iteration must be smaller than  $10^{-5}$  and  $10^{-7}$ , respectively). Once convergence is obtained the simulation goes to the next time step to repeat the above procedures.

### 6.5.2 Grid Study

Considering the symmetry of the geometry and boundary conditions, only half of the pool (shaded part in Figure 6.1) is considered in the calculation. A uniform grid of  $100 \times 30$  (x direction  $\times$  y direction) was tested and the results were compared with a grid of  $200 \times 60$ . The time step size was chosen to be 0.001 sec for both cases. Results for the total condensation rate and average velocity at the free surface are shown in Table 6.1 for

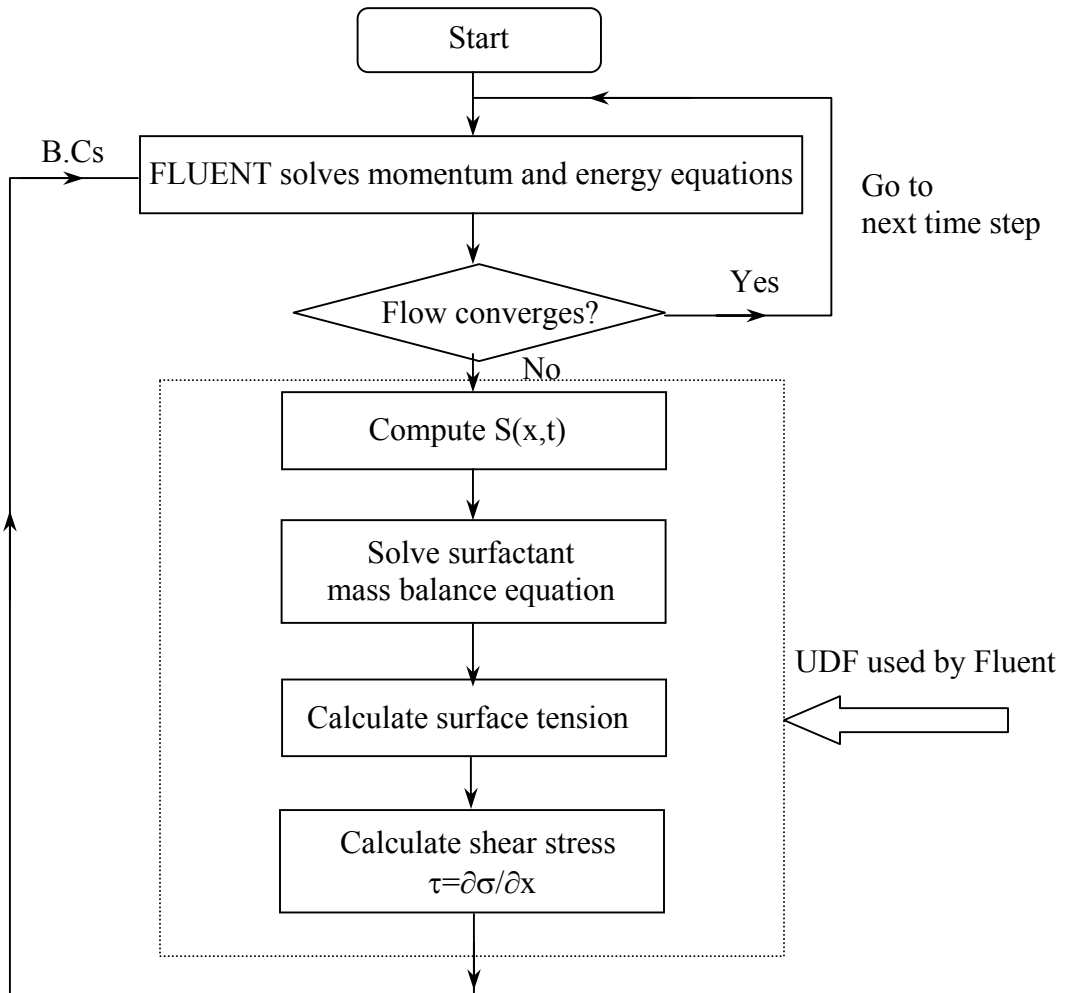


Figure 6.3 Flow chart for the Fluent based simulation of Marangoni convection during condensation in the presence of surfactant in the vapor

a representative case (time = 5 sec). The flow features at time = 5 sec are dominated by the effect of surfactant surface concentration (discussed further in Section 6.6) and thus the results in Table 6.1 represent the effect of the grid density on calculation accuracy for this problem. Because the differences between the simulation values for the two cases is small, in order to save computing time, the  $100 \times 30$  grid was used for the subsequent simulations.

Table 6.1 Grid study results showing total condensation rate and average velocity at the free surface (time = 5 sec) for two grid choices.

	<b>Grid = <math>100 \times 30</math></b>	<b>Grid = <math>200 \times 60</math></b>	<b>Relative error</b>
Total condensation rate (mg/s)	1.300	1.256	3.4%
<b>Average velocity at free surface (mm/s)</b>	1.581	1.488	5.9%

### 6.5.3 Relationship Between Surface Tension and Surface Concentration

Figure 6.4 shows the relationship between the surface tension and the 2EH surface concentration for water used in this simulation. For comparison, the data obtained from the Gibbs analysis (Equation 4.7 and Figure 4.2) is included in Figure 6.4. The results based on the Gibbs analysis indicate a steep reduction in surface tension with surface concentration when the surface concentration approaches the saturation value of  $\Gamma = 0.59 \text{ mg/m}^2$ . It was found that this caused difficulty in the simulation because surface tension is very sensitive to 2EH surface concentration and therefore it required a very small time step for convergence. As a compromise to allow completion of the simulation

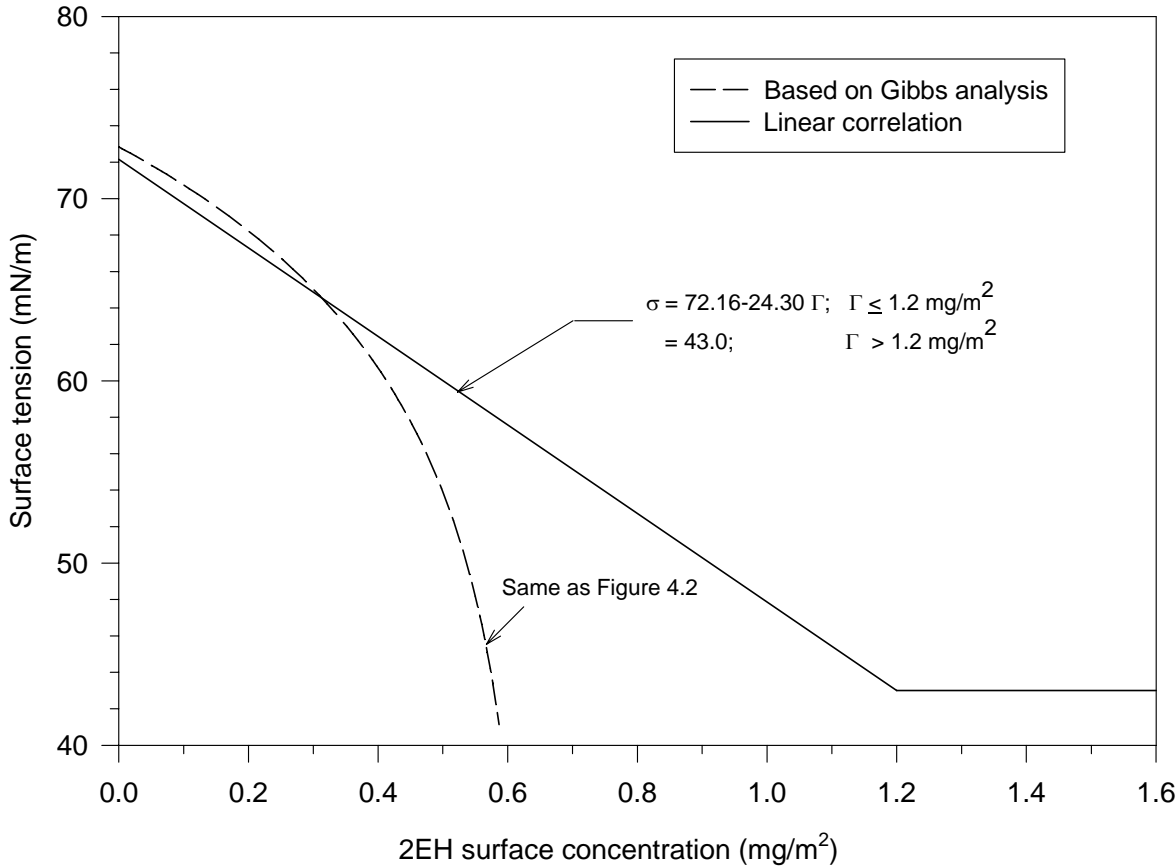


Figure 6.4 Relationship between surface tension and surfactant surface concentration used in simulation

in an acceptable time period (two weeks for a run on a Sun workstation with a clock speed of 286 MHz), a linear relationship was used which approximately matches the experimental surface concentration data from 0 to 0.5 mg/m<sup>2</sup>. A comparison of the results from this linear relationship and the relationship based on Gibbs analysis was conducted. In the most interesting surface concentration range (surface concentration below 0.5 mg/m<sup>2</sup>), the heat flux value only deviated within 1% as two different relationships were used.

#### **6.5.4 Mass Diffusivity of 2EH in Water and Aqueous LiBr**

Mass diffusivity is one of the fluid properties necessary for the simulation study. However, only limited diffusivity information for 2EH in water was found in the literature. One predictive equation is from the correlation by Wilke and Chang (1955) as follows

$$D_{1,2} = 7.4 \times 10^{-12} \frac{T}{\mu_2} \frac{(CM_2)^{0.5}}{V_1^{0.6}} \quad 6.20$$

where:  $D_{1,2}$  diffusion coefficient of solute 1 in solvent 2, m<sup>2</sup>/s

$T$  temperature, K

$\mu_2$  dynamic viscosity of solvent 2, mPa·s

$M_2$  molecular weight of solvent 2, kg/kmol

$V_1$  molar volume of solute 1 at its boiling temperature at 1.013 bar, cm<sup>3</sup>/mol

$C$  association factor of solvent 2,  $C = 2.6$  for water;  $C = 1.5$  for ethyl alcohol

The diffusion coefficient of the solute (1) in the solvent (2),  $D_{1,2}$ , can be determined from the dynamic viscosity,  $\mu_2$  and the molecular weight,  $M_2$ , of the solvent. The association factor of the solvent,  $C$ , is 2.6 for water. Based on this correlation, the diffusion coefficients of all liquids and gases in liquids fall in the range of  $5 \times 10^{-10}$  to  $5 \times 10^{-9}$  m<sup>2</sup>/sec. The other source is from Kim and Janule (1994), who report diffusion coefficients of 2EH in water as  $4.1 \times 10^{-10}$  m<sup>2</sup>/sec. Based on these results, the diffusivity of 2EH in the solution is believed to be in the range of  $10^{-9}$  to  $10^{-10}$  m<sup>2</sup>/sec.

In early simulations, divergence occurred for such low values of diffusivity and an artificially high value ( $D = 10^{-3}$  m<sup>2</sup>/sec) was run. A series of cases with diffusivity  $D = 10^{-7}$  m<sup>2</sup>/sec are discussed and compared with the high diffusivity case ( $D = 10^{-3}$  m<sup>2</sup>/sec). The runs for  $D = 10^{-7}$  m<sup>2</sup>/sec cases took approximately 500 CPU hrs because a very small time step, on the order of  $10^{-4}$  sec was used. However, because the results for the two values of diffusivity did not exhibit large differences, the case with  $D = 10^{-7}$  m<sup>2</sup>/sec is expected to give realistic features.

### **6.5.5 Time Step Size**

Although an implicit scheme is used in the UDF (user defined function) for the 1-D surfactant mass balance equation and an implicit scheme is chosen in FLUENT for solving the momentum and energy equations, the calculation was found to diverge unless very small time steps, on the order of  $10^{-4}$  sec, were used for the cases with diffusivity of  $D = 10^{-7}$  m<sup>2</sup>/sec. The small time steps meant that a single run takes between 2-3 weeks of CPU time on a Sun workstation with a clock speed of 286 MHz. In practice, the surfactant source values, the velocity profile and the shear stress profile on the free

surface are transferred between Fluent and the UDF at each time step. Therefore, the equations are solved sequentially and the entire scheme is not fully implicit. As a result, the stability of the calculation is dependent on the time step size implying small time steps and long run times.

### 6.5.6 Numerical Approximation of the Advection Term

Several tests were run to find an appropriate scheme for the advection term in the 1-D surfactant mass balance with high accuracy for both high and low diffusivity values. Another potential benefit from this is to find which scheme can postpone divergence with the same time step size. Three schemes (upwind scheme, power law scheme and hybrid scheme) were examined. The coefficients  $A(|Pe|)$  for the discretization equation are as follows:

$$A(|Pe|) = \begin{cases} 1 & \text{Upwind scheme} \\ \left[0, (1 - 0.1|Pe|)^{0.5}\right] & \text{Power law scheme} \\ \left[0, 1 - 0.5|Pe|\right] & \text{Hybrid scheme} \end{cases} \quad 6.21$$

where  $[a,b]$  denotes the greater of a and b. Based on the results, little difference was found among the three schemes for the condensation rate, but the power law scheme was found to postpone divergence slightly. Therefore, the power law scheme was used for further simulations.

## 6.6 Results and Discussion

In the simulation results discussed in this section, the diffusivity of the surfactant along the surface is set as  $D = 10^{-7} \text{ m}^2/\text{sec}$  unless otherwise noted, and the surfactant concentration in the vapor is set as  $X_{vapor} = 120 \text{ ppm}$ . Natural convection is turned on. The water properties are taken as constant and evaluated at 20°C.

Figure 6.5 shows the condensation flux and surfactant surface concentration along the free surface near the beginning of the condensation process (time = 5 sec). The condensation flux is localized in the region above the cooling section of the base due to conduction and natural convection in the slow moving pool. The flux of condensate brings surfactant from the vapor phase to the surface. Due to slow diffusion and advection of surfactant, the surface concentration is non-uniform with the maximum surface concentration gradient appearing in the region  $1 \leq x \leq 2 \text{ cm}$ . This is also the location of the maximum surface tension gradient that drives the surface convection. The surface convection brings cool liquid up to the surface locally (around  $x = 1 \text{ cm}$ ) and thus the condensation flux peak is found at that location. This localized condensation flux peak delivers a large flux of 2EH to the surface locally which tends to increase the gradient in surface concentration.

Figures 6.6 and 6.7 show the shear stress distribution and surfactant surface concentration distribution as a function of position and time on the free surface (note that the average surfactant surface concentration at a particular time,  $X_{s,aver}$ , has been subtracted from the surface concentration in Figure 6.7 to emphasize the surface concentration gradient). These plots are discussed together since the plotted variables are

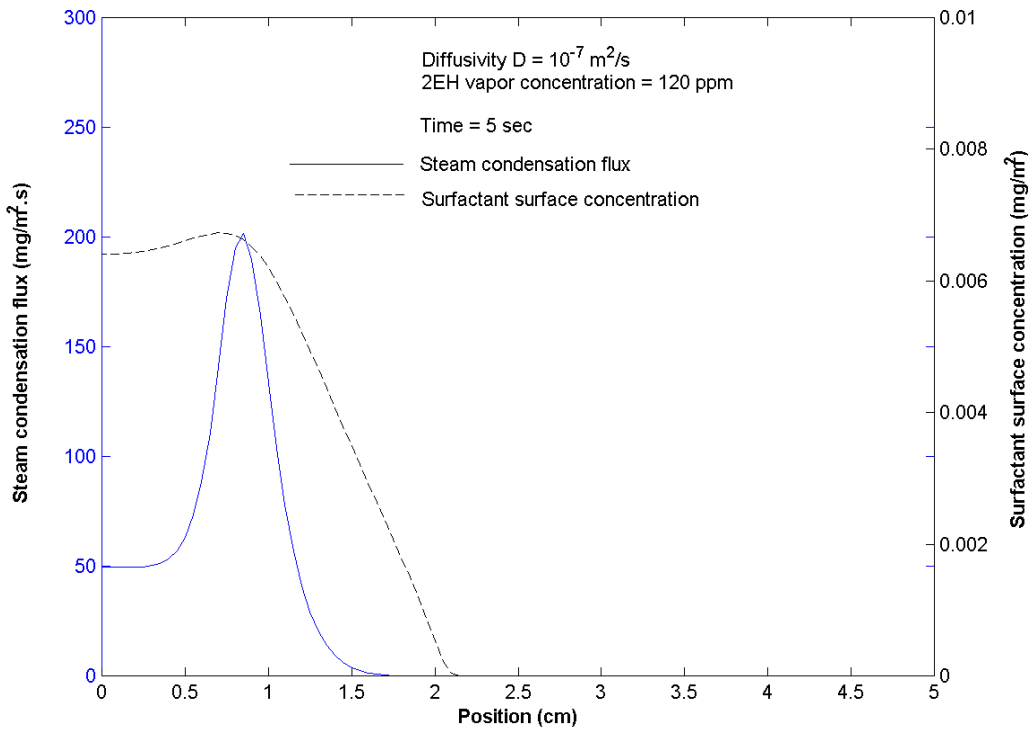


Figure 6.5 Surfactant surface concentration and steam condensation flux

directly linked by Equation 6.6. It can be seen that the shear stress first increases to a maximum close to time = 7.5 sec where it begins to decrease. The shear stress eventually goes to zero when the surfactant surface concentration reaches saturation, which is approached by approximately time = 70 sec. The surfactant surface concentration gradient is seen to peak around time = 7.5 sec as expected.

During the initial stage of the process ( $0 < \text{time} < 2.5$  sec), the major heat transfer mode in the pool is conduction and thus the condensation flux is small as shown in Figure 6.8. As a result, the surfactant source from the vapor phase is small as shown by the relatively uniform surface concentration (Figure 6.7). Due to the low surface velocity during this initial stage, the distribution of surfactant is governed mainly by diffusion and

condensation. As the surfactant concentration gradient increases, the velocity of the surface increases rapidly as shown in Figure 6.9, and then advection becomes prominent. However, at the same time, advection moves the surfactant towards the right boundary ( $x = 5$  cm), and this tends to smooth the surfactant distribution along the upper surface. These two factors compete resulting in a maximum shear stress around time = 7.5 sec (Figure 6.6). As the process proceeds further, the shear stress decreases resulting in a lower velocity. When the velocity becomes small, diffusion again dominates both the heat transfer and surfactant distribution resulting in a small shear stress and relatively uniform surfactant distribution as experienced in the initial stage of the process.

The condensation flux data in Figure 6.8 for time = 5 sec is identical to that in Figure 6.5. A condensation flux peak is observed at the edge of the cooling section at time = 5 sec and it reaches a local maximum value at time = 7.5 sec. As time goes on, more cooled water is driven to the surface in the center range, causing an increase in condensation flux in the center range with a maximum value at the center around time = 15 sec.

Figure 6.8 shows that the condensation flux reaches a maximum and then begins to decline. This can be seen more clearly in Figure 6.10 where the total condensation rate at the upper surface is shown for five cases as a function of time. The conduction and natural convection cases were calculated to establish a baseline, and the results for the high diffusivity cases ( $D = 10^3$  m<sup>2</sup>/sec) in the presence of surfactant, with and without natural convection, are included for comparison. For the conduction case, fluid motion is not permitted and conduction is the only energy transport mode. The condensation rate rises toward the steady state value (referred to as the condensation rate corresponding to

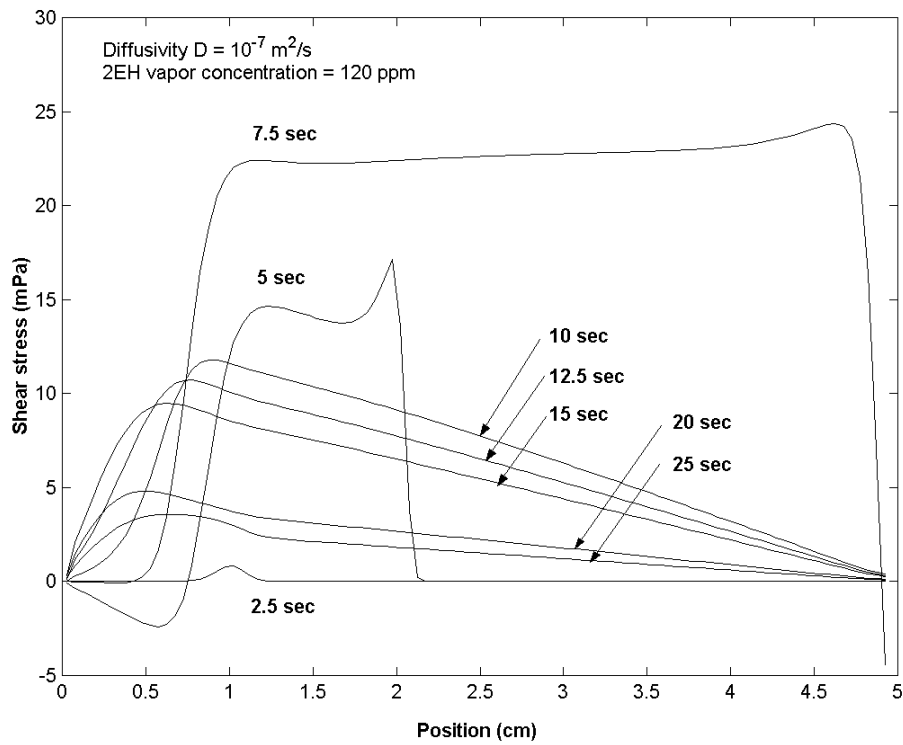


Figure 6.6 Shear stress distribution at upper surface as a function of position and time

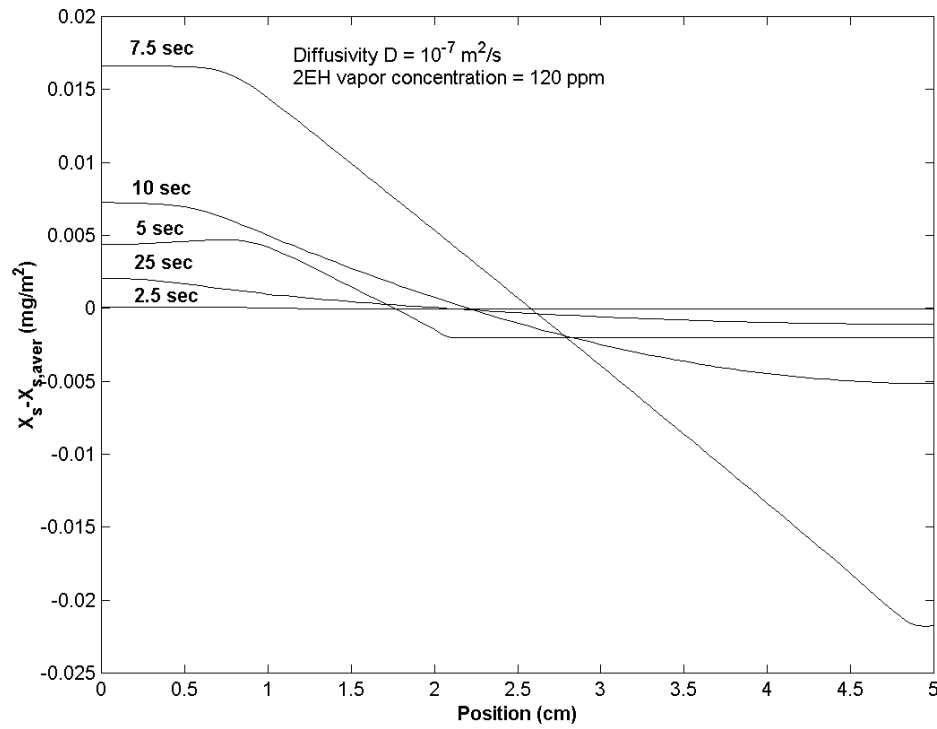


Figure 6.7 Surfactant surface concentration distribution as a function of position

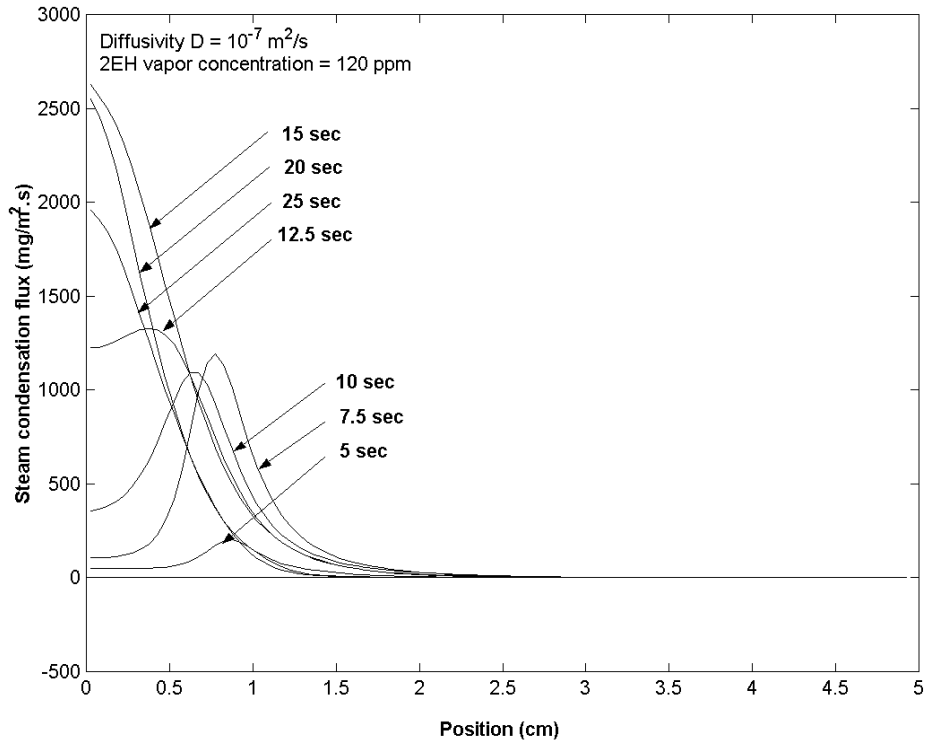


Figure 6.8 Condensation flux distribution along surface as a function of position

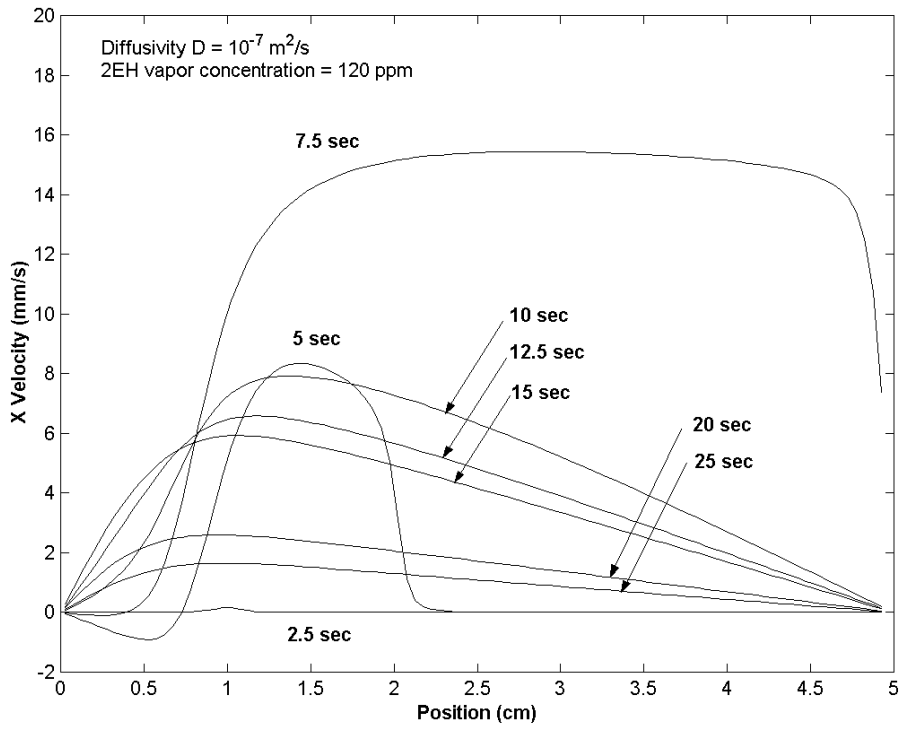


Figure 6.9 Velocity distribution along surface as a function of position and time

the cooling rate in Figure 6.10) as the two-dimensional temperature field is established. The conduction case was computed as a limiting case to assist in understanding the results from the convection cases. It was initially expected that natural convection would augment the condensation process over that seen for pure conduction. However, the somewhat non-intuitive result is that natural convection causes the average temperature of the liquid to fall slightly faster than for pure conduction. To enable the energy balance for the constant cooling rate at the bottom, the effect of that drop in internal energy on condensation is a slight reduction in the condensation rate. As expected, both cases rise toward the same steady state value for large time.

The result for diffusivity  $D = 10^{-3}$  m<sup>2</sup>/sec without natural convection shows the highest peak in Figure 6.10. It is observed that the surfactant-induced flow enhances condensation significantly as compared to the conduction and natural convection cases. This enhancement can be attributed to the important role of advection in bringing the cold fluid to the upper surface. The results show that the condensation rate reaches a maximum around time = 16.1 sec. After this, the flow in the pool slows down resulting in a decreasing condensation rate. An interesting observation for this run is that the condensation rate exceeds the rate corresponding to the cooling rate from time 16.0 to 18.0 sec. This overshoot is induced by advection. During the initial stage, the water at the bottom of the pool is cooled by conduction, but since the velocity in the pool at that time is small, the subcooled water stays near the bottom. As the surface tension gradients increase, the water velocity increases gradually, until most of the water is involved in the circulation in the pool. The circulation brings the subcooled water to the surface, and the condensation rate at the surface becomes large. However, as the process continues, the

water flowing past the cooling area becomes warmer. This occurs because the water now passes by the cooling area more quickly. As a result, the condensation rate declines.

The result for diffusivity  $D = 10^{-3}$  m<sup>2</sup>/sec with natural convection is also shown in Figure 6.10. It can be seen that the condensation rate reaches a maximum around time = 15.0 sec. After 15.0 sec the flow in the pool slows down, resulting in a decreasing condensation rate, until the flow settles into the natural convection pattern. For this case, the overshoot feature is eliminated by natural convection because natural convection and Marangoni convection drive the flow in opposite directions in the region close to the cooling section. By comparing the condensation rate between the cases for  $D = 10^{-3}$  m<sup>2</sup>/sec with and without natural convection, the maximum condensation rate is decreased by about 25% by natural convection, which means that the effect of natural convection on enhancement is significant. Even so, the surfactant-induced flow still dominates and enhances condensation significantly as compared to both conduction and natural convection (without Marangoni convection).

The results for diffusivity  $D = 10^{-7}$  m<sup>2</sup>/sec with natural convection show a similar peak to the case for  $D = 10^{-3}$  m<sup>2</sup>/sec. It can be seen that the condensation rate increases slowly from 0 to 5 sec and then increases rapidly from 5 to 8 sec. At time = 8 to 9 sec, a flat step is seen before it rises again. A discussion of this step is provided at the end of this section after introduction of all the simulation data. The maximum condensation rate is achieved around time = 16 sec, after which, the condensation rate decreases and finally follows the natural convection curve after 25 sec.

The condensation rate is enhanced from 5 to 25 sec. After 25 sec, it follows the natural convection curve. The enhancement caused by the surfactant is time dependent.

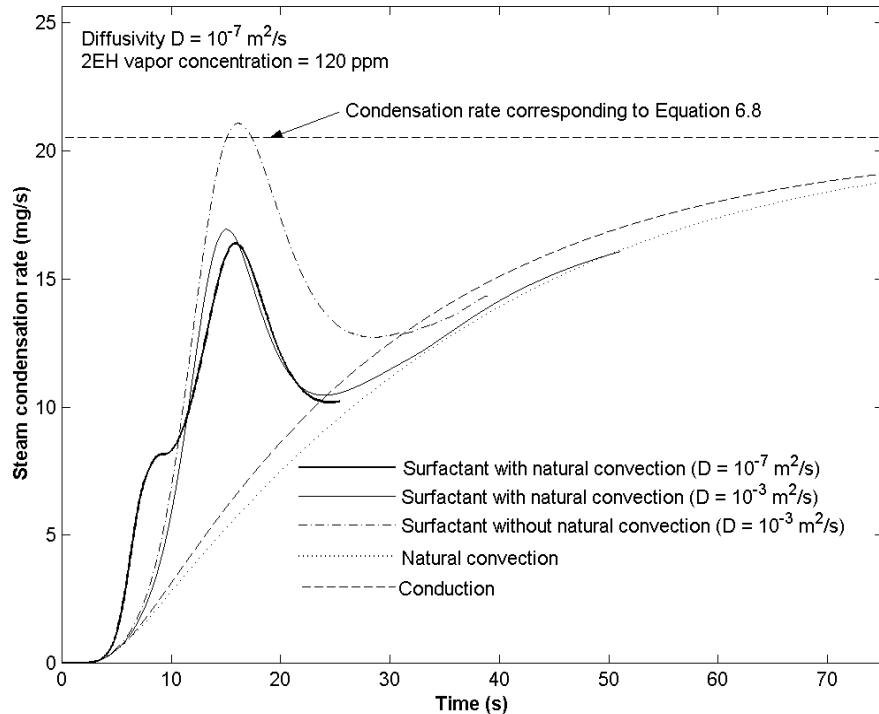


Figure 6.10 Condensation rate versus time for surfactant enhanced condensation simulation

This can be explained by reference to the surfactant concentration gradient shown in Figure 6.7. Because of the small surface concentration gradients before 2.5 sec and after 25 sec, the Marangoni convection is weak during these time periods. As can be seen in Figure 6.7, the maximum 2EH surface concentration gradient was achieved around 7.5 sec. However, the maximum average velocity in the region from 0 to 1 cm is achieved at time = 15 sec. The maximum condensation rate correlates closely with the maximum average velocity in the vicinity of the cooling chip.

Figure 6.11 is a plot of surfactant surface concentration versus time at two surface locations along with the average value for the entire surface. As can be seen, the surface

concentration rises continuously all along the surface. The maximum surfactant surface concentration difference between 1 and 2 cm is achieved at around 7.5 sec. This result is consistent with the results shown in Figure 6.7.

In addition, Figure 6.11 shows that the maximum surface concentration is about  $0.5 \text{ mg/m}^2$  at 25 sec. Therefore, the linear relationship between the surface tension and surface concentration which was introduced in Section 6.3 (see Equation 6.14 and Figure 6.4) avoids the convergence problem and also gives good accuracy for this case.

In order to better understand the flow regimes, Figure 6.12 shows a series of streamline contours at different times (notice that the y axis in each of these plots is expanded by a factor of 2 to enhance readability). In each plot, eight contours equally

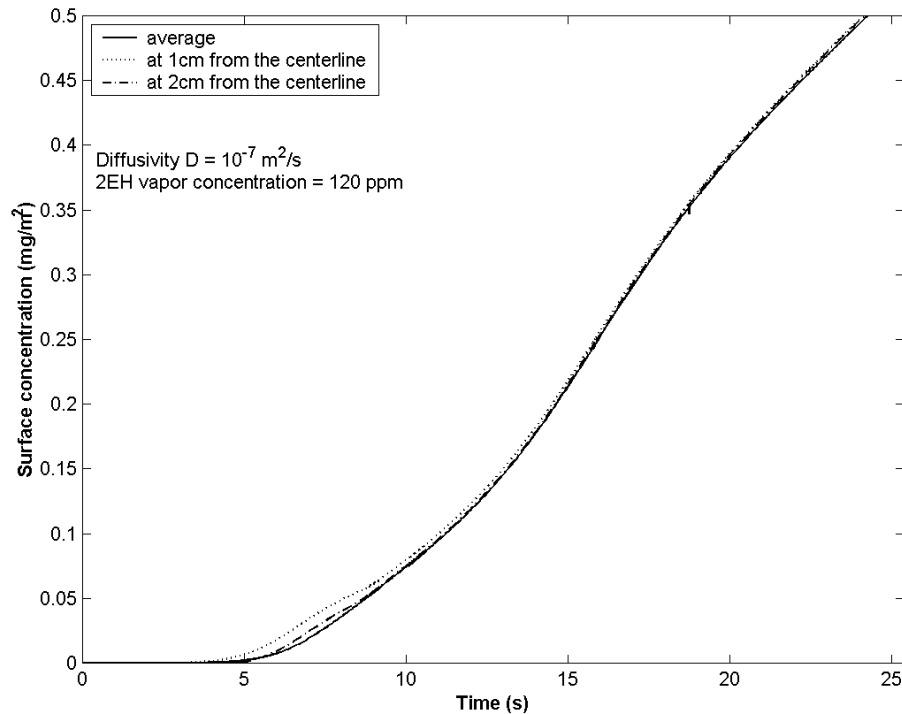


Figure 6.11 Surfactant surface concentration versus time at different locations

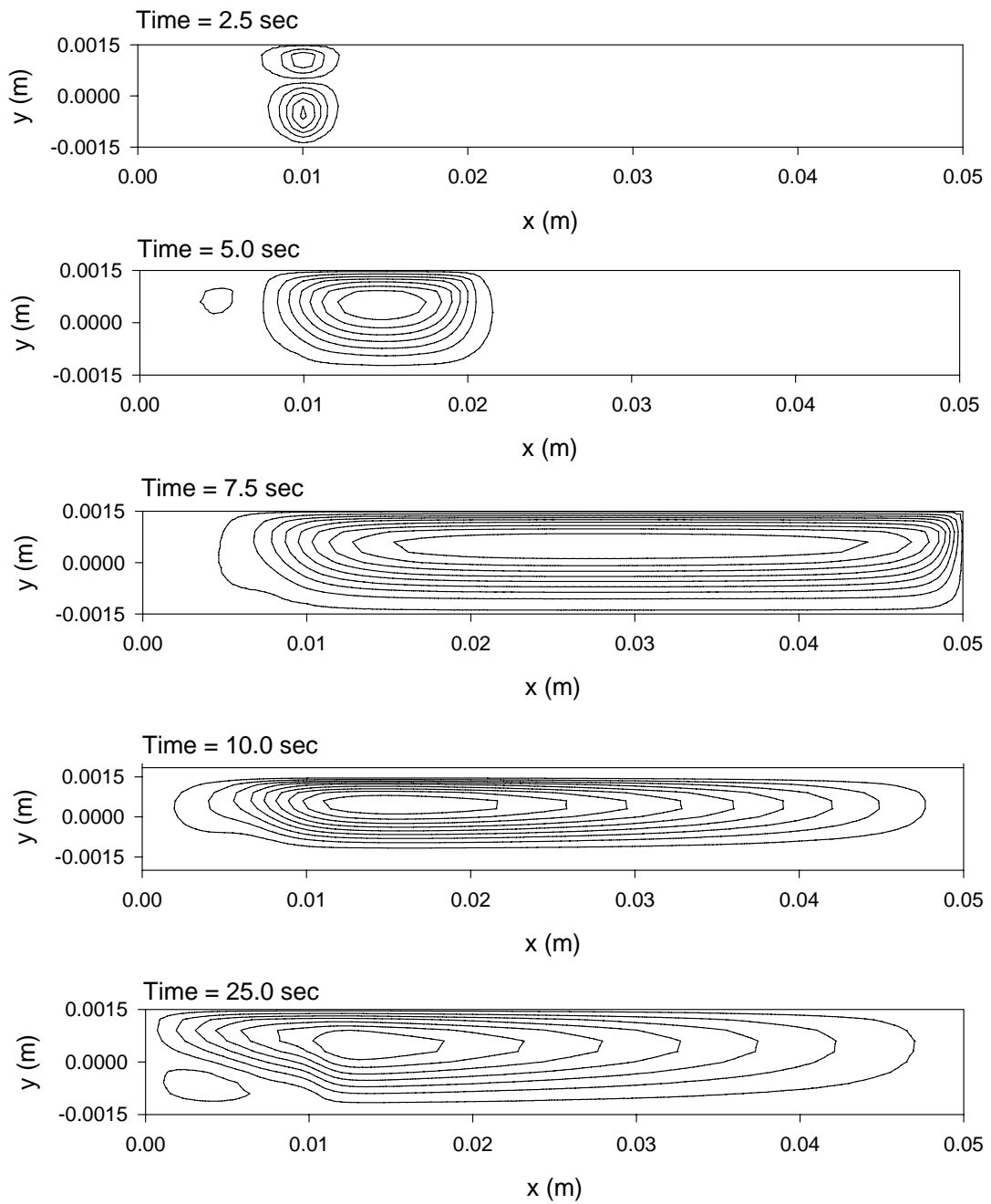


Figure 6.12 Streamline contours ( $D = 10^{-7} \text{ m}^2/\text{sec}$ )

divide the stream function value from 0 to the maximum value (notice that the maximum values are different for each plot) with the highest stream function value at the center of the cell represented by the concentric contours. At 2.5 sec, the pool is largely stationary, but a small cell on the surface, induced by the surface tension gradient, is seen. The lower cell is due to natural convection induced by the cooling localized in the center region. During the time period from 5 to 7.5 sec, the cell expands rapidly until the entire pool is in motion except the center range. After 7.5 sec the cell evolves slowly as the velocity declines.

In Figure 6.10, a flat step appears for the case of diffusivity  $D = 10^{-7} \text{ m}^2/\text{sec}$  at about 10 sec. This feature is not observed in the case of diffusivity  $D = 10^{-3} \text{ m}^2/\text{sec}$ . This step feature is attributed to two effects: 1) the low mass diffusivity of 2EH, and 2) the circulation of cold water from the bottom of the pool to the free surface in the center region.

Due to the low diffusivity ( $D = 10^{-7} \text{ m}^2/\text{sec}$ ), surfactant diffusion is slow. Because the condensation is localized near the cooling section ( $x = 1 \text{ cm}$ ), the largest surfactant surface concentration gradient appears at that location. The concentration gradient drives the surface flow away from the cooling section and brings cold water to the surface from the bottom of the pool. This cold water further enhances condensation in the center region. Figure 6.8 shows this feature and the heat flux peak is found at 7.5 sec. However, as the process proceeds, more water is involved in the circulation and non-uniformity of the surface concentration declines which results in a decrease in the peak value after 7.5 sec. On the other hand, the cold water brought to the surface causes an increase of heat flux in the center region (Figure 6.8). Therefore, the reduction of heat flux at  $x = 1 \text{ cm}$

and the increase of heat flux at center region results in an almost constant average heat flux from 7.5 to 10 sec resulting in a flat step in the condensation rate curve.

## **CHAPTER 7**

## **DISCUSSION**

This chapter presents a discussion of the main results from the thesis including 1) the surface tension measurements, 2) surface concentration analysis, and 3) the Marangoni convection experiments. Simulation results are also compared with experimental results in this chapter. The objective of this chapter is to explain the effect of the surfactant 2-ethyl-hexanol (2EH) on surface tension, surface concentration and Marangoni convection, with emphasis on the differences seen as 2EH is delivered from either the vapor or liquid sides.

### **7.1 Effect of Surfactant 2-ethyl-hexanol on Surface Tension**

The surface concentration calculations, discussed in Section 4.3, show that the saturated 2EH surface concentration is approximately the same order for both water and 60% aqueous LiBr ( $0.59 \text{ mg/m}^2$  for water and  $0.99 \text{ mg/m}^2$  for 60% aqueous LiBr). However, the surface tension data show that the time needed to reach the saturated surface concentration is different for these two systems. This is due to differences in both the diffusivity and solubility of 2EH in the liquid phase. Because of the low solubility (27 ppm) and low diffusivity ( $2.81 \times 10^{-7} \text{ cm}^2/\text{sec}$  (Kim, 1994)) of 2EH in 60% aqueous LiBr, the 2EH delivered to the surface from the vapor stays largely on the surface for the time scales of interest in this work. Therefore, for 60% aqueous LiBr experiencing a certain surface flux of surfactant, the surface concentration can reach the equilibrium surface

concentration in a short time and the surface tension measured by the drop weight method is found to be independent of the drop frequency if the drop frequency is smaller than 0.1 Hz. In contrast, because of the higher solubility (835 ppm) and the higher diffusivity ( $4.07 \times 10^{-6}$  cm<sup>2</sup>/sec, (Kim, 1994)) of 2EH in water, a large fraction of the 2EH delivered to the surface dissolves into the liquid bulk, and therefore, the amount of 2EH remaining on the surface is less in the same time interval. The surface tension data for water show frequency dependence even at the lowest tested frequency of 0.03 Hz.

Extensive measurements of surface tension with surfactant 2EH in air and in liquid, for both water and 60% aqueous LiBr, were conducted. The results show that for aqueous LiBr, the effect of 2EH from the vapor side is dominant in determining surface tension and the effect of 2EH from the liquid side is negligible at a nominal drop frequency of 0.03 Hz. Therefore, the 2EH vapor concentration is a primary variable in understanding the surface tension of such systems. One conclusion is that, in order to obtain repeatable and accurate equilibrium surface tension data, the 2EH vapor concentration must be allowed to reach equilibrium and this process is time consuming, often providing a bottleneck to the experimental process.

The results for water show that 2EH in the vapor also exhibits significant effects. However, due to the higher diffusivity of 2EH in water, when the 2EH was delivered from the vapor side a fraction of 2EH dissolves in water and only part of the 2EH stays on the surface. As a result, the surface concentration slowly reaches equilibrium and the surface tension is more dependent on drop frequency. On the other hand, when the 2EH was delivered from the liquid side, the 2EH was found to diffuse to the surface rapidly causing a very low surface tension even at the highest frequency tested (0.3 Hz).

The measurements and calculations included in Section 4.3 show that the solubility limit of 2EH decreases from 858 to 37 ppm with increases of mass fraction of LiBr from 0 to 60%. For the same change, the surface concentration of 2EH increases from 0.587 to 0.993 mg/m<sup>2</sup> and the surface tension plateau decreases from 41.1 to 36.8 mN/m (Tables 4.1 and 4.2). These results indicate that for the same 2EH system concentration, more 2EH molecules are expelled from LiBr liquid bulk to the surface with increases of mass fraction of LiBr and hence surface concentration of 2EH increases and the surface tension is lower.

Surface tension data were also taken for water in the presence of 2EH in the vapor by Zhou et al. (2001) using a different procedure. The large surface tension plateau value observed by Zhou (49 mN/m) seems to indicate that the 2EH surface concentration did not reach an equilibrium value. After checking the experimental procedure used by Zhou et al. (2001), it was found that the drop frequency used was 0.04-0.056 Hz. Although this drop frequency is small enough for the 2EH surface concentration to reach equilibrium for the case with 2EH in the liquid only (Figure 3.7 shows that the surface tension is independent of drop frequency with drop frequency lower than 0.1 Hz), it is not small enough for the case with 2EH in the vapor (Figure 3.5 shows that the surface tension is dependent on the drop frequency even when the drop frequency is smaller than 0.04 Hz). This explains why Zhou et al. (2001) found the surface tension plateau to be larger and the 2EH surface concentration to be smaller as compared with the results found in the present study. However, it should be repeated that the relationship between the surface tension and the drop frequency is much different for water and aqueous LiBr. Figure 3.9

shows that for 60% aqueous LiBr the surface tension was totally independent of the drop frequency when the drop frequency is smaller than 0.1 Hz.

In addition to the effect of 2EH surface concentration, the effects of solution temperature and LiBr mass fraction on the surface tension were considered. The change of the surface tension can be written in general as:

$$\Delta\sigma = \frac{\partial\sigma}{\partial\Gamma_{2EH}}\Delta\Gamma_{2EH} + \frac{\partial\sigma}{\partial T}\Delta T + \frac{\partial\sigma}{\partial X_{LiBr}}\Delta X_{LiBr} \quad 7.1$$

where  $\partial\sigma/\partial\Gamma_{2EH}$  was calculated based on surface tension results shown in Figure 4.5, which is about  $-64$  (mN/m)/(mg/m<sup>2</sup>). The terms  $\partial\sigma/\partial T$  and  $\partial\sigma/\partial X_{LiBr}$  were found from the literature which are about  $0.38$  (mN/m)/K (Kim and Berman, 1994) and  $33$  (mN/m)/(kg/kg) (Foote Mineral Co., 1995).

In the current study, we are interested in the change of surface tension along the free surface so we interpret Equation 7.1 as

$$\frac{d\sigma}{dx} = \frac{\partial\sigma}{\partial\Gamma_{2EH}}\frac{d\Gamma_{2EH}}{dx} + \frac{\partial\sigma}{\partial T}\frac{dT}{dx} + \frac{\partial\sigma}{\partial X_{LiBr}}\frac{dX_{LiBr}}{dx} \quad 7.2$$

where x is the spatial coordinate along the surface. For the case of condensation, the surface temperature would be expected to be closely isothermal due to the nature of water condensation and the large energy transport that occurs during the phase change. Thus for condensation, only the first term on the right hand side of Equation 7.2 remains. For absorption, the surface will also approach saturation but the mixture properties complicate the situation such that neither the temperature nor the LiBr concentration will be uniform along the surface. However, for absorption in the absence of surfactant, no Marangoni convection was observed. Thus, it is concluded that the influence of

temperature and LiBr mass fraction on surface tension are relatively small effects compared to the dominant influence of surfactant surface concentration.

## 7.2 Effect of Surfactant Vapor on Marangoni Convection

The effect of 2EH vapor on Marangoni convection was observed in a bench top test (Section 5.1) in which a liquid drop of 2EH was positioned close to, but not touching, the aqueous LiBr surface. The presence of the drop causes a surface flow radially away from the drop position. Further experiments to ascertain the effect of 2EH vapor on Marangoni convection were conducted in an absorption/condensation pool apparatus. In the experiments, 2EH was introduced into the absorption/condensation pool with steam from the vapor side as described in Section 5.2.2. The results show that the presence of 2EH in the vapor causes Marangoni convection, and the strength of the convection and the flow patterns that develop are dependent on the 2EH concentration in the vapor.

In the case of adiabatic absorption, if the 2EH vapor concentration is lower than 200 ppm, Marangoni flow was not observed. This is attributed to the relatively low flux of 2EH arriving at the surface that is insufficient to create the surface tension gradients needed to cause a flow.

When the 2EH vapor concentration was in the range 400 to 1500 ppm, a slow-moving multi-cell flow was formed initially followed by a vigorous sweeping flow. In each cell of multi-cell flow there was a circulation from the center to the edge of the cell on the surface and back from the edge to the center of the cell underneath the surface. The vigorous surface motion that followed involved the entire surface of the pool and was faster than that in the multi-cell flow. As time went on, the Marangoni convection

finally stopped. The circulation in each cell of the multi-cell flow is caused by higher 2EH surface concentration and thereby lower surface tension at the center of each cell due to non-uniform absorption of 2EH vapor. The breakup of the cells is apparently due to a sudden increase in absorption at one of the cells that causes it to erupt and destabilize the cellular flow pattern. After the vigorous surface motion occurs, the surface motion gradually dies out and stops. This is apparently due to the surface becoming saturated with surfactant.

For the case where the 2EH vapor concentration was 2500 ppm, only the multi-cell flow was observed but the circulation in each cell was much weaker as compared with the case of 2EH vapor concentration in the range of 400 to 1500 ppm. No vigorous surface motion was observed for this case. When the 2EH vapor concentration was 7800 ppm or higher, Marangoni flow was not observed. It is believed that the large concentration of 2EH vapor presents vapor side mass transfer resistance that limits the absorption rate when the 2EH vapor concentration is above 1500 ppm.

Based on the observations of the surface movement and the measurements of the pressure in the present study, it is found that there is an optimal 2EH vapor concentration (i.e. 400 to 1500 ppm in the present study) that results in vigorous Marangoni convection and maximum absorption. Near this optimal 2EH vapor concentration, large surface tension gradients are formed during absorption resulting in vigorous surface motion and high absorption rate.

### **7.3 Absorption and Condensation in the Presence of 2-ethyl-hexanol Vapor**

Based on the present study, the features of Marangoni flow during absorption in an aqueous LiBr pool and condensation in a water pool in the presence of 2EH in the vapor have some similarities but also have clear differences. As mentioned in Section 7.2, in the case of absorption, a much less organized vigorous surface movement with a speed of about 20 mm/sec was observed at 2EH vapor concentration in the range 400 to 1500 ppm, and both multi-cell flow and vigorous flow presented depending on the 2EH concentration in the vapor. By comparison, in the case of condensation as discussed in Section 5.5.2, no surface movement was found at 2EH vapor concentration of 1500 ppm and surface movement was very weak at 2EH concentration in the range 3500 to 5000 ppm, and a clear surface movement was seen when 2EH vapor concentration was above 10000 ppm. Instead of the multi-cell flow or vigorous surface movement observed in absorption case, the particles on the surface move as a united group.

Measurements of the pressure in the absorption/condensation chamber show that the change of pressure during absorption was at a rate of about 1.8 mmHg/min, while the change of pressure during the condensation test was at a rate of about 0.18 mmHg/min. Based on the pressure data, the flux of water plus surfactant condensed on the surface in absorption is a factor of 10 higher than in condensation.

The reasons for the differences in Marangoni flow in absorption and condensation can be explained as follows. For condensation, the driving force (pressure in system – saturation pressure) was low ( $25.8 - 17.7 = 8.1$  mmHg in Table 5.3), and the 2EH vapor side mass transfer resistance is high because of high 2EH vapor concentration (10000 ppm). Therefore, the condensate flux was low. If the amount of 2EH adsorbed on the

surface is assumed to be proportional to the product of the condensate flux and the 2EH concentration in the vapor, the amount of 2EH adsorbed on the surface for the condensation case with 2EH concentration 10000 ppm is on the same order as that for the absorption case. However, because of the high solubility (835 ppm) and diffusivity of 2EH in water ( $4.07 \times 10^{-6}$  cm<sup>2</sup>/sec, (Kim, 1994)), the largest portion of the 2EH dissolves in the liquid and only a small portion of the 2EH is expected to stay on the surface. A larger condensation flux would be expected to produce a vigorous Marangoni convection in this configuration.

In comparison, for absorption, because of the high driving force ( $23.9 - 1.6 = 22.3$  mmHg in Table 5.3), and low 2EH vapor side mass transfer resistance due to low 2EH vapor concentration (400 ppm), the absorption flux is calculated to be 0.7 kW/m<sup>2</sup> (based on measured data for the case of adiabatic absorption with 2500 ppm 2EH discussed in Sections 5.4.1.1 and 5.4.1.2, absorption flux is  $670 \text{ J}/(3 \text{ min} \times 54 \text{ cm}^2) = 0.7 \text{ kW/m}^2$ ), which is much higher as compared with that for condensation (0.14 kW/m<sup>2</sup>, based on measured data for the case of adiabatic condensation with 10300 ppm 2EH discussed in Section 5.5.1, condensation flux is calculated to be  $(89.69 - 84.25) \text{ kJ/kg} \times 17 \text{ g}/(2 \text{ min} \times 54 \text{ cm}^2)$ ). Furthermore, because of the low solubility (27 ppm) and low diffusivity ( $2.81 \times 10^{-7}$  cm<sup>2</sup>/sec (Kim, 1994)) of 2EH in 60% aqueous LiBr, the 2EH delivered to the surface stays largely on the surface. Spatial non-uniformities in absorption flux cause local gradients in 2EH surface concentration which then drive Marangoni convection. The Marangoni convection supports and enhances spatial non-uniformities in absorption flux completing a positive feedback mechanism of enhancement.

## **7.4 Comparison of Numerical and Experimental Results**

This section provides a comparison of the experimental and numerical results for the absorption case with applied cooling.

### **7.4.1 Comparison of Geometries and Assumptions in Simulations and Experiments**

For both the computational and experimental models, the configuration of the pool is 3 mm in depth. The pool is 10 cm in diameter in the experiments and 10 cm in the 2-D simulations. The upper surface is exposed to water vapor containing surfactant, and the cooling chip (2 cm in diameter for experiment and 2 cm in width in the simulations) is positioned in the center under the bottom of the pool.

The computational work was based on the properties of water (density and specific heat) for simplicity; however, the application to lithium bromide solutions is a direct extension. It is assumed in the computational work that the surfactant stays on the surface after it condenses. Compared to water, both the solubility and the mass diffusivity of the surfactant are much less in a brine. Therefore, the assumption that the surfactant stays on the surface in the model is more accurate for the absorption problem with a LiBr solution. Thus, the simulation results represent a mixed case that is not directly comparable to the experiments.

The surface movements were observed in the experimental study under several operating modes. The mode where the cooling was turned on at the start is the case that was simulated. The pool was static before the cooling was applied and the surface movement was induced by the cooling.

The 2EH diffusion coefficient used in the simulations was  $1 \times 10^{-7}$  m<sup>2</sup>/sec, which is different from the value in the literature ( $1 \times 10^{-9}$  to  $1 \times 10^{-10}$  m<sup>2</sup>/sec in Kim and Janule (1994)). Based on the fact that the simulation results for the two values of diffusivity ( $1 \times 10^{-3}$  m<sup>2</sup>/sec and  $1 \times 10^{-7}$  m<sup>2</sup>/sec) did not exhibit large differences, it is expected that the simulation results are generally representative of the physics of interest.

#### 7.4.2 Discussion of Major Results

Based on results from both the simulations and experiments, the surface movement started at the edge of the cooling chip. This location corresponds to the point of highest heat flux (as shown in Figure 6.8), which has a high local value of surfactant surface concentration and high gradient in surface concentration. After the surface movement was initiated, the liquid on the surface moved from the center toward the edge of the pool eventually reaching a steady state circulation. The surface liquid moved radially outward from the edge of the cooling chip and then radially inward below the surface. The surface moves at a maximum speed of about 1 cm/s in the experiments and 0.8 cm/s in the simulations (Figure 6.9), and the surface involved in the liquid circulation extends to a maximum diameter of about 4 cm for both the experiments (Figure 5.7) and the simulations (Figure 6.12).

Although the applied cooling power and 2EH vapor concentration were much higher in the experiments as compared to the simulations, the time from applying the cooling to reaching the maximum liquid speed in the pool was much shorter for the simulation. One explanation for this difference is that the solution can still dissolve a portion of the 2EH although the solubility is low and the diffusivity is small. Therefore,

compared with the amount of 2EH dissolved in the liquid bulk, the amount of 2EH adsorbed on the surface is small. This dissolving of 2EH in the liquid results in a longer time needed to form a sufficient surface concentration gradient and surface tension gradient in the experiments.

The experiments show a dead zone in the center of the system (Figures 5.8 and 5.9), which was also present in the simulations (Figure 6.12). Relatively uniform 2EH surface concentration in the region above the cooling chip (Figure 6.7) is believed to be a main reason. Furthermore, it was observed in experiments that the surface velocity from the center toward the edge of the pool was about 0.5 cm/s (when a steady state circulation with a diameter of 4 cm was formed) whereas the return velocity (under the surface) was about 0.25 cm/s. Based on a mass balance, the depth involved in the flow from the center to the edge of the pool is about one-third of the depth of the pool. The simulation results shown in Figure 6.12 is consistent with this experimental observation.

Thus, the simulation confirmed that the surface movement after the cooling turned on discussed in Section 5.4.2 was induced by non-uniform 2EH surface concentration from the vapor side delivered to the surface by bulk flow of the condensing vapor.

## 7.5 Interpretation of Results in Terms of the Vapor Surfactant Theory

The recently proposed Vapor Surfactant theory of absorption enhancement in absorption chillers holds that the surfactant reaches the surface of the solution mainly from the vapor phase (Kulankara and Herold, 2000). In this theory, the bulk flow of water vapor from the vapor phase to the surface is identified as the primary source of surfactant on the surface, and the non-uniformity of surfactant arriving at the surface causes a non-

uniform surfactant surface concentration. Since the surface tension is largely determined by the surface concentration, the non-uniform surface concentration causes Marangoni convection, the ultimate mechanism of enhancement of heat and mass transfer, by providing mixing of the surface film. Based on the present study, a deeper understanding of the Vapor Surfactant theory was obtained as discussed next.

In the context of the Vapor Surfactant theory, the most important variables that influence the delivery of surfactant to the surface of the liquid are the surfactant vapor concentration and the mass flux of water vapor being absorbed. The flux of surfactant arriving at the surface is the product of these two variables. Once the surfactant arrives at the surface, a portion of it dissolves in the liquid. For this solvation process, two properties that govern the process are the solubility of the surfactant in the liquid and the mass diffusivity of the surfactant in the liquid. Two systems were studied which differ greatly in these properties. Aqueous lithium bromide has low values for both of these variables and, as a result, surfactant delivered to the liquid surface from the vapor tends to stay on the surface whereas water has much larger values and the experiments show that a significant amount of the surfactant delivered to the surface dissolves rapidly in the liquid.

The strength of Marangoni convection and absorption/condensation enhancement was observed to be dependent on the 2EH concentration in the vapor. In the present study, if 2EH vapor concentration was in the range of 400 to 1500 ppm, the strongest absorption occurred with a vigorous surface motion. If 2EH vapor concentration was outside this range, the Marangoni convection was much weaker. Therefore, it is concluded that there is an optimal 2EH vapor concentration, at which surface tension

gradients are maximized resulting in strong Marangoni convection and effective absorption/condensation enhancement.

Based on the measurements of surface tension for 60% LiBr solution (Section 3.3.2), surface tension is very sensitive to 2EH in the vapor, and relatively insensitive to 2EH in the liquid. Therefore, the 2EH vapor concentration is a dominant variable in absorption enhancement. In contrast, for the case of the measurements of surface tension of water, the surface tension was found to be sensitive to 2EH in both the vapor and the liquid. This difference is apparently due to the fact that in water, dissolved 2EH can diffuse to the surface rapidly. These differences in the way 2EH is transported in the liquid have a strong influence on the vapor conditions for optimum enhancement with condensation requiring a higher vapor concentration of surfactant for optimum enhancement.

Similar observations were made based on the absorption/condensation experiments. The optimum surfactant flux for absorption was identified and when a similar flux was tried for condensation, no Marangoni convection was observed. Only when a much larger flux of surfactant was imposed did the surface move during condensation.

# CHAPTER 8

## CONCLUSIONS AND RECOMMENDATIONS

## FOR FUTURE WORK

This chapter presents a summary of the work, conclusions regarding the effect of surfactants on surface tension, surface concentration and Marangoni convection in aqueous lithium bromide (LiBr) and water systems, and recommendations for future work.

### **8.1 Summary**

The novel surface tension measurement facility used in this work maintains a constant vapor concentration of 2-ethyl-hexanol (2EH) flowing past a drop weight surface tension setup. This facility was used for surface tension measurements on water and aqueous LiBr with controlled surfactant 2EH concentration in air. These measurements yield a probable error of  $\pm 1.43$  mN/m in surface tension, which is well below the deviations seen in the literature between different investigations. The ability to control the concentration of the surfactant in the vapor allowed a new understanding of dominant role that surfactant vapor plays in this system.

The absorption/condensation pool apparatus used in this work delivers steam, along with surfactant vapor, to the test chamber. This facility was used for absorption/condensation studies to understand the effect of vapor phase surfactants. Absorption and condensation, with and without cooling, were investigated and the

influence of key variables, such as the concentration of the surfactant in the vapor and vapor mass flux, was quantified. Although similar pool absorption/condensation experiments have been done previously, this is the first study where such experiments were done with controlled concentration of the surfactant in the vapor.

Based on the experimental and numerical analysis in the current study, it was found that the presence of surfactant (2EH) vapor alone is sufficient to cause a large reduction of surface tension due to a large increase of surfactant surface concentration. The Marangoni convection that results in significant heat and mass enhancement (up to 300%) in absorption chillers is found to be caused largely by surfactant delivered to the surface via bulk flow (along with water vapor).

The interaction of the surfactant with aqueous lithium bromide is strongly dependent on the concentration of the LiBr. In particular, the surfactant solubility is higher when the LiBr content is lower. Also, the diffusivity of surfactant in the liquid is retarded by the presence of the LiBr. Thus, although the basic mechanisms of enhancement are identical in condensation and absorption, the conditions under which maximum enhancement is obtained are different for pure water versus 60% LiBr. These effects are quantified throughout the thesis.

The importance of the surfactant vapor in absorption technology is highlighted in this work. The fact that the surface tension of aqueous lithium bromide can be reduced to the lowest values ever measured for this system by simply blowing air with 400 ppm of surfactant past the surface is a very important realization. On the other hand, if air with no surfactant is blown past the surface, the presence of surfactant in the liquid does not reduce the surface tension. Combined, these observations show that although the liquid in

the absorber does carry a small dissolved fraction of surfactant, which dissolved fraction plays only a minor role in enhancement. The dominant role is played by the surfactant vapor that passes through the absorption machine in a surfactant cycle and which returns to the absorber surface with the vapor coming from the evaporator. The work done in this thesis has quantified several aspects of this process and provided basic data that will allow others to pursue these ideas further.

## 8.2 Conclusions

- The equilibrium surface tension measurement results show that for both water and aqueous LiBr the surface tension is reduced with increased 2EH concentration in the system, and the plateau (i.e. minimum) surface tension values are experimentally determined to be 41 mN/m for water and 37 mN/m for 60% aqueous LiBr.
- An important property, solubility, is determined by a new method, called Solubility Limit of Vapor Surfactant with Adsorption (SLVSA), which accounts for the effect of 2EH adsorbed on the wall and 2EH in the vapor. The solubility of 2EH in aqueous LiBr decreases with mass fraction of aqueous LiBr. The solubility limits of 2EH in water and 60% aqueous LiBr were measured to be  $835 \pm 45$  ppm and  $27.1 \pm 0.56$  ppm, respectively, which are significantly different than previously reported values.
- The results of surface tension measurements show that surface tension decreases at a rate of 0.25 mN/m/ppm for 60% aqueous LiBr and in a rate of 0.075 mN/m/ppm for water with increases of 2EH concentration in vapor from 0 to 200 ppm. The results of 2EH surface concentration show that 2EH surface concentration increases with 2EH system concentration at a rate of 0.009 mg/m<sup>2</sup>/ppm for 60% aqueous LiBr and at a

rate of  $0.003 \text{ mg/m}^2/\text{ppm}$  for water with increases of 2EH system concentration from 0 to 100 ppm. The higher sensitivity of surface tension and surface concentration to vapor side delivery of surfactant exhibited by 60% aqueous LiBr as compared to water is mainly due to the differences in the mass diffusivity of 2EH and the solubility of 2EH in the two systems.

- The results of surface tension measurements show that for aqueous LiBr, the presence of 2EH in the liquid, even at its solubility limit, is not sufficient to cause a large reduction in surface tension (i.e. surface tension reduces from 96 mN/m with no 2EH to 87 mN/m with 100 ppm of 2EH in the liquid). By comparison surfactant levels of 100 ppm in the air flow, with no surfactant in the liquid, are sufficient to cause a significant reduction in the surface tension (i.e. the surface tension reduces from 96 mN/m with no 2EH to 56 mN/m with 100 ppm of 2EH in the air flow). Therefore, 2EH concentration in the vapor is concluded to be a primary variable in determining the surface tension of aqueous LiBr. Therefore, surfactant vapor concentration is understood to be a primary variable in the stimulation of Marangoni enhancement of absorption.
- The surface tension measurements for water show a much stronger dependence on drop frequency as compared to aqueous LiBr (60% aqueous LiBr was found to be essentially independent of drop frequency below 0.2 Hz while water showed sensitivity even at the lowest frequencies tested as shown in Figure 3.5). These results are apparently due to higher diffusivity and solubility of 2EH in water as compared to aqueous LiBr. For water, a large fraction of the 2EH delivered to the surface dissolves into the liquid bulk instead of staying on the surface.

- Surfactant in the vapor was observed to have a significant effect on the surface tension measurements and a lack of control of surfactant vapor conditions is thought to explain the large deviations in reported surface tension values for aqueous LiBr. Equilibrium surface tension results require that the vapor, liquid and surface all be in equilibrium but the slow diffusion rate of 2EH in the liquid implies that long times are required for the vapor to reach equilibrium if the 2EH is supplied solely by mixing in the liquid.
- The surface concentration values of 2EH are calculated from the new equilibrium surface tension data using a Gibbs analysis for both water and LiBr solutions. The presence of LiBr causes a reduction in 2EH solubility in the liquid and the surface concentration of 2EH increases as the concentration of LiBr is increased. The saturated surface concentrations are  $0.59 \text{ mg/m}^2$  for water and  $0.99 \text{ mg/m}^2$  for 60% LiBr solution.
- To achieve saturated surface concentration values of 2EH, it required on the order of 1000 ppm of 2EH vapor in air for water and on the order of 600 ppm for 60% aqueous LiBr. Since 2EH vapor concentration is based on the mass of air, this demonstrates the sensitivity of surface concentration of 2EH to vapor borne surfactant. In other words, addition of 2EH to the vapor side is a very efficient method to cause an increase of surface concentration of 2EH and thereby a reduction of surface tension.
- The strength of Marangoni convection and absorption enhancement is dependent on the 2EH concentration in the vapor. There is an optimal surfactant concentration to achieve maximum enhancement. In the current study, in a 60% aqueous LiBr

absorption pool with no 2EH in the solution, the maximum enhancement is achieved at a level of 1500 ppm of 2EH in vapor, accompanied by a vigorous surface motion.

Based on pressure history data, the absorption flux is calculated to be about  $0.2 \text{ g/m}^2 \cdot \text{s}$ , corresponding to heat flux of  $0.5 \text{ kW/m}^2$ . If the 2EH vapor concentration is lower than 200 ppm, relatively low flux of 2EH arriving at the surface is insufficient to cause a Marangoni flow. If the 2EH vapor concentration is higher than 2500 ppm, the large concentration of 2EH in the vapor presents a mass transfer resistance that limits the absorption and thus limits the Marangoni flow.

- Based on the numerical analysis (described in Chapter 6) on surfactant-induced condensation enhancement, the maximum condensation enhancement is achieved in the time range from 5 to 25 sec, when the corresponding surfactant surface concentration is in the range of 0 to  $0.5 \text{ mg/m}^2$ , which is below the saturation surface concentration in this case. Unfortunately, the experiments done in this work do not match the conditions of the simulation. Thus, the predictions made by the simulation will have to wait for further data for verification.
- The numerical analysis shows that the flow field is controlled by different factors at different times. In the current study, it is first controlled by natural convection (from 0 to 2.5 sec), and then dominated by Marangoni convection (from 2.5 to 25 sec). After 25 sec, the effect from natural convection is seen again.

### 8.3 Recommendations for Future Work

Recommendations for future work based on the current study are:

- The novel surface tension measurements reported in Section 3.2.1 use air as a carrier fluid. Similar surface tension measurements should be run using steam as the carrier fluid to isolate any effects caused by air. This would more closely mimic the conditions in an absorption chiller.
- To better understand the absorption and condensation enhancement due to Marangoni convection by surfactant, the experimental studies on absorption and condensation in a falling film absorber and condenser should be carried out with controlled vapor concentrations of surfactants and report the heat flux or mass flux as a key experimental variable.
- Expand the numerical analysis of absorption/condensation pool to include the evaporation, adsorption and diffusion of surfactant to replace the simple model used here which assumes that the surfactant stays on the liquid surface
- Expand theoretical analyses to configurations other than the pool.
- Expand theoretical analysis to include a stability analysis on the vapor surfactant absorption process.
- The non-linearity in the relationship between surface concentration and surface tension provides considerable complexity and slows down numerical simulations. However, this is one of the most important aspects of surfactant physics and should be included in numerical analysis of the basic fluid equations.
- To obtain high accuracy theoretical predictions, accurate values of surfactant diffusivity are needed.

## **APPENDIX A**

### **SOURCE CODE FOR 1-D SURFACTANT MASS TRANSFER EQUATION**

In the simulation of Marangoni convection during condensation in the presence of surfactant in the vapor (Chapter 6), Fluent, a commercial fluid flow code, was used with the 1-D surfactant mass transfer equation (Equation 6.4 in Section 6.3) solved as a user defined function (UDF) to find surfactant surface concentration. The surface tension and shear stress are also calculated in this UDF and are used as the boundary conditions for solving the momentum and energy equations in the main body of Fluent for the next iteration. This iteration process continues until the convergence criterion is satisfied and the simulation goes to the next step. The UDF is written in C language and the detailed source code is provided in this Appendix.

```
/*=====
```

This is a UDF (User Defined Function) code, which is used for  
1) Simulate the surfactant surface concentration.  
2) Find the surface tension based on surfactant surface concentration.  
3) Supply the boundary conditions for the main body of Fluent.  
4) Get the velocity profile and source term from main body for surfactant surface concentration simulation.

```
=====*/
```

```
#include "udf.h"                                /*Required by Fluent */  
#include "sg.h"                                  /*Required by Fluent */  
#include "math.h"                                /*Load math library */  
#define ND 101                                    /*Number of nodes */  
#define NC (ND-1)                                 /*Number of control volume */  
#define vapor_ppm 120.0                            /*Surfactant concentration in the vapor */  
#define controlPad 1e-7                            /*Diffusion coefficient, unit: m2/s */  
#define latent_heat 2437000.0                      /*Latent heat of steam at 1atm */  
#define length 0.05                               /*The length of the pool, unit: m */  
#define max(a, b) (((a) > (b)) ? (a) : (b))      /*Self defined function, to get the greater from a and b */  
  
#define WALL_ID 3                                 /*3 is a ID number corresponding to the top surface, which is decided during building the grid by Gambit, you need check this ID if you plan to make your own grid */  
  
enum  
{  
    conc,  
  
    conc_old,  
    timeold  
};  
  
/* UDS definition */  
  
/*1. Delete the output of S_C[]  
2. Delete the output of gSur[] */  
  
/* The UDF is comprised of two parts:  
1. Calculation of surfactant source from vapor phase.  
    Approach: correlate surfactant flux to steam absorption, then to heat flux;  
2. Define the B.Cs for top surface.  
    Approach: shear stress is controlled by surface tension that is related to the surfactant surface concentration */  
  
/* Global variables definition */  
static double Q[NC];                                /* surfactant source from vapor */  
  
DEFINE_PROFILE(shearstress_profile, thread, position)  
{  
    /* variable declarations */  
    double time;                                     /* time of current calculation */  
    double dt;                                       /* length of time step (s) */  
    double gSur[ND];                                 /* grid surfactant conc. for time step t */  
    double time_old;                                /* time of last iteration */  
    double gSur_old[ND];                            /* grid surfactant conc. for time step t */
```

```

double velocity[NC];
double r[ND_ND];
double x;
face_t f;
cell_t c;

int i;
float x1,x2;

float dx=length/(NC);
int jj;
/* FILE *gsurfle; */
double outputshst;
double shearStress[NC];
double old_time;
FILE *mass;

/* note that only cell values are used */

/* defined function in Fluent, to get temperature on
the face of the cell*/
/* defined function in Fluent, to get average
temperature on the cell*/

/* these variables are used to stored the gSur and
gSur_old of [ND-1] */

/* where stored in time_old[8] and time_old[18] */

/* shear stress on surface, CELL value */

/* file for storage of Q */

/* Function forward declarations */
double functionA(double P, int choice);
void TDMA(double a[ND-1],double b[ND],double c[ND],double d[ND]);
int gridConcentration(double *,int,double *,double,double,double,double,double,double);
int SMBE(double *,double *, int,double,double,double *,double *);
double interpolate( double x, double dx, double shearstress[NC]);

/* Function body */
time=RP_Get_Real("flow-time");
dt=RP_Get_Real("physical-time-step");
old_time=0.0;

/* 1. Read in time, time step size, velocity profile, concentration profile */
/* data needed: time, dt, gSur, gSur_old and velocity. Find the definitions of data in the variable section */

/* If this is the first iteration, the initial condition is specified here */
if(time<dt*(1+1e-6))
{
begin_c_loop(c,thread)
{
C_UDSI(c,thread,conc_old)=0.0;
C_UDSI(c,thread,timeold)=0.0;
}
end_c_loop(c,thread)
}
/* read in the time_old of last time iteration */
i=NC-1;
begin_c_loop(c,thread)
{
if(i==3)
    time_old=C_UDSI(c,thread,timeold);
    i--;
if (i==8)
    x1=C_UDSI(c,thread,timeold);          /* timeold[5..10] store gSur_old[ND-1] */
if (i==18)
    x2=C_UDSI(c,thread,timeold);          /* timeold[10..] store the gSur[ND-1] */
}
end_c_loop(c,thread)

```

```

/* input of velocity profile */
i=NC-1;
begin_c_loop(c,thread)
{
    velocity[i]=C_U(c,thread);
    i--;
}
end_c_loop(c,thread)

/* Update the time_old and gSur_old based on whether or not the last iteration lead to a new time step, these
values are stored in the arrays in this function for calculation */

if(fabs(time-dt)<1e-6)
{
    time_old=0;
    for(jj=0;jj<ND;jj++)
        gSur_old[jj]=0;
}
else if( (time-time_old-dt)>-1e-6) /* This means that the last time iteration leads to a
time step forward */
{
}

/* update the additive concentration of last time step with value get in lastest successful try */
i=NC-1; /* fprintf(gsurfile,"%f\n",time_old+222); */
begin_c_loop(c,thread)
{
    gSur_old[i]=C_UDSI(c,thread,conc);
    i--;
}
end_c_loop(c,thread)
gSur_old[ND-1]=x2;

/* update the time_old, tell FLUENT calculation has marched to the time now, but not simply another
iteration */
time_old=time;
}
else /* This means that the last iteration fails to march
into a new time step */
{
    /* use the time_old and gSur_old of last iteration */
    i=NC-1;
    begin_c_loop(c,thread)
    {
        gSur_old[i]=C_UDSI(c,thread,conc_old);
        i--;
    }
    end_c_loop(c,thread)
    gSur_old[ND-1]=x1;
}

/* update the UDS items about the time_old and gSur_old, this is done with the above operation */
i=NC-1;
begin_c_loop(c,thread)
{
    C_UDSI(c,thread,conc_old)=gSur_old[i];
}

```

```

        i--;
    }
end_c_loop(c,thread)

i=NC-1;
begin_c_loop(c,thread)
{
    if (i<=5)
        C_UDSI(c,thread,timeold)=time_old;
    if ((i>5) && (i<10))
        C_UDSI(c,thread,timeold)=gSur_old[ND-1];
    i--;
}
end_c_loop(c,thread)

/* 2. Calculate the proper shear stress and new surfactant concentration */
SMBE(shearStress,gSur,1999,time,dt,gSur_old,velocity);

/* 3. Tell FLUENT the shear stress at surface and time of this iteration (later
   used for judging of convergence, as well as surfactant concentration update)*/

begin_f_loop(f,thread)
{
    F_CENTROID(r,f,thread);
    x=r[0];
    F_PROFILE(f,thread,position)=interpolate(x,dx,shearStress);
}
end_f_loop(f,thread)

/* update the gSur_old in UDS, this has been done in the lines above */
/* update the gSur stored in UDS, this value will be used for a new gSur_old if this iteration converges */
i=NC-1;
begin_c_loop(c,thread)
{
    C_UDSI(c,thread,conc)=gSur[i];
    i--;
}
end_c_loop(c,thread)

/* update time_old in UDS and gSur_old[ND-1] and gSur[ND-1] */
i=NC-1;
begin_c_loop(c,thread)
{
    if(i<=5)
        C_UDSI(c,thread,timeold)=time_old;
    if ((i>15) && (i<20))
        C_UDSI(c,thread,timeold)=gSur[ND-1];
    i--;
}
end_c_loop(c,thread)

/* fclose(gsurfile); */
} /* end of the DEFINE_PROFILE */

/* This function calculate the grid value of additive concentration for one time step*/
int gridConcentration(double gSur[ND],int DIV,

```

```

double gSur_old[ND],double velocity[ND],double gama,double dx,double omg,double time,
double qLeft,double qRight)
{
int i;
double position; /* position of the cell center along surface, left most
is zero. */
double a[ND-1], b[ND], c[ND-1], d[ND]; /* coefficient of mass balance equation*/

/* set the coefficient for the discreted mass balance equation of additive */
double D=gama/dx; /* cell diffusion coefficient */
double Ve, Vw; /* cell velocity at east and west of the present point*/
double Fe, Fw; /* cell convection coefficient at west & east point to
present */
double Pe, Pw; /* ratio of convection intensity to diffusion intensity
*/
double S_c[ND], Sp=0; /* the source from vapor phrase is Sc[]+Sp*C */
int ch; /* discretion scheme 0 for upwind, 1 for power law,
and 2 for hybrid */

double functionA(double P, int choice);
void TDMA(double a[ND-1],double b[ND],double c[ND],double d[ND]);
int gridConcentration(double *,int,double *,double *,double,double,double,double,double);
int SMBE(double *,double *, int,double,double,double *,double *);
double interpolate( double x, double dx,double shearstress[NC]);
```

/\* Upwind scheme is used in this calculation \*/  
ch=1;

/\* 1. Calculation of surfactant absorption strength along nodes points \*/  
/\* in unit of mg/m \*/  
for(i=0;i<ND;i++)  
{  
  
if(i==0)  
S\_c[i]=Q[i];  
else if(i==ND-1)  
S\_c[i]=Q[i-1];  
else  
S\_c[i]=(Q[i]+Q[i-1])/2;  
if(S\_c[i]<0) /\* to avoid initial trivial problem \*/  
S\_c[i]=0;  
}

/\* 2. Set up the discretization equation of mass balance of surfactant over surface \*/  
for(i=0;i<ND;i++)  
{  
if(i==0)  
{  
position=0.5\*dx;  
Ve=velocity[i];  
Fe=Ve;  
Pe=Fe/D;  
  
/\* coefficient for ApXp=AeXe+AwXw+S \*/  
b[i]=omg/2+Fe+D\*(functionA(Pe,ch)+max(-1\*Pe,0));  
c[i]=D\*(functionA(Pe,ch)+max(-1\*Pe,0));

```

d[i]=qLeft+gSur_old[i]*omg/2;

/* for the source term from vapor phrase */
b[i]=-Sp*dx*0.5;
d[i]+=S_c[i]*dx*0.5;

/* coefficient for TDMA */
c[i]*=-1;
}

else if(i==ND-1)
{

position=(i+0.5)*dx;
Vw=velocity[i-1];
Fw=Vw;
Pw=Fw/D;

/* coefficient for ApXp=AeXe+AwXw+S */
a[i-1]=Fw+D*(functionA(Pw,ch)+max(-1*Pw,0));
b[i]=omg/2+D*(functionA(Pw,ch)+max(-1*Pw,0));
d[i]=omg/2*gSur_old[i]-qRight;

/* for the source term from vapor phrase */
b[i]=-Sp*dx*0.5; /* half cell ! */
d[i]+=S_c[i]*dx*0.5;

a[i-1]*=-1; /* coefficient for TDMA */
}

else
{
position=(i-0.5)*dx;
Vw=velocity[i-1];
Ve=velocity[i];
Fe=Ve;
Fw=Vw;
Pe=Fe/D;
Pw=Fw/D;

/* coefficient for ApXp=AeXe+AwXw+S */
a[i-1]=D*functionA(Pw,ch)+max(Fw,0);
c[i]=D*functionA(Pe,ch)+max(-1*Fe,0);
b[i]=omg+a[i-1]+c[i]+Fe-Fw;
d[i]=gSur_old[i]*omg;

/* for the source term from vapor phrase */
b[i]=-Sp*dx;
d[i]+=S_c[i]*dx;

/* coefficient for TDMA */
a[i-1]*=-1;
c[i]*=-1;
}

/* 3. solve the equation to get grid values of this time step */
TDMA(a,b,c,d);

```

```

/* 4. store the result of grid surfactant concentration into gSur[] */
for(i=0;i<ND;i++)
    gSur[i]=d[i];
return DIV;
}

double functionA(double P, int choice)
{
    double coeff;
    P=fabs(P);
    switch (choice)
    {
        case 0:
            coeff=1;
            break;
        case 1:
            coeff=max(0,pow(1-0.1*P, 5));
            break;
        case 2:
            coeff=max(0,1-0.5*P);
            break;
    }
    return coeff;
}

/* Following is a part to get the coefficients by Tri-diagonal Matrix Algorithm */
void TDMA(double a[ND-1],double b[ND],double c[ND],double d[ND])
{
    int ii;
    for(ii=1;ii<ND;ii++)
    {
        a[ii-1]=a[ii-1]/b[ii-1];
        b[ii]-=a[ii-1]*c[ii-1];
        d[ii]-=a[ii-1]*d[ii-1];
    }
    d[ND-1]=d[ND-1]/b[ND-1];
    for (ii=ND-2;ii>-1;ii--)
        d[ii]=(d[ii]-c[ii]*d[ii+1])/b[ii];
    return;
}

double interpolate( double x, double dx, double shearStress[NC])
{
    int cellno,next;
    double x1,x2;
    double result;
    double temp;

    x=x-dx/2;                                /* from the center of first cell */
    temp=x/dx;

    cellno=temp;                               /* cell before it */
    x1=cellno*dx;

    next=cellno+1;                            /* cell after it */
    x2=next*dx;
}

```

```

if(x<0)                                /* before the center of first CV */
    result=shearStress[0];
else if(x>dx*(NC-1))                  /* after the center of last CV */
    result=shearStress[NC-1];
else
    result=shearStress[cellno]+(shearStress[next]-shearStress[cellno])/(x2-x1)*(x-x1);

return result;
}

double C_F(double concen)
{
double tension;

/* the input of the formulation is in unit of mg/m^2, and the output is in unit of mN/m */
/* Note: Used after 7/7/00. One linear correlation from 0 to 1.2mg/m^2 */

if(concen<=1.2)
    tension=69.72852604-24.29566932*(concen-0.1);
else
    tension=43.00328979;

return tension/1000;                      /* convert into N/m which is used in all UDF */
}

int shearStressCalculation(double shearStress[NC],double gSur[ND],double dx)
{
int i;
for(i=0;i<NC;i++)
    shearStress[i]=(C_F(gSur[i+1])-C_F(gSur[i]))/dx;
return 0;
}

int SMBE(double shearStress[NC],double gSur[ND],
         int DIV,
         double time,double dt,double gSur_old[ND],double velocity[NC])
{
/* Section I. Variable Define      */
/* Specify the domain of calculation and grid specification */
double width=length;                      /* length of the free surface, (m) */
double dx=width/NC;
double omg=dx/dt;
double qLeft=0;
double qRight=0;                          /* additive output from right side (g/s) */

/* Specify the additive property      */
double gama=controlPad;                  /* diffusion coefficient of surfactant (m^2/s) */
int i;

/* Section II. Calculation surfactant concentration on surface */
gridConcentration(gSur,1999,gSur_old,velocity,gama,dx,omg,time,qLeft,qRight);

/* Section III. Calculate the shear stress on surface */
shearStressCalculation(shearStress,gSur,dx);

return DIV;
}

```

```

}

/* Part II. Solve for surfactant absorption
Approach: Use DEFINE_ADJUST() to calculate surfactant before each iteration */

DEFINE_ADJUST(gradient, domain)
{
face_t f;
cell_t c0;

real F_coord[ND_ND];
real C_coord[ND_ND];
real x, y, z;
real s0[ND_ND];
real A[ND_ND];
real At;
real alpha0;
real p0[ND_ND];
real beta0;
real dT_dn;

int i=NC-1;

Thread * wall_thread = Lookup_Thread(domain, WALL_ID);
Thread *fluid_thread = THREAD_T0(wall_thread); /* for cells next to WALL_ID */

Alloc_Storage_Vars(domain, SV_T_RG, SV_T_G, SV_NULL);
T_derivatives(domain);
Free_Storage_Vars(domain, SV_T_RG, SV_NULL);

/* find the surfactant flux at each cell */
begin_f_loop(f, wall_thread)
{
/* get index of cells next to WALL_ID */
c0 = F_C0(f, wall_thread);

/* get cell and face centroids */
C_CENTROID(C_coord, c0, fluid_thread);
F_CENTROID(F_coord, f, wall_thread);

x = F_coord[0];
y = F_coord[1];

NV_VV(s0, =, F_coord, -, C_coord);
F_AREA(A, f, wall_thread);
At = NV_MAG(A);

alpha0 = NV_DOT(A, A)/NV_DOT(A, s0);
NV_VS_VS(p0, =, A, /, alpha0, -, s0, *, 1);
beta0 = NV_DOT(p0, C_T_G(c0, fluid_thread));

/* temperature gradient along top surface */
dT_dn = (F_T(f, wall_thread) - C_T(c0, fluid_thread) + beta0)*alpha0/At;
/* heat absorbed though surface in unit of W */
Q[i]=dT_dn*C_K_L(c0,fluid_thread);
}

```

```

/* steam condensation in uit of kg/(s.m)*/
Q[i]=Q[i]/latent_heat;

/* surfactant flux in unit of kg/(s.m) */
Q[i]=Q[i]*vapor_ppm*1e-6;

/* surfactant flux in unit of mg/(s.m) */
Q[i]=Q[i]*1e6;

    i--;
}
end_f_loop(f, wall_thread)
}

/* This part specifies the cooling power along bottom surface */
DEFINE_PROFILE(coolingLine, thread, position)
{
    float time;
    float heatFlux;
    float x,r[ND_ND];
    face_t f;
    int i=0;
    time=RP_Get_Real("flow-time");

begin_f_loop(f,thread)
{
    F_CENTROID(r,f,thread);
    x=r[0];
    if(time<2)
    {
        if(x<0.01)                                /* cooling is confined in the left corner at the bottom
                                                       */
            heatFlux=-5000;
        else
            heatFlux=0;
    }
    else
    {
        if(x<0.01)
            heatFlux=-5000;
        else
            heatFlux=0;
    }
    F_PROFILE(f,thread,position)=heatFlux;
}
end_f_loop(f,thread)
}                                         /* end of the DEFINE_PROFILE */

```

## **APPENDIX B**

### **EXPERIMENTAL PROCEDURE FOR POOL ABSORPTION/CONDENSATION MEASUREMENTS**

Included here is a data sheet used in the experimental study of Marangoni convection in absorption/condensation in the presence of surfactant vapor. This data sheet summarizes the experimental procedure that was followed in order to observe the Marangoni convection and to obtain the quantitative data. The experimental procedure consists of eight main steps:

- 1) Clean the system with compressed air.
- 2) Set up the absorption/condensation pool, including loading the sample solution into the petri dish and positioning the thermocouples in the solution.
- 3) Introduce micro-sphere particles (for flow visualization) to the sample solution.
- 4) Introduce a measured amount of 2EH and water to the sample flask with all valves in the system closed.
- 5) Evacuate the chamber, the mixing flask and sample flask, respectively. The final pressure should be same as the vapor pressure of the liquid, zero and about 50 mmHg, respectively.
- 6) Warm the sample flask with the sample flask heater and then deliver sample vapor to the mixing flask with Valve 5 opened and Valves 1,2 and 3 closed (see Figure 5.1).

- 7) Open the valve 2 between the mixing flask and the static pool chamber (see Figure 5.1) and record the Marangoni convection on video tape and record temperature and pressure history from the transducers.
- 8) Repeat the data collection with cooling or heating applied in the center of the petri dish.

## ABSORPTION/CONDENSATION POOL MEASUREMENTS

Date and time: \_\_\_\_\_

Room temperature: \_\_\_\_\_;      Ambient pressure: \_\_\_\_\_

### The procedure for the experiments (Check the box next to each item)

- a. Clean the system by compressed air about 30mins (No water and 2EH?)
- b. Set up the thermal pad and thermal grease
- c. Introduce sample solution to the petri dish

W. of petri dish: \_\_\_\_\_(g); W. of aqueous LiBr : \_\_\_\_\_(g); Total: \_\_\_\_\_ (g)

Density and depth of the solution: \_\_\_\_\_ g/cm<sup>3</sup>; \_\_\_\_\_ (mm); (Note: Dia. of petri dish = 8.3cm)

Micro particles w: \_\_\_\_\_ (g) (0.015 is recommended)

- d. Set up the thermocouples in the liquid and vapor (Don't block the view)
- e. Close the cover (don't too tight the bolts)
- f. 2EH vapor concentration:

W<sub>2EH</sub> = \_\_\_\_\_ (g); W<sub>water</sub> = \_\_\_\_\_ (g; 1.0g recommended);

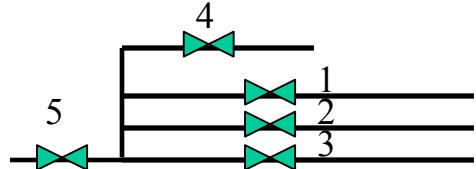
2EH conc. in water = \_\_\_\_\_ (ppm)

- g. Set the camera
- h. Close all valves
- i. Set up the pressure for the system including absorption/condensation pool

- The system pressure and temperature before evacuation:

p=\_\_\_\_\_ (mmHg); t=\_\_\_\_\_ (°C)

- Open valves V2 and V4
  - Turn on the vacuum pump and then open valve V1 very slowly to evacuate the system to 50mmHg. Actual pressure:\_\_\_\_\_ (mmHg)
  - Close valve V1 and then V2
  - Open valve V5 slowly (p=\_\_\_\_\_ mmHg)
  - Close V5 and reopen V1 to evacuate the pressure to 50mmHg again (p=\_\_\_\_\_ mmHg)
  - Close valve V1 and open valve V5 again. The pressure of sample flask: \_\_\_\_\_ (mmHg) (Final p ≤ 50mmHg)
  - Close valve V5
  - Open valve V1 and then V2 to evacuate the absorption/condensation pool until the pressure reaches the lowest value. The pressure of absorption/condensation pool: \_\_\_\_\_ (mmHg)
    - Maintain this status for 10 mins to check the leakage condition. (p from \_\_\_\_\_ to \_\_\_\_\_ (mmHg))
    - Air bubbles still in solution? \_\_\_\_\_



- ( ) j. Close valve V1 and then switch off vacuum pump
- ( ) k. Heat sample in the sample flask by a heater (see the condensation on the wall)
- ( ) l. Start the recording the videotape
- ( ) m. Switch off the heater and open the valve 5. Record the pressure and temperature
- ( ) n. Power on the cooling chip after initial movement stops and turn on the fan for the cooling chip
- ( ) o. After finishing the test, introduce the air to the system **very slowly** to protect the sealing (15mins at least)
- ( ) p. Weigh the petri dish: W = \_\_\_\_\_ (g), absorption amount: \_\_\_\_\_ (g)

The history of pressure and temperature after delivering 2EH

Time (s)	-0.1	0	10	20	30	40	50	60	70	80	90	120
Pressure (mmHg)												
Temp (center)												
Temp (edge)												
Temp (vapor)												
Time	150	180	210	240	270	300	330	360	390	420	450	480
Pressure (mmHg)												
Temp (center)												
Temp (edge)												
Temp (vapor)												

Observation of the surface movement during the period of 2EH delivering, cooling and heat modes

Time						
Status	Before evacuation	After evacuation	Right after V5 opened			
Pressure						
Temp (center)						
Temp (edge)						
Temp (vapor)						
Observation						
Time						
Status						
Pressure						
Temp (center)						
Temp (edge)						
Temp (vapor)						
Movement						

## APPENDIX C

### **REGRESSION OF THE PROPERTIES OF AQUEOUS LITHIUM BROMIDE BY GIBBS FREE ENERGY METHOD**

#### **C.1 Introduction**

An accurate expression for the thermodynamic properties of aqueous lithium-bromide is important for the current study and furthermore for design and testing of LiBr-based absorption machines. Therefore, a significant effort was spent in finding such an accurate expression based on available data (Yuan and Herold, 2005a). This appendix presents a summary of the work in obtaining an analytical expression for the properties of aqueous LiBr.

The traditional method in obtaining such an expression is based on a single property correlation. The single property correlation is usually available only for limited temperature and mass fraction ranges and usually leads to inconsistency in thermodynamic properties. To overcome these weaknesses, a multi-property correlation method based on the Gibbs free energy function is used for this study.

The multi-property correlation method combines and correlates all thermodynamic property data in a single expression. To do so, a functional form for the Gibbs free energy is first created; all available thermodynamic property data over the full temperature and mass fraction range are used to calculate the coefficients of Gibbs free energy. The resulting function is used to calculate particular thermodynamic properties

by thermodynamic theory resulting in complete thermodynamic consistency between properties so obtained.

However, thermodynamic consistency does not necessarily imply accuracy. To obtain an accurate expression, special attention was paid to obtain accurate experimental data over a wide range and to find an appropriate functional form for the Gibbs free energy.

## C.2 Multi-property Gibbs Free Energy Correlation Method

The multi-property correlation method combines and correlates all thermodynamic property data in a single expression based on a functional form for the Gibbs free energy. The steps to create this function and to use it for finding other thermodynamic properties are:

1. A functional form for the Gibbs free energy which is a function of solution temperature, mass fraction and vapor pressure is first formed.
2. And then, verified high-quality literature data for vapor pressure, specific heat data (mainly from our measurements) and density (volume) are combined together and regressed to obtain the coefficients of the Gibbs free energy.
3. The resulting function is then used to derive particular thermodynamic properties by differentiation and/or combination of terms of the Gibbs free energy by thermodynamic theory.

In order to find an appropriate functional form for the Gibbs free energy and to get good accuracy for the results, an arbitrary function was first postulated guided by experience obtained in earlier work (Herold, 1985). Each term of this functional form

was then tested individually against the data by knocking the term out and judging its contribution to the overall quality of the fit. Some terms were modified and additional terms were then added based on observations about the data and the fit. The final result is the empirical best fit based on a large number of attempts. The final function/efficient set is called SSC-4 (the fourth major variation coming out of the Sorption Systems Consortium effort).

### C.3 SSC-4 Correlation

#### C.3.1 Database Used to Generate the SSC-4 Correlation

A summary of the entire data set used for this correlation is given in Table C.1. The sources of experimental data used in SSC-4 are given in Table C.2. The data set consists of a mix of vapor pressure values from 13 authors, each of which covers a different range of temperature and concentration. The specific heat data in the literature was found to be inconsistent and an effort was initiated to measure the specific heat of aqueous lithium bromide over the complete range of temperature and concentration of interest. This new data set (see Figure C.5) was measured and then used in the correlation (see Appendix E for details). Density (volume) data were taken from 5 authors (it is noted that the density data for this system is very regular and the data from different authors is largely consistent).

Table C.1 Summary of the property data set used to generate SSC-4

Data Property	No. of data points	The range of data			Weight factor	No. of authors
		T(°C)	x(%)	p(kPa)		
<b>Vapor pressure</b>	641	T=1~350,	x=4~76,	p=0.7~15696	1	13
<b>Vapor pressure (H<sub>2</sub>O)</b>	12	T=0~220,	x=0,	p=0.26~2318	3	1
<b>Specific heat</b>	450	T=5~260,	x=5~74.76,		150	1
<b>Specific heat (H<sub>2</sub>O)</b>	53	T=0~260,	x=0		450	1
<b>Volume</b>	556	T=-60~220,x=1~65			1000000	5
<b>Volume (H<sub>2</sub>O)</b>	50	T=0~220,	x=0		1000000	1
<b>Enthalpy (Ref. point)</b>	1	T=0,	x=50,	p=0.153	200	
<b>Entropy (Ref. point)</b>	1	T=0,	x=50,	p=0.153	200	
<b>Total</b>	1764					22

Table C.2 The sources of experimental vapor pressure and density data used in SSC-4

The sources of experimental vapor pressure data used in SSC-4
Boryta, D.A., Maas, A.J., Giant, C. B., 1975, "Vapor Pressure-Temperature-Concentration Relationship for System Lithium Bromide and Water (40-70% Lithium Bromide)", J. Chem. Eng. Data, Vol. 20, pp. 316- 319.
Fedorov, M.K., Antonov, N.A., Lvov, S.N., 1975, "Vapor Pressure of Saturated Aqueous Solutions of LiCl, LiBr, and LiI and Thermodynamic Characteristics of the Solvent in these Systems At Temperatures of 150-350°C and Pressures Up To 1500 Bar", Translated from Zhurnal Prikladnoi Khimii, Vol. 49, No. 6, pp. 1226-1232 (taken from Eng. Trans : J. App. Chem. USSR, 1976).
Feuerecker, G., Scharfe, J., Greiter, I., 1993, "Measurement of Thermophysical Properties of Aqueous LiBr- Solutions at High Temperatures and Concentrations", International Absorption Heat Pump Conference, AES-Vol. 31, pp. 493-499.
I.C.T, 1928, International Critical Tables, McGraw-Hill.
Lenard, J.L.Y., Jeter, S.M., Teja, A.S., 1992, "Properties of Lithium Bromide-Water Solutions at High Temperatures and Concentrations - Part IV: Vapor Pressure", ASHRAE Transactions, Vol. 2, pp. 167-172.
Lower, H., 1960, "Thermodynamische und physikalische Wigenhaftungen der Wassrigen Lithium bromid- Losung", Ph.D. Dissertation, Technischen Hochschule Karlsruhe.
Matsuda, A., Munakata, T, Yoshimaru, T., 1980, "Measurement of Vapor Pressures of Lithium Bromide Water Solutions" (in Japanese), Kagaku-kogaku Ronbunshu, Vol. 6, pp. 119-122.
Maust, E.E., Jr., 1966, "New Absorbent-Refrigerant Combinations For Air

Conditioning Absorption Refrigeration", Ph.D Dissertation, University of Maryland.
McNeely, L. A., 1979, "Thermodynamic properties of aqueous solution of LiBr", ASHRAE Trans. Vol. 3, pp. 413-434.
Murakami, K., Sato, H., Watanabe, K., 1993, "Measurements of Bubble-Point Pressures for the Binary LiBr/H <sub>2</sub> O Pair", International Absorption Heat Pump Conference, AES-Vol. 31, pp. 509-515.
Patil, K.R., Tripathi, Atri D., Pathak, G., Katti, S.S., 1990, "Thermodynamic Properties of Aqueous Electrolyte Solutions. 1 Vapor Pressure of Aqueous Solutions of LiCl, LiBr, and LiI", J. Chem. Eng. Data, Vol. 35, pp 166-168.
Pennington, W., 1955, "How to Find Accurate Vapor Pressures of Lithium Bromide Water Solutions", Refrig. Eng., Vol. 63, pp. 57-61.
Wark, K., 1995, "Advanced thermodynamics for engineering", McGraw-Hill, Inc.
<b>The sources of experimental density (volume) data used in SSC-4</b>
Bogatykh,S.A., Evnovich, I.D., 1965, "Investigation of Densities of aqueous LiBr, LiCl, and CaCl <sub>2</sub> solutions in relation to conditions of gas drying", Zhurnal Prikladnoi Khimii, Vol. 38, No. 4, pp. 945-946.
I.C.T, 1928, International Critical Tables, McGraw-Hill, Density - Aqueous Inorganic Solutions, pp. 77.
Lee, R.J., DiGuilio, R.M., Jeter, S.M., Teja, A.S., 1990, "Properties of Lithium Bromide-Water Solutions at High Temperatures and Concentrations - II: Density and Viscosity ", ASHRAE Transactions, Vol. 96. No part1, pp709-714
Mashovets et al., 1971, "Viscosity and Density of Aqueous LiCl, LiBr, and LiI Solutions at Moderate and Low Temperatures", Lensoviet Leningrad Technological Institute, Translated from Zhurnal Prikladnoi Khimii, Vol. 44, No. 9, pp. 1981-1986.
Wimby,J. M., Berntsson,T.S., 1994, "Viscosity and Density of Aqueous Solutions of LiBr, LiCl, ZnBr <sub>2</sub> , CaCl <sub>2</sub> , and LiNO <sub>3</sub> . 1. Single Salt Solutions", J. Chem. Eng. Data, Vol. 39, pp. 68-72.

### C.3.2 Functional Form of Gibbs Free Energy and Other Thermodynamic Properties

After considerable effort in testing and analyzing numerous terms, the final functional form for the SSC-4 Gibbs free energy expression is given here, which involved 42 terms and coefficients.

**Gibbs free energy (kJ/kg):**

$$\begin{aligned}
g(x, T, p) = & (A_0 + A_1x + A_2x^2 + A_3x^3 + A_4x^{1.1}) \\
& + T(B_0 + B_1x + B_2x^2 + B_3x^3 + B_4x^{1.1}) \\
& + T^2(C_0 + C_1x + C_2x^2 + C_3x^3 + C_4x^{1.1}) \\
& + T^3(D_0 + D_1x + D_2x^2 + D_4x^{1.1}) \\
& + T^4(E_0 + E_1x) \\
& + \frac{F_0 + F_1x}{T - T_0} \\
& + p(V_0 + V_1x + V_2x^2 + V_3T + V_4xT + V_5x^2T + V_6T^2 + V_7xT^2) \\
& + \ln(T)(L_0 + L_1x + L_2x^2 + L_3x^3 + L_4x^{1.1}) \\
& + T \ln(T)(M_0 + M_1x + M_2x^2 + M_3x^3 + M_4x^{1.1})
\end{aligned}$$

Based on the thermodynamic property expression, the coefficients  $A_1$  and  $B_1$  cannot be decided from the selected data set. However,  $A_1$  and  $B_1$  can be decided if the reference points for enthalpy and entropy are given. The coefficients  $A_1$  and  $B_1$  were selected to obtain enthalpy and entropy zero at  $x = 50\%$  and  $T = 0^\circ\text{C}$ .

The form of the terms for pure water, given next, are similar to those used in the NBS Steam Tables (Haar et al., 1984);

$$\begin{aligned}
& T(B_0 + B_1x + B_2x^2 + B_3x^3 + B_4x^{1.1}) \\
& + \ln(T)(L_0 + L_1x + L_2x^2 + L_3x^3 + L_4x^{1.1}) \\
& + T \ln(T)(M_0 + M_1x + M_2x^2 + M_3x^3 + M_4x^{1.1})
\end{aligned}$$

These terms improve the fitting of  $c_p$  data in the middle temperature range.

In order to improve the correlation in the low temperature range,  $(F_0 + F_1x)/(T - T_0)$  is included. It significantly changes the chemical potential of water in the low temperature range and improves the accuracy for the regression of vapor pressure.

The terms  $(E_0 + E_1x)T^4$  were added to improve the characteristics of the fit in the high temperature range from 260 to 300°C, which is beyond the available data range.

Furthermore, the terms with power 1.1 improved the deviation between our enthalpy data and McNeely's results for mass fractions from 10 to 40%.

By using thermodynamic relations between the Gibbs free energy and other thermodynamic properties (Bejan, 1997), other thermodynamic properties are derived as follows.

### **Chemical potential of water (kJ/kg):**

$$\begin{aligned}
 \mu_w(x, T, p) &= g - x \left( \frac{\partial g}{\partial x} \right)_{T, p} \\
 &= (A_0 - A_2 x^2 - 2A_3 x^3 - 0.1A_4 x^{1.1}) \\
 &\quad + T(B_0 - B_2 x^2 - 2B_3 x^3 - 0.1B_4 x^{1.1}) \\
 &\quad + T^2(C_0 - C_2 x^2 - 2C_3 x^3 - 0.1C_4 x^{1.1}) \\
 &\quad + T^3(D_0 - D_2 x^2 - 0.1D_4 x^{1.1}) \\
 &\quad + T^4(E_0) \\
 &\quad + \frac{F_0}{T - T_0} \\
 &\quad + p(V_0 - V_2 x^2 + V_3 T - V_5 x^2 T + V_6 T^2) \\
 &\quad + \ln(T)(L_0 - L_2 x^2 - 2L_3 x^3 - 0.1L_4 x^{1.1}) \\
 &\quad + T \ln(T)(M_0 - M_2 x^2 - 2M_3 x^3 - 0.1M_4 x^{1.1})
 \end{aligned}$$

### **Volume (m<sup>3</sup>/kg):**

$$\begin{aligned}
 v(x, T) &= \left( \frac{\partial g}{\partial p} \right)_T \\
 &= V_0 + V_1 x + V_2 x^2 + V_3 T + V_4 x T + V_5 x^2 T + V_6 T^2 + V_7 x T^2
 \end{aligned}$$

**Specific heat (kJ/kg.K):**

$$\begin{aligned}
c_p(x, T) &= -T \left( \frac{\partial^2 g}{\partial T^2} \right)_{p,x} \\
&= -2T(C_0 + C_1x + C_2x^2 + C_3x^3 + C_4x^{1.1}) \\
&\quad - 6T^2(D_0 + D_1x + D_2x^2 + D_4x^{1.1}) \\
&\quad - 12T^3(E_0 + E_1x) \\
&\quad - 2 \frac{(F_0 + F_1x)T}{(T - T_0)^3} \\
&\quad - 2pT(V_6 + V_7x) \\
&\quad + \frac{1}{T}(L_0 + L_1x + L_2x^2 + L_3x^3 + L_4x^{1.1}) \\
&\quad - (M_0 + M_1x + M_2x^2 + M_3x^3 + M_4x^{1.1})
\end{aligned}$$

**Entropy (kJ/kg.K):**

$$\begin{aligned}
s(x, T, p) &= - \left( \frac{\partial g}{\partial T} \right)_{p,x} \\
&= -(B_0 + B_1x + B_2x^2 + B_3x^3 + B_4x^{1.1}) \\
&\quad - 2T(C_0 + C_1x + C_2x^2 + C_3x^3 + C_4x^{1.1}) \\
&\quad - 3T^2(D_0 + D_1x + D_2x^2 + D_4x^{1.1}) \\
&\quad - 4T^3(E_0 + E_1x) \\
&\quad + \frac{F_0 + F_1x}{(T - T_0)^2} \\
&\quad - p(V_3 + V_4x + V_5x^2 + 2V_6T + 2V_7xT) \\
&\quad - \frac{1}{T}(L_0 + L_1x + L_2x^2 + L_3x^3 + L_4x^{1.1}) \\
&\quad - (\ln(T) + 1)(M_0 + M_1x + M_2x^2 + M_3x^3 + M_4x^{1.1})
\end{aligned}$$

### Enthalpy (kJ/kg):

$$\begin{aligned}
h(x, T, p) &= g + Ts = g - T \left( \frac{\partial g}{\partial T} \right)_{p,x} \\
&= (A_0 + A_1x + A_2x^2 + A_3x^3 + A_4x^{1.1}) \\
&\quad - T^2(C_0 + C_1x + C_2x^2 + C_3x^3 + C_4x^{1.1}) \\
&\quad - 2T^3(D_0 + D_1x + D_2x^2 + D_4x^{1.1}) \\
&\quad - 3T^4(E_0 + E_1x) \\
&\quad + (F_0 + F_1x) \left( \frac{1}{T - T_0} + \frac{T}{(T - T_0)^2} \right) \\
&\quad + p(V_0 + V_1x + V_2x^2 - V_6T^2 - V_7xT^2) \\
&\quad + (\ln(T) - 1)(L_0 + L_1x + L_2x^2 + L_3x^3 + L_4x^{1.1}) \\
&\quad - T(M_0 + M_1x + M_2x^2 + M_3x^3 + M_4x^{1.1})
\end{aligned}$$

### Vapor pressure (kPa):

Vapor pressure cannot be calculated directly like the other thermodynamic properties. It is derived from the Gibbs free energy expression by the following steps.

Given: Solution temperature T and mass fraction x

Guess: Vapor pressure p

Compute: Chemical potential  $\mu_w(x, T, p)$  of water in aqueous LiBr

Compute: Gibbs free energy g of steam at T, p

If  $g \neq \mu_w$ , guess a new pressure value by iteration until  $g = \mu_w$ .

### C.3.3 SSC-4 Regression Results

The coefficients for the SSC-4 correlation are given in Table C.3. The standard error and R. squared are 3.914 and 0.99993, respectively.

Table C.3 Coefficients for SSC-4

$A_0 = 5.506219979E+3$	$B_0 = 1.452749674E+2$	$C_0 = 2.648364473E-2$
$A_1 = 5.213228937E+2$	$B_1 = -4.984840771E-1$	$C_1 = -2.311041091E-3$
$A_2 = 7.774930356$	$B_2 = 8.836919180E-2$	$C_2 = 7.559736620E-6$
$A_3 = -4.575233382E-2$	$B_3 = -4.870995781E-4$	$C_3 = -3.763934193E-8$
$A_4 = -5.792935726E+2$	$B_4 = -2.905161205$	$C_4 = 1.176240649E-3$
$D_0 = -8.526516950E-6$	$E_0 = -3.840447174E-11$	$F_0 = -5.159906276E+1$
$D_1 = 1.320154794E-6$	$E_1 = 2.625469387E-11$	$F_1 = 1.114573398$
$D_2 = 2.791995438E-11$		
$D_3 = -8.511514931E-7$		
$V_0 = 1.176741611E-3$	$L_0 = -2.183429482E+3$	$M_0 = -2.267095847E+1$
$V_1 = -1.002511661E-5$	$L_1 = -1.266985094E+2$	$M_1 = 2.983764494E-1$
$V_2 = -1.695735875E-8$	$L_2 = -2.364551372$	$M_2 = -1.259393234E-2$
$V_3 = -1.497186905E-6$	$L_3 = 1.389414858E-2$	$M_3 = 6.849632068E-5$
$V_4 = 2.538176345E-8$	$L_4 = 1.583405426E+2$	$M_4 = 2.767986853E-1$
$V_5 = 5.815811591E-11$		$T_0 = 220K$
$V_6 = 3.057997846E-9$		
$V_7 = -5.129589007E-11$		
Units: Temperature (K)	Gibbs free energy (J/g)	
Mass fraction (%)	Enthalpy (J/g)	
Pressure (kPa)	Entropy (J/g-K)	
Volume (m <sup>3</sup> /kg)		

## C.4 Verification and Discussion

Error plots are given for vapor pressure, specific heat and volume in Figures C.1 to C.3. These plots show the results of the SSC-4 correlation compared against the input data. The average error for vapor pressure, specific heat and volume are 2.99%, 0.754% and 0.172%, respectively. Where the average error is defined as:

$$Y_{\text{exp},ave} = \frac{1}{n} \sum \frac{|Y_{\text{exp},i} - Y_{\text{SSC-4},i}|}{Y_{\text{SSC-4},i}} \times 100\%$$

As can be seen from Figure C.1, a large deviation for one line of data was found in the vapor pressure error plot, which is from Lower's (1960) pressure data. Because of limited data in this region, these data were retained. By comparison, the average errors for specific heat and volume are much smaller. The small error indicates that our experimental data has good consistency.

Furthermore, comparisons of vapor pressure, specific heat and volume between the SSC-4 correlation and some selected experimental data from the literature were made. Figure C.4 shows a comparison of specific heat between the SSC-4 correlation and our experimental data. As can be seen, the SSC-4 correlation matches both our experimental data and the pure water data very well over the entire data range.

A comparison between the SSC-4 correlation and McNeely's [1979] data for vapor pressure is given in Figure C.5. It should be noted that these data were not used in the Gibbs free energy regression and so this comparison represents an independent check. Good consistency is obtained over most of the domain. However, some deviation is observed at mass fraction 70%. This deviation helps to explain the deviation in the enthalpy data discussed in the next paragraph. A comparison of volume between the SSC-4 correlation and the data of Lee et al. (1990) and I.C.T. (1928) is shown in Figure C.6 and the agreement is very good as well.

For further verification, a comparison of enthalpy between calculated values from the SSC-4 correlation and the McNeely correlation (1979) was made. The enthalpy comparison is shown in Figure C.7 and the enthalpy difference is also given in Table C.4. The largest deviation was found at 70% LiBr and is attributed to insufficient experimental data. In the range above 130°C, the deviation is due to the different vapor pressure data from the SSC-4 correlation and McNeely's data, which can be seen in Figure C.5. The method for calculating the enthalpy in McNeely (1979) is based on the slope of the vapor pressure at constant mass fraction. Thus, different vapor pressure values cause a deviation in enthalpy value. It should be noted that no enthalpy data were used in the SSC-4 correlation. This makes the agreement shown here more impressive

both as an indication of the usefulness of the formulation and as an indication of the level of consistency among all the properties.

Table C.4 Enthalpy difference between the SSC-4 correlation and McNeely's data  
(Unit for enthalpy difference: kJ/kg)

	A	B	C	D	E	F	G	H	I
1	<b>Enthalpy difference between SSC-4 correlation and McNeely's data</b>								
2	Note: $h'$ =Enthalpy from SSC-4 correlation, $h$ =McNeely's enthalpy data								
3									
4									
5	<b>t (°C)</b>	<b>x=0%</b>	<b>x=10%</b>	<b>x=20%</b>	<b>x=30%</b>	<b>x=40%</b>	<b>x=50%</b>	<b>x=60%</b>	<b>x=70%</b>
6		<b>h'-h</b>	<b>h'-h</b>	<b>h'-h</b>	<b>h'-h</b>	<b>h'-h</b>	<b>h'-h</b>	<b>h'-h</b>	<b>h'-h</b>
7	<b>0.0</b>	-0.6	-2.6	0.5	-2.1	-3.6	-0.0	-1.2	12.4
8	<b>10.0</b>	-0.6	-0.9	3.0	0.7	-1.1	2.1	1.1	15.5
9	<b>20.0</b>	-0.7	0.5	4.8	2.7	0.6	3.3	2.4	17.1
10	<b>30.0</b>	-0.8	1.4	5.8	2.9	0.5	3.2	2.4	17.0
11	<b>40.0</b>	-0.7	2.2	6.4	3.9	1.2	3.2	2.7	17.0
12	<b>50.0</b>	-0.6	3.5	7.8	5.0	1.9	3.5	2.8	17.0
13	<b>60.0</b>	-0.5	3.9	8.2	5.6	2.1	3.5	2.8	16.9
14	<b>70.0</b>	-0.4	5.0	9.3	6.8	3.2	3.5	2.7	16.8
15	<b>80.0</b>	-0.4	1.9	8.8	7.0	3.2	3.7	2.8	16.7
16	<b>90.0</b>	-0.3	5.6	9.3	7.6	3.4	3.7	2.7	16.4
17	<b>100.0</b>	-0.3	6.1	9.6	7.9	3.9	3.8	3.0	16.4
18	<b>110.0</b>	-0.4	6.4	9.9	8.0	4.4	4.1	3.2	16.6
19	<b>120.0</b>	-0.5	6.8	10.1	8.2	4.8	4.4	3.7	16.3
20	<b>130.0</b>	-0.6	6.9	10.6	8.3	5.1	4.9	4.5	16.3
21	<b>140.0</b>	-0.7	6.4	9.9	8.8	5.5	5.4	5.3	16.4
22	<b>150.0</b>	-0.9	6.5	9.8	8.7	5.8	5.7	5.9	16.5
23	<b>160.0</b>	-1.1	5.6	9.8	9.0	6.2	6.2	7.0	16.9
24	<b>170.0</b>	-1.2	4.9	9.6	9.0	6.9	6.8	7.6	17.8
25	<b>180.0</b>	-1.3	4.3	9.0	8.9	7.4	7.4	8.6	19.4

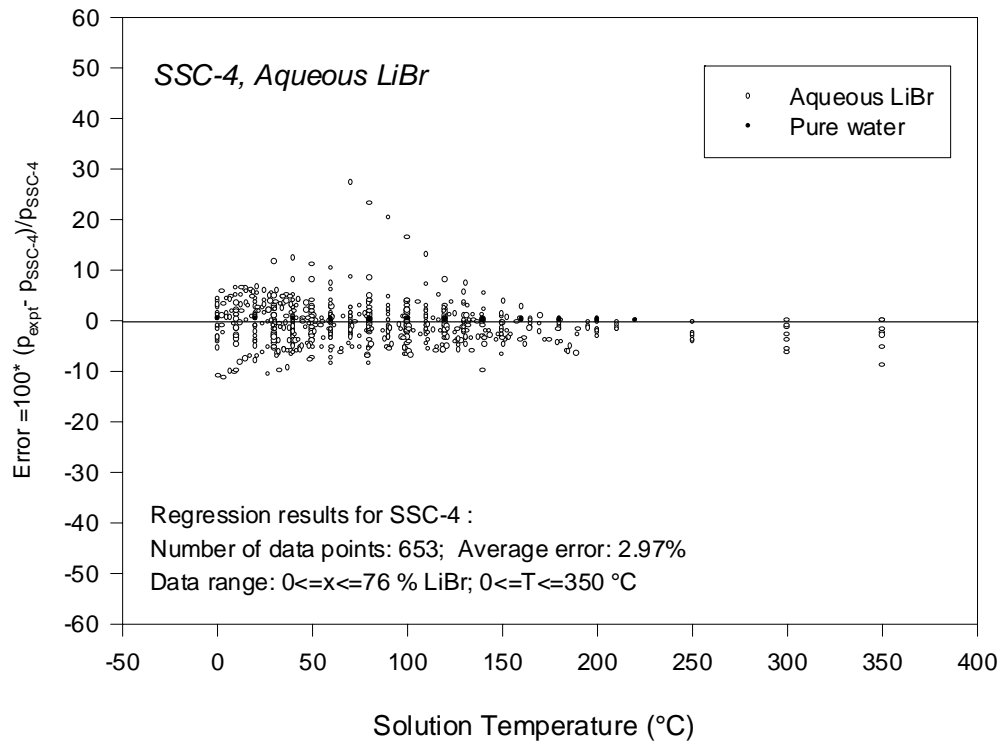


Figure C.1 Vapor pressure error plot

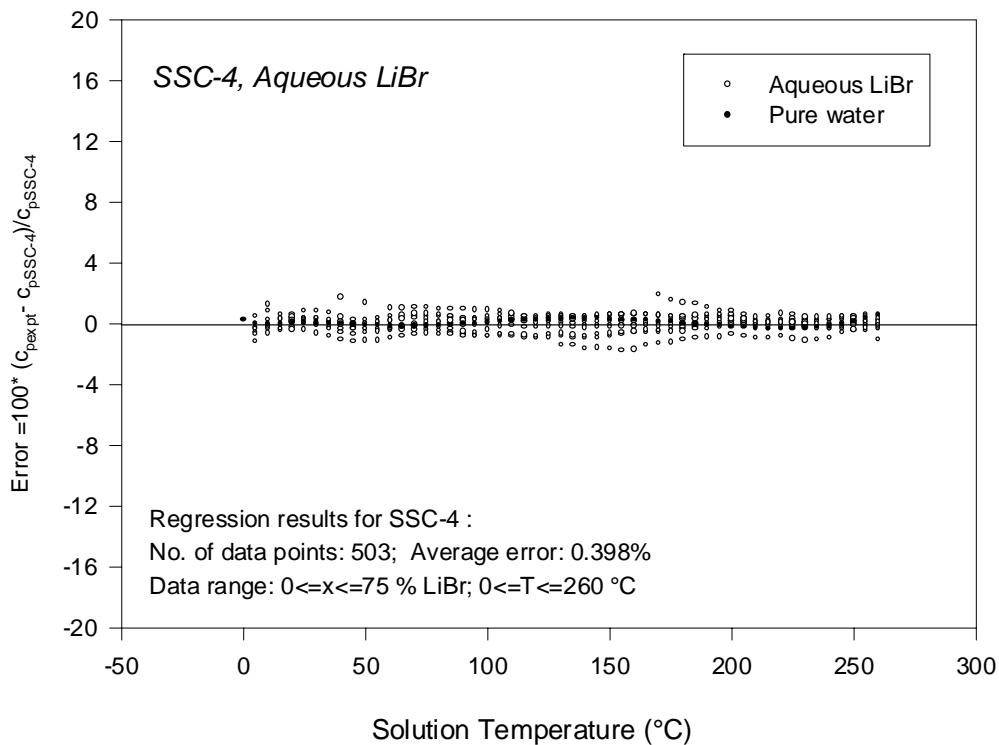


Figure C.2 Specific heat error plot

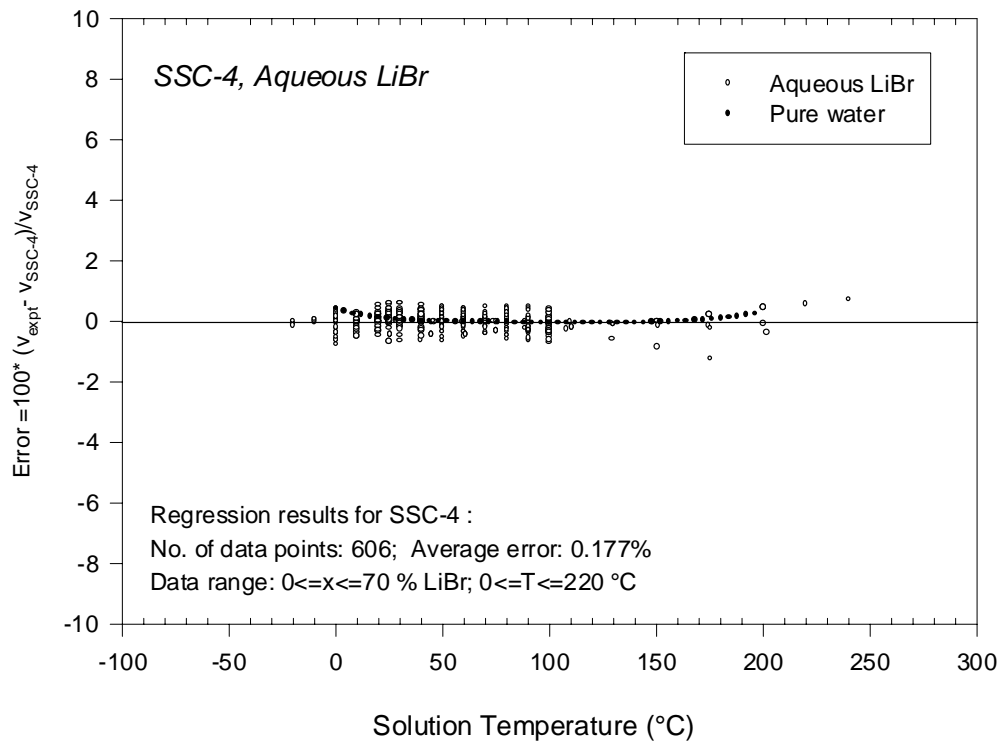


Figure C.3 Volume error plot

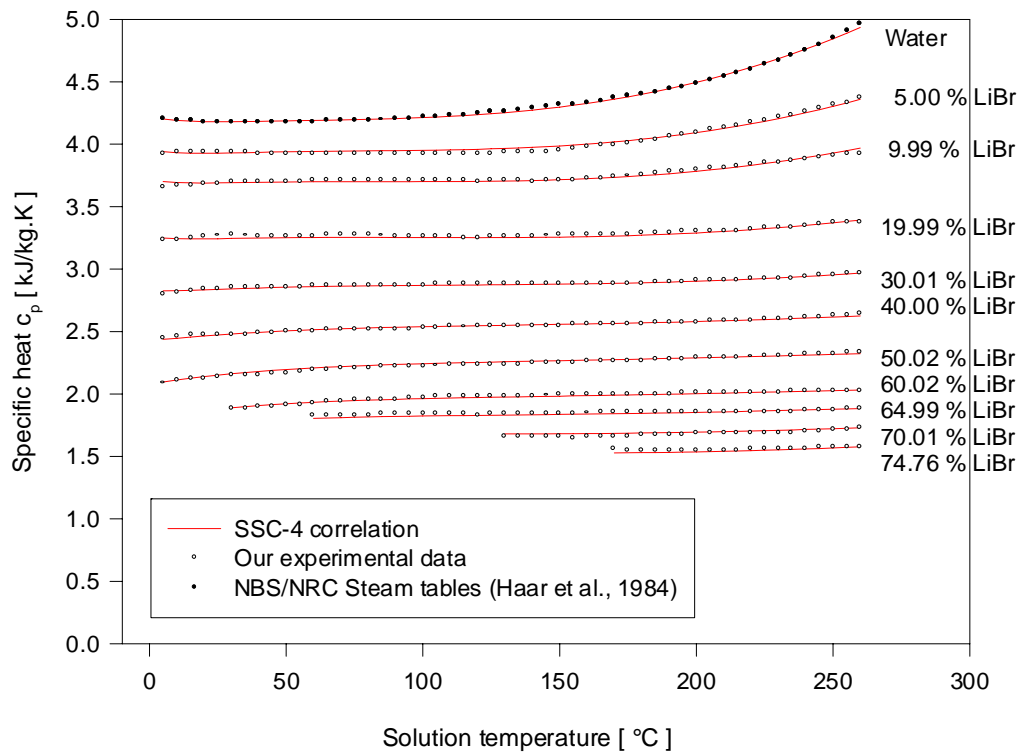


Figure C.4 Comparison of specific heat between SSC-4 correlation and experimental data

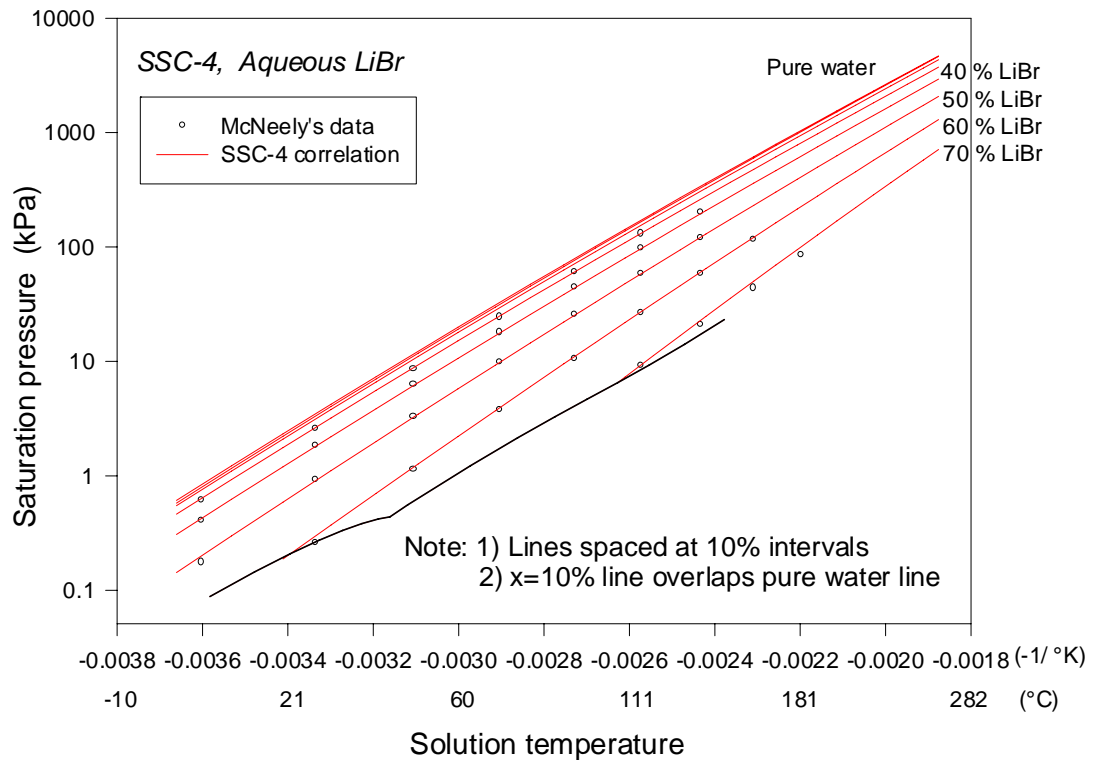


Figure C.5 Comparison of vapor pressure between SSC-4 correlation and McNeely's data

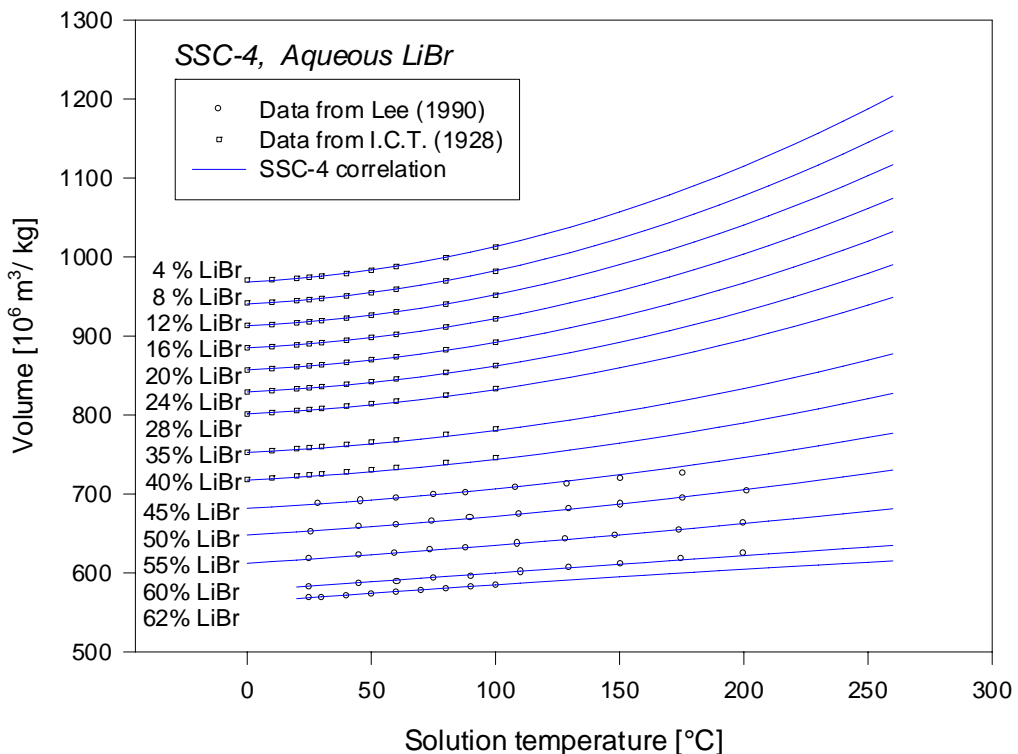


Figure C.6 Comparison of volume between SSC-4 correlation and experimental data

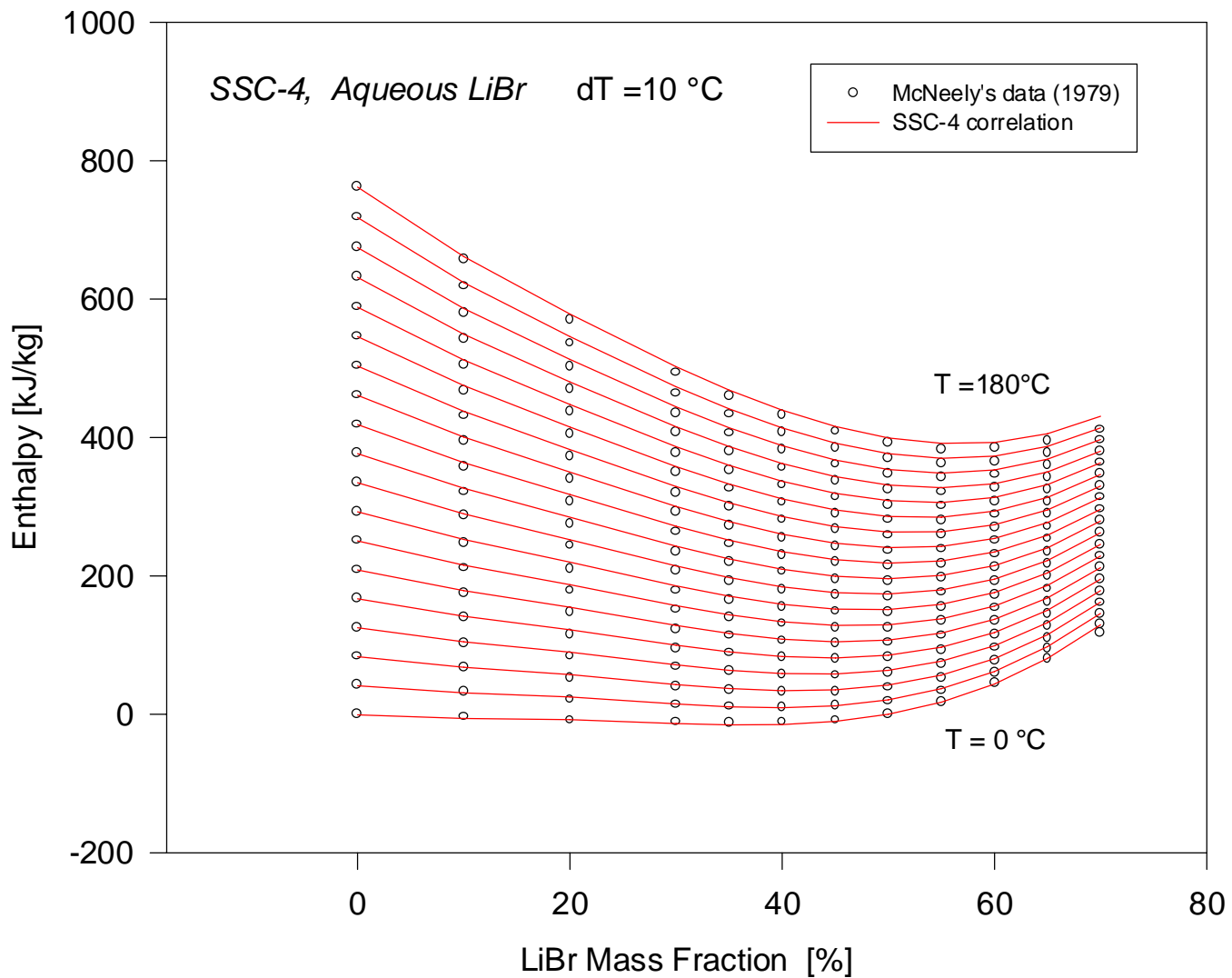


Figure C.7 Comparison of enthalpy between SSC-4 correlation and McNeely's data

## C.5 Thermodynamic Property Plots

Besides the thermodynamic properties mentioned in Section C.4, other thermodynamic properties including Gibbs free energy, chemical potential of water in solution and entropy are shown in Figures C.8 to C.10, with a full range of temperature from 0 to 300°C and mass fraction from 0 to 70% LiBr. Based on these plots, it can be said that the SSC-4 correlation exhibits smooth behavior even near the edges of the input data range. This, again, is an indication of the usefulness of formulation and the consistency among the thermodynamic properties.

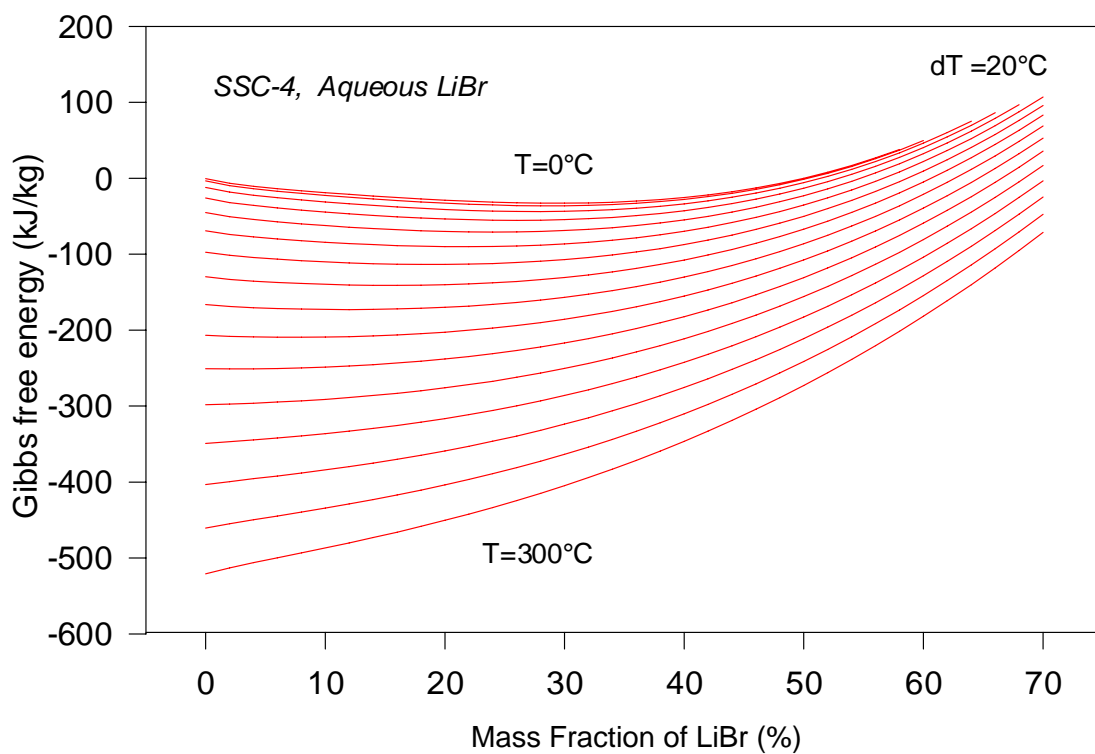


Figure C.8 Gibbs free energy property plot

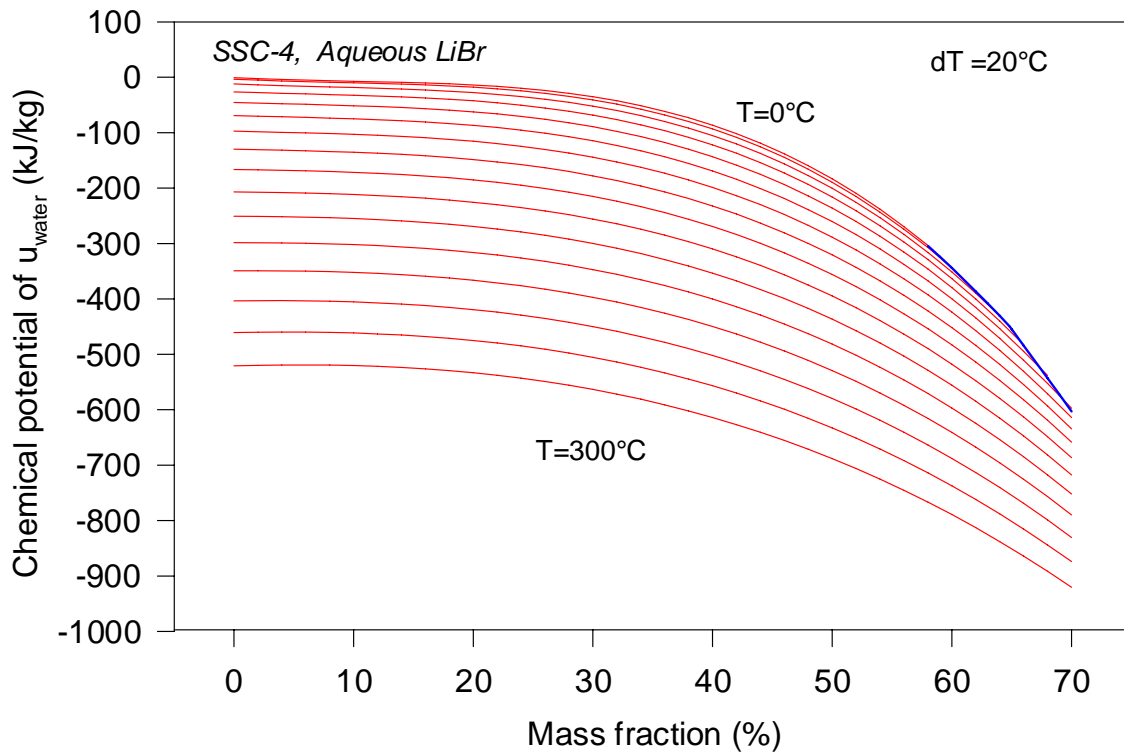


Figure C.9 Chemical potential of water property plot

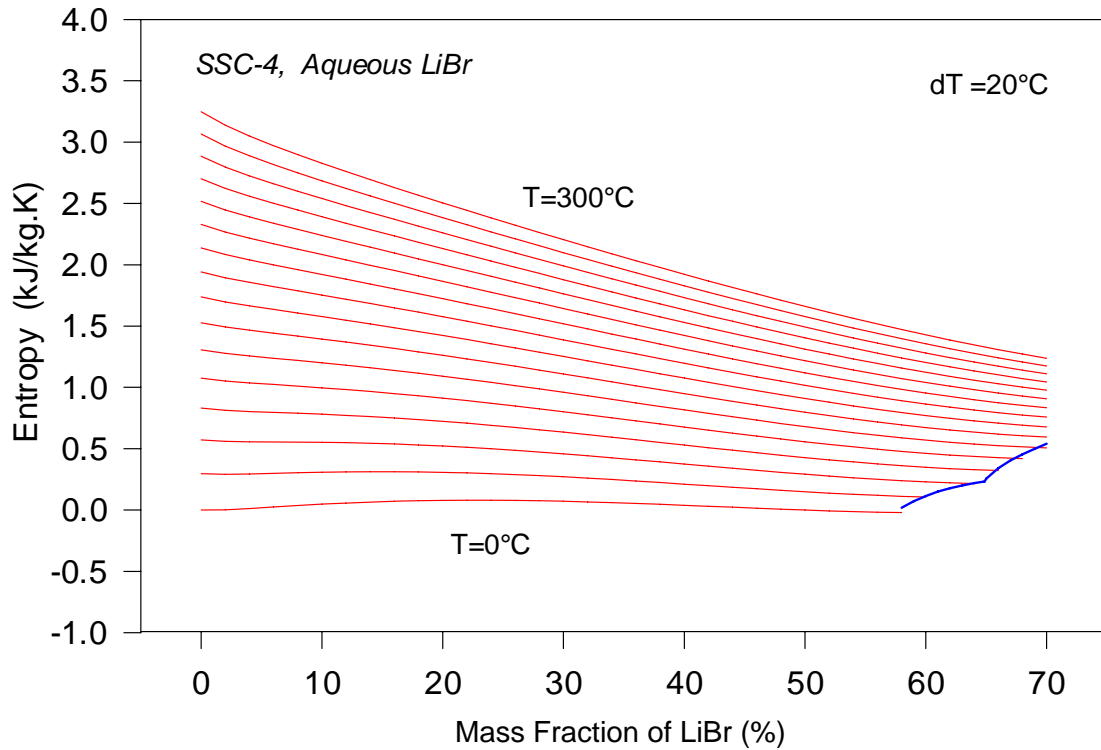


Figure C.10 Entropy property plot

## C.6 Conclusion

A multi-property correlation method using a Gibbs free energy functional form was used to regress the thermodynamic properties of aqueous LiBr. The final version, SSC-4, was obtained after careful examination of each term of the correlation and verification with literature data. This SSC-4 correlation can be used in the range of temperature from 0 to 260°C and the mass fraction of aqueous LiBr from 0 to 75%. The main advantage of using this form is that the thermodynamic properties are consistent, and it also gives good accuracy for most properties of interest in the full temperature and mass fraction range for the current study and for the ranges of interest for design and application of absorption machines.

## APPENDIX D

### PROPERTY ROUTINE: FOR AQUEOUS LIBR AND WATER IN VISUAL BASIC

#### **D.1 Introduction**

The work described in this appendix is a programming effort in Visual Basic. The purpose of this work was to create a user-friendly computer program that allows properties of aqueous LiBr and water to be utilized easily during the data processing in the current study. In this Visual Basic routine, the SSC-4 correlation (Yuan and Herold, 2005a) is used for aqueous LiBr properties and NBS/NRC Steam Tables data (Harr et al., 1984) is used for water properties. This routine includes most variables of interest and is applicable over the range of temperature from 0 to 260°C and mass fraction of aqueous LiBr from 0 to 75%.

#### **D.2 Visual Basic Routine and Its Main Features**

Figure D.1 is an About window from the property software. As described in Appendix C, the correlation for aqueous LiBr properties is based on a Gibbs free energy function. The correlation for water properties is from NBS/NRC Steam Tables (Haar, 1984) and is based on a Helmholtz energy function. Both thermodynamic and transport properties are included in this routine.

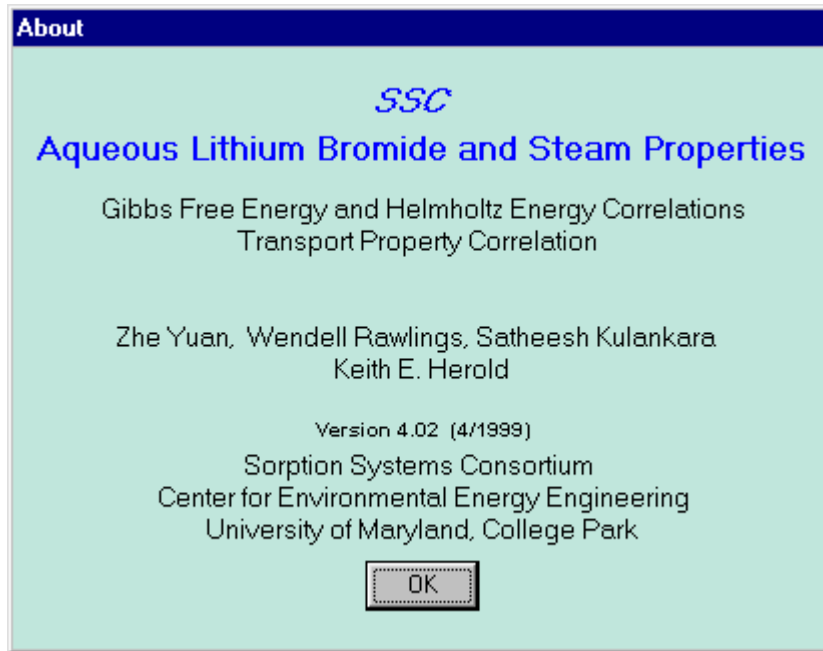


Figure D.1 About window in Visual Basic routine

Figure D.2 is a screen shot of the main window for calculating the properties of aqueous LiBr and water. The main features and functions of this window are listed as follows:

- a. SSC and McNeely's correlations for aqueous LiBr are included. For single phase states the available input variable pairs for the SSC correlation are temperature and pressure (T,p), temperature and mass fraction (T,x), pressure and mass fraction (p,x), enthalpy and mass fraction (h,x) and temperature and volume/density/specific gravity (T, v/d/sg); and for two phase states, available input triples for SSC correlation are temperature, mass fraction and enthalpy (T, x, h) or pressure, mass fraction and enthalpy (p, x, h). Twelve thermodynamic and transport properties are calculated. The applicable ranges for SSC-4 correlation are:  $0 < T < 260^{\circ}\text{C}$ ,  $0 < x < 75\%$ ,  $0.26 < p < 15000 \text{ kPa}$ . and for McNeely's correlation are:  $5 < T < 175^{\circ}\text{C}$ ,  $45 < x < 75\%$ .

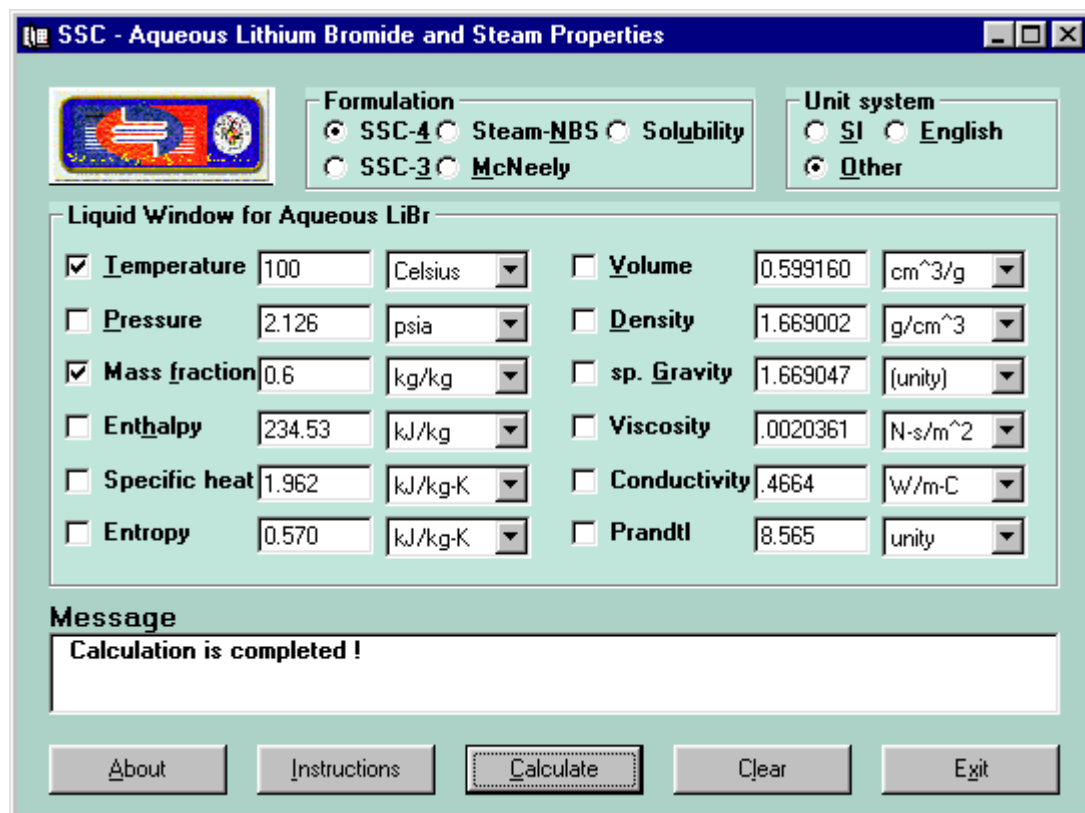


Figure D.2 Main window in Visual Basic routine

- b. The Steam-NBS correlation for water properties is from the NBS/NRC Steam Tables (Haar et al., 1984). For water calculations, mass fraction is replaced by quality. Other input and output variables are similar to those for aqueous LiBr. For both single and two phase states, the available input variable pairs include temperature and density/volume/specific gravity (T,d/v/sg), enthalpy and pressure (h,p). For single phase states, an additional input variable pair is temperature and pressure (T,p). For two phase states, two additional input variable pairs are temperature and quality (T,q) and pressure and quality (p,q).

The applicable ranges are:  $0 < T < 800^{\circ}\text{C}$ ,  $0 < q < 1$ ,  $0.26 < p < 1000$  bar. If the calculated quality is 1.01, the state is superheated. If the calculated quality is -0.01, the state is a sub cooled state.

- c. Solubility of aqueous LiBr is provided and the correlation is based on the data from Boryta (1970). Either temperature or mass fraction is an input variable. The applicable range are:  $-49.3 < T < 120^{\circ}\text{C}$  and  $48.47 < x < 71.9\%$
- d. SI and English units are available. The units can also be mixed as desired by users. The unit choice is saved for future ease of use.
- e. The check boxes are used to designate chosen input variables.
- f. Controls can be selected by mouse, Tab key and access key (underlined letter).
- g. A message window shows important information during the calculation.

Figure D.3 is a window for calculating aqueous LiBr properties in the two-phase range. It provides the properties of both liquid and vapor states. The properties in the two-phase range are useful for many cases like a flashing calculation at an absorber inlet.

When temperature, mass fraction and enthalpy ( $T$ ,  $x$ ,  $h$ ) or pressure, mass fraction and enthalpy ( $p$ ,  $x$ ,  $h$ ) are chosen as input variables in main window, the code will first determine the state. If the state is in the liquid phase, the main window is maintained. If the state is in the two phase region, the two-phase window is automatically displayed and the quality, LiBr mass fraction in liquid and the enthalpy, specific heat, entropy, density, viscosity and thermal conductivity for both the liquid and vapor phases are calculated.

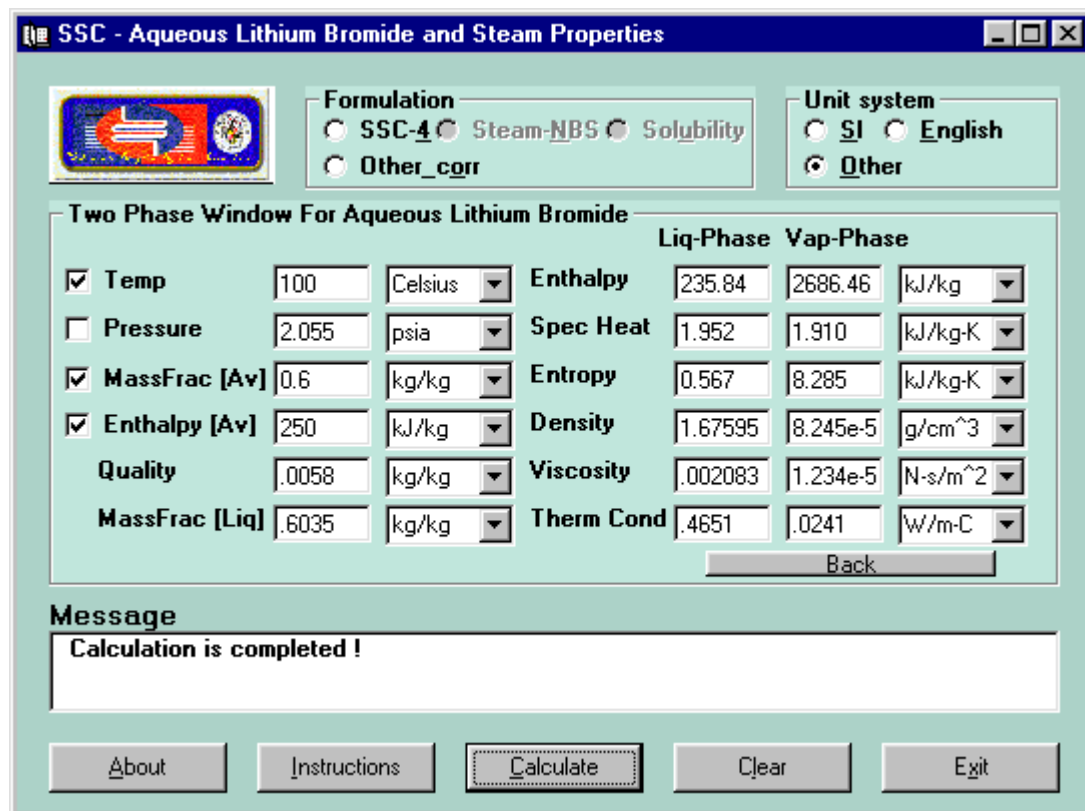


Figure D.3 Two phase window for aqueous lithium bromide

For the two-phase calculation, the vapor properties from the NBS Steam Tables (Haar et al., 1984) are used in conjunction with the SSC correlation to determine the state. The “Back” button in the two-phase window is designed for toggling to the main window. All control, command keys and units in main window also work for the two phase window.

### D.3 Verification

The property routines for aqueous LiBr and pure water have been thoroughly checked for values and different unit systems.

For the SSC-4 correlation, the check was implemented over the range of temperature from 0 to 260°C and mass fraction from 0 to 70%. The values from different input pairs show good consistency, and the values are consistent with the available experimental data.

The values for water properties from Steam-NBS correlation also give good consistency from different input pairs. The results from this routine were compared with NBS water data (Haar, 1984) over the range of  $0.01 < T < 800^{\circ}\text{C}$ ,  $0.0061 < p < 1000$  bar in superheat, compressed liquid and two phase ranges. The results show at least five digits are same, which is a very high accuracy.

#### D.4 Summary

A user-friendly routine for the calculation of the properties of aqueous LiBr and water is developed in Visual Basic with a user-friendly interface. This routine is very easily utilized and gives most variables of interest in the design and application of absorption refrigeration, and the present study benefited from this routine. This software has been used widely in several key refrigeration companies in the U.S and can be free downloaded from Dr. Herold's website.

## **APPENDIX E**

### **SPECIFIC HEAT MEASUREMENTS ON AQUEOUS LITHIUM BROMIDE**

In the design and application of lithium bromide (LiBr) based absorption machines, McNeely's correlation for enthalpy is widely used. This correlation is derived from vapor pressure and specific heat data. The McNeely correlation applies in the range of mass fraction of aqueous LiBr from 45 to 75% and temperature from 5 to 175°C. Therefore, high temperature applications require a new correlation. In addition, after a literature survey on aqueous LiBr specific heat data, it was found that the data are limited and inconsistent. The need for consistent data, including high temperature data, motivated us to measure specific heat in the full range of mass fraction of liquid aqueous LiBr and the temperature range from 5 to 260°C (Yuan and Herold, 2005b). The new data were then used to create an updated correlation as discussed in Appendix C. The measurements of specific heat discussed here were performed using a Setaram C80 calorimeter. The accuracy of the measurement method is estimated to be  $\pm 2\%$  based on comparisons with high accuracy data for pure water and estimates of uncertainty in the other variables. Comparison of our specific heat data with other data sources indicates that reasonable agreement is obtained over the central range of the independent variables. However, certain systematic deviations in the low temperature range and a different tendency in the high temperature range are observed. A main contribution of this study is the extended temperature and mass fraction range of this new specific heat data set.

## **E.1 Introduction**

The motivation for the present work comes from design and analysis of absorption refrigeration systems based on aqueous lithium bromide as the working fluid. A key working fluid property in the analysis of such systems is the specific heat. Various correlations and data sources exist in the literature including the widely used McNeely correlation (1978) which is restricted to temperatures below 175°C due primarily to the lack of specific heat data. Recent high temperature concepts for advanced cycles represent a significant motivation to obtain more data. The data obtained in this study cover the range of temperature from 5-260°C and the full range of liquid concentration from pure water to crystallization.

## **E.2 Measurement Method**

The specific heat measurements were conducted using a Setaram C80 dual-cell, heat flux calorimeter for which a layout is shown in Figure E.1. The aqueous LiBr solution is loaded in a sample vessel that is placed in one of the two cells in the calorimeter. The other cell holds an empty vessel as a reference. Two symmetrical heat flux detectors composed of conductive thermocouples, connected in series, surround both cells and connect them thermally to the calorimetric block. A difference in heat flowing into the two cells, as is expected during temperature changes when the cells have different thermal capacitance, results in an electrical signal that represents the magnitude of that difference.

During the measurement, the calorimeter block is heated at a steady rate so that the temperatures of the cells increase linearly with time. The calorimeter measures the

differential heat flow between the sample and reference cells. The symbol P represents the signal obtained during a data run with the sample loaded, and  $P_0$  represents the signal from a separate run with both cells empty. A small differences in mass between the two metal vessels results in a non-zero  $P_0$ . Data from the heat flux sensors (P), temperature of the calorimeter block (T) and time (t) are recorded every minute during the run. The specific heat is related to the measured parameters as

$$c_p = \frac{P - P_0}{S m \frac{dT}{dt}} \quad (\text{E.1})$$

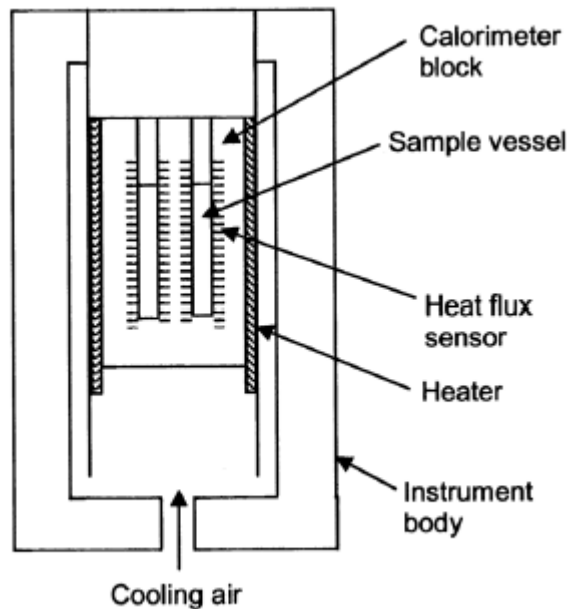


Figure E.1 Layout of Setaram C80 heat flux calorimeter

where  $m$  is the mass of the sample and  $S$  is a sensitivity function supplied by the calorimeter manufacturer.

Aqueous LiBr solution was obtained from FMC Corp and adjusted to the desired concentration by adding or removing (by boiling) water. Concentration was inferred from

density measurements made using a 50 ml volumetric flask, with a volume measurement accuracy of  $\pm 0.1$  ml, and a balance, with an accuracy of  $\pm 0.01$  g, based on well-established density data (SSC-4 correlation in Appendix C). The sample vessel was loaded with the desired aqueous LiBr sample at atmospheric pressure and then sealed. The sample vessel was weighed before and after each run to make sure no leakage occurred. An analysis showed that the mass of the air sealed in the sample vessel at atmospheric conditions is negligible. The sample vessel (nominal 12.5 cc sample volume) was loaded with sufficient liquid such that the vessel was at least 80% full of liquid by volume resulting in sample mass of 10-17 g depending on the LiBr concentration. It was necessary to provide sufficient vapor space so as to avoid the very high pressures that can result from thermal expansion of a liquid filled system and which might damage the calorimeter.

For the measurements at mass fractions above 65%, the high crystallization temperature required a different loading procedure. Powdered LiBr from Fisher Co. (99% LiBr) was directly loaded into the sample vessel and a measured quantity of distilled water was added to the sample vessel to achieve the desired LiBr mass fraction. The sample was held at a temperature above the crystallization temperature overnight so that all crystals dissolved before taking the data.

The calorimeter was programmed to ramp the temperature at a fixed rate ( $\sim 0.18^\circ\text{C}/\text{min}$ ) that was kept identical for all runs. The ramp rate was chosen based on a series of preliminary runs which showed that the results are independent of ramp rate for rates below  $0.5^\circ\text{C}/\text{min}$ . Plots showing data for a typical run over the temperature range from 27 to  $266^\circ\text{C}$  are shown in Figure E.2. The slope of the temperature was obtained by

a linear fit to the data over the temperature range of interest and was found to be constant between runs within  $\pm 0.1\%$ . The power signals were first smoothed by averaging over  $1^{\circ}\text{C}$  increments and linearly interpolated to rounded values of temperature.  $P_0$  was then subtracted from  $P$  at the same temperature. Finally, the specific heat at each temperature was calculated using Eq. E.1. Although both  $P$  and  $P_0$  are plotted on the same time axis in Figure E.2, it is noted that these two traces were obtained in separate runs.

The measurement method involves charging the sample vessel partially full of the liquid being investigated and then sealing the vessel at atmospheric pressure. The cylindrical sample vessel is made from stainless steel with a wall thickness of 2 mm and, thus, is essentially rigid as long as the pressure does not exceed the vapor pressure of the liquids of interest. The conditions of the experiment are essentially constant volume heating of a two-phase system. Because the majority of the mass in the two-phase system is liquid, the heat input required to change the temperature of this system is closely related to the amount of heat required to change the temperature of the liquid at constant pressure (i.e. the specific heat  $c_p$ ).

Once the sample is charged in the sample vessel, the system is heated at a constant ramp rate and the differential heat between the two cells is recorded. At any given temperature, the majority of the sample mass is liquid while a small fraction is vapor. The amount of mass in each phase depends on the initial charge and the specific volume of each of the phases. As the temperature increases, the pressure rises exponentially causing the specific volume of the vapor to decrease. For the purposes of the specific heat measurement, it is of interest to know whether mass is evaporating or condensing during the temperature changes since both processes occur, depending on the

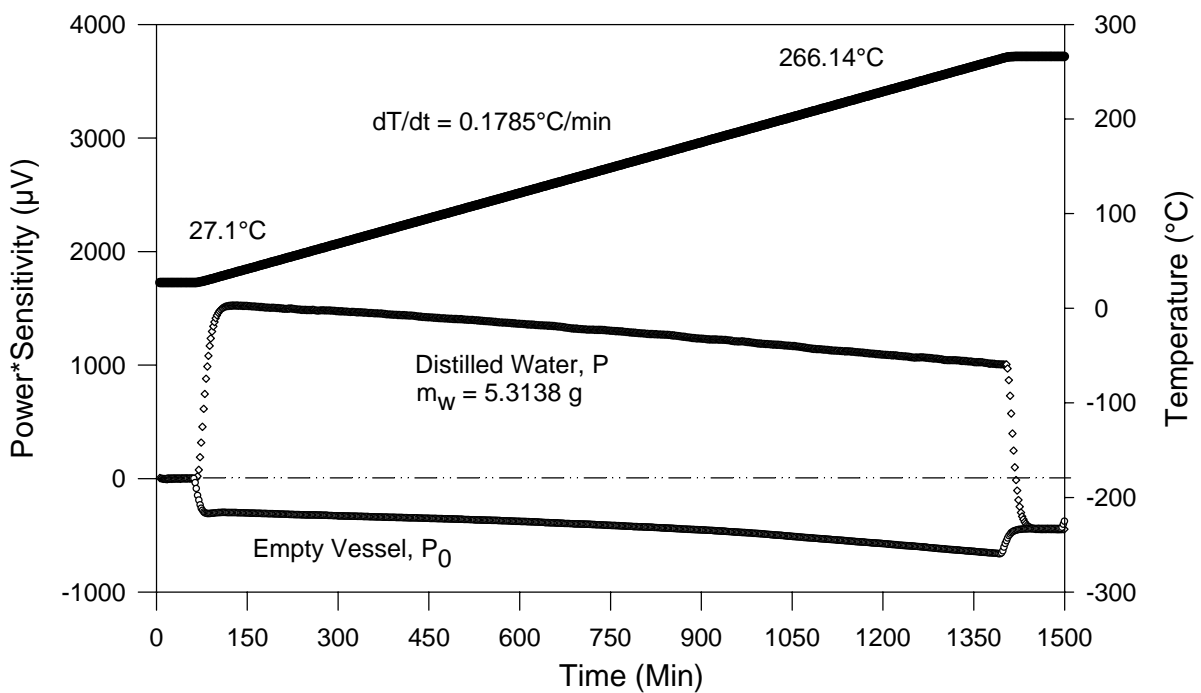


Figure E.2 C80 output for a run with distilled water

conditions, and both contribute errors. Simulations were run which show that the errors introduced by phase change are small as long as the size of the initial vapor space is small.

Simulations were done over the full operating condition range to determine the maximum error due to the various effects discussed and it was found that the most important factor is that the error is larger when the initial vapor space is larger. When the initial vapor space is less than 15% of the total volume, the largest error was found to be less than  $\pm 1\%$  but it is noted that the properties of pure water do not allow such a starting condition because it leads to a liquid filled system at high temperature. Thus, for the very

low salt concentration cases, the errors at high temperature were estimated to be more like -1.5%.

### E.3 Specific Heat Results

The results of our measurements of specific heat of aqueous LiBr are shown in Figure E.3. These measurements were accomplished in three parts. First, measurements were taken over the range of temperature from 35 to 260°C with a 10% mass fraction interval from 0 to 60%, 5% and 65%. Then a similar set of measurements were taken over the range of temperature from 5 to 40°C by placing the calorimeter in a freezer maintained at -25°C. Finally, measurements were made at high mass fraction (70 to 75%). The overlapping data in the temperature range from 35 to 40°C are averaged. The major operational issues in this test series included: 1) great care was taken to measure concentration accurately through an optimized technique arrived at after long experience with the method, and 2) concern about condensation on the calorimeter during testing in the freezer led to a procedure that minimized door openings of the freezer and a shutdown procedure that allowed the system to warm to room temperature while remaining in the low humidity environment of the freezer box.

The data are plotted in Figure E.3 at 1°C increments. A low-amplitude wiggle in the data is observed, which represents the stability of the temperature controller. It is seen that the specific heat is less sensitive to temperature at higher LiBr mass fraction. However, at lower mass fractions, the solution data reflects the temperature dependence of pure water. The scatter in the data is on the order of  $\pm 0.05$  J/g-K but appears to be randomly distributed about a mean trend line. To eliminate the scatter, the data were

averaged over neighboring-temperature data points at the same concentration (11 points used in average) and the averages, at 5°C intervals, are used in all subsequent discussions. The averaged data are given in Table E.1 and are plotted in Figure E.4 along with a correlation obtained through a multiproperty curve fit of specific heat, vapor pressure and volume data as discussed in Appendix C. The form of the specific heat correlation is

$$\begin{aligned}
c_p(x, T, p) &= -T \left( \frac{\partial^2 g}{\partial T^2} \right)_{p,x} \\
&= -2T(C_0 + C_1x + C_2x^2 + C_3x^3 + C_4x^{1.1}) \\
&\quad - 6T^2(D_0 + D_1x + D_2x^2 + D_4x^{1.1}) \\
&\quad - 12T^3(E_0 + E_1x) - 2 \frac{(F_0 + F_1x)T}{(T - T_0)^3} - 2pT(V_6 + V_7x) \\
&\quad + \frac{1}{T}(L_0 + L_1x + L_2x^2 + L_3x^3 + L_4x^{1.1}) \\
&\quad - (M_0 + M_1x + M_2x^2 + M_3x^3 + M_4x^{1.1})
\end{aligned} \tag{E.2}$$

The coefficients in Eq. E.2 are given in Table E.2 and an error plot showing the difference between the data and the correlation is shown in Figure E.5. The error falls within the band  $\pm 2\%$  with an average error of 0.398%.

## E.4 Comparison With Selected Literature Data

The specific heat results are compared with selected literature data and plotted in Figures E.6 and E.7. As shown in Figure E.6, comparison between our results for pure water and the NBS water data shows very good consistency over the full temperature range with a maximum deviation of 0.76%. Lower's data (1960) and the data from Murakami's correlation (1995) are also shown in Figure E.6. The comparison indicates that the literature data agrees closely with our results and shows identical trends as our

new data in the range of mass fraction of usual interest to absorption technologists. However, at the extremes, significant differences are observed. In the low temperature range, Lower's data shows much more curvature as temperature decreases. In addition, significant deviations are observed at lower mass fraction as temperature increases. The Murakami correlation results are shown (as data points) because no other high temperature data are available for comparison. The comparison shows significant systematic differences in trend between our results and those of Murakami, particularly at high mass fraction.

A more recent data set, in a volume translated from Russian, is the work of Zaytsev and Ayelev (1992) which references the early German sources (1928, 1951). A comparison between our results and these data is shown in Figure E.7 where it is seen that they show good agreement in the central range and again show deviation at the extremes. Unlike the data from Lower, the data from Zaytsev and Ayelev shows essentially no temperature dependence at low temperature. At the high temperature end, both Lower and Zaytsev and Ayelev show a steeper slope with temperature than our results.

## E.5 Verification of Measurement Method Accuracy

Verification of the sensitivity function was performed using our data set for pure water and high accuracy data for the specific heat of pure water (Haar et al., 1984). Eq. E.1 was used to compute the sensitivity function from our power readings and the literature value for specific heat. The results of this calculation are shown in Figure E.8 along with the sensitivity function provided by the calorimeter manufacturer. Good

consistency is observed over the whole range except for several wiggles which are traced to the stability of the temperature controller. The maximum relative deviation between the two sources is 0.76%.

Measurements were also performed using anhydrous ethanol, a well-characterized system with a lower value of specific heat, and the results are shown in Figure E.9. A small systematic error is observed between the two data sets with the slope of our data set being somewhat higher. However, the maximum relative error between the two data sets is smaller than 2% which is remarkable considering the difficulty in avoiding contamination by water when working with ethanol.

## E.6 Uncertainty Analysis

Uncertainty analysis provides information defining the accuracy of the measured data and also gives insight as to what is the main error source. The uncertainty analysis discussed here follows Moffat (1985). Because the mass fraction  $x$  can be expressed as a function of mass  $m$ , volume  $V$  and temperature  $T$ , the uncertainties for density  $\rho$  and mass fraction  $x$  can be written as

$$\Delta\rho = \left[ \left( \frac{1}{V} \Delta W \right)^2 + \left( \frac{W}{V^2} \Delta V \right)^2 \right]^{0.5} \quad (\text{E.3})$$

$$\Delta x = \left[ \left( \frac{\partial x}{\partial d} \Delta \rho \right)^2 + \left( \frac{\partial x}{\partial T} \Delta T \right)^2 \right]^{0.5} \quad (\text{E.4})$$

Where  $\partial x/\partial \rho$  and  $\partial x/\partial T$  are calculated using the SSC-4 correlation. The total probable error of mass fraction is calculated as  $\pm 0.235\%$  LiBr.

The uncertainty of the specific heat data consists of two parts. One is from the measurement using the calorimeter and the other is from the uncertainty in mass fraction discussed above. For the uncertainty introduced by the calorimeter, an analysis based on pure water as a standard reference fluid was performed. The probable error in specific heat was calculated as  $\pm 0.242\%$ . Over the same temperature range, pure water has approximately twice the specific heat of a typical LiBr solution (e.g.  $4.2/2.2 = 1.9$ ). Consequently, for a typical LiBr sample, the calorimeter probable error is estimated to be  $\pm 0.46\%$ .

The uncertainty in the mass fraction of the LiBr solution is another possible source of error in specific heat. The error in specific heat due to error in mass fraction can be calculated as  $\pm 0.705\%$  LiBr. Thus the combined probable error of specific heat is calculated as  $\pm 0.84\%$ .

## E.7 Conclusion

Measurement of specific heat of aqueous LiBr solution was accomplished using a heat flux calorimeter. Measurements are reported here over the range of temperature from 5 to 260°C at mass fractions from 0 to 75% LiBr. These data significantly increase the available data at high temperature and high mass fraction. The verification of the measurement method and uncertainty analysis shows that this measurement method provides a specific heat accuracy (probable error) of  $\pm 0.84\%$ .

Table E.1 Experimental specific heat data for aqueous Lithium Bromide

T (°C)	Mass fraction LiBr (%)										
	0	5	9.99	19.99	30.01	40	50.02	60.02	64.99	70.01	74.76
<b>10</b>	4.189	3.942	3.670	3.241	2.816	2.466	2.107	1.854			
<b>20</b>	4.183	3.942	3.682	3.261	2.837	2.474	2.130	1.868			
<b>30</b>	4.183	3.942	3.692	3.272	2.851	2.478	2.148	1.887			
<b>40</b>	4.183	3.931	3.694	3.262	2.851	2.484	2.157	1.895	1.815		
<b>50</b>	4.182	3.924	3.697	3.260	2.854	2.496	2.171	1.910	1.820		
<b>60</b>	4.183	3.925	3.706	3.267	2.865	2.507	2.187	1.927	1.823		
<b>70</b>	4.187	3.929	3.718	3.275	2.873	2.518	2.203	1.942	1.830		
<b>80</b>	4.194	3.928	3.717	3.273	2.870	2.522	2.212	1.952	1.834		
<b>90</b>	4.204	3.920	3.712	3.265	2.865	2.520	2.217	1.960	1.837		
<b>100</b>	4.216	3.919	3.710	3.262	2.872	2.528	2.224	1.971	1.840		
<b>110</b>	4.231	3.923	3.710	3.259	2.883	2.540	2.232	1.978	1.838		
<b>120</b>	4.248	3.923	3.705	3.254	2.880	2.540	2.235	1.980	1.835		
<b>130</b>	4.266	3.933	3.708	3.260	2.884	2.546	2.243	1.986	1.839	1.657	
<b>140</b>	4.287	3.936	3.704	3.264	2.879	2.546	2.244	1.987	1.841	1.653	
<b>150</b>	4.311	3.955	3.712	3.274	2.884	2.551	2.252	1.993	1.847	1.654	
<b>160</b>	4.337	3.976	3.721	3.279	2.885	2.557	2.259	1.998	1.850	1.654	
<b>170</b>	4.367	3.998	3.738	3.282	2.886	2.561	2.264	2.000	1.851	1.663	1.558
<b>180</b>	4.401	4.024	3.758	3.285	2.889	2.564	2.268	2.001	1.853	1.669	1.551
<b>190</b>	4.441	4.059	3.776	3.295	2.897	2.571	2.276	2.003	1.859	1.675	1.549
<b>200</b>	4.486	4.100	3.800	3.304	2.906	2.579	2.286	2.008	1.863	1.682	1.549
<b>210</b>	4.539	4.131	3.814	3.306	2.909	2.583	2.289	2.008	1.855	1.682	1.547
<b>220</b>	4.600	4.174	3.833	3.320	2.919	2.593	2.299	2.013	1.857	1.689	1.556
<b>230</b>	4.671	4.215	3.856	3.331	2.925	2.601	2.306	2.015	1.862	1.690	1.559
<b>240</b>	4.753	4.263	3.881	3.346	2.938	2.614	2.316	2.021	1.866	1.699	1.566
<b>250</b>	4.850	4.315	3.911	3.369	2.958	2.629	2.326	2.028	1.876	1.715	1.573
<b>260</b>	4.965	4.367	3.927	3.381	2.966	2.637	2.330	2.031	1.885	1.725	1.575

Table E.2 Coefficients for the specific heat correlation for aqueous lithium bromide (Eq. E.2)

	0	1	2	3	4
C <sub>i</sub> , i = 0..4	2.648364473E-2	-2.311041091E-3	7.559736620E-6	-3.763934193E-8	1.176240649E-3
D <sub>i</sub> , i = 0..2, 4	-8.526516950E-6	1.320154794E-6	2.791995438E-11	NA	-8.511514931E-7
E <sub>i</sub> , i = 0..1	-3.840447174E-11	2.625469387E-11	NA	NA	NA
F <sub>i</sub> , i = 0..1	-5.159906276E+1	1.114573398	NA	NA	NA
L <sub>i</sub> , i = 0..4	-2.183429482E+3	-1.266985094E+2	-2.364551372	1.389414858E-2	1.583405426E+2
M <sub>i</sub> , i = 0..4	-2.267095847E+1	2.983764494E-1	-1.259393234E-2	6.849632068E-5	2.767986853E-1
V <sub>i</sub> , i = 6..7	3.057997846E-9	-5.129589007E-1	NA	NA	NA
Average error:	Specific heat = 0.398 %				
Additional notes:					
1. T <sub>0</sub> = 220 K					
2. Units in Equation 8 are: T (K), X(LiBr mass fraction expressed in %), p (kPa)					
3. NA indicates that there is no coefficient for that position					

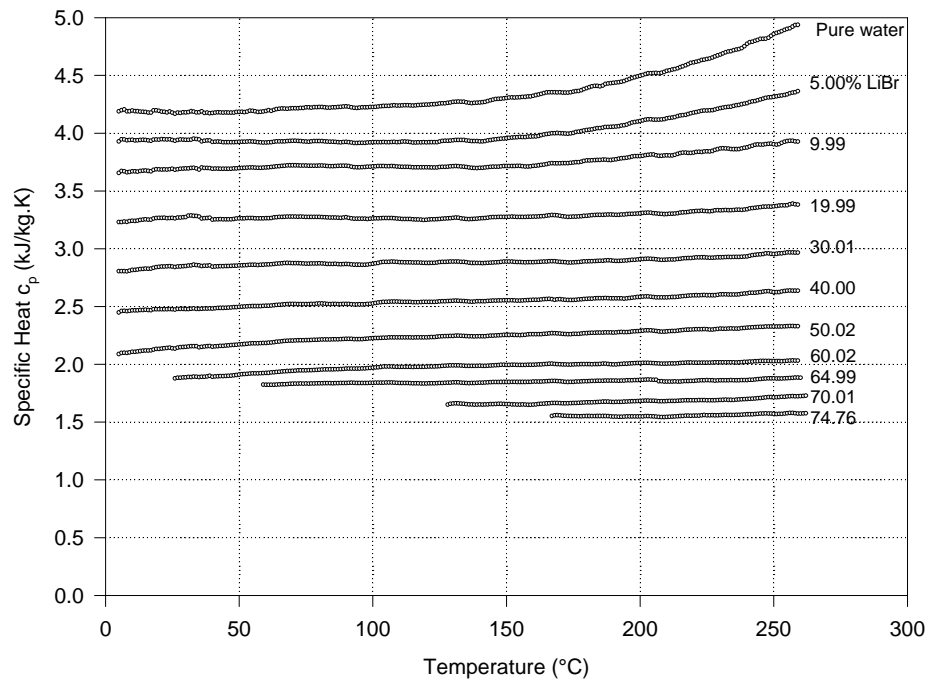


Figure E.3 Specific heat data of aqueous LiBr solution

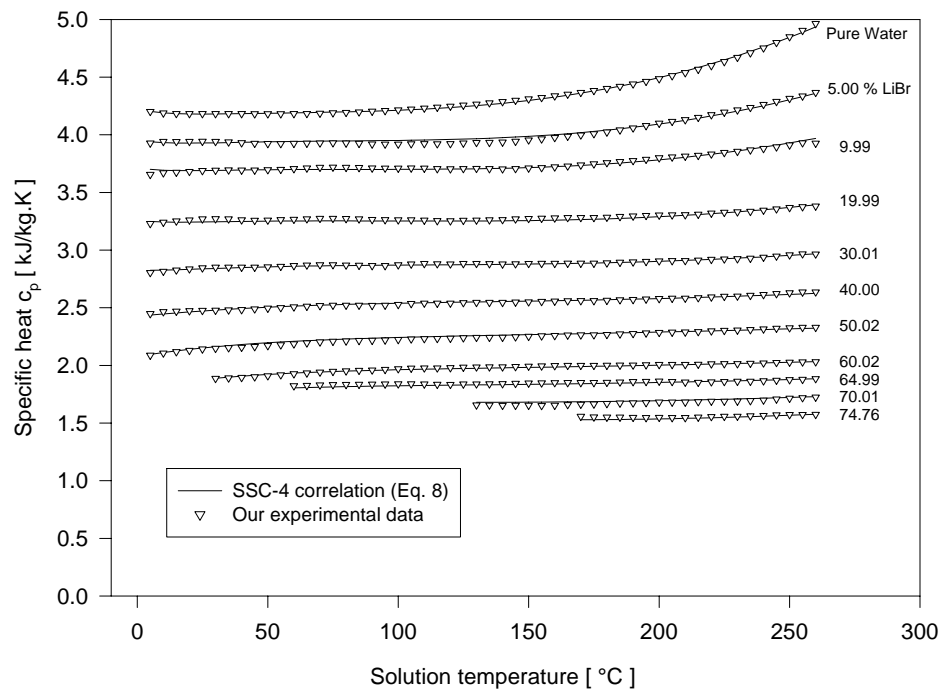


Figure E.4 Specific heat data compared with SSC-4 correlation

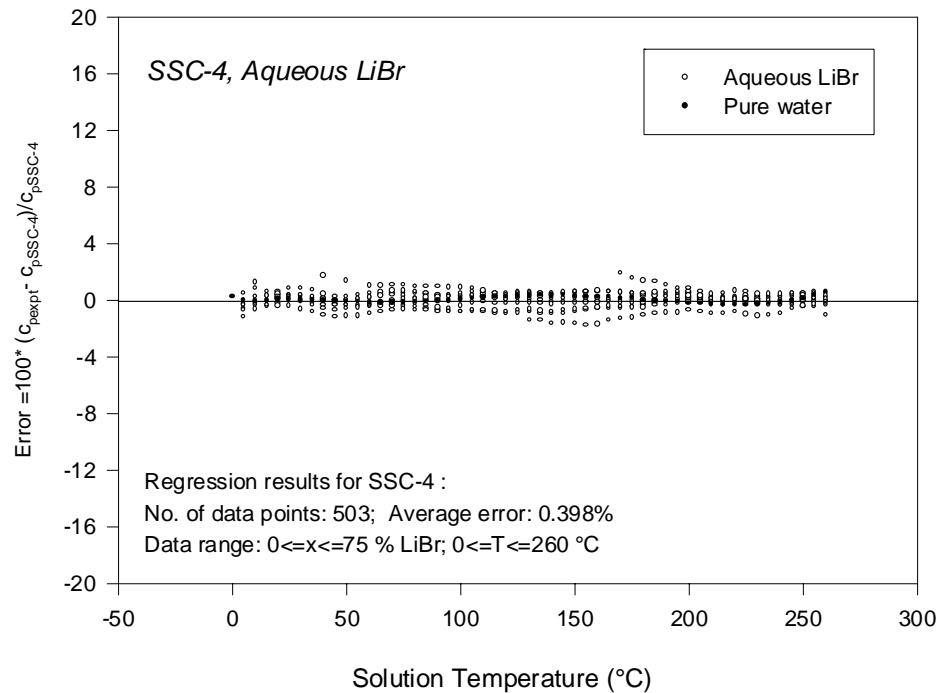


Figure E.5 Error plot of differences between our experimental data and the SSC-4 correlation.

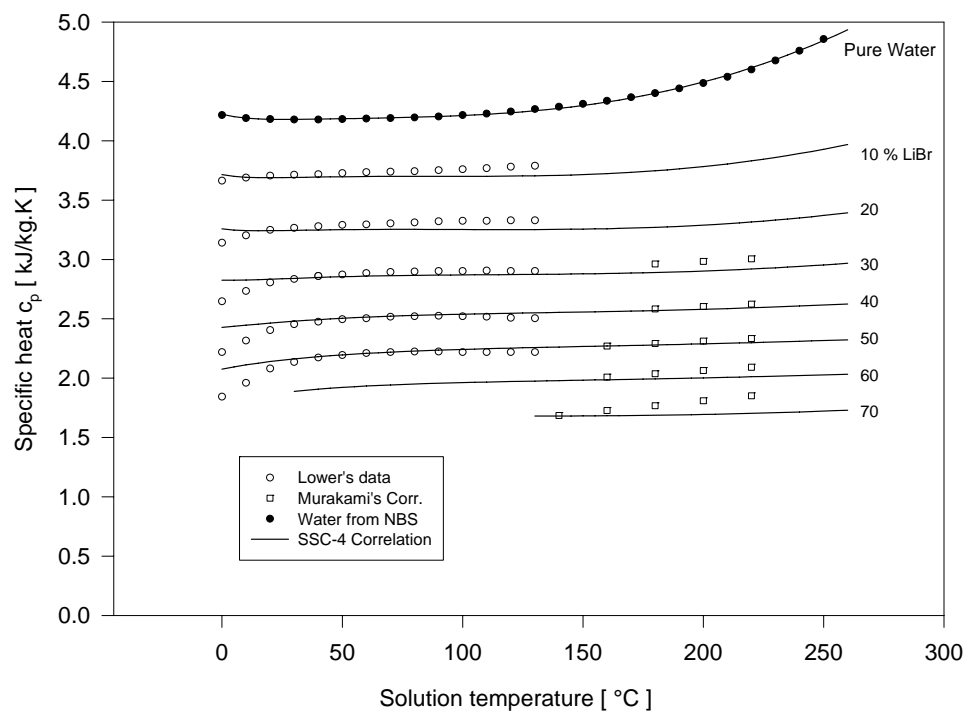


Figure E.6 Comparison of specific heat between our correlation and other data sources

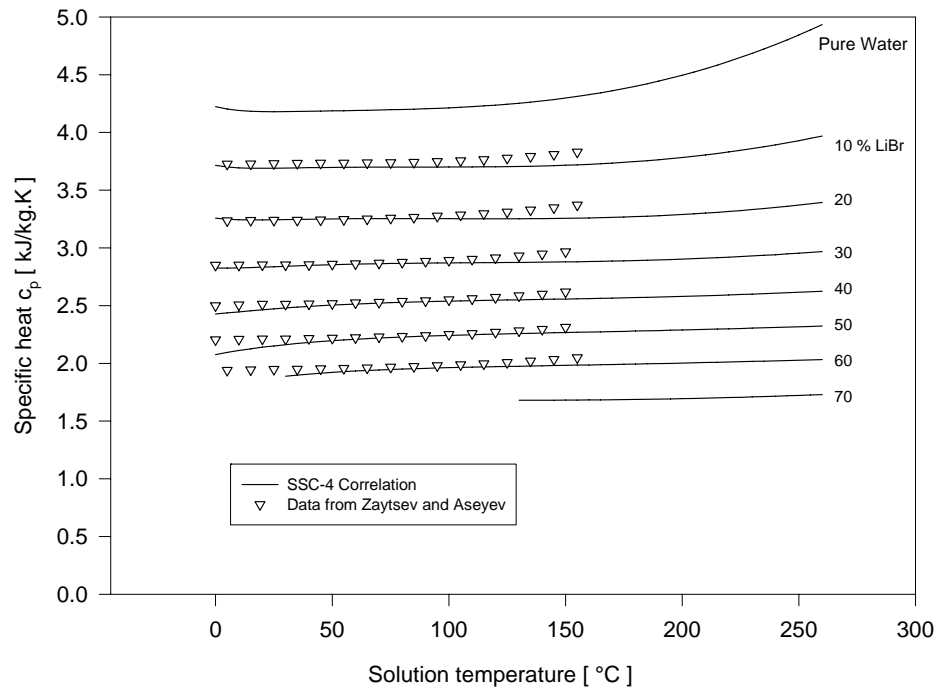


Figure E.7 Comparison of specific heat between our correlation and the data of Zaytsev and Aseyev (1992)

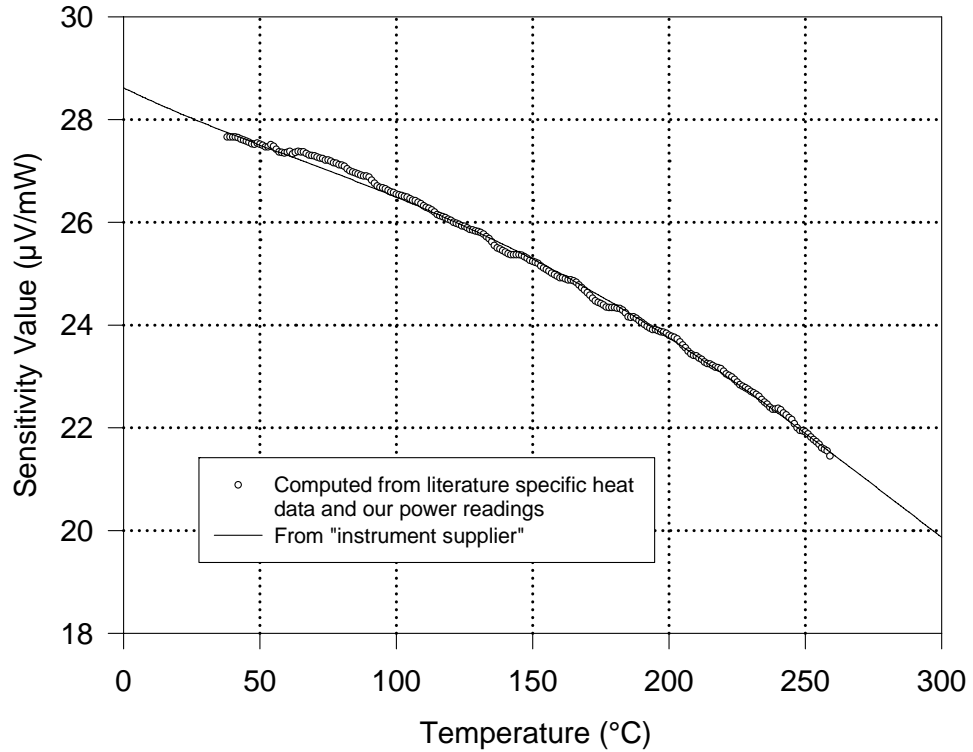


Figure E.8 Calorimeter sensitivity function verification using pure water literature data

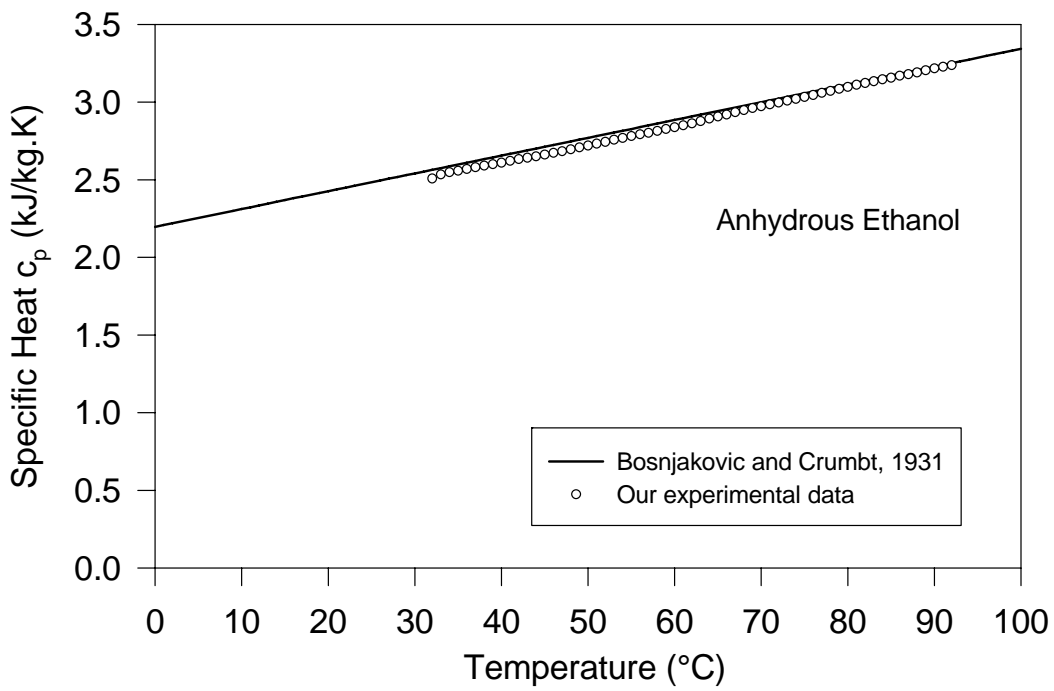


Figure E.9 Verification of the specific heat measurement system for a sample (ethanol) with lower specific heat

## BIBLIOGRAPHY

- Agble, D., Mendes-Tatsis, M.A., 1999, "The Effect of Surfactants on Interfacial Mass Transfer in Binary Liquid-Liquid Systems", *International Journal of Heat and Mass Transfer*, Vol. 43, pp. 1025-1034.
- Albertson, C.E, Krueger, R.H., 1971, "Heat and Mass Transfer Additives for Absorbent Solutions", *U.S. Patent*, No. 3580759.
- Becher, P., 1965, *Emulsions: Theory and Practice*, 2<sup>nd</sup> Edition, Reinhold Publishing Corp., New York.
- Baranenko, A.V., Zyukanov, V.M., 1990, "Raising Absorber Heat Transfer Performance in a Lithium Bromide Refrigerator", *Chemical and Petroleum Engineering*, Vol. 26, No. 9, pp. 466-469.
- Bergles, A.E., 1997, "Heat Transfer Enhancement: The Encouragement and Accommodation of High Heat Fluxes", *Journal of Heat Transfer*, Vol. 119, pp. 8-19.
- Beutler, A., Greiter, I., Wagner, A., Hoffmann, L., Schreier, S., Alefeld, G., 1996, "Surfactant and Fluid Properties", *International Journal of Refrigeration*, Vol. 19, No. 5, pp. 342-346.
- Beutler, A., Hoffmann, L., Ziegler, E., Alefeld, G., Gommed, K., Grossman, G., Shavit, A., 1996, "Experimental Investigation of Heat and Mass Transfer in Film Absorption on Horizontal and Vertical Tubes", *Proceedings of International Absorption Heat Pump Conference*, Montreal, Vol. 1, pp. 409-419.
- Bikerman, J.J., 1970, *Physical Surfaces*, Academic Press, New York.
- Borwankar, R.P., Wasan, D.T., 1983, "The Kinetics of Adsorption of Surface Active Agents at Gas-liquid Surfaces", *Chemical Engineering Science*, Vol. 38, No. 10, pp. 1637-1649.
- Bourne, J.R., 1976, "Alcohol Circulation System", *U.S. Patent*, No. 3977204.
- Bourne, J.R., 1976, "Alcohol Separator", *U.S. Patent*, No. 3977211.
- Bourne, J.R., Eisberg, K.V, 1966, "Maintaining the Effectiveness of an Additive in Absorption Refrigeration Systems", *U.S Patent*, No. 3276217.
- Brian, P.L.T., 1971, "Effect of Gibbs Adsorption on Marangoni Instability", *AIChE Journal*, Vol. 17, No. 4, pp. 765-771.

Burnet, J.C., Himmelbau, D.M, 1970, "The Effect of Surface Active Agent on Interphase Mass Transfer", *AICHE Journal*, Vol. 16, No. 2, pp. 185-193.

Castro, J., Leal, L., Perez-Segarra, C.D., Pozo, P., 2004, "Numerical Study of the Enhancement Produced in Absorption Processes Using Surfactants", *International Journal of Heat and Mass Transfer*, Vol. 47, pp.3463-3476.

Chattoraj, D.K., Birdi, K.S., 1984, *Adsorption and the Gibbs Surface Excess*, Plenum Press, New York.

Chi, C.W., Macriss, R.A., Rush, W.F., 1971, "Secondary Alcohol Additives for Lithium Bromide-Water Absorption Refrigeration System", *U.S. Patent*, No. 3609087.

Clint, J. H., 1991, "Surfactant Aggregation", *Chapman and Hall*, New York.

Cosenza, F., Vliet, G.C., 1990, "Absorption in Falling Water/LiBr Films on Horizontal Tubes", *ASHRAE Transactions*, Vol. 96, pp. 693-701.

Cyprus Foote Mineral, 1995, "Technical Data: Lithium Bromide", Bulletin 145.

Dai, Y.Q. and Zheng, Y.Q., 1980, *LiBr Based Absorption Chiller*, Industry Publication, Inc., (in Chinese).

Daiguji, H., Hihara, E., Saito, T., 1997, "Mechanism of Absorption Enhancement by Surfactant", *International Journal of Heat and Mass Transfer*, Vol. 40, No. 8, pp. 1743-1752.

Edmonstone, B.D., Matar, O.K., 2004, "Simultaneous Thermal and Surfactant-induced Marangoni Effects in Thin Liquid Films", *J. of Colloid and Interface Science*, Vol 274, pp. 183-199.

Eigen, M. and Wicke, E., 1951, "Ionenhydration und spezifische Wärme wässriger Elektrolytlösungen. Zeitschrift für Elektrochemie". Vol. 55, No. 5, pp.354-363.

Elkassabgi, Y.M., Perez-Blanco, H., 1991, "Experimental Study of the Effects of Alcohol Additives in Lithium Bromide/Water Pool Absorbers", *ASHRAE Transactions*, Vol. 97, No. 2, pp. 403-405.

FLUENT Inc, 2000, FLUENT, Version 5.2.

Ford, J.D., Missen, R.W., 1968, "On the Conditions for Stability of Falling Films Subject to Surface Tension Disturbances; the Condensation of Binary Vapors", *The Canadian Journal of Chemical Engineering*, Vol. 46, pp. 309-312.

Frances, V.M.S., Ojer, J.M.P., 2004, "Multi-factorial Study of the Absorption Process of H<sub>2</sub>O (vap) by a LiBr(aq) in a Horizontal Tube Bundle Using 2-ethyl-1-hexanol as Surfactant", *International J. of Heat and Mass Transfer*, Vol. 47, pp. 3355-3373.

Fujita, I., Hihara, E., 1999, "Surface Tension–Driven Instability of Thin Liquid Film of LiBr Aqueous Solution Absorbing Water Vapor", ISHPC'99, *Proceeding of the International Sorption Heat Pump Conference*, Munich, Germany, 1999, pp.367-379.

Gavrish, A.S., Rifert, V.G., Sardak, A.I., Pobereznny, V.L., 1993, "A New Dropwise Condensation Promoter for Desalination and Power Plants", *Heat Transfer Research*, Vol. 25, No. 1, pp. 82-86.

Ghosh, K., Zhou, X., Herold, K.E., 2002, "Circulation of 2-Ethyl-Hexanol in an Absorption Chiller", ASHRAE Transactions, Vol. 108, No. 1, pp. 861-866.

Glebov, D., Setterwall, F., 2002, "Experimental Study of Heat Transfer Additive Influence on the Absorption Chiller Performance", *Int. J. of Refrigeration*, Vol. 25, pp.538-545.

Goto, M., Fujii, T., 1982, "Film Condensation of Binary Refrigerant Vapors on a Horizontal Tube", *Proceedings of the 7<sup>th</sup> International Heat Transfer Conference*, Munich, Vol. 5, pp. 71-76.

Grosman, E.R., Naumov, S.E., 1984, "In Povyshenie Effektivnosti Kholodilnykh Mashin", Lensoviet Technological Institute, Leningrad, pp.3-7.

Gustafsson, M., Ternstrom, G., Setterwall, F., 1996, "Surface Tension of Aqueous Lithium Bromide and Sodium Hydroxide Solutions with Surfactants", *International Absorption Heat Pump Conference*, Montreal, Vol. 1, pp. 61-65.

Haar, L., J.S. Gallagher, Kell, G.S., 1984, *NBS/NRC Steam Tables*, Hemisphere Publishing Corporation, New York.

Harkins, W.D., 1952, "The Physical Chemistry of Surface Films", Reinhold, New York.

Herold, K.E., 2005, "Surfactant Vapor Experiments", *International Sorption Heat Pump Conference*, Denver, USA, ISHPC-021-2005

Hihara, E., Saito, T., 1991, "Behavior of the Liquid Film in an Absorber", *Proceedings of 18<sup>th</sup> International Congress of Refrigeration, Montreal, Canada*, Vol. 2, pp. 524-527.

Hijikata, K., Fukasaku,Y., Nakabeppu, O., 1996, "Theoretical and Experimental Studies on the Micro-structure of Pseudo-dropwise Condensation of a Binary Vapor Mixture", *Journal of Heat Transfer*, Vol. 118, pp. 140-147.

Hijikata, K., Fukasaku, Y., Nakabeppu, O., 1994, "Theoretical and Experimental Studies on Pseudo-dropwise Condensation of a Binary Vapor Mixture", *Proceedings of International Mechanical Engineering Congress and Exposition, ASME-HTD*, Chicago, Vol. 291, pp. 57-62.

Hoffmann, L., Greiter, I., Wagner, A., Weiss, V., Alefeld, G., 1996, "Experimental Investigation of Heat Transfer in a Horizontal Tube Falling Film Absorber with Aqueous Solutions of LiBr with and without Surfactants", *International Journal of Refrigeration*, Vol. 19, No. 5, pp. 331-341.

Hozawa, M., Inoue, M., Sato, J., Tsukada, T., Imaishi, N., 1991, "Marangoni Convection During Steam Absorption into Aqueous LiBr Solution with Surfactant", *Journal of Chemical Engineering of Japan*, Vol. 24, No. 2, pp. 209-214.

I.C.T., 1928, International Critical Tables. McGraw-Hill.

Ishida, K., Mori, Y.H., 1996, "Surface Tension of Aqueous Lithium Bromide Solutions Containing 1-Octanol as a Heat-Transfer Additive", *International Communications in Heat and Mass Transfer*, Vol. 23, No. 7, pp. 907-915.

Ji, W., Bjurstrom, H., Setterwall, F., 1993, "A Study of the Mechanism of Heat Transfer Additives in an Absorption System", *Journal of Colloid and Interface Science*, Vol. 160, No. 1, pp. 127-140.

Ji, W., Setterwall, F., 1994, "Effects of Surfactant on the Stability of Failing Liquid Films", *Proceedings of the International Absorption Heat Pump Conference*, New Orleans, Vol. 31, pp. 33-40.

Joo, S.W., Davis, S.H., Bankoff, S.G., 1996, "A Mechanism for Rivulet Formation in Heated Falling Films", *Journal of Fluid Mechanics*, Vol. 321, pp. 279-298.

Jung, S.H., Sgamboti, C., Perez-Blanco, H., 1994, "An Experimental Study of the Effect of Some Additives on Falling Film Absorption", *Proceedings of the International Absorption Heat Pump Conference (IAHPC)*, New Orleans, ASME AES-Vol. 31, pp. 49-55.

Kang, Y.T., Akisawa, A., Kashiwagi, T., 1999, "Experimental Investigation of Marangoni Convection in Aqueous LiBr Solution with Additives", *Transactions of the ASME, Journal of Heat Transfer*, Vol. 121, pp. 1088-1091.

Kang, Y.T., Akisawa, A., Kashiwagi, T., 1999, "Visualization and Model Development of Marangoni Convection in NH<sub>3</sub>-H<sub>2</sub>O System", *International Journal of Refrigeration*, Vol. 22, pp. 640-649.

Kang, Y.T., Kashiwagi, T., 2002, "Heat Transfer Enhancement by Marangoni Convection in the NH<sub>3</sub>-H<sub>2</sub>O Absorption Process", *International Journal of Refrigeration*, Vol. 25, pp. 780-788.

Kashiwagi, T., 1988, "Basic Mechanism of Absorption Heat and Mass Transfer Enhancement by the Marangoni Effect", *Newsletter of the IEA Heat Pump Center*, Vol. 64, pp. 2-6.

Kashiwagi, T., Kurosaki, Y., Shishido, H., 1985, "Enhancement of Vapor Absorption into a Solution Using Marangoni Effect", *Transactions of JSME*, pp. 1002-1009.

Kashiwagi, T., Rie, D.H., Kurosawa, S., Nomura, T., Omata, K., 1993, "Marangoni Effect on the Process of Steam Absorption into a Falling Film of an Aqueous Solution of LiBr", *Heat Transfer-Japanese Research*, Vol. 22, No. 4, pp. 355-371.

Killon, J.D., Grarimella, S., 2000, "A Critical Review of Falling-film Absorption Heat and Mass Transfer Models", *34<sup>th</sup> National Heat Transfer Conference*, Pittsburgh, Pennsylvania, PP. 1-34.

Kim, J., Choi, C.K., Kang, Y.T., 2004, "Instability Analysis of Marangoni Convection for Absorption Process Accompanied by Heat Transfer", *International J. of Heat and Mass Transfer*, Vol. 47, pp.2395-2402.

Kim, J., Kang, Y.T., Choi, C.K., 2004, "Effects of Gas and Additive Properties on Marangoni Instability for Absorption Process in a Horizontal Fluid Layer", *Int. J. of Refrigeration*, Vol. 27, pp.140-149.

Kim, J.S., Lee, H., Yu, S.I., 1999, "Absorption of Water Vapour Into Lithium Bromide-Based Solutions with Additives Using a Simple Stagnant Pool Absorber", *International Journal of Refrigeration*, Vol. 22, pp. 188-193.

Kim, K.J., Berman, N.S., Wood, B.D., 1996, "The Interfacial Turbulence in Falling Film Absorption: Effects of Additives", *International Journal of Refrigeration*, Vol. 19, No. 5, pp. 322-330.

Kim, K.J., Berman, N.S., Wood, B.D., 1994, "Experimental Investigation of Enhanced Heat and Mass Transfer Mechanisms Using Additives for Vertical Falling Film Absorber", *Proceedings of the International Absorption Heat Pump Conference (IAHPC 1993)*, New Orleans, ASME AES-Vol. 31, pp. 41-47.

Kim, K.J., Berman, N.S., 1994, "Surface Tension of Aqueous Lithium Bromide + 2-Ethyl-1-hexanol", *J. of Chemical and Engineering Data*, Vol. 39, No. 1, pp. 122-124.

Kim, K.J., Berman, N.S., Wood, B.D., 1996, "Absorption of Water Vapor Into LiBr Solutions with 2-Ethyl-1-Hexanol", *AIChE Journal*, Vol. 42, No. 3, pp. 884-888.

Kim, K.J., Janule, V.P., 1994, "Dynamic Surface Tension of Aqueous Lithium Bromide with 2-Ethyl-1-Hexanol", *International Communications in Heat and Mass Transfer*, Vol. 21, No. 6, pp. 839-848.

Kim, K.J., Kulankara, S., Herold, K.E., 1995, "Experimental Evaluation of Enhancement Additives for the Absorption of Water Vapor into Aqueous LiBr", *Heat Pump and Refrigeration Systems Design*, ASME AES-Vol. 34, pp. 183-192.

Kim, K.J., Kulankara, S., Herold, K.E., Miller, C, 1996, "Heat Transfer Additives for Use in High Temperature Applications", *International Absorption Heat Pump Conference*, Montreal, Vol. 1, pp. 89-97.

Kiyota, M., Morioka, I., Ousaka, A., Fujikawa, K., 1996, "Steam Absorption into Films of Aqueous Solution of LiBr Flowing over Multiple Horizontal Pipes", *Heat Transfer-Japanese Research*, Vol. 25, No. 7, pp. 476-485.

Klein, S.A., 1992, "Engineering Equation solver (EES) for Microsoft Windows Operating Systems", University of Wisconsin at Madison.

Koenig, M.S., Grossman, G., Gommed, K., 1999, "Additive Induced Enhancement of Heat and Mass Transfer in a Static Absorber: A Numerical Study", *ISHPC'99, Proceeding of the International Sorption Heat Pump Conference*, Germany, March, 1999. pp. 359-365.

Koenig, M.S., Grossman, G., Gommed, K., 2003, "The Role of Surfactant Adsorption Rate in Heat and Mass Transfer Enhancement in Absorption Heat Pumps", *Int. J. of Refrigeration*, Vol. 26, pp.129-139.

Kulankara, S., 1999, "Effect of Enhancement Additives on the Absorption of Water Vapor by Aqueous Lithium Bromide," Ph.D. Dissertation, University of Maryland.

Kulankara, S., Herold, K.E., 2000, "Theory of Heat/Mass Transfer Additives in Absorption Chillers", *International Journal of Heating, Ventilating, Air-Conditioning and Refrigeration*, Vol. 6, No. 4, pp. 369-380.

Kulankara, S., Herold, K.E., 2002, "Surface Tension of Aqueous Lithium-bromide with Heat/Mass Transfer Enhancement Additive: the Effect of Additive Vapor Transport", *International Journal of Refrigeration*, Vol. 25, pp. 383-389.

Lange, E. and Schwartz E, 1928, "Losungs- und Verdunnungswarmen von Salzen von der aussersten Verdunnung bis zer Sättigung. Zeitschr. fur Physik. Chemie", Vol.133, pp.129-150.

Lower, H., 1960, "Thermodynamiche und physikalische Wigenhaftent der Wassrigen Lithium bromid- Losung", *Technischen Hochschule Karlsruhe*.

Lu, H.H., Yang, Y.M., Maa, J.R., 1997, "On the Induction Criterion of the Marangoni Convection at the Gas/Liquid Interface", *Industrial Engineering Chemistry Research*, Vol. 36, No. 2, pp. 474-482.

Lu, H.H., Yang, Y.M., Maa, J.R., 1997, "Surfactant Effects on Absorption in the Presence of Induced Interfacial Turbulence", *AIChE Journal*, Vol. 43, No. 7, pp. 1909-1913.

McGillis, W.R., Carey, V.P., 1996, "On the Role of Marangoni Effects on the Critical Heat Flux for Pool Boiling of Binary Mixtures", *Journal of Heat Transfer*, Vol. 118, pp. 103-109.

McTaggart, C.L., 1983, "Convection Driven by Concentration and Temperature Dependent Surface Tension", *Journal of Fluid Mechanics*, Vol. 134, pp. 301-310.

McNeely, L.A., 1978, "Thermodynamic Properties of Aqueous-Solutions of Lithium Bromide". *ASHRAE Journal-American Society of Heating Refrigerating and Air-Conditioning Engineers*. Vol. 20, No.12, pp.54-55.

Mirkovich, V.V., Missen, R.W., 1961, "Non-filmwise Condensation of Binary Vapors of Miscible Liquids", *The Canadian Journal of Chemical Engineering*, Vol. 39, pp. 86-87.

Mirkovich, V.V., Missen, R.W., 1963, "A Study of the Condensation of Binary Vapors of Miscible Liquids II: Heat Transfer Coefficients for Filmwise and Non-filmwise Condensation", *The Canadian Journal of Chemical Engineering*, Vol. 41, pp. 73-78.

Modahl, R., Lynch, P.J., 1974, "Absorption Heat Exchange Systems, Methods and Absorbent Compositions", *U.S. Patent*, No. 3783631.

Moffat, R.J., 1985, "Using Uncertainty Analysis in the Planning of an Experiment. Journal of Fluids Engineering", *Transactions of the ASME*, Vol.107, No.2, pp.173-178.

Moller, R., Knoche, K.F., 1996, "Surfactant with NH<sub>3</sub>-H<sub>2</sub>O", *International Journal of Refrigeration*, Vol. 19, No. 5, pp. 317-321.

Morrison, J.N.A., Deans, J., 1997, "Augmentation of Steam Condensation Heat Transfer by Addition of Ammonia". *International Journal of Heat and Mass Transfer*, Vol. 40, No. 4, pp. 765-772.

Morrison, J.N.A., Philpott, C., Deans, J., 1998, "Technical Note: Augmentation of Steam Condensation Heat Transfer by Addition of Methylamine", *International Journal of Heat and Mass Transfer*, Vol. 41, pp. 3679-3683.

Murakami, K., Sato, H., Watanabe, K. 1995, "Duhring Charts and Enthalpy-Concentration Charts for the LiBr/H<sub>2</sub>O and LiCl/H<sub>2</sub>O Solutions. in 19th International Congress of Refrigeration", pp.428-435.

Nordgren, M., Setterwall, F., 1996, "An Experimental Study of the Effects of Surfactant on a Falling Liquid Film", *International Journal of Refrigeration*, Vol. 19, No. 5, pp. 310-316.

Oscik, J., Cooper, I.L., 1982, *Adsorption*, John Wiley & Son, New York.

Park, C.W., Cho, H.C., Kang, Y.T., 2004, "The Effect of Heat Transfer Additive and Surface Roughness of Micro-scale Hatched Tubes on Absorption Performance", *Int. J. of Refrigeration*, Vol. 27, pp. 264-270.

Park, C.W., Cho, H.C., Kang, Y.T., 2004, "The Effect of Heat Transfer Additive and Surface Roughness of Micro-scale Hatched Tubes on Absorption Performance", *International Journal of Refrigeration*, Vol. 27, pp. 264-270.

Patankar, S.V., 1980, *Numerical Heat Transfer and Fluid Flow*, McGraw-Hill, New York.

Patel, S.S., 1996, "Effect of Surfactant Concentration and Film Area on the Stability of Film of Surfactant Solutions", *Journal of Colloid and Interface Science*, Vol. 183, pp. 603-606.

Patnaik, V., Perez-Blanco, H., 1996, "A Study of Absorption Enhancement by Wavy Film Flows", *International Journal of Heat and Fluid Flow*, Vol. 171, pp. 71-77.

Pearson, J.R.A., 1958, "On Convection Cells Induced by Surface Tension", *Journal of Fluid Mechanics*, Vol. 4, pp. 489-500.

Perez-Blanco, H., Sheehan, D.S., 1995, "Effect of Additive Concentration on Falling Film Absorption", *HVAC&R Research*, Vol. 1, No. 4, pp. 273-281.

Persson, L.H., Holmberg, P.A., 1994, "Heat Transfer by Falling Film Desorption of Concentrated Lithium Bromide Aqueous Solutions With Surfactant Octanol Addition", *Proceedings of the International Absorption Heat Pump Conference*, New Orleans, ASME AES-Vol. 31, pp. 57-63.

Qiao, R., Yuan, Z., Herold, K.E., 2000, "Surface Tension Driven Film Flow Due to Condensation with a Vapor Borne Surfactant", *Proceedings of IMECE 2000, International Mechanical Engineering Congress & Exhibition*, Orlando, Florida, pp. 169-174.

Reid, R.C., Prausnitz, J.M., Poling, B.E., 1988, *The Properties of Gases and Liquids*, 4<sup>th</sup> Edition, McGraw-Hill, New York.

Rie, D.H., Kashiwagi, T., 1991, "Experimental Study of Steam Absorption Enhancement in Accordance with Interfacial Turbulence into Aqueous Solution of LiBr (the Influence of a Non-condensable Gas)", *JSME International Journal*, Vol. 34, No. 4, pp. 502-508.

Rie, D.H., Kashiwagi, T., 1991, "Computer Simulation of Vapor-Absorption Enhancement into H<sub>2</sub>O/LiBr Absorbent by Marangoni Convection", *JSME International Journal, Series 2*, Vol. 34, No. 3, pp. 355-361.

Riffat, S.B., James, S.E., Wong, C.W., 1998, "Experimental Analysis of the Absorption and Desorption Rates of HCOOK/H<sub>2</sub>O and LiBr/H<sub>2</sub>O", *International Journal of Energy Research*, Vol. 22, pp. 1099-1103.

Rosen, M.J., 1989, *Surfactant and Interfacial Phenomena*, John Wiley & Sons, New York.

Rowlinson, J.S. and Swinton, F.L., 1982, Liquids and Liquid Mixtures. *London: Butterworth Scientific*.

Rush, W.F., Wurm, J., Perez-Blanco, H., 1991, "A Brief Review of the Uses and Effect of Additives for Absorption Enhancement", *Environment-Friendly Technologies for the 21st Century (IAHPC 1991)*, Tokyo, pp. 183-187.

Scheele, G.F., Meister, B.J., 1968, "Drop Formation at Low Velocities in Liquid-Liquid Systems", *AIChE Journal*, Vol. 14, No. 1, pp. 9-15.

Schick, M.J., 1962, "Surface Films of Nonionic Detergents — I. Surface Tension Study", *Journal of Colloid Science*, Vol. 17, pp. 801-813.

Scriven, L.E., 1960, "Dynamics of a Fluid Interface", *Chem. Engineering Science*, Vol. 12, pp. 98-108.

Scriven, L.E., Sternling, C.V., 1960, "The Marangoni Effects", *Nature*, Vol. 187, pp. 186-188.

Scriven, L.E., Sternling, C.V., 1964, "On Cellular Convection Driven by Surface-tension Gradients: Effects of Mean Surface Tension and Surface Viscosity", *Journal of Fluid Mechanics*, Vol. 19, pp. 321-340.

Setoguchi, T., Perez-Blanco, H., 1991, "Effect of Additives in Ammonia Absorption in Water in a Static Pool", *Environment-Friendly Technologies for the 21st Century (IAHPC 1991)*, Tokyo, pp. 177-182.

Setterwall, F., Yao, W., Ji, W., Bjurstrom, H., 1991, "Heat Transfer Additives in Absorption Heat Pumps", *Environment-Friendly Technologies for the 21st Century (IAHPC 1991)*, pp. 73-78.

Sheehan, D.S., Perez-Blanco, H., Prescott, P.J., 1996, "Investigation of Additive Effectiveness with Infrared Sensor and Dynamic Surface Tension Measurements",

Proceedings of *International Ab-sorption Heat Pump Conference*, Montreal, Vol. 1, pp. 75-82.

Shen, Y.R., 1989, "Surface Properties Probed by Second-harmonic and Sum-frequency Generation", *Nature*, Vol. 337, No. 9, pp. 519-525.

Shinoda, K., Yamaguchi, T., Hori, R., 1961, "The Surface Tension and the Critical Micelle Concentration in Aqueous Solution of  $\beta$ -D-Alkyl Glucosides and Their Mixtures", *Bulletin of the Chemical Society of Japan*, Vol. 34, No. 2, pp. 237-241.

Smith, K.A., 1966, "On Convective Instability Induced by Surface-Tension Gradients", *Journal of Fluid Mechanics*, Vol. 24, No. 2, pp. 401-414.

Sternling, C.V., Scriven, L.E., 1959, "Interfacial Turbulence" Hydrodynamic Instability and the Marangoni Effect", *AICHE Journal*, Vol. 5, No. 4, pp. 514-523.

Suzuki, Y., Noguchi, S., Longtin, J.P., Hijikata, K., 1996, "Combined Concentration and Temperature-Induced Marangoni Convection in a Binary Mixture", *Proceeding of the ASME Heat Transfer Division*, Vol. 3, pp. 77-83.

Tennekes, H., Lumley, J.L., 1982, *A First Course in Turbulence*, The MIT Press.

Tsai, B.B., Perez-Blanco, H., 1998, "Limits of Mass Transfer Enhancement in Lithium Bromide-Water Absorbers by Active Techniques", *International Journal of Heat and Mass Transfer*, Vol. 41, No. 15, pp. 2409-2416.

Tsuji, K., 1997, *Surface Activity*, Academic Press, New York.

Utaka, Y., 1995, "Measurement of Condensation Characteristic Curves for Binary Mixtures of Steam and Ethanol Vapor", *Heat Transfer-Japanese Research*, Vol. 24, No. 1, pp. 57-67.

Utaka, Y., 1998, "On Condensation Heat Transfer for Water and Ethanol Vapor Mixture (Observation of Drop Formation and Departure Processes for Marangoni Dropwise Condensation)", *Nippon Kikai Gakkai Ronbunshu, B-hen*, Vol. 64, No. 626, pp. 221-230.

Vliet, G.C., Cosenza, F.B., 1991, "Absorption Phenomena in Water-Lithium Bromide Films", *Environment-Friendly Technologies for the 21st Century (IAHPC 1991)*, Tokyo.

Wilke, C.R., Chang, P., 1955, "Correlation of Diffusion Coefficients in Dilute Solutions", *AICHE Journal*, Vol. 1, No. 2, pp. 264-270.

Wilkinson, M.C., 1972, "Extended Use of, and Comments on, the Drop Weight (drop Volume) Technique for the Determination of Surface and Interfacial Tensions", *Journal of Colloid and Interface Science*, Vol. 40, No. 1, pp. 14-26.

Yao, W., Bjurstrom, H., Setterwall, F., 1991, "Surface Tension of Lithium Bromide Solutions with Heat-Transfer Additives", *Journal of Chemical and Engineering Data*, Vol. 36, No. 1, pp. 96-98.

Yaws, C.L., 1994, *Handbook of Vapor Pressure*, Gulf Publishing Company, Houston, Vol. 3.

Yuan, Z., Herold, K.E., 2001, "Surface Tension of Aqueous Lithium Bromide with Controlled Vapor Concentration of 2-Ethyl-Hexanol", *ASHRAE Transaction*, Vol. 107, Pt.1, 2001.

Yuan, Z., Herold, K.E., 2001a, "Surface Tension of Pure Water and Aqueous Lithium Bromide with 2-ethyl-hexanol", *Applied Thermal Engineering*, Vol. 21, No. 8, pp. 881-897.

Yuan, Z., Herold, K.E., 2005a, "Thermodynamic Properties of Aqueous Lithium-Bromide Using a Multi-property Free Energy Correlation", *International Journal of Heating, Ventilating, Air-conditioning and Refrigeration*, Vol.11, No.3, pp. 377-393.

Yuan, Z., Herold, K.E., 2005b, "Specific Heat Measurements on Aqueous Lithium-Bromide", *International Journal of Heating, Ventilating, Air-conditioning and Refrigeration*, Vol.11, No.3, pp. 361-375.

Zaytsev, I.D. and Aseyev, G.G., 1992, "Properties of Aqueous Solutions of Electrolytes". Translated by Lazarev, M.A., Sorochenko, V.R., CRC Press.

Ziegler, F., Grossman, G., 1996, "Review Paper: Heat Transfer Enhancement by Additives ", *International Journal of Refrigeration*, Vol. 19, No. 5, pp. 301-309.

Zhou, X., Yuan, Z. and Herold, K.E., 2002, "Phase Distribution of the Surfactant 2-ethyl-hexanol in Aqueous Lithium Bromide", *HVAC&R Research*, Vol.8, No. 4, pp.371-381.

